Final Technical Report

Project Title:	A Novel Flash Ironmaking Process
Award Number:	DE-EE0005751 / 0013
Project Period:	02:2012 – 08:2018
American Iron and Steel Institute Principal Investigator:	Michael Sortwell msortwell@steel.org 412-458-5820
Berry Metal Company Principal Investigator:	George Boy gboy@berrymetal.com 724-453-1658
University of Utah Principal Investigator:	H. Y. Sohn h.y.sohn@utah.edu 801-581-5491
Recipient:	American Iron and Steel Institute 25 Massachusetts Avenue NW Suite 800 Washington DC 20001
Project Team Organizations:	ArcelorMittal USA TimkenSteel United States Steel Corporation
Date of Report:	11:2018

Acknowledgment: "This material is based upon work supported by the Department of Energy's Office of Energy Efficiency and Renewable Energy Advanced Manufacturing Office under Award Number DE-EE0005751."

Table of Contents

Acronyms

BMC – Berry Metal Company
CFD – Computational Fluid dynamics
DRI – Direct Reduced Iron
FIT – Flash ironmaking Technologies
LSBR – Large Scale Bench Reactor

Executive Summary

The goal of this project was to develop an entirely new transformative process for alternate ironmaking based on the direct gaseous reduction of iron oxide concentrate in a flash reduction process, with the ultimate objective of significantly lowering energy consumption and reducing environmental emissions, especially CO_2 emissions, versus the conventional blast furnace ironmaking route.

The Novel Flash Ironmaking Technology (FIT) developed in this project uses natural gas and generates hot reducing gas mixture of hydrogen and carbon monoxide, together with water vapor and carbon dioxide. The developed technology is to be applied to the production of iron as a feed to the subsequent steelmaking process, competing with other alternate ironmaking processes and eventually possibly replacing the blast furnace. The process could also be a part of a continuous direct steelmaking process.

The scope of this project included the design, installation, and commissioning of the Large Scale Bench Reactor (LSBR), testing and fine tuning the LSBR, performing computational fluid dynamics (CFD) modeling of the LSBR, and determining the next step for FIT development.

The LSBR was designed to fit in the existing laboratory. The commissioning of the LSBR was successful and the project advanced to the second phase – testing. The testing phase of the project proved the FIT was achievable. The goal of 95% metallization was exceeded by reducing the iron ore fines to a full 100% metallization. The project advanced to the third phase where additional testing was performed in order to determine the optimum operating conditions. A pilot plant was designed to perform additional tests to validate FIT at the next appropriate scale up size.

FIT is competing with alternate ironmaking processes that have plants in operation that are sized for approximately 1,600,000 tonnes/year. The LSBR was sized for 43 tonnes/year, but it was never operated in a manner to achieve that level of production. In order to scale the process to a level comparable with other similar technologies, there will be at least one intermediary size plant. The next stage of FIT is a pilot plant that was designed to produce 3,000 tonnes/year. This size was selected because it was large enough to gather sufficient information, and small enough to cost effectively modify components and adjust operating profiles. The technology is not ready for commercialization at this level. The next step in FIT is to establish a project team interested in constructing the 3,000 tonnes/year pilot plant. The pilot plant testing will answer additional questions on the viability of the technology and further determine the path towards commercialization.

Introduction

The work performed during this project was to develop a high intensity process to produce iron from iron ore. The primary method for producing iron includes coke ovens, iron ore pelletization, and a blast furnace. The Flash Ironmaking Technology would eliminate the need for iron ore pelletizing and coke ovens. Eliminating these processes would provide significant energy savings from the current method of steel production.

The FIT process feeds iron ore concentrate through a flash furnace at temperatures around 1300°C with a residence time of 2 to 10 seconds. The iron ore concentrate can successfully be reduced to 95-100% metallization. The temperature in the furnace is kept below the melting point of the iron ore concentrate to avoid sticking and fusion of the particles.

This project focused on the overall goal of creating an entirely new transformational process for alternate ironmaking based on the direct gaseous reduction of iron oxide concentrates in a flash reduction process. The ultimate objective is to significantly increase energy productivity and reduce environmental emissions. This project furthered the process development of Flash Ironmaking Technology. A kinetic feasibility project took place from 2005-2007 and a proof of concept at lab scale project ran from 2008-2011. This project scaled up the technology for process validation.

The FIT is targeted towards the steel industry. It would be beneficial for a steel producer to install this process at their steelmaking facility. Another option for the location of the technology would be at the iron ore mines. This option would require more logistics to package and transport the finished product. The energy analysis for FIT shows greater than 35% energy savings per tonne compared to the established a blast furnace technology and it also offers fewer emissions.

The experiments to date along with CFD modeling and analysis have shown the FIT is a technology worth pursuing. The next stage in the technology is a pilot plant to further prove the technology with a new reactor design and larger scale material handling.

Background

One of the core technical problems facing the U.S. steel industry today is to develop a new technology to produce steel from iron ore. An ideal process would replace the blast furnace and coke oven; would use domestic iron ores especially concentrates which the US has in abundance; and would greatly reduce energy requirements. It should also be a high intensity process requiring much less capital investment than the blast furnace/coke oven combination, and must be capable of producing 5,000 – 10,000 tonnes of metal per day so that it can support existing steel mills.

The project goal is to develop an entirely new transformational process for alternate ironmaking based on the direct gaseous reduction of iron oxide concentrates in a flash reduction process, with the ultimate objective of significantly increasing energy productivity and reducing environmental emissions, especially CO_2 emissions, versus the conventional blast furnace ironmaking route. The Novel Flash Ironmaking Process uses gaseous reducing agents, such as natural gas, hydrogen, other syngas, or a combination thereof. The proposed technology is to be applied to the production of iron as a feed to the steelmaking process, eventually replacing the blast furnace and other alternate ironmaking processes. The process can also be a part of a continuous direct steelmaking process.

This project had three phases: 1. Design, installation, and commissioning of the LSBR. 2. Testing and validation. 3. Determining optimum operating conditions and pilot plant design. The two primary contributors to this project were Dr. H. Y. Sohn of the University of Utah and the project team at Berry Metal Company.

Dr. Sohn is considered a world expert on gas-solid reaction analysis. He developed the idea to reduce iron ore fines using hydrogen. He faced some opposition on this idea, but was able to find errors in his opponents' analysis. One of Dr. Sohn's students had become the head of research and development at a steel producing company. Dr. Sohn spoke with him about the possibility of this technology and shortly after the development of Flash Ironmaking Technology began.

Dr. Sohn and his staff at the University of Utah were primarily responsible for the testing and validation of the technology. They also worked on determining optimum operating parameters, computational fluid dynamics, and contributed to pilot plant design.

Berry Metal Company (BMC) is a leading provider of furnace technology for steelmaking and ironmaking. Their goal is to provide customers the latest technology to improve efficiency, lower operating costs, and increase throughput in the steelmaking and ironmaking process. Over seven decades in business, BMC has earned a strong reputation for continuous development, quality products, dependable deliveries, and knowledgeable repair services.

BMC was primarily responsible for the design, installation, and commissioning of the LSBR. BMC offered technical support for the testing phase of the project. BMC was the lead for the pilot plant design and performed computational fluid dynamics modeling.

Results and Discussion

The primary objective of this project was to achieve greater than 95% metallization of iron ore fines. The project testing was successful as results of 100% metallization were achieved. This project achieved everything that it was supposed to and will prove to be an integral phase in the progression of Flash Ironmaking Technology.

Extensive discussion of the testing and modeling work can be found in Appendix A. Additional modeling work with regards to the next step in FIT can be found in Appendix B.

Benefits Assessment

When compared with similar technologies FIT offers equivalent or less energy usage in the production phase of iron. The most efficient DRI plants such as Midrex or HYL are around 10.8 GJ/tonne while a typical blast furnace uses 16.3 GJ/tonne. The energy analysis with conservatively high calculations for a FIT 500,000 tonnes/year plant resulted in 10.8 GJ/tonne. FIT also offers savings in the steelmaking process as it contains less gangue than the other processes and will not require as much energy in the steel refining process and it does not require pelletization. FIT can also offer better environmental emissions as hydrogen for reducing the ore can be generated in a number of carbon free emission processes.

Commercialization

Flash Ironmaking Technology began in a drop tube reactor and then progressed to a bench reactor. For this project, the FIT testing was performed in the Large Scale Bench Reactor which was capable of 43 tonnes/year but never run to that capacity. The project team evaluated the next logical size of the FIT process and determined a pilot plant capable of 3,000 tonnes/year. At this stage in the technology, it is too early for commercialization. Depending on the outcome of the pilot plant testing, FIT could move to a demonstration plant size. A description on the decision process for the next stage of FIT can be found in Appendix B.

Accomplishments

The major accomplishment of this project was proving the process of reducing iron ore fines in a flash furnace and determining this process would be less energy intensive than other similar technologies along with providing environmental benefits. The project resulted in many publications, multiple graduate student theses, and a patent application. A list of publications can be found in Appendix A.

Conclusions

This project was an important and integral step in the advancement of Flash Ironmaking Technology. Over the six year project the team learned a lot including material selection, temperature selection, feed rate, gas mixture and flow. The project team learned the difference between reactor shapes and design which resulted in the decision for the next reactor to be built long and skinny with a first in first out type product flow. The project team also learned about product loss and has built into the next phase a cyclone separator to practically eliminate product loss. Many of the lessons learned and how they factored into decisions for the pilot plant can be found in Appendix B.

Recommendation

The recommendation is to continue advancing Flash Ironmaking Technology by constructing and testing a 3,000 tonnes/year plant.

Appendices

Appendix A – University of Utah Final Project Report

Appendix B – Berry Metal Company Pilot Plant Preliminary Design Final Report

A Novel Flash Ironmaking Process

Final Project Report

September 2018

Prepared by

H. Y. Sohn

h.y.sohn@utah.edu

Department of Metallurgical Engineering,

University of Utah

Salt Lake City, Utah 84112

DOE/EERE/Office of Advanced Manufacturing Program (AMO)

FINAL PROJECT REPORT

Project Title: **A Novel Flash Ironmaking Process**

Project Period: 09/01/2012 through 08/31/2018

Date of Report: September 2018

Recipient: American Iron and Steel Institute (AISI)

Subcontractor: University of Utah, Salt Lake City, Utah 84112

Contact: H.Y. Sohn, 801-581-5491, h.y.sohn@utah.edu

Award Number: DE-EE0005751/0013

Partners: University of Utah, Salt Lake City, Utah 84112
Berry Metal Company, Harmony, Pa 16037
ArcelorMittal USA, East Chicago, Indiana 46312
United States Steel Corporation, Pittsburgh, Pa 15219
TimkenSteel, Canton, Ohio 44706

TABLE OF CONTENTS

1. PROJECT GOALS / OBJECTIVES

The goal of this project was to develop an entirely new transformative process for alternate ironmaking based on the direct gaseous reduction of iron oxide concentrate in a flash reduction process, with the ultimate objective of significantly lowering energy consumption and reducing environmental emissions, especially CO_2 emissions, versus the conventional blast furnace ironmaking route.

The Novel Flash Ironmaking Technology (FIT) developed in this project uses natural gas and generates hot reducing gas mixture of hydrogen and carbon monoxide, together with water vapor and carbon dioxide. The developed technology is to be applied to the production of iron as a feed to the subsequent steelmaking process, eventually replacing the blast furnace and other alternate ironmaking processes. The process can also be a part of a continuous direct steelmaking process.

The major task in this project was the test of the Flash Ironmaking Technology (FIT) in a Large Scale Bench Reactor (LSBR) in the laboratory. Additional tasks included a more detailed determination of the concentrate reduction kinetics by H_2+CO mixtures and experiments in a smaller laboratory flash reactor termed Utah Flash Reactor (UFR).

2. BACKGROUND

One of the core technical problems facing the U.S. steel industry today is to develop a new technology to produce iron from iron ore. An ideal process would replace the blast furnace and coke oven; would use domestic iron ores especially iron ore concentrate, which the U.S. has in abundance; and would greatly reduce energy requirements. It should also be a high intensity process requiring much less capital investment than the blast furnace/coke oven combination, and must be capable of producing 5,000 – 10,000 tons of iron per day so that it can support existing steel mills.

The fundamental question regarding the feasibility of adapting the flash furnace to ironmaking concerns the speed of reaction, i.e. can iron oxide concentrates be sufficiently reduced in the few seconds of residence time typically available in a flash furnace. Research performed under the AISI/DOE Technology Roadmap Program (DE-FC36-97ID13554) at the University of Utah using iron ore concentrate (~30 μm size) showed that 90 – 99% reduction can be achieved within 1 – 7 seconds of residence time at temperatures of 1300°C or higher [Choi and Sohn, 2010]. This was verified by additional laboratory-scale testing. Thus, the question on whether the reduction rate of concentrate particles is fast enough for a flash reduction process has been resolved conclusively to be affirmative.

The studies also established that because of the high temperature and absence of significant contact between the iron ore particles in flash furnaces, sticking and fusion of the particles is eliminated. Sticking is a crucial problem that has beset other alternative ironmaking processes and eliminated them as a replacement for the blast furnace.

Additional large-scale laboratory tests supported by AISI under the CO_2 Breakthrough Program (2008-2011) included successful operation of an oxy-fuel burner as a supply source of both heat and reducing gases in an industrial operation. Detailed material and energy balances showed that Flash Ironmaking Technology can use a number of reductants/fuels. A natural gas fired flash smelter will generate only 39% of the carbon dioxide of a blast furnace. CO_2 emissions using coal gas or hydrogen are 69% or 4%, respectively, in the ironmaking step. The

Flash Ironmaking Process also eliminates the iron ore pelletizing and indurating steps and, of course, eliminates the need for coke and coke ovens.

Once fully developed, the technology is to be applied to the production of iron as a feed to the steelmaking process, eventually replacing the blast furnace and other alternative ironmaking processes. The process can also be a part of a continuous direct steelmaking process.

3. SUMMARY OF ACCOMPLISHMENTS

The following is a summary list of major accomplishment from this project:

- Achieved more than 90% metallization with 1.5 times the minimum theoretical amount of reducing gas using a Large-Scale Bench Reactor (LSBR) operating at temperature 1350 °C and concentrate feeding rate of 5 kg/h.
- Operated the LSBR under various conditions in the temperature range of 1150-1400 °C and concentrate feeding rate 1-7 kg/h.
- Determined the effects of temperature and partial pressures of hydrogen and carbon monoxide on the reduction kinetics of magnetite concentrate using two drop-tube reactors (DTRs) in the temperature range of 1150 - 1600 °C.
- Achieved more than 90% metallization with 2 times the minimum theoretical amount of reducing gas using the laboratory scale flash reactor (UFR) operating at temperatures of 1150-1200 °C and the concentrate feeding rate of 0.1-0.5 kg/h.
- Completed formulation of a CFD model for the LSBR in terms of temperature, gas-phase composition, and reacting particles.
- Complete formulation of a CFD model for the existing lab-scale reactor, Utah Flash Reactor (UFR), in terms of temperature, gas-phase composition, and reduction kinetics of magnetite.
- Complete formulation of a CFD model for a drop-tube reactor (DTR) in terms of temperature, gas-phase composition and reduction kinetics of magnetite.
- Developed a rigorous computational algorithm to accurately determine the particle residence time and temperature in two DTRs. This is critical in developing the reduction rate equations.

4. RESULTS OF EXPERIMENTAL WORK

4.1 Tests with Smaller Laboratory Reactors

Experimental work was first performed using a drop-tube reactor (DTR) available at the University of Utah and a smaller laboratory reactor named the Utah Flash Reactor (UFR). These tests were performed to deliver essential information and experience for establishing an experimental campaign for the larger LSBR. During the extended period of work using the UFR, tests were done with natural gas in addition to hydrogen. These tests generated information on preferred operating gas ratios and gas/particle injection configurations in preparation for the tests with the LSBR, including different injector/burner designs.

Experimental work with DTR determined the kinetics of magnetite reduction by H_2 + CO gas mixtures to be generated by internal partial combustion of natural gas. In particular, the effects of temperature, partial pressures of hydrogen and carbon monoxide, and particle size on the kinetics were established. The results were instrumental for selecting the optimal operating conditions; that is, reaction temperature, reducing gas composition, and particle residence time

for testing in LSBR. In addition, the results will contribute to the design of the industrial pilot reactor. This DTR had a maximum operating temperature of only 1400 °C. Thus, to facilitate the collection of basic kinetics data at higher temperatures, a new DTR system was set up (1400 – 1600 °C). This expanded the temperature range to that tested in the LSBR. Below are the details of the major findings from the UFR and the two DTR systems.

4.1.1 Drop-Tube Reactors

Experiments were performed on the drop tube reactors to study the kinetics of the magnetite reduction with H_2, CO, and H_2+CO gas mixture. The effect of temperature, particle size, and reducing gases partial pressures was studied.

The calculations of the nominal particle residence time, excess driving force and excess reducing gases were performed using the same method adopted for the UFR calculations except that the reactor does not have a flame. All the experiments were performed to maintain excess reducing gas of more than 500% so that the gas composition remains largely constant. It is noted that the specific barometric pressure of Salt Lake City is 0.85 atm (1 atm = 101.32 kPa), which was used in all the experimental design and analysis in all the experimental work.

The reduction of magnetite concentrate particles with hydrogen and by carbon monoxide was investigated in the temperature range of 1150–1600 °C at ~50°C increments. Due to the fusion of the particles at temperatures higher than 1350 °C, the rate investigation was divided into two temperature ranges: 1150-1350 °C and 1350-1600 °C. Global reaction rate equations were formulated for the two temperature ranges for the reduction by an individual gas using the nucleation and growth model. The effects of temperature, particle size, and gas partial pressures were incorporated in the rate equations. The rate equation for the reduction by H_2 and CO mixture was then developed based on the rate equations developed for the reduction by individual gases.

(a) Reduction of Magnetite Concentrate by H_2

Reduction degrees of > 90% were achieved in a few seconds that are typically available in a flash reactor at temperatures as low as 1236 °C. The rate equation was described with the Avrami model with an Avrami parameter n = 1. The rate dependence on hydrogen partial pressure was first order and the activation energy was 193 kJ/mol in the temperature range of 1150-1350 °C. The particle size effect was negligible in this temperature range. The complete rate equation in this temperature range of 1150-1350 °C is

$$[-\mathrm{Ln}(1-X)] = 8.65 \times 10^6 \times e^{\left(\frac{-193{,}000}{RT}\right)} \times \left[p_{H_2} - \left(\frac{p_{H_2O}}{K_H}\right)\right]_{lm} \times t \qquad (1)$$

where R is 8.314 J/mol K, T is in K, p is in atm, and t is in seconds.

In the higher temperature range of 1350-1600 °C, the activation energy was 170 kJ/mol and the particle size effect was significant as increasing particle size decreased the reduction rate. The complete rate equation is

$$[-\mathrm{Ln}(1-X)] = 2.5 \times 10^7 \times e^{\left(\frac{-170{,}000}{RT}\right)} \times (d_p)^{-1} \times \left[p_{H_2} - \left(\frac{p_{H_2O}}{K_H}\right)\right]_{lm} \times t \qquad (2)$$

where R is 8.314 J/mol K, T is in K, p is in atm, d_p in μm, and t is in seconds.

(b) Reduction of Magnetite Concentrate by CO

The reduction rate by CO was much slower than that by H_2 and little reduction by CO was obtained at temperatures lower than 1239 °C when the residence time was as high as 8 s. The Avrami model was used to describe the reduction kinetics with an Avrami parameter $n = 0.5$ and first order dependence on the carbon monoxide partial pressure. The activation energy was 430 kJ/mol with no effects of the particle size in the temperature range of 1200-1350 °C. The complete rate equation is

$$[-\mathrm{Ln}(1-X)]^{1/0.5} = 1.21 \times 10^{13} \times e^{\left(\frac{-430{,}000}{RT}\right)} \times \left[p_{CO} - \left(\frac{p_{CO_2}}{K_C}\right)\right]_{lm} \times t \qquad (3)$$

where R is 8.314 J/mol K, T is in K, p is in atm, and t is in seconds.

In the higher temperature range of 1350-1600 °C, the particle size effect was the same as the case of reduction by H_2 in the same temperature range. The activation energy was 73 kJ/mol as the temperature had a smaller effect on the reduction rate in this range. The complete rate equation is:

$$[-\mathrm{Ln}(1-X)]^{1/0.5} = 2.39 \times 10^{3} \times e^{\left(\frac{-73{,}000}{RT}\right)} \times (d_p)^{-1} \times \left[p_{CO} - \left(\frac{p_{CO_2}}{K_C}\right)\right]_{lm} \times t \qquad (4)$$

where R is 8.314 J/mol K, T is in K, p is in atm, d_p in μm, and t is in seconds.

(c) Reduction of Magnetite Concentrate by H_2+CO Mixture

The analyses of magnetite reduction by the individual gases proved that H_2 was the main reductant as the reduction rate by H_2 was much faster than that by CO. The rate equations for reduction by individual gases were used to develop a rate equation for the reduction kinetics by H_2 + CO gas mixtures. The presence of CO increased the reduction rate to be higher than the simple sum of the rates by individual gases. In order to account for the enhanced effects, the reduction contribution due to H_2 was amplified by a constant for the case of reduction by H_2 + CO mixtures.

The rate expression for the H_2 + CO gas mixtures in the temperature range of 1150–1350 °C was established as

$$\left.\frac{dX}{dt}\right|_{H_2+CO} = 1.3 \cdot \left.\frac{dX}{dt}\right|_{H_2} + \left.\frac{dX}{dt}\right|_{CO} \qquad 1150°C \leq T < 1350\ °C \qquad (5)$$

where $\left.\frac{dX}{dt}\right|_{H_2}$ and $\left.\frac{dX}{dt}\right|_{CO}$ are the instantaneous rate of reaction obtained from the reaction rates individually by H_2 and CO, respectively, in the temperature range of 1150-1350 °C.

For the reduction of magnetite by H_2+CO gas mixtures in the temperature range of 1350-1600°C, the rate equation is

$$\left.\frac{dX}{dt}\right|_{H_2+CO} = 2 \cdot \left.\frac{dX}{dt}\right|_{H_2} + \left.\frac{dX}{dt}\right|_{CO} \qquad 1350°C \leq T < 1600\ °C \qquad (6)$$

where $\left.\frac{dX}{dt}\right|_{H_2}$ and $\left.\frac{dX}{dt}\right|_{CO}$ are the instantaneous rate of reaction obtained from the reaction rates individually by H_2 and CO, respectively, in the temperature range of 1350-1600 °C.

This kinetics investigation was the first to be performed on the reduction of magnetite concentrate by H_2 and CO in the temperature range of 1150-1600 °C. The rate equations have a great significance for the development of the flash ironmaking technology. They are instrumental in designing and testing a larger scale flash reactor in which the reduction of magnetite concentrate are carried out in a H_2+CO mixture produced from the partial oxidation of natural gas. This will allow the utilization of the abundant and inexpensive natural gas in ironmaking. Validation of the developed rate equations are shown in Figures 1-6.

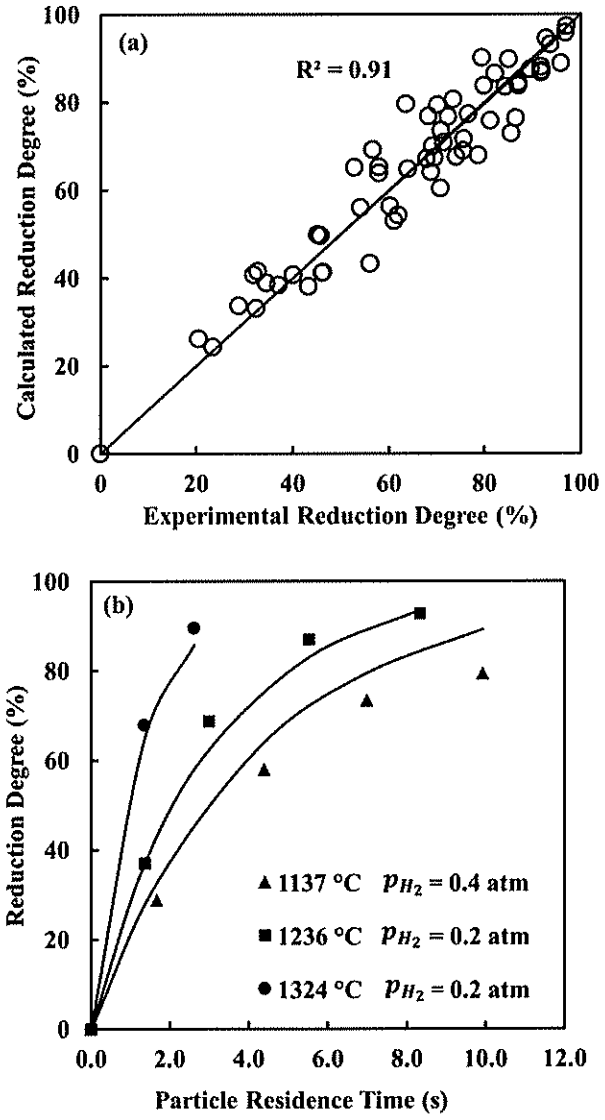

Figure 1. Validation of developed rate equation for reduction by H_2 at 1150-1350 °C. (a) Comparison between the calculated reduction degree (%) by the developed rate equation and the experimental results. (b) Experimental reduction degree (%) vs. particle residence time where the solid lines represent the calculated reduction degree by the developed rate equation.

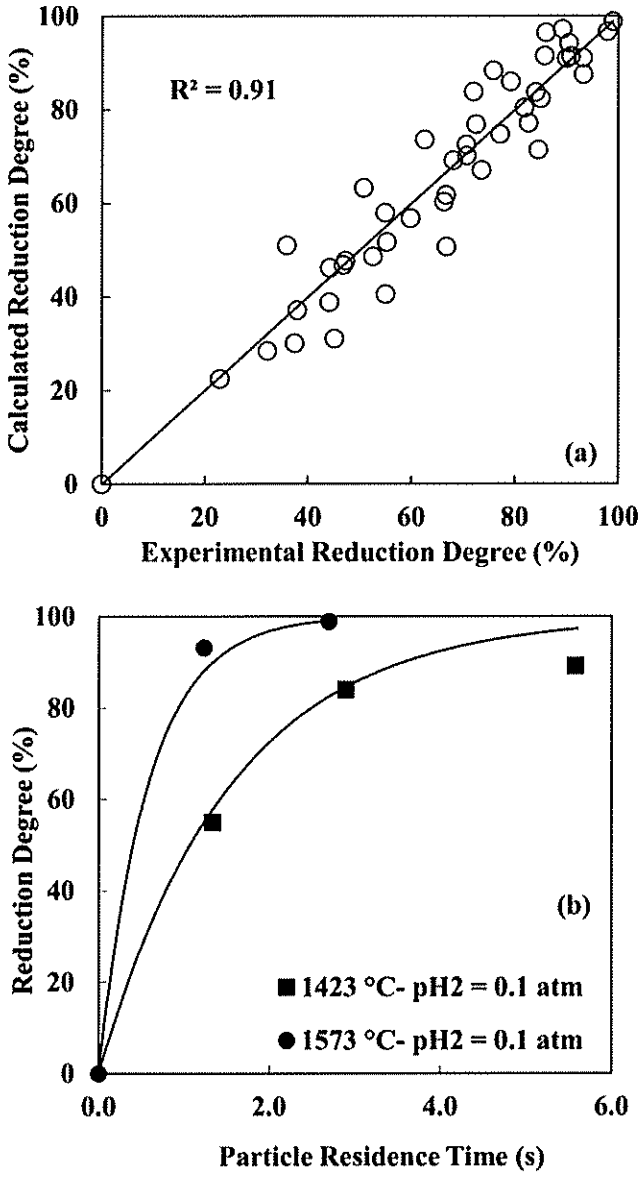

Figure 2. Validation of developed rate equation for reduction by H_2 at 1350-1600 °C. (a) Comparison between the reduction degree (%) calculated by the developed rate equation and the experimental results. (b) Experimental reduction degree (%) vs. particle residence time where the solid lines represent the reduction degree calculated by the developed rate equation.

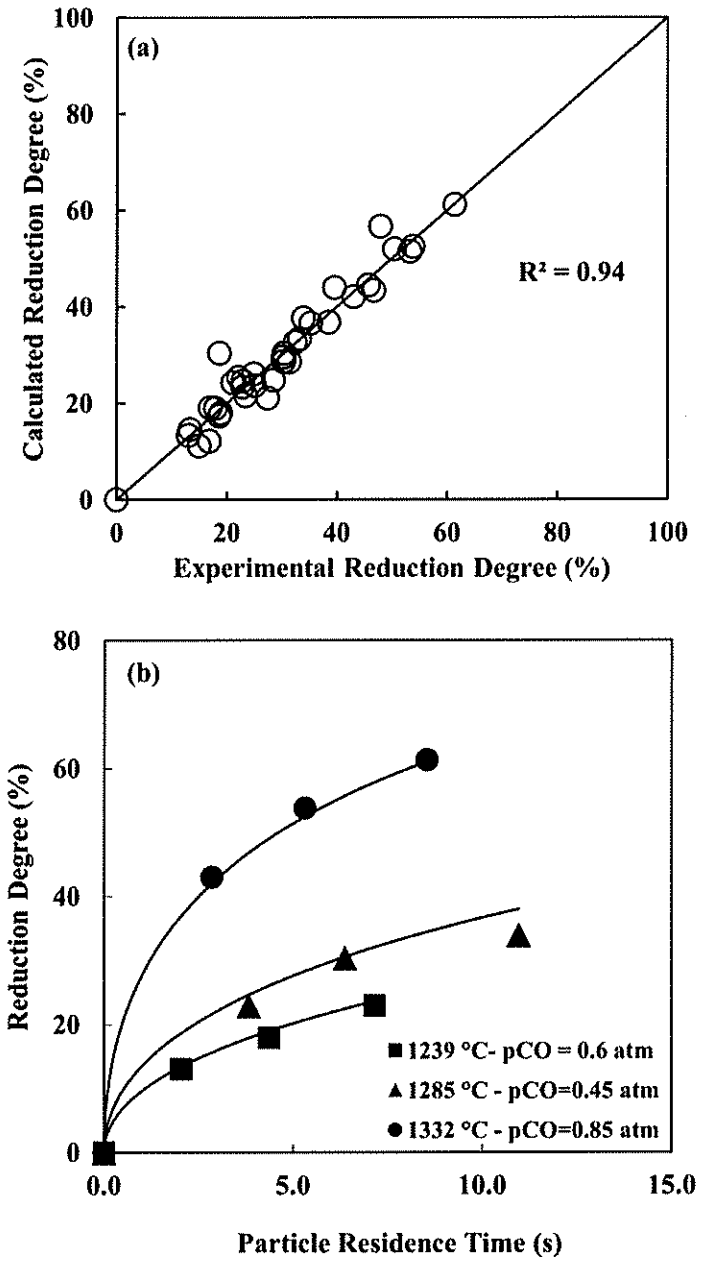

Figure 3. Validation of the developed rate equation for reduction by CO at 1150-1350 °C (a) Comparison between the reduction degree (%) calculated by the developed rate equation and the experimental results. (b) Experimental reduction degree (%) vs. particle residence time where the solid lines represent the reduction degree calculated by the developed rate equation.

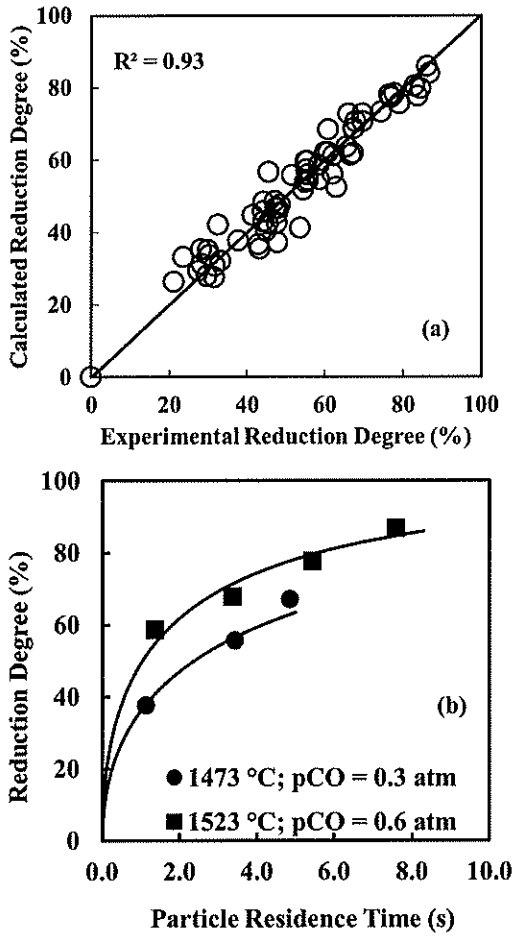

Figure 4. Validation of developed rate equation for reduction by CO at 1350-1600 °C (a) Comparison between the reduction degree (%) calculated by the developed rate equation and the experimental results. (b) Experimental reduction degree (%) vs. particle residence time where the solid lines represent the reduction degree calculated by the developed rate equation.

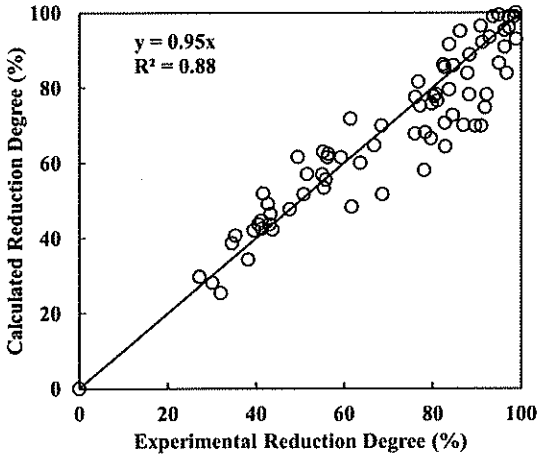

Figure 5. Comparisons between the calculated reduction degrees vs. experimental results when H_2+CO mixtures are the reducing gas at 1150-1350 °C.

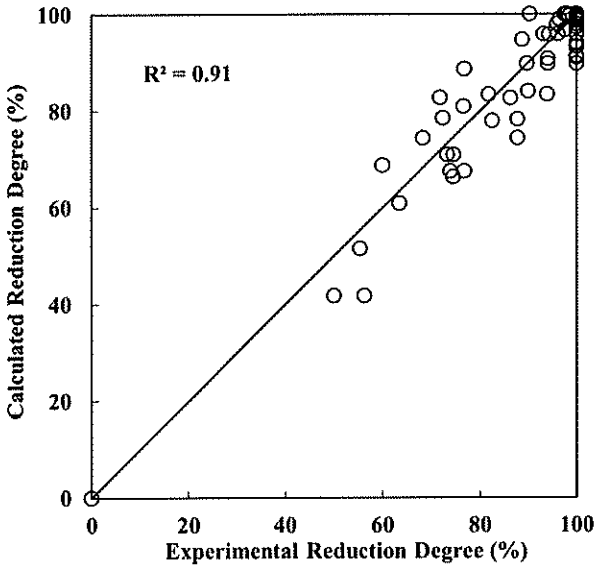

Figure 6. Comparisons between the calculated reduction degrees vs. experimental results with H_2+CO mixtures as the reducing gas at 1350-1600 °C.

4.1.2 Utah Flash Reactor (UFR)

The tests in UFR, the reactor tube of which was made of stainless steel 316 with 0.19 m ID and 2.13 m length and more fully described elsewhere [Fan et al., 2016c], delivered useful information and experience for the experimental campaign in the Large Scale Bench Reactor (LSBR). Hydrogen and methane (the major constituent of natural gas) were used as the fuels/reductants. The main goal of the UFR runs was to determine operating conditions that yielded a product powder with a high reduction degree (> 90 %). The UFR operating conditions are defined in terms of the *excess driving force (EDF)* and the *residence time of the concentrate particles*, the definitions of which are given below:

(a) *Excess Driving Force (EDF)*

To represent the excess amount of hydrogen over the equilibrium requirement of the reduction of wüstite ($Fe_{0.947}O$) by hydrogen [$Fe_{0.947}O + H_2 = 0.947Fe + H_2O$], the term "excess driving force (EDF)," defined by the following equation, is used:

$$EDF = \frac{\dfrac{p_{H_2,\text{off-gas}}}{p_{H_2O,\text{off-gas}}} - \dfrac{p_{H_2,eq}}{p_{H_2O,eq}}}{\dfrac{p_{H_2,eq}}{p_{H_2O,eq}}} \tag{7}$$

where $p_{H_2,\text{off-gas}}$ and $p_{H_2O,\text{off-gas}}$ are the partial pressures of hydrogen and water vapor in the off-gas, respectively, and $p_{H_2,eq}$ and $p_{H_2O,eq}$ are the partial pressures of hydrogen and water vapor at equilibrium in the presence of wüstite and iron. The "theoretical minimum amount of reducing gas" is defined as the sum of the stoichiometric amount of reducing gas required for the overall

reduction [e.g., $Fe_3O_4 + 4H_2 = 3Fe + 4H_2O$ for magnetite concentrate] of the iron oxide and the amount of reducing gas required for the iron-wüstite equilibrium.

(b) *Residence Time*

The duration of the reduction reaction of iron oxide concentrate particles is determined by the "residence time (τ) of the particles" in the reaction zone. In the UFR, the reaction zone is defined as the reactor length in which the particles experience a temperature higher than 1150 °C, a temperature level at which the reduction rate begins to be significant based on the previous work (AISI/DOE Technology Roadmap Program - DE-FC36-97ID13554 [Sohn, 2008] and AISI CO_2 Breakthrough Program). Temperature profiles obtained using thermocouples placed at 20, 30, and 40 inches below the upper flange of the reactor in the axial direction and at 3.25 inches away from the center of the reactor in the radial direction indicated that the reaction zone has an approximate length of 0.46 m (18 inches). The nominal residence time of the particles is thus calculated by

$$\tau = \frac{L}{u_g + u_t} \tag{8}$$

where L is the length of the reaction zone, u_g is the average gas velocity (volumetric flow rate divided by cross-sectional area), and u_t is the terminal falling velocity of the particles for the creeping flow region, which is expressed by Stoke's law assuming that the particles fall at a constant velocity in the reaction zone:

$$u_t = d_p^2 g(\rho_p - \rho_g)/18\mu \tag{9}$$

where d_p is particle size (22.4 μm), g is the gravitational acceleration (9.81 m/s^2), ρ_g is the gas density (kg/m^3), ρ_p is the particle density (5170 kg/m^3), and μ_g is the viscosity of the gas (Pa s).

It is noted that the calculated nominal residence time of the particles is a simple approximation of the actual residence time that the particles experience inside the UFR. As particles flow downward inside the reactor, they disperse and, as a result, they experience different gas velocities (due to the presence of a radial velocity component) and different temperatures (due to the presence of the flame). Therefore, CFD work on the UFR, which provides computed distributions of velocity, temperature and species concentrations, was subsequently used to calculate the residence times of the particles more accurately.

(c) *Potential Further Reaction in the Collection Area*

In order to ascertain that no further reduction occurs in the main collection locations, a bowl and a flange, at the bottom of the reactor (the flash reduced powder stays there for about an hour and a half), two experiments were performed. In the first experiment, the temperature was continuously recorded in the collection bowl during an experimental run. The temperature was 345 ± 5 °C which is low for the reduction reaction to be significant. In the second experiment, partially reduced sample from a previous UFR run was loaded to these two collection locations. The powder was spread in a thin layer in the collection bowl and on the flange. The experiment was performed without feeding the powder and then the two samples were collected and

analyzed. There was no change in the reduction degree of the two samples before and after the experiment, which indicated that the samples collected during the main runs did not undergo any further changes.

(d) *Determination of the Reaction Zone*

As shown in Eq. (8), the length of the reaction zone is required to calculate the particle nominal residence time in the Utah Flash Reactor (UFR).

Temperature was measured near the wall and at the center of the reactor tube during representative runs using a 90" K-type thermocouple, as presented in Table 1 and Figure 7. Temperature profiles were measured under the highest and lowest possible flame powers that are expected to be tested in the UFR experimental campaign. The measurements were recorded at two inch intervals. The temperature profile was measured under experimental conditions that included concentrate feeding, as shown in Table 1. The reaction zone in the UFR was defined as the zone where the temperature is 1175 ± 25°C with the length of 27". All calculations of the particle nominal residence time were based on the 27" reaction zone. In this reaction zone, the temperature difference between the center and the wall varied from 5 to 10°C. This temperature difference was considered small, and therefore, the radial temperature in the UFR was considered uniform at the measured value.

Table 1. Conditions under which temperature profiles were measured.

Profile	Input Flow Rates (L/min)			Iron Concentrate Feeding		% Excess H_2	EDF	Particle Residence Times (s)	Product Analysis		Notes	Reaction Zone Length (in)
	(H_2)	(O_2)	(N_2)	Rate (g/min)	Injection Point*				RD%	Met%		
a	20	2.96	2.8	2.2	SS	40.30%	0.45	7.5	80.3	73.8	Center	30
b	20	2.96	2.8	1.9	SS	45.50%	0.5	7.5	96.8	95.7	Side	30
c	60	9.65	2.8	2.2	SS	49.50%	0.51	3.4	74.2	65.6	Center	26
d	60	9.65	2.8	2.1	SS	49.80%	0.52	3.4	79.5	72.7	Side	28
e	60	9.65	1.85	1.5	B'	53.80%	0.55	1.9	74.9	66.5	Side New flame	24

**SS represents 2-side feeding with old flame configuration and B' represents feeding through the center and applying the new flame configuration in Fig.9.*

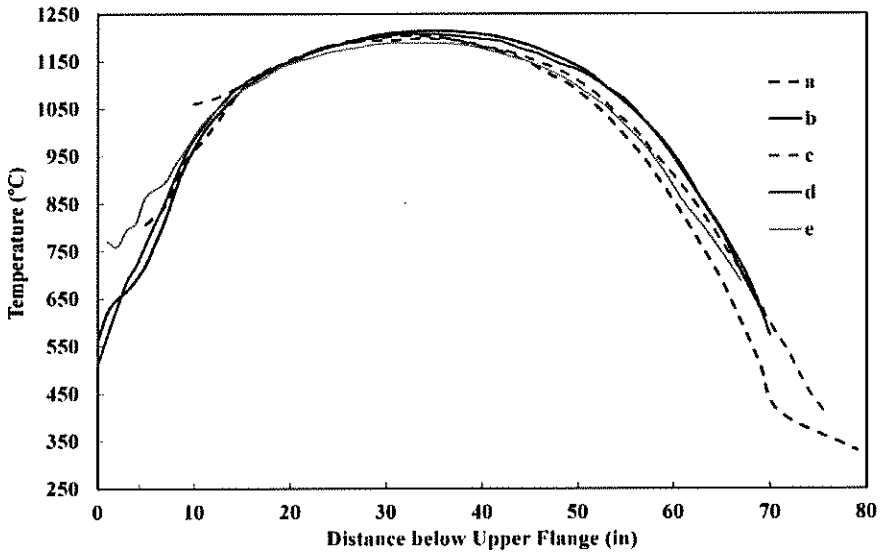

Figure 7. Comparison between the temperature profiles measured at the center and at the side for experiment with using different flame powers.

(e) Feeding Ports and Flame Configuration

The UFR tests delivered useful information and experience for establishing an experimental campaign for the new Large Scale Bench Reactor (LSBR).

Experiments in the Utah Flash Reactor (UFR) were performed using hydrogen or methane as the fuels/reductant and magnetite ore concentrate. The powder was fed to the system at a constant rate of 0.12 ± 0.01 kg/h. The particles were fed mainly through the upper flange of the system either through the center of burner (namely burner feeding) or through two inlets on the side of the burner (namely two side feeding), as shown in Figure 8. When feeding was through the burner inlet, the feeding rate was approximately 0.12 kg/h whereas in feeding through the two side inlets the feeding was approximately 0.06 kg/h through each inlet with an approximate total feeding rate of 0.12 kg/h. It is noted that the specific barometric pressure of Salt Lake City is 0.85 atm (1 atm = 101.32 kPa), which was used in all the experimental design and analysis in all the experimental work.

The flame configuration inside the reactor was changed in some experiments by swapping the hydrogen and oxygen feeding ports in the burner nozzle. In the new flame configuration oxygen flow surrounds hydrogen feed stream. The old flame configuration had the two gas streams reversed. When the concentrate is fed through the center tube, the new configuration prevents the particles from being heated excessively and melting, as shown by temperature contours in the two simulated configurations shown in Figure 9 below.

Various combinations of particles residence time, excess driving force, feeding ports, and flame configuration were tested.

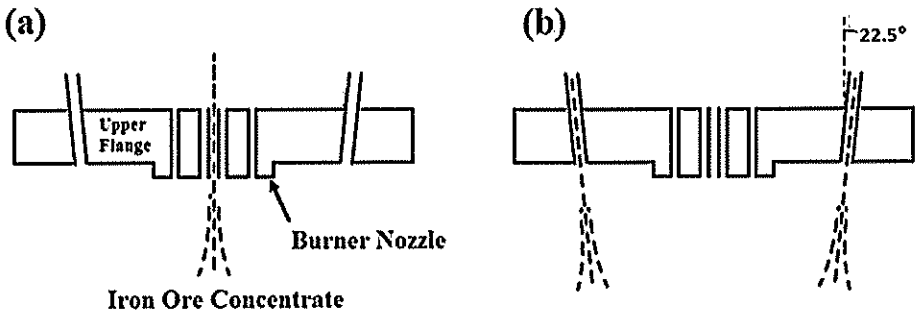

Figure 8. Powder feeding modes: (a) burner and (b) Two side feeding.

(f) UFR Runs and Results: Hydrogen Runs

A reduction degree of 96% and metallization degree 95% with % excess hydrogen of less than 100 at temperature as low as 1175 °C and a feeding rate of ~ 0.12 kg/h in a few seconds of residence time was achieved. Some experiments were performed using a 45° tilted port but the powder hit the opposite wall of the reactor and accumulated then fell as chunks in the collection. The powder injection through the two side feeding ports was adjusted to be within 0-25° from the perpendicular axis of the feeding port to avoid any accretion on the wall.

Sixty-six complete experiments were performed on the UFR using hydrogen gas as the reductant/fuel and magnetite as the reactants. Table 2 shows all the experiments conducted, conditions and results. When feeding through the two side inlets, increasing the particle residence time and the excess driving force increased the reduction degree as shown in Figure 10.

Changing the feeding port from the two side inlets to the burner inlet resulted in lowering the reduction degree significantly due to the particles melting as a result of exposure to the high temperature in the center of the flame, as shown in the SEM micrographs in Figure 11. As can be seen in Figure 9(a), the temperature at the center of the flame where the particles are fed in the burner feeding mode using the old flame configuration reaches 2600 K. Melting and rounding reduces the active sites on the particles as compared with side feeding where the particles retain their irregular shape and reactivity that produced higher reduction degrees.

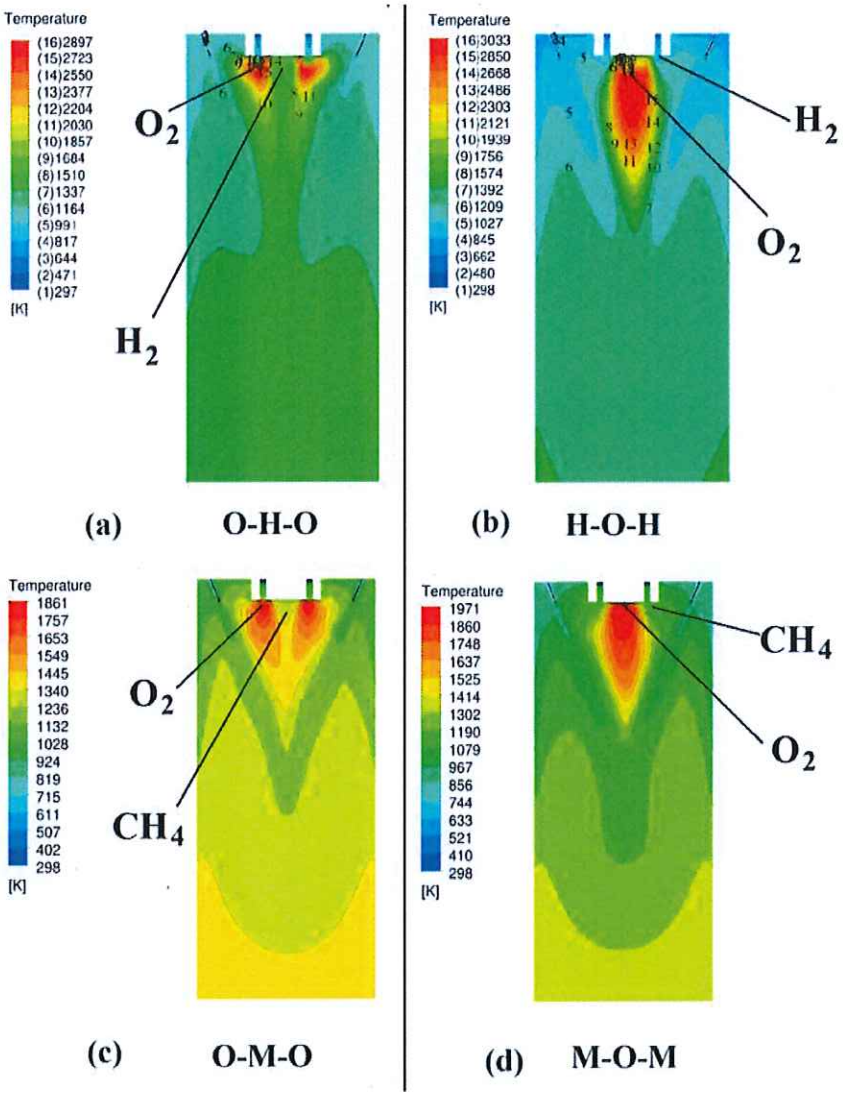

Figure 9. The flame configuration and temperature contours: (a) old configuration and (b) new configuration.

Table 2. The experimental conditions and results for the hydrogen/magnetite UFR experiments.

Date	Experiment Code	Iron Concentrate Rate (kg/hr)	Iron Concentrate Injection Point*	Chemical Driving Force $Fe_{0.947}O + H_2 = 0.947\ Fe + H_2O$ % Excess H_2	Chemical Driving Force EDF	Nominal Particle Residence Time (s)	RD (%)	Met. (%)	Comment
10/18/2013	UFR-131018	0.067	S	898.1%	10.46	4.4	83.7	78.2	
10/22/2013	UFR-131022	0.064	S	283.8%	3.20	7.4	88.5	84.7	
10/25/2013	UFR-131025	0.066	S	126.7%	1.37	7.6	81.8	75.8	
10/29/2013	UFR-131029	0.064	S	87.7%	0.94	7.6	77.7	70.3	
11/5/2013	UFR-131105	0.068	T	43.2%	0.46	7.7	72.9	63.9	
11/8/2013	UFR-131108	0.069	T	131.2%	1.39	5.8	85.5	80.7	
11/12/2013	UFR-131112	0.062	T	51.1%	0.53	5.9	66.7	55.6	
11/15/2013	UFR-131115	0.066	T	90.9%	0.95	5.8	74.9	66.6	
11/19/2013	UFR-131119	0.071	T	92.9%	0.95	3.4	75.3	67.0	
11/22/2013	UFR-131122	0.067	T	48.2%	0.49	3.4	70.9	61.2	
11/26/2013	UFR-131126	0.068	T	140.6%	1.45	3.4	78.4	71.3	
12/10/2013	UFR-131210	0.130	SS	131.8%	1.43	4.6	91.5	88.7	
12/13/2013	UFR-131213	0.129	SS	44.2%	0.47	4.7	76.7	68.9	
12/20/2013	UFR-131220	0.118	SS	7.6%	0.08	7.5	62.8	50.4	
12/23/2013	UFR-131223	0.128	SS	5.3%	0.06	8.8	56.9	42.6	
12/31/2013	UFR-131231	0.111	SS	22.6%	0.25	7.5	82.6	76.8	
1/3/2014	UFR-140103	0.122	SS	19.8%	0.22	8.8	69.5	59.3	
1/7/2014	UFR-140107	0.113	SS	43.7%	0.50	8.7	79.8	73.0	
1/10/2014	UFR-140110	0.110	SS	46.0%	0.51	7.5	84.0	78.6	
1/17/2014	UFR-140117	0.103	SS	32.6%	0.36	8.7	76.2	68.2	
1/21/2014	UFR-140121	0.111	SS	31.1%	0.34	7.5	80.1	73.4	
1/31/2014	UFR-140131	0.112	SS	21.1%	0.24	8.8	70.3	60.4	Repeat
2/7/2014	UFR-140207	0.115	SS	21.4%	0.22	3.9	64.0	52.0	
2/14/2014	UFR-140214	0.120	SS	10.9%	0.11	3.4	46.3	28.4	
2/21/2014	UFR-140221	0.112	SS	51.1%	0.53	3.4	74.3	65.7	
2/25/2014	UFR-140225	0.121	SS	5.8%	0.06	3.4	49.3	32.4	
3/7/2014	UFR-140307	0.115	SS	44.5%	0.49	7.5	90.4	87.2	Repeat
3/24/2014	UFR-140324	0.110	SS	46.0%	0.51	7.5	105.8	107.7	Powder size < 20μ
3/28/2014	UFR 140328	0.109	SS	9.2%	0.10	7.5	83.3	77.8	Powder size < 20μ
4/4/2014	UFR 140404	0.120	B	46.6%	0.52	4.6	25.8	1.1	
4/7/2014	UFR 140407	0.123	B	50.0%	0.52	1.9	53.2	37.7	
4/11/2014	UFR 140411	0.121	B	132.3%	1.53	4.4	45.8	27.7	
4/14/2014	UFR 140414	0.121	B	145.6%	1.53	1.8	50.9	34.5	
4/16/2014	UFR 140416	0.120	B	95.4%	1.03	2.9	48.1	30.9	
4/21/2014	UFR 140421	0.112	B	99.4%	1.04	1.8	59.1	45.4	
4/25/2014	UFR 140425	0.116	B	92.3%	1.04	4.4	28.6	4.7	
5/2/2014	UFR-140502	0.121	B	48.8%	0.52	2.9	45.6	27.4	
5/7/2014	UFR-140507	0.119	B	140.3%	1.53	2.9	33.9	11.9	
5/9/2014	UFR-140509	0.128	SS	49.5%	0.51	3.4	63.3	51.0	Repeat
5/12/2014	UFR-140512	0.116	SS	44.2%	0.49	7.5	77.2	69.6	Repeat
5/15/2014	UFR-140515	0.122	SS	45.1%	0.48	4.7	56.4	41.8	Repeat
5/22/2014	UFR-140522	0.118	B	50.5%	0.52	1.9	59.3	45.7	Repeat
5/29/2014	UFR-140529	0.119	B	133.5%	1.54	4.4	40.8	21.1	Repeat
6/2/2014	UFR-140602	0.118	B	133.9%	1.55	4.4	94.4	92.5	Repeat
6/5/2014	UFR-140605	0.120	B	132.8%	1.53	4.4	43.7	24.9	Repeat
7/17/2014	UFR-140717	0.116	SS	21.4%	0.22	3.4	58.2	44.3	
7/21/2014	UFR-140721	0.109	SS	20.9%	0.22	3.4	63.8	51.7	Repeat
7/24/2014	UFR-140724	0.107	SS	21.1%	0.22	3.4	65.0	53.3	Repeat
7/30/2014	UFR-140730	0.120	SS	29.0%	0.30	3.4	71.9	62.5	
1/8/2014	UFR-140801	0.120	SS	42.9%	0.44	3.4	69.1	58.9	
9/17/2014	UFR-140917	0.119	SS	45.0%	0.50	7.5	96.8	95.7	Temperatur Profile-Side
9/19/2014	UFR-140919	0.114	SS	49.6%	0.52	3.4	79.5	72.7	Temperatur Profile-Side
10/10/2014	UFR-141010	0.122	B'	51.8%	0.54	1.9	59.6	46.1	New Flame Structure
10/15/2014	UFR-141015	0.119	B'	53.6%	0.55	1.9	74.9	66.5	New Flame Structure-Temperature Profile-Side
10/17/2014	UFR-141017	0.139	B'	21.0%	0.22	1.9	57.8	43.8	New Flame Structure
11/21/2014	UFR-141121	0.100	SS'	46.1%	0.52	8.7	82.7	77.0	New Flame Structure
11/24/2014	UFR-141124	0.113	SS'	49.7%	0.52	3.4	82.7	77.0	New Flame Structure
11/26/2014	UFR-141126	0.128	SS'	46.1%	0.48	4.7	90.1	86.8	New Flame Structure
12/3/2014	UFR-141203	0.105	SS'	42.8%	0.46	4.65	87.0	82.7	New Flame Structure-141126
12/5/2014	UFR-141205	0.088	SS	49.2%	0.51	3.38	74.2	65.6	Temperatur Profile-Center
12/10/2014	UFR-141210	0.120	B'	52.2%	0.54	1.85	56.1	41.5	New Flame Structure
12/12/2014	UFR-141212	0.106	B'	51.9%	0.57	4.55	44.0	25.3	New Flame Structure
3/1/2015	UFR-150103	0.127	SS	39.8%	0.44	7.46	80.3	73.8	Temperatur Profile-Center
10/1/2015	UFR-150110	0.116	SS	93.4%	1.07	7.38	95.9	94.6	
2/26/2015	UFR-150226	0.139	SS	50.1%	0.52	3.38	69.4	59.2	Measuring Bowl Temp.
2/28/2015	UFR-150228	0.131	SS	63.7%	0.64	3.38	Sample in Bowl-no change		Temperature Profile-Side-No Feeding

** S represents one side inlet; T represents tilted inlet; SS represents two side inlets, old flame configuration; SS' represents two side inlets, new flame configuration; B represents Burner inlet, old flame configuration; and B' represents Burner inlet, new flame configuration.*

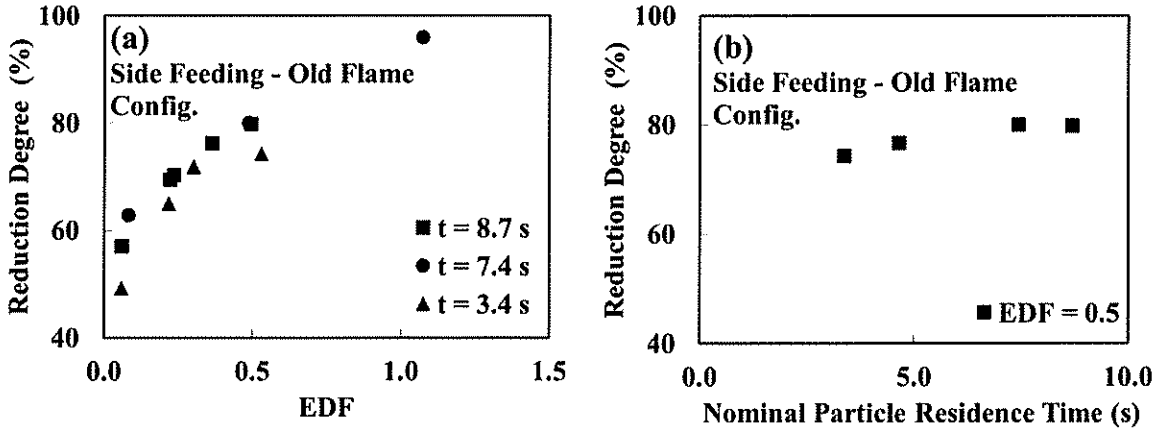

Figure 10. Feeding through the two side-inlets using the old flame configuration. (a) Effect of EDF on reduction degree (%) (b) Effect of nominal particle residence time.

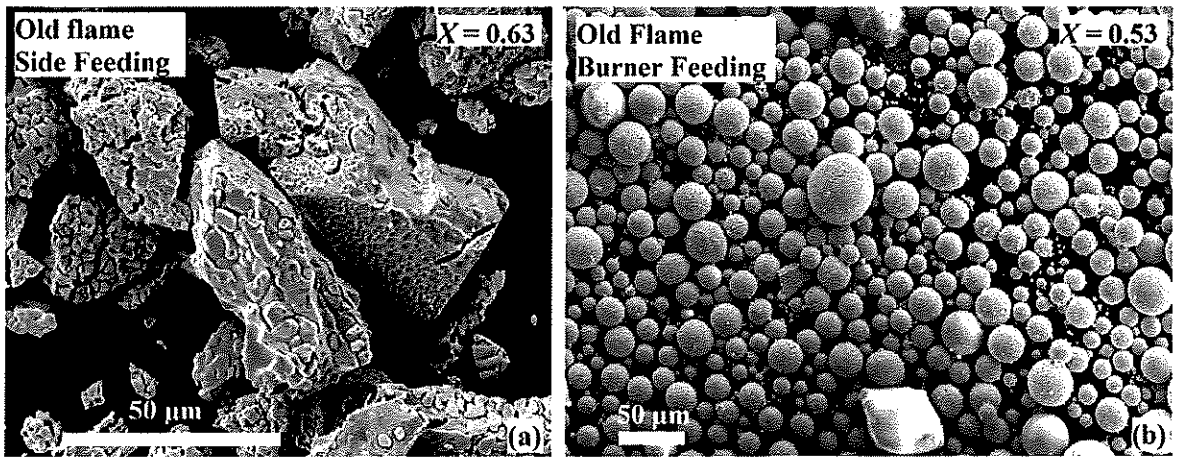

Figure 11. SEM micrograph for samples obtained with H_2 flow rate = 60 L/min and O_2 flow rate = 9.7 L/min and feeding through (a) side (RD = 63%) and (b) burner feeding (RD% = 53%).

Under the same hydrogen flow rate, the flame power increases with oxygen flow rate. As mentioned earlier the particle nominal residence time is mainly controlled by the gas flow rates in this experiment. This means the power of the flame (directly linked to the flame temperature) increases with a decrease in residence time under the same excess driving force and temperature. For example, at 1175 °C and EDF of 0.5, the flow rates of hydrogen 60 L/min and 9.7 L/min of oxygen (nominal particle residence time of ~ 1.9 s), respectively, generated higher flame power than that the hydrogen flow rates of 20 L/min and 2.9 L/min of oxygen (nominal particle residence time of ~ 4.6 s). In the former case, the high flame power results in increasing the particles temperature in the reaction zone and therefore increased the reduction degree of the particles (RD = 60%, although shorter residence time of 1.9 s) compared with the latter case with a lower flame power (RD = 30%, although longer residence time, 4.6 s), as shown in Figure 12.

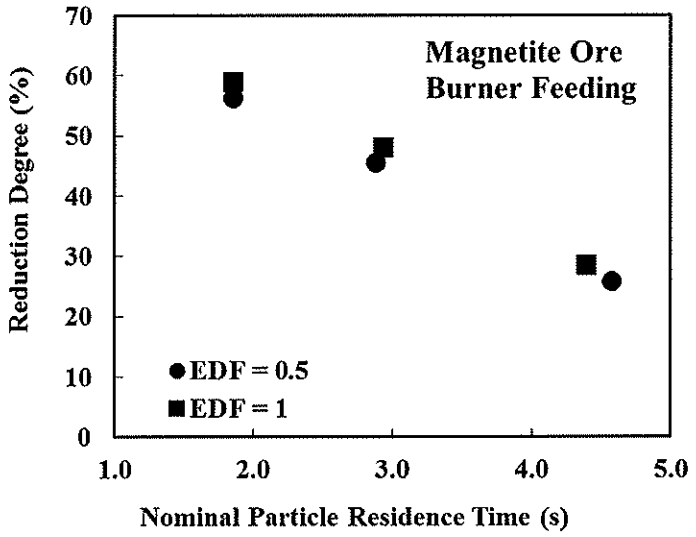

Figure 12. Reduction degree (%) vs. nominal particle residence time at different EDF when feeding through the burner inlet.

Changing the flame configuration by swapping the hydrogen and oxygen inlets ports resulted in changing the temperature profile at the top of the reactor. When feeding through the two side inlets, the particles experience higher temperature compared to the old flame configuration specially for higher flame power experiments where the H_2 flow rate is 40-60 L/min and EDF = 0.5, as shown in Figure 13.

In burner feeding with the new flame configuration, the temperature in the center of the flame was lower [see Figure 9(b)] than in the old flame configuration [see Figure 9(a)]. Thus, particle melting was not evident; rather the particles retained their irregular shape even when passing through the flame. Figure 13 shows the change in the reduction degree (%) with the residence time while Figure 14 shows the change in the particles shape with the flame configuration under otherwise the same conditions.

(g) UFR Runs and Results: Methane Runs

In these runs, methane was partially oxidized by oxygen, producing hydrogen and carbon monoxide reductants. The equilibrium composition of the gas from the partial oxidation of methane was calculated using HSC 5.1 thermodynamics software to define the reducing gas composition. Different experimental conditions were investigated, including various percentage excess hydrogen and particles nominal residence time.

A reduction degree of 88% with excess hydrogen driving force of 0.5 at the low temperature of 1175 °C and a feeding rate of ~ 0.12 kg/h in a few seconds of residence time was achieved. At this low temperature the reduction rate by carbon monoxide, although its excess driving force is also about 0.5, is very slow compared with that by hydrogen.

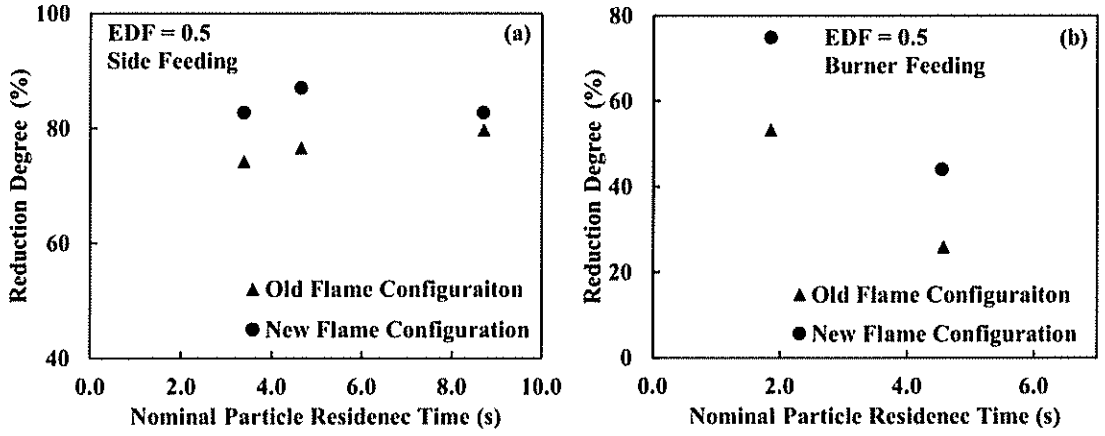

Figure 13. Reduction degree (%) vs. nominal particles residence time with EDF = 0.5 and different flame configurations for (a) side and (b) burner feeding.

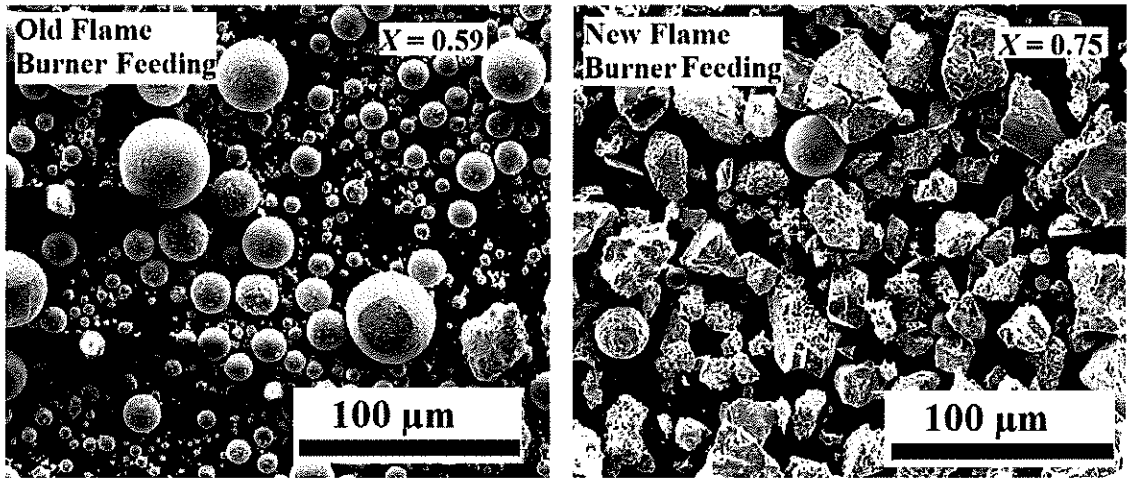

Figure 14. SEM micrographs of the powders from the collection plate from experiment with EDF = 0.5, particle residence time = 1.9 s, and feeding through the burner using (a) new (RD = 75%) and (b) old flame configurations (RD = 59%).

Twenty-five complete experiments were performed using gas mixtures from partial oxidation of methane as the reductant and magnetite as the reactant, as shown in Table 3. In all methane experiments soot formation was observed mainly on the upper part of the reactor stainless steel tube which is believed to have catalyzed the soot formation. This caused a limitation in the experimental conditions especially when trying to increase the methane flow rate as it caused off-gas lines clogging among other operational problems during the runs.

Increasing the EDF from 0.5 to 1 increased the reduction degree at the same nominal particle residence time as shown in Figure 15.

Table 3. The experimental conditions and results for the methane/magnetite UFR experiments.

Date	Reference	Iron Concentrate Feeding		Chemical Driving Force		Nominal Particle Residence Time (s)	RD (%)	Met. (%)	Comment
		Rate (kg/hr)	Injection Point*	$Fe_{0.947}O + H_2 = 0.947\ Fe + H_2O$ EDF (H_2)	$Fe_{0.947}O + CO = 0.947\ Fe + CO_2$ EDF (CO)				
8/21/2014	UFR-140821	0.0879	SS	0.64	0.64	5.6	82.1	76.2	
8/26/2014	UFR-140826	0.1075	SS	0.60	0.60	5.6	74.6	66.2	Repeat
8/29/2014	UFR-140829	0.1135	SS	0.60	0.60	5.6	76.3	68.4	Repeat
9/3/2014	UFR-140903	0.1164	SS	0.60	0.60	5.6	82.2	76.3	Repeat
9/5/2014	UFR-140905	0.1138	SS	0.10	0.10	5.6	51.0	34.7	
9/9/2014	UFR-140909	0.1200	SS	0.07	0.07	8.4	16.6	-11.2	
9/24/2014	UFR-140924	0.1200	SS	0.07	0.07	8.4	38.7	18.3	Repeat
1/10/2014	UFR-141001	0.1189	SS	0.07	0.07	8.4	46.4	28.5	Repeat
10/24/2014	UFR-141024	0.1135	B'	0.60	0.60	3.1	78.3	71.1	
10/29/2014	UFR-141029	0.1215	B'	0.10	0.10	3.1	49.6	32.8	
10/31/2014	UFR-141031	0.1184	B'	0.07	0.07	5.0	33.2	10.9	
12/11/2014	UFR-141112	0.1215	B'	0.07	0.07	5.0	26.8	2.4	Repeat
11/14/2014	UFR-141114	0.1218	B'	0.01	0.01	8.1	72.7	63.6	
12/27/2014	UFR-141227	0.1193	SS	0.35	0.35	5.6	74.1	65.5	
1/17/2015	UFR-150117	0.1076	SS	0.50	0.51	8.4	87.5	83.3	
1/24/2015	UFR-150124	0.1272	SS	0.50	0.51	8.4	57.1	42.8	Repeat
1/31/2015	UFR-150131	0.1233	SS	0.50	0.51	8.4	58.8	45.0	Repeat
7/2/2015	UFR-150207	0.1262	SS	0.50	0.51	8.4	73.6	64.8	Repeat
2/14/2015	UFR-150214	0.1281	SS	0.50	0.51	8.4	78.6	71.5	Repeat
7/10/2015	UFR-150710	0.1200	SS'	0.50	0.51	8.3	83.0	77.4	
7/16/2015	UFR-150716	0.1226	SS	1.06	1.06	8.3	75.8	67.8	
7/23/2015	UFR-150723	0.1410	SS	1.06	1.06	8.4	63.7	51.6	
7/30/2015	UFR-150730	0.1224	SS'	0.50	0.51	8.4	41.5	22.0	
8/6/2015	UFR-150806	0.1190	SS'	0.50	0.51	5.5	46.1	28.1	
9/10/2015	UFR-150910	0.1200	SS'	1.06	1.07	8.4	39.1	18.9	Repeat

** SS represents two side inlets, old flame configuration; SS' represents two side inlets, new flame configuration; and B' represents Burner inlet, new flame configuration.*

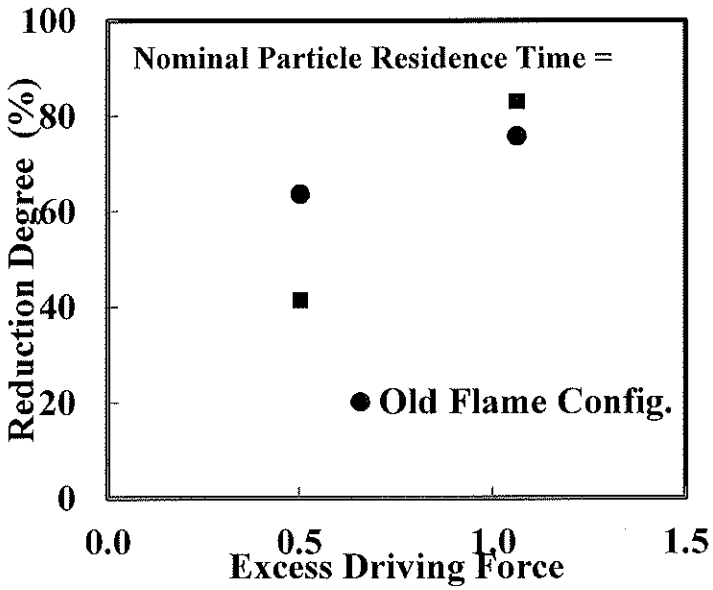

Figure 15. Reduction degree (%) vs. excess driving force with nominal particle residence time = 8.3 s and different flame configurations.

4.1.3 Development of an ICP-OES Method for Iron Content Determination

The traditional titrimetric analysis method was compared with an ICP-OES method developed during this project for determining the total iron fraction in iron ores and DRI samples [Mohassab et al., 2016]. Both analyses were of the similar accuracy and precision, but the ICP-OES method is much faster and easier than the titrimetric method. The ICP method can be easily used for high or low silica-containing iron samples. Titrimetric method introduces error when analyzing samples with high silica content due to the difficulty in using HF.

Table 4 shows the various iron-containing samples and their total iron content used in this study. Tables 5 and 6 show the results of both analysis methods with the calculated *SD* and *%RSD* (% relative standard deviation). From the comparison of the *%RSD* values for the samples by the two methods, it is clear that both methods have similar precision for samples with no or extremely low silica contents, as shown in Figure 16(a). For the samples with high silica content (> 5 mass %), ICP method gave results with much higher precision than the trimetric method, as

Table 4. Chemical analysis of the samples used in the analysis.

Samples	Code	Expected Iron Fraction
Certified Reference Sample	CRM	0.6685
Pure Fe_2O_3 Reference Sample	RM 1	0.699
Pure Fe_3O_4 Reference Sample	RM 2	0.724
Fe_2O_3 Chinese Ore	H	0.657
Flash Reduced Magnetite with High Reduction Degree	FRMH	0.90
Flash Reduced Magnetite with Low Reduction Degree	FRML	0.75
Flash Reduced Hematite with High Reduction Degree	FRHH	0.90
Flash Reduced Hematite with Low Reduction Degree	FRHL1	0.72
Flash Reduced Hematite with Low Reduction Degree	FRHL2	0.67

shown in Figure 16(b). Both methods were found to be of similar accuracy as Figure 17 shows. It is worth noting that a skilled operator can at most analyze 6-10 samples in an 8-hours shift using the titrimetric method, whereas using the ICP method 30 – 50 samples can be analyzed.

Table 5. Analysis results of the titration method.

Sample	Reference Iron Fraction	Analysis 1	2	3	4	5	6	Mean	SD	RSD (%)	Diff. (%)
CRM	0.6685	0.6693	0.6690	0.6727				0.670	0.002	0.303	0.273
RM1	0.7235	0.7272	0.7276	0.7276				0.727	0.000	0.031	0.541
RM2	0.6991	0.7012	0.6902	0.7075	0.6926	0.6908	0.7033	0.698	0.007	1.052	0.212
FRMH	N/A	0.9072	0.9047	0.8977				0.903	0.005	0.543	
FRML	N/A	0.7481	0.7488	0.7558				0.751	0.004	0.565	
H	N/A	0.6592	0.6453	0.6504				0.652	0.007	1.079	
FRHL1	N/A	0.7243	0.7067	0.7151				0.715	0.009	1.233	
FRHH	N/A	0.6415	0.5904	0.6054				0.612	0.026	4.285	

Table 6. Analysis results of the ICP method.

Sample	Expected Iron Fraction	Analysis 1	2	3	4	5	6	7	Mean	SD	RSD (%)	Diff. (%)
CRM	0.6685	0.6719	0.6751	0.6693	0.6752	0.675	0.6716		0.6730	0.0025	0.3646	0.676
RM1	0.7235		0.7196	0.7317	0.7246	0.7245	0.7329	0.7334	0.7278	0.0057	0.7796	0.592
RM2	0.6991	0.7018	0.6969	0.7029	0.693	0.696	0.7031		0.6990	0.0042	0.6045	0.021
FRMH	N/A	0.9069	0.9071	0.9047	0.9047	0.8951	0.9048	0.9159	0.9056	0.0061	0.6725	
FRML	N/A	0.7524	0.758	0.7596	0.758	0.7501	0.7562		0.7557	0.0037	0.4890	
H	N/A	0.6513	0.6525	0.6471	0.6546				0.6514	0.0032	0.4851	
FRHL2	N/A	0.6667	0.6657	0.6719					0.6681	0.0033	0.4982	
FRHH	N/A	0.89999	0.9012	0.8962	0.9087				0.9015	0.0052	0.5810	

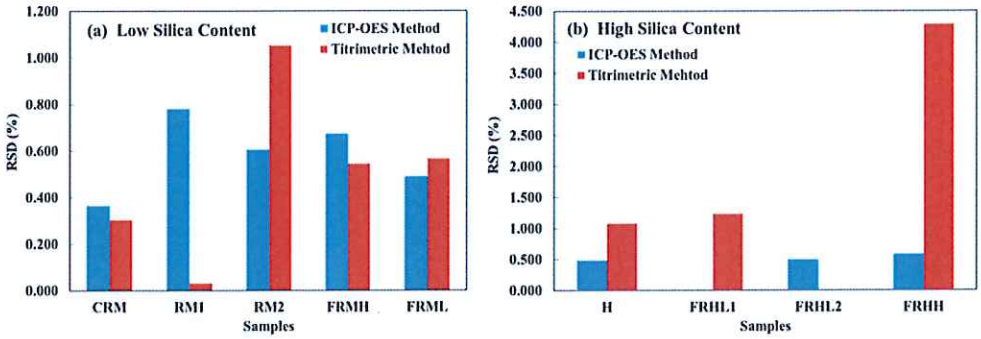

Figure 16. RSD values for the ICP-OES and titrimetric methods for samples with (a) low and (b) high silica contents.

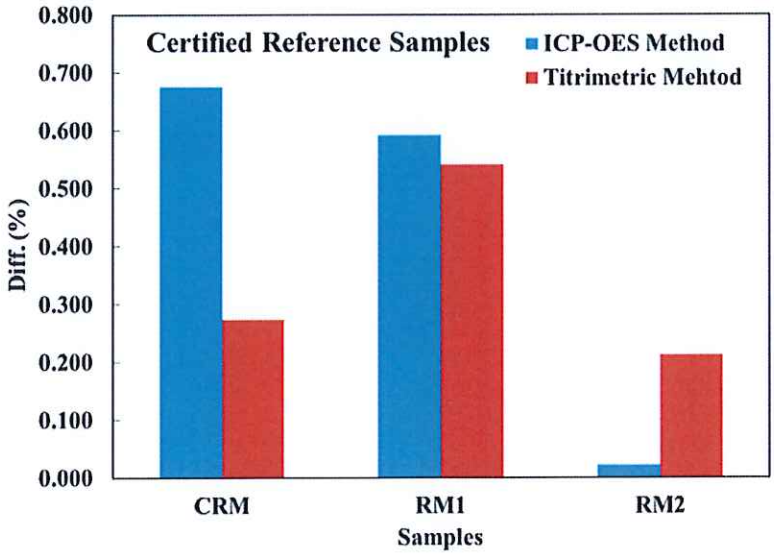

Figure 17. Comparison of the accuracy of the two methods.

4.2 Large Bench-Scale Reactor Installation and Operation

The UTAH Project Team consisting of the P.I., graduate and undergraduate assistants worked with Berry Metal Co. (BMC) and University Construction Services to coordinate, support and monitor the construction and installation activities for the Large-Scale Bench Reactor (LSBR) at the reactor host site (ITL laboratory at the University of Utah). The UTAH team reviewed and edited the gas flow rates, the cool down programs of LSBR, and the process control instruments, and provided the required input and specifications. UTAH also evaluated BMC's proposed burner design based on CFD analysis and developed specifications for LSBR operation: standard operating procedures and sequence of operation. The UTAH team carried out hot commissioning, with the assistance of BMC, to test the different components. The LSBR was tested to prepare it for operation in the experimental mode during the commissioning:

- The furnace was preheated to 1450 °C and the temperature was held for 10 hours while finalizing other steps.
- The main burner was started by HMI.
- Magnetite concentrate was fed through the main burner at a rate of 2.5 kg/h for 1 hour.
- During the run, 7 out of 18 water chillers failed due to over pressurizing resulting in cracks formation and water leaking from them. 4 embedded T/Cs failed during the run.
- After the system cooled down, the system was opened for inspection and it was found that:
- The roof refractory had deep cracks extending all the way to the carbon steel shell.
- The powder accumulated on the cone-shaped part of the reactor bottom which prevented it from falling all the way to the collection bin.
- The zirconia tips protecting the main burner had severe conditions and needed to be replaced.

The Utah team prepared the LSBR for a restart including refractory repair, the embedded thermocouples in the system were C-type, which is a high temperature thermocouple, but they failed easily in a cyclic temperature conditions (heating and cooling of the reactor). We experienced the loss of more than half of the thermocouples embedded in the reactor refractory after each run. All the C-type thermocouples in the roof and reactor wall were replaced with B-type thermocouples, which are more robust in the testing conditions of the reactor. The lead wires of the thermocouples were replaced with wires compatible with the B-type. The programming of the HMI program was adjusted to read the B-type thermocouples.

The roof of the LSBR was fixed using mortar to fill the cracks to a depth of 0.75-1". The cracks at the bottom part of the reactor were also filled. The opening at the bottom cone of the reactor vessel was enlarged from 5" to 8" in order to improve the powder collection. The zirconia blocks of the main burner and preheat burner were replaced with new blocks.

After fixing the programming problems, 11 start-up runs were performed on the LSBR as shown in Table 7. During this period, feeding and collecting powder was tested at room temperature under conditions to mimic the experimental conditions. Nitrogen gas was flowed through the main burner at flow rates close to those that will be used in the actual experiments. The concentrate was fed at a rate of 1.5 kg/h for 2 hours. 3 kg was fed and 1.6 kg was collected in the collection bin. Calibration of the concentrate feeder also took place to get feeding rates in the range of 1-5 kg/h.

These experiments had many problems with respect to product powder collection and it was hard to collect representative samples. Therefore, new collection methods using a series of magnets placed in strategic positions were implemented in the reactor for better collection and quality of the sample. After fixing the collection problem, the reactor was operated for collecting the required data. The off-gas composition was monitored during the experiment and the excess driving force (EDF) of hydrogen was calculated on the HMI. The flow rates of oxygen and natural gas were adjusted till the required EDF was achieved. After feeding a certain amount of the magnetite concentrate, the system was shut down by switching off the flame in the reactor. The flare stack was kept running for 5 minutes longer to burn any remaining gases from the reactor. The reactor was left to cool down to temperature lower than 400 °C in the vessel and room temperature in the quench tank, which took 4 days. After the quench tank reached room temperature, the flange of the tank was opened and the reduced sample was collected. The collected sample was analyzed by ICP to determine its reduction degree. The results of these runs were used to verify the CFD simulation model.

Table 7. LSBR Experiments during commissioning

Run #	Target Temperature	Status
1	1250	The system was heated up successfully to the target temperature without any problems. No gases flowed through the MFC during the experimental mode.
2	1250	
3	1250	
4	1250	Once the gases were fed through the main burner, the cooling water temperatures increased by 20 °C and the system was shut down.
5	1300	
6	1300	An experiment was performed and concentrate was fed for 55 min. with feeding rate 1 kg/h.
7	1300	The system was shut down by itself after 5 min. in the experimental mode.
8	1300	The system was shut down by itself after 10 min. in the experimental mode.
9	1300	Concentrate was fed for 2.5 hours with feeding rate 1 kg/h.
10	1150	Concentrate was fed for 50 min. with feeding rate 2.5 kg/h.
11	1200	Concentrate was fed for 3.5 hours with feeding rate 2 kg/h.

The results of the LSBR runs are expected to be useful in designing the industrial reactor, including the identification of the difficulties and how to improve the various aspects of operation. This reactor was simulated by CFD to optimize the operating conditions to achieve a sufficiently high reduction degree at the optimum conditions and reactor sizes to be used in an industrial reactor. The results obtained from the developed CFD model was compared with the actual results of the reactor operation and good agreement was achieved. Table 8 shows the results of the 'successful' runs performed in the reactor.

Excessive swirl in the main burner caused problems in sample collection as described in the next section. Lower flow rates of natural gas and oxygen were used in the experiments to moderate the swirl effect. These low flow rates caused the inner wall temperature of the reactor to drop with time. Many of the experimental runs were designed to yield a wide range of

reduction degree at less than 90 % reduction to better examine the effects of the operating conditions and validate the CFD model in these different conditions.

In this reactor, no soot was formed during the experiments. LECO analysis was performed on some of the samples collected from the experiments and less than 0.24% C was found.

The experiments were performed at different temperatures and EDF with the aim of obtaining data for designing the industrial flash reactor. The results showed good reproducibility within ±5% of the average reduction degree. This represents a very high degree of reproducibility, considering the complexity of the operation and design of this large unit.

The LSBR was the first of its kind and the design and operation of such a large reactor posed a number of challenges. It took much effort to fix many of these difficulties. Others remained parts of the system design that must be avoided while designing the industrial reactor. This

Table 8. The results of main runs performed in LSBR.

Inner Wall Temperature (°C)	Magnetite Concentrate Feeding Rate (kg/h)	Gas Flow Rate (SLPM)* Main Burner NG (SLPM)	O_2 (SLPM)	H_2 EDF	Nominal Residence Time (s)	RD (%)
1200-1130	5.0	404	321	0.76	12.5	65
1290-1220	1.8	410	293	0.84	12.0	79
1290-1210	2.9	410	293	0.96	12.0	82
1290-1230	2.5	358	270	1.00	13.3	83
1290-1240	3.5	512	327	1.07	10.2	76
1330-1230	4.7	330	200	1.36	15.3	89
1330-1230	4.5	330	200	1.44	15.3	87
1330-1230	5.2	500	290	3.00	10.6	80
1330-1230	4.3	500	290	3.00	10.6	82
1355-1260	5.5	235	190	0.03	18.3	7
1350-1300	4.0	255	209	0.15	17.0	49
1350-1270	4.5	275	212	0.20	16.2	31
1340-1280	5.0	280	209	0.21	16.2	37
1350-1290	4.6	280	230	0.50	15.6	80
1400-1300	6.3	300	240	0.82	14.4	88
1400-1300	5.0	330	200	1.51	14.6	100
1415-1350	4.5	220	191	0.07	18.0	18
1410-1360	4.0	240	195	0.33	17.1	32

1410-1330	5.0	295	221	0.50	14.7	66
1410-1330	6.0	300	210	0.70	14.9	74
1410-1320	5.0	300	210	0.82	14.9	82

* The flow rates of natural gas and O_2 in the pilot burner were 9.6 and 37.6 SLPM, respectively. The flow rate of N_2 in the powder feeder was 10.7 SLPM.

would provide valuable findings from this type of a testing program. One of the biggest problems encountered in operation was the cracking of the quench tank. The reactor vessel consisted of a carbon steel shell and layers of insulation while the quench tank was made of stainless steel. The connection between the vessel and the quench tank was a stainless steel cylinder which was connected to the vessel with a flange and welded to the tank. In this region, the high temperature gas coming from the vessel was quenched with a high flow of N_2 gas. However, this part was not well insulated and due to the rapid cooling of the hot gases, a crack was formed there which caused a gas leak. This crack was welded and then moldable ceramic fiber insulation was used to form an insulation layer, which stopped cracking and overheating of this part.

There was a problem in the powder collection in the last experiments performed on the reactor. The reactor inner diameter was 80 cm while the opening where the gas and particles flowed through to the quench tank was only 20 cm. This opening was smaller in size compared with the reactor inner diameter due to the limitation of overall reactor size to be built inside the facility at the University of Utah. That reduction in diameter required designing a conical part as shown in Figure 18 to reduce the diameter from 80 cm to 20 cm within a short height. Unfortunately, that conical shape resulted in particle accumulation on its surface during the run, which adhered to the alumina walls and stayed there forming a solid accretion layer. This accretion is hard to remove as shown in Figure 18. This accumulation resulted in a limited amount of sample collected from the experiment compared to the amount fed (about 10% of the amount collected). The more accumulated particles formed, the rougher the cone surface and the more particles trapped in this part. After the last experiments, that opening was completely blocked and the blockage was very hard to remove.

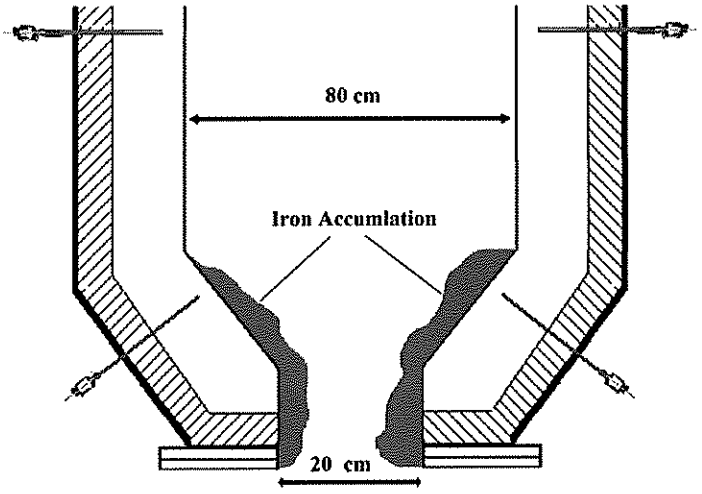

Figure 18. Product particles accumulated in the bottom part of the reactor.

5. CFD MODEL DEVELOPMENT

The CFD work in this project focused on the simulation of the flash ironmaking reactors, in which the temperature, gas-phase composition, particle distribution in the reactor vessels, and particle reduction were calculated.

The gas phase was treated as a continuum in the Eulerian frame of reference, and the particles are tracked using a Lagrangian approach in which the trajectory and velocity are determined by integrating the equation of particle motion. In addition, a heat balance on the particle that relates the particle temperature to convection and radiation was applied. The realizable k-ε model was chosen for simulating the spread of the carrier gas jet. Radiation was taken into account using the discrete ordinate (DO) model. As the volume fraction of the solid phase in the reactor is in the order of $10^{-6} - 10^{-5}$, the flow is categorized as a dilute flow. Thus, the inter-particle collisions were neglected. The change in the particle mass was related to the chemical reaction, and the particle temperature was calculated by taking into consideration the heat of reaction, convection and radiation. The stochastic trajectory model was used to describe particle dispersion due to turbulence. The partial combustion of H_2 or natural gas by O_2 was also incorporated. The temperature profiles and reduction degrees obtained from the simulations were compared with the experimental measurements for validation of the model. The obtained rate expressions were used in the CFD model for the design of an industrial pilot flash reactor.

5.1 LSBR CFD Modeling

Simulation runs were made to study the effects of various operating conditions on the reduction degree of the magnetite concentrate in the LSBR:

a) Effect of the inlet oxygen to natural gas ratio with the same total gas flow rate:

Natural gas is partially combusted by oxygen to produce the reducing gases (H_2 and CO) in the temperature range of 1150-1600 °C. The reducing gases reduce the magnetite concentrate particles to produce metallic iron. The flow rates of natural gas and oxygen in the LSBR affect the operating temperature of the reactor. The oxygen/natural gas ratio also changes the mole percentages of hydrogen, carbon monoxide, carbon dioxide, and water vapor, thus affecting the value of the excess driving force (EDF).

For the total gas flow rates of 726, 1036 and 1810 SLPM, an oxygen/natural gas ratio of 0.7 resulted in a reduction degree of 85±9%. The runs with a ratio of oxygen/natural gas of 1.0 gave an operating temperature of the LSBR above the melting point of iron. An oxygen/natural gas ratio of 0.8 achieved a high reduction degree of 99.2±0.7%.

b) Effect of total gas flow rate with constant oxygen/natural gas ratio:

The total gas flow rate at a constant oxygen/natural gas ratio affects the operating temperature and the particle residence time. Although the latter decreases at a higher gas flow rate, the resulting higher operating temperature affects the reduction degree more strongly.

The LSBR vessel is shown schematically in Figure 19. The burner used in the LSBR is shown in Figure 20. The reactor vessel is made up of the layers of refractory, insulation, and carbon steel. The inclined angle of the oxygen inlet ports (total of ten ports) causes a swirl flow in the reactor, which increases the particles residence time. This particular design of the burner shortens the flame length and ensures a larger uniform temperature zone in the whole reactor.

The following assumptions were made in the simulation:

1- Steady state conditions: The gas phase responds to changes much more quickly compared to condensed phases such as walls, as the density of the gas is about three orders of magnitude lower. Thus, the transient term for the gas phase energy balance is much smaller than other terms in the gas phase energy equation. Thus, the steady state condition is assumed for the gas-particle phase.

2- Inter-particle collisions between magnetite concentrate particles in the reactor are neglected as the volume of the solid particles occupying the reactor is three orders of magnetite lower than the volume of the gas.

The ANSYS Fluent 17.1 software was used for modeling and simulating the LSBR where the gas/solid phase interactions occur.

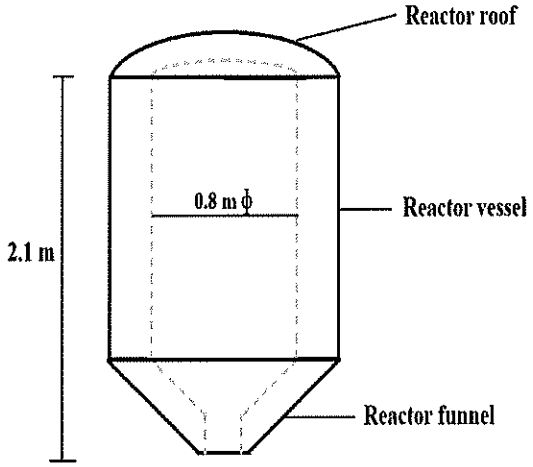

Figure 19. Schematic representation of the LSBR

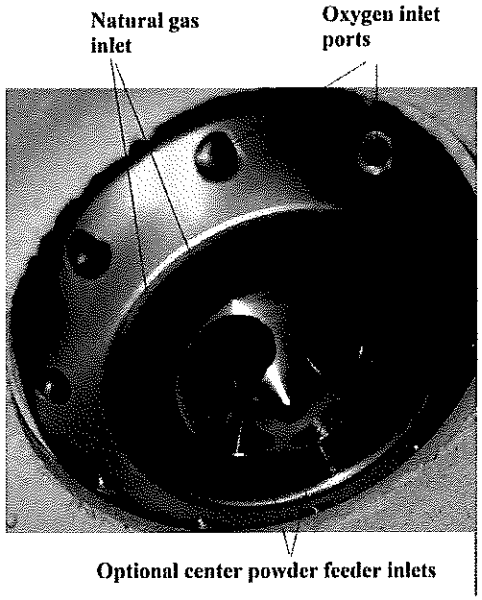

Figure 20. Burner used in the LSBR

The reaction kinetics for the partial combustion of natural gas [with the actual composition of 96 mol% CH_4, 2 mol% C_2H_6, and 2 mol% nitrogen] was incorporated in the simulation. Natural gas was considered as 100.6 mol% CH_4 (1 mol% of C_2H_6 equivalent to 2.6 mol% of CH_4 in heat production and 2 mol% of CH_4 in hydrogen and carbon monoxide production, both for generating a representative hot gas mixture from the partial combustion; thus considering these two factors, 1 mol% of C_2H_6 was treated as being equivalent to 2.3 mol% of CH_4) and 2 mol% nitrogen to avoid the complexity of including ethane. The kinetics of natural gas oxidation used in this work consisted of four chemical reactions involving six species [Jones and Lindstedt, 1988], as shown in Table 9. The eddy dissipation concept (EDC) approach was used to take the turbulence-chemistry interaction into consideration [Gran and Magnussen, 1996].

Table 9. Arrhenius constant, temperature exponent, and activation energy of CH_4-O_2 partial combustion reactions

	Reaction	A	β	$E_{a,i}$ (cal mol^{-1})
1	$CH_4+0.5O_2=CO+2H_2$	4.40×10^{14} m$^{2.25}$ mol$^{-0.75}$ s^{-1}	0.0	30,000
2	$CH_4+H_2O=CO+3H_2$	3.00×10^{11} m^3 mol^{-1} s^{-1}	0.0	30,000
3	$H_2+0.5O_2=H_2O$	2.50×10^{19} m$^{2.25}$ mol$^{-0.75}$ s^{-1}K	-1.0	40,000
4	$H_2O+CO=CO_2+H_2$	2.75×10^{12} m^3 mol^{-1} s^{-1}	0.0	20,000

The rates of reactions, according to Jones and Lindstedt [1988], are given by

$$r_1 = k_{f,1} C_{CH_4}{}^{0.5} C_{O_2}^{1.25} \tag{10}$$

$$r_2 = k_{f,2} C_{CH_4} C_{H_2O} \tag{11}$$

$$r_3 = k_{f,3} C_{H_2}{}^{0.25} C_{O_2}^{1.5} \tag{12}$$

$$r_4 = k_{f,4} C_{H_2O} C_{CO} - k_{b,4} C_{CO_2} C_{H_2} \tag{13}$$

The forward reaction rate constant for each reaction is given by

$$k_{f,i} = AT^{\beta} exp\left(-\frac{E_{a,i}}{RT}\right) \tag{14}$$

The backward reaction rate constant was linked to the forward reactions by equilibrium relationships in the fourth reaction:

$$k_{b,4} = \frac{k_{f,4}}{K_{c,4}} \tag{15}$$

$$K_{C,4} = \left(\frac{C_{CO_2} C_{H_2}}{C_{H_2O} C_{CO}}\right)_{eq} \tag{16}$$

The particle phase was treated as a discrete phase. The force balance that equates the particle inertia with the forces (mainly gravitational force and drag force) acting on the particle is expressed in the Lagrangian frame of reference as

$$\frac{d\vec{u}_p}{dt} = F_D\left(\vec{u} - \vec{u}_p\right) + \frac{\vec{g}(\rho_p - \rho)}{\rho_p} \tag{17}$$

$$F_D = \frac{3\mu c_D R_e}{4\rho_p d_p^2} \tag{18}$$

$$c_D = \begin{cases} 0.44, & R_e > 1000 \\ \frac{24}{R_e}(1 + 0.15R_e^{0.678}), & R_e \leq 1000 \end{cases} \tag{19}$$

The particle thermal energy equation is expressed as

$$m_p c_p \frac{dT_p}{dt} = hA_p(T - T_p) - \frac{dm_o}{dt} H_{reac} + A_p \varepsilon_p \sigma(T^4 - T_p^4) \tag{20}$$

where the term $\frac{dm_o}{dt}$ is related to particle chemical reaction rate. The rate equations for reduction used in this work based on those developed by Fan et al. [2016a] where both H_2 and CO gases contributed to the reduction of magnetite concentrate particles. Thus, the global nucleation and growth rate expressions for magnetite reduction by H_2 [$Fe_3O_4 + 4H_2 = 3Fe + 4H_2O$] and by CO [$Fe_3O_4 + 4CO = 3Fe + 4CO_2$] were used in the kinetics. The mass balance of the particle is described by the following equation [Fan et al., 2016b]:

$$\frac{dm_O}{dt} = m_O^{\circ} \cdot \frac{dX}{dt} \tag{21}$$

$$\frac{dX}{dt} = [1 + (-0.004T + 7.004) \cdot \frac{p_{co}}{p_{co} + p_{H_2}}] \cdot \left.\frac{dX}{dt}\right|_{H_2} + \left.\frac{dX}{dt}\right|_{CO}; \; T \text{ in K and } t \text{ in s} \tag{22}$$

where m_O is the mass of iron-bonded oxygen in the particle at time t, m_O° is the initial mass of oxygen in the particle, and $\frac{dX}{dt}$ is the rate of fractional reduction. A user defined function (UDF) code was created to add the reduction kinetics of iron concentrate. The UDF code, shown in the Appendix, was imported into the CFD simulation. The gas-particle heat transfer coefficient h was evaluated using the correlation of Ranz and Marshall [1952]. A value of 0.8 was chosen as the particle emissivity ε_p, as recommended by Hahn and Sohn [1990] and Theodore et al. [2011].

The gas-phase governing equations were discretized and solved using the commercial CFD software package ANSYS FLUENT 17.1. Three-dimensional mesh was generated using ICEM-CFD ANSYS with a total number of 398,380 hexahedral cells. Mesh optimization was confirmed by doubling the number of cells without changing the computational results. Figure 21 shows the meshing of the LSBR. Total particle streams of 480 were released from the injection ports to establish a statistical representation of the spread of the particles due to turbulence. Turbulence effect on the particles dispersion was considered by using the stochastic tracking model. In the stochastic tracking approach, ANSYS Fluent predicts the turbulent dispersion of particles by integrating the trajectory equations for individual particles, using the instantaneous fluid velocity, $\bar{u}+u'(t)$, along with the particle path during the integration. The path in this manner is computed for a sufficient number of representative particles (termed the "number of tries"). A stochastic method (random walk model) is used to determine the instantaneous gas

velocity. In the discrete random walk (DRW) model, the fluctuating velocity components are discrete piecewise constant functions of time. Their random value is kept constant over an interval of time given by the characteristic lifetime of eddies. The particle trajectories and velocities were determined by numerically integrating the equation of particle motion, Eq. (17). As the particle trajectory was computed, Eqs. (20) - (22) were integrated to obtain the particle temperature and mass. The calculation was carried out by a steady state pressure-based solver and the convergence was achieved by having a residual less than 10^{-3} in the momentum equation, less than 10^{-6} in the energy balance equation, and less than 0.01% variation in the mass-weighted average temperature at the exit of the LSBR for more than 500 consecutive iterations. A second-order upwind scheme was chosen for momentum, species transport and energy equation discretization for the convection term. Other details of the CFD modeling of the LSBR are given in a dissertation by Abdelghany [2018].

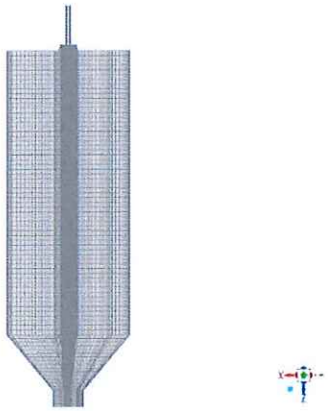

Figure 21. Meshing of the LSBR

Six typical operating conditions of the LSBR listed in Table 10 were simulated.

Table 10. The experimental conditions for the LSBR

Parameters	Run 1	Run 2	Run 3	Run 4	Run 5	Run 6
Concentrate feeding rate, kg h^{-1}	2.5	4.3	5.0	5.0	4.6	4.0
Particle size range, μm	32 - 90	less than 90	less than 90	32 - 90	less than 90	less than 90
Mass average particle size, μm (used for simulation)	45	32	32	45	32	32
Natural Gas flow rate,* m^3 h^{-1}	25.2	30.6	20.4	24.8	17.4	15.9
Natural Gas input temperature, K	300	300	300	300	300	300
O_2 flow rate,* m^3 h^{-1}	19.8	19.7	14.3	21.5	16.4	14.8
O_2 input temperature, K	300	300	300	300	300	300
Total inlet gas flow rate,* m^3 h^{-1}	45.0	50.2	34.6	46.3	33.7	30.7
O_2 to Natural Gas mole ratio	0.79	0.64	0.70	0.87	0.94	0.93

Inner wall temperature,** K	1483-1563	1503-1603	1573-1673	1403-1473	1563-1623	1573-1623
Inner wall temperature, K (used for simulation)	1526	1548	1626	1440	1594	1599

*Flow rates are calculated at 298 K and 0.85 atm, the barometric pressure at Salt Lake City (1 atm = 101.32 kPa).

** Wall temperatures were measured during feeding of the concentrate in the experiment.

The simulated temperature distributions and particle streams under the six experimental conditions are shown in Figures 22 and 23, respectively.

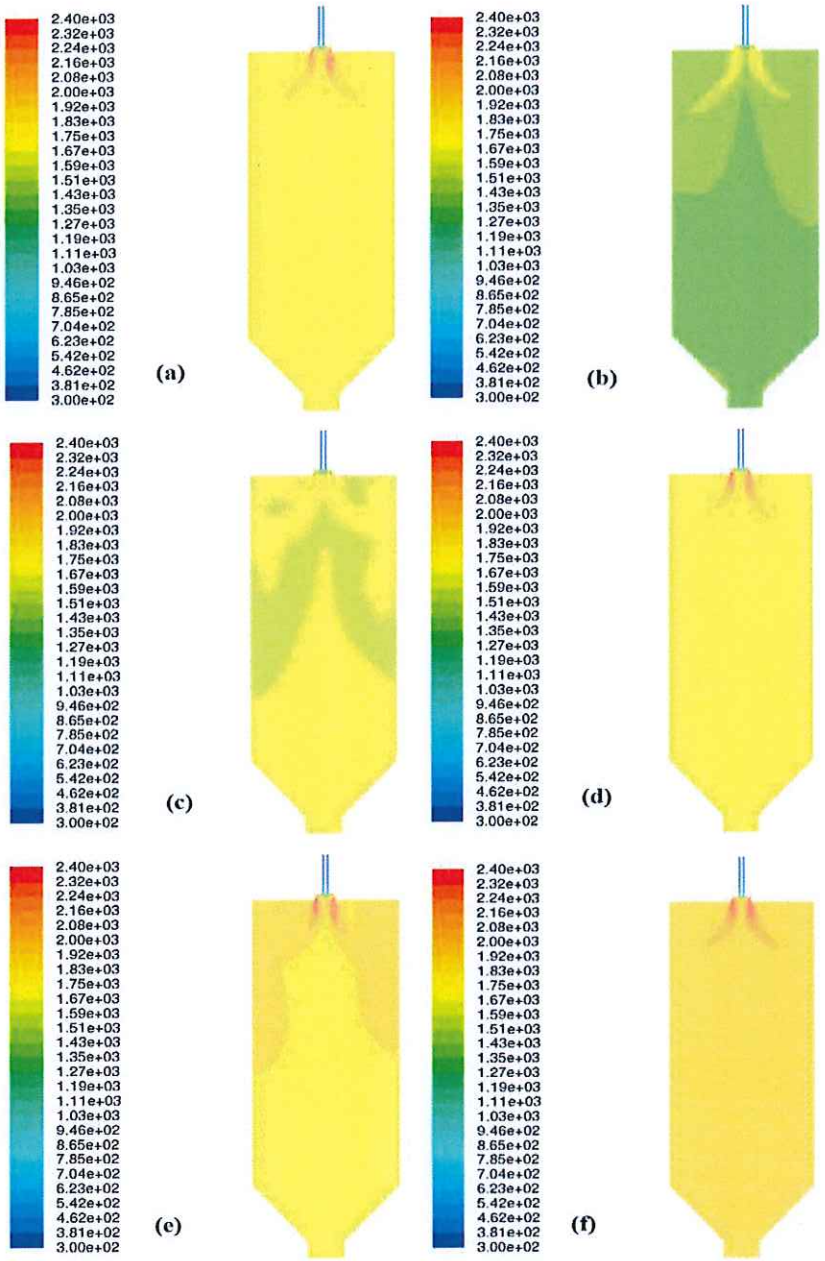

Figure 22. Temperature distributions in K: (a) Run 1 (b) Run 2 (c) Run 3 (d) Run 4 (e) Run 5 (f) Run 6

Higher temperatures compared with other runs are noticed for runs 5 and 6 in which the higher mole ratio of oxygen to natural gas was at 0.94 and 0.93, respectively. The lowest temperature is noticed for run 2 where the mole ratio of oxygen to natural gas was the lowest at 0.64. The temperature distribution of the six runs show largely uniform temperature distributions and short flame lengths thanks to the particular design of the burner.

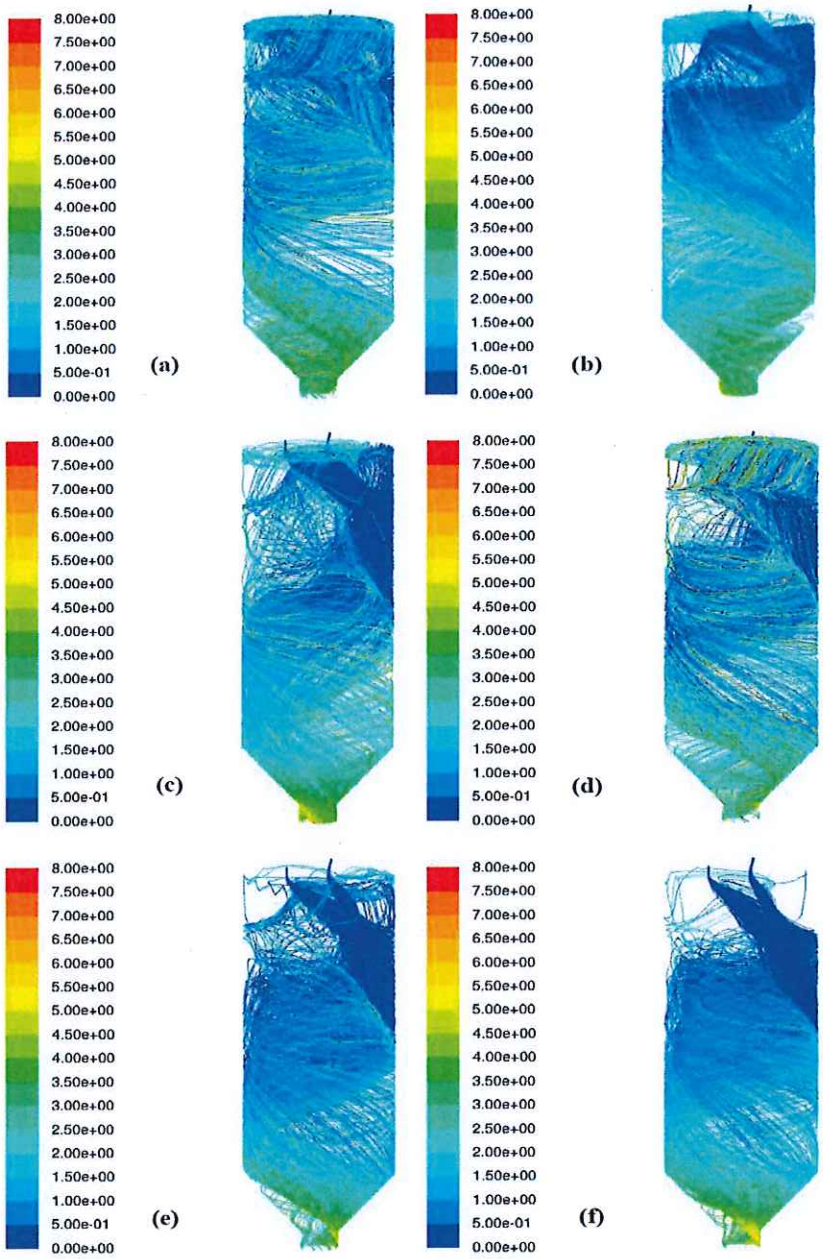

Figure 23. Particle stream distribution with time in s: (a) Run 1 (b) Run 2 (c) Run 3 (d) Run 4 (e) Run 5 (f) Run 6

The particle streams for the six runs show a swirl flow because of the particular design of the burner. The particle streams of runs 5 and 6 occupy smaller volumes of the LSBR compared to

the other runs, which can be explained by the smaller total inlet gas flow rates of 33.7 and 30.7m^3 h^{-1}, respectively.

Comparisons of the measured off-gas contents of H_2, CO, CO_2, and H_2O with the computed values for the six runs are shown in Figure 24.

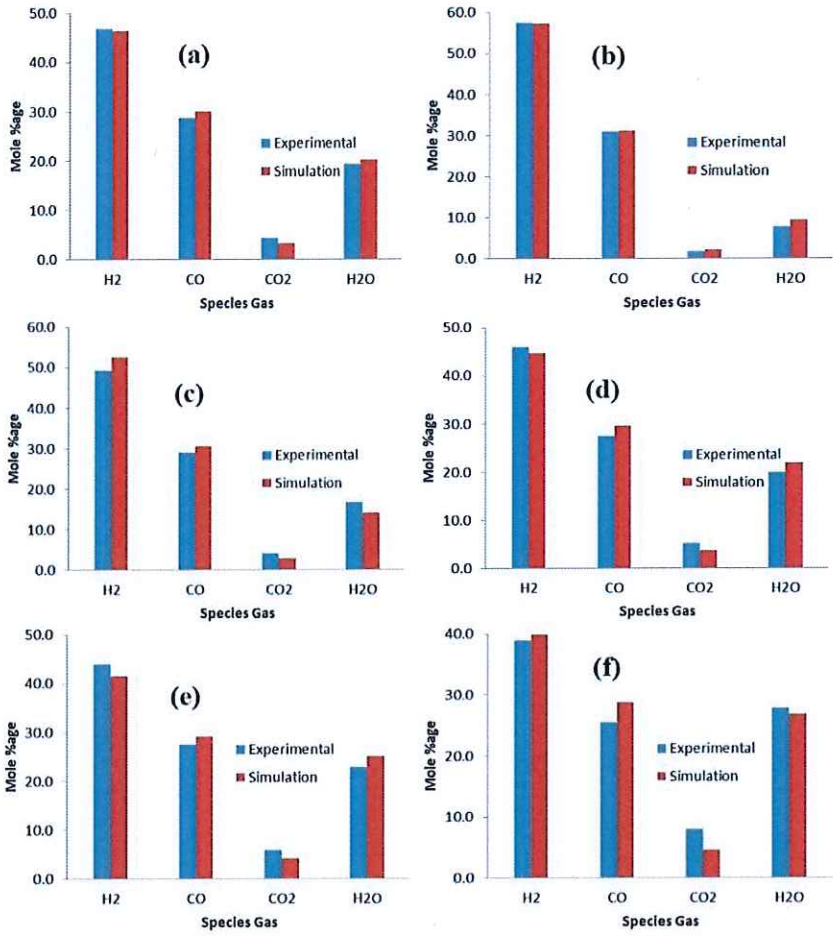

Figure 24. Comparison of the measured off-gas contents of H_2, CO, CO_2, and H_2O with the computed values: (a) Run 1 (b) Run 2 (c) Run 3 (d) Run 4 (e) Run 5 (f) Run 6

It can be seen that overall a good agreement is achieved. The simulation model was able to predict the contents of the reducing gases H_2 and CO with accuracies greater than 93% compared to experimental data in most of the runs.

The experimental reduction degrees and the gas composition of the runs versus the calculated values are listed in Table 11.

Table 11. Experimental vs calculated reduction degrees

Run	Experimental (pct)	Simulation (pct)
1	94.0	99.8
2	80.0	84.5
3	94.5	99.6

4	74.0	99.8
5	72.5	99.5
6	50.0	85.0

There is a good agreement for the reduction degree in the first three runs. The last three runs do not show a good agreement between simulation and experiment, the reason may be the assumption of no interactions between particles is not accurate at the runs of 4, 5, and 6. The later three runs have higher oxygen to natural gas ratio and higher gas temperatures compared to other runs. Gas temperatures in those runs were above 1850 K which is higher than the melting point of iron (1811 K). Particle at these high temperatures will melt to become droplet and will tend to coalesce together. This effect has been previously pointed out to be significant in copper flash smelting [Kimura et al., 1986; Kemori et al., 1988; Themelis et al. 1988]. Particles coalescence slows down the reaction and cause lower reduction degree in experimental compared to the simulation in those runs. Although, the gas temperature in run 1 is high and above 1850 K, the mass feeding rate of concentrate powder in this run is nearly half the values in runs 4, 5, and 6. The low mass feeding rate greatly decreases the probability of droplet to coalesce in run 1. We could not check that suggested reason experimentally because of the complexity of the system and the lack of quantitative measurements to observe changes on the particles.

The model proposed in this work described accurately the fluid flow and heat transfer within the LSBR. The model also predicted the reduction degrees with good agreement for those experiments where the gas temperature was below the melting/fusion point of iron (1811 K). The off-gas composition obtained by incorporating the user defined function for reduction kinetics of H_2 and CO gases with iron concentrate, previously determined in a drop-tube reactor at our research lab, agreed with the off-gas composition readings from the experiments. The model can be used in the design and optimization of much larger reactors when the gas operating temperature is within the range of 1423 – 1811 K. The model had lower degree of agreement for reduction degree in the experiments where the gas temperature was above iron melting, which caused the particles to melt and coalescence. Particle/droplet coalescence made the assumption of no interactions between particles less accurate. This points out to the need to incorporate the particle/droplet coalescence into the model to improve its performance at operating temperatures above 1811 K.

5.2 CFD Design of a Pilot-Scale Reactor of the Same Configuration as LSBR

The LSBR model was adjusted to design a "pilot-scale" reactor with a target production rate 100,000 ton metallic iron per year. The throughput rate was decided considering that the costs of facility and testing operation should be low and yet the reactor should be sufficiently large as a last test one step before a commercial reactor. The dimensions of the reactor as well as the operating conditions were refined, and CFD simulation was performed based on the new parameters.

5.2.1 Geometry

The dimension for the 100,000 ton-per-year flash iron making reactor was determined to be 4 meters in diameter and 25 meters in height in order to achieve 95% metallization for the product. The geometry is shown in Figure 25. The reactor is design to feed the fuel and oxygen through a main burner installed on the roof of the reactor. Symmetric powder feeding configuration is used. The powder is fed through four powder feeders that are 1 m away from the centerline of the reactor, which is shown in Figure 26. The bottom part of reactor is design to have a convergent shape for powder collection.

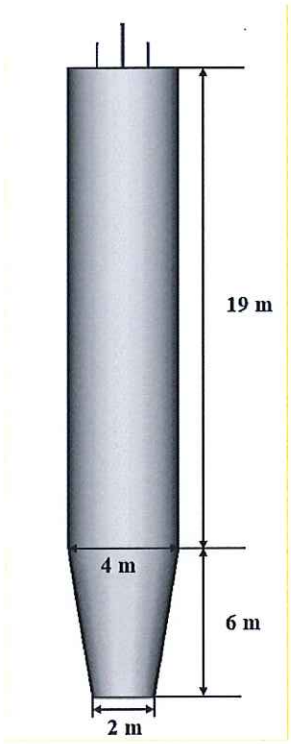

Figure 25. Geometry of the pilot-scale flash reactor.

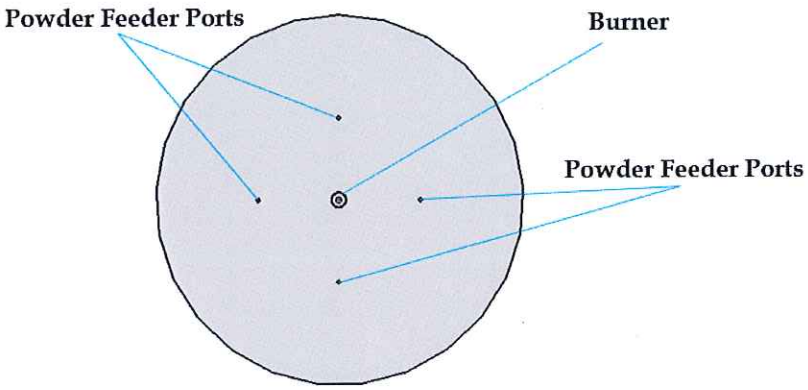

Figure 26. Top view of the reactor.

The reactor wall consists of three layers, namely, the refractory layer, insulation layer and steel shell layer from the inner to outer surface, as shown in Figure 27. The thickness of the refractory layer, insulation layer and steel shell layer are kept as 0.15 m, 0.08 m and 0.0254 m, respectively.

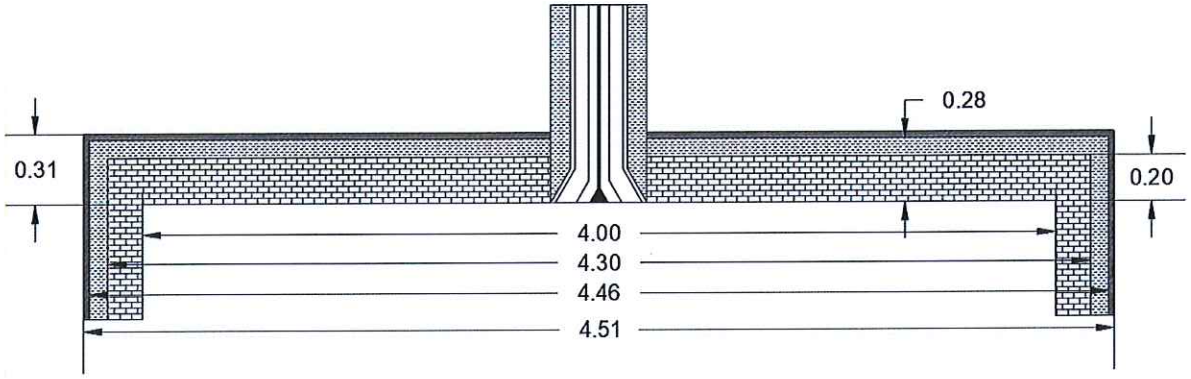

Figure 27 Wall structure (units in m)

5.2.2 Burner Configuration

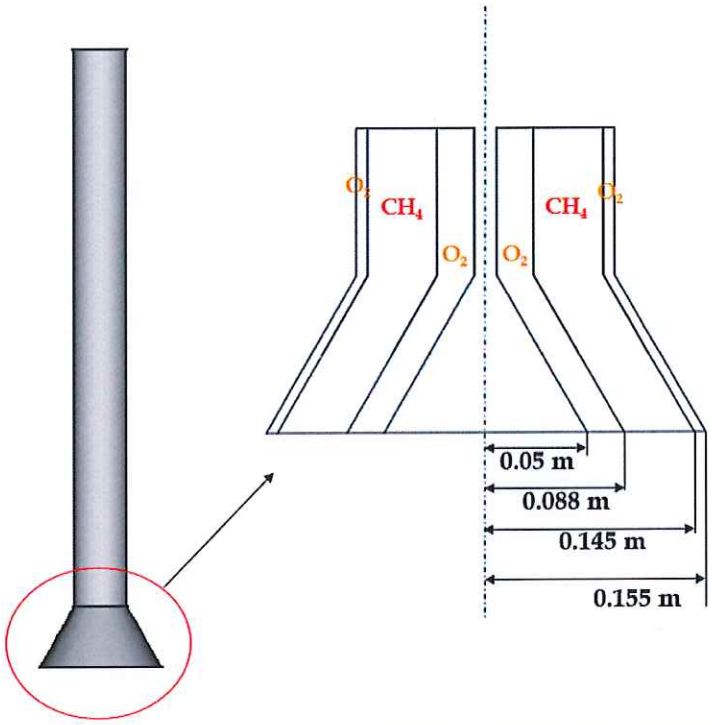

Figure 28. Burner configuration.

A non-premixed burner with two oxygen slots and one natural gas slot is used for the partial oxidation of NG, which is shown in Figure 28. The fuel used in the simulations is natural gas, which is partially oxidized to produce reducing gases CO and H_2, and at the same time, provides the heat needed for the overall process. Depending on operational needs, the natural gas can be

preheated before entering the reactor. In the following results, five sets of operating parameters have been tested, which are shown in the following Tables 12-16. The annual production rate of metallic iron was aimed at 100,000 tons for all operating conditions.

Table 12. Operating Parameters (run #1)

Parameter	Value	Input Temp. (°C)
Total Production rate	100,000 tpy	NA
Total CH_4	7,240 kg/h	25
Total O_2	10,656 kg/h	25
Concentrate	15.1 tons/h	25

The same mass flow rates were used for the two oxygen slots (50% of the total flow rate each). The O_2/CH_4 ratio for run #1 was kept at 0.74.

Table 13. Operating Parameters (run #2)

Parameter	Value	Input Temp. (°C)
Total Production rate	100,000 tpy	NA
Total CH_4	8,640 kg/h	25
Total O_2	12,816 kg/h	25
Concentrate	15.1 tons/h	25

The same mass flow rates were used for the two oxygen slots (50% of the total flow rate each). The O_2/CH_4 ratio for run #2 was also maintained at 0.74.

Table 14. Operating Parameters (run #3)

Parameter	Value	Input Temp. (°C)
Total Production rate	100,000 tpy	NA
Total CH_4	10,800 kg/h	25
Total O_2	16,416 kg/h	25
Concentrate	15.1 tons/h	25

In run #3, 50% of the total O_2 was fed through O_2 slot #1, and the rest of 50% was fed through O_2 slot #2. The O_2/CH_4 ratio for run #2 was also maintained at 0.74.

Table 15. Operating Parameters (run #4)

Parameter	Value	Input Temp. (°C)
Total Production rate	100,000 tpy	NA
Total CH_4	10,800 kg/h	600
Total O_2	11,740 kg/h	600
Concentrate	15.1 tons/h	600

In run #4, the amount of O_2 fed through the each of oxygen slots was also kept at the same mass flow rate. An O_2/CH_4 ratio of 0.74 was also maintained at input. As the input gases were preheated before entering the reactor, the total amount of fuel needed is less than that when input gases were charged at room temperature. Therefore, the 95% metallization can be achieved with a shorter reactor length. The total reactor length for run #4 was kept at 21 meter.

Table 16. Operating Parameters (run #5)

Parameter	Value	Input Temp. (°C)
Total Production rate	100,000 tpy	NA
Total CH_4	7,050 kg/h	1000
Total O_2	9,070 kg/h	1000
Concentrate	15.1 tons/h	1000

In run #5, the gas input temperature was further preheated to 1000 **°C** before entering the reactor. The amount of O_2 fed through the each of oxygen slots was also kept at the same mass flow rate. The total reactor length for this simulation was kept at 18 m.

5.2.3 Results

Run #1

The temperature distribution is shown in Figure 29. The final product temperature is 1200 °C. The distributions of H_2 and H_2O mole fractions in the reactor are shown in Figures 30 and 31, respectively. The mole fractions of H_2 and H_2O at the exit of the reactor are 0.38 and 0.26, respectively.

The average particle residence time and reduction degree at the exit are 6.3 seconds and 78%, respectively. The reduction degree in this simulation run does not meet the 95% metallization criterion as the operating temperature is relatively low.

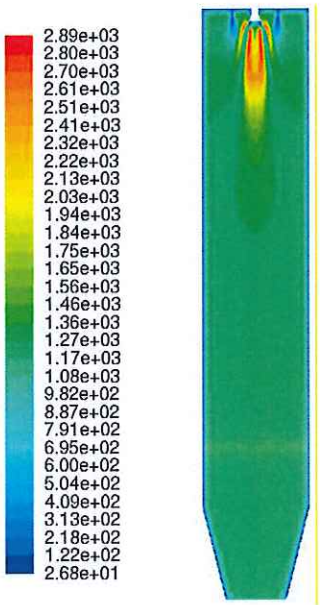

Figure 29. Temperature distribution (temperature in °C)

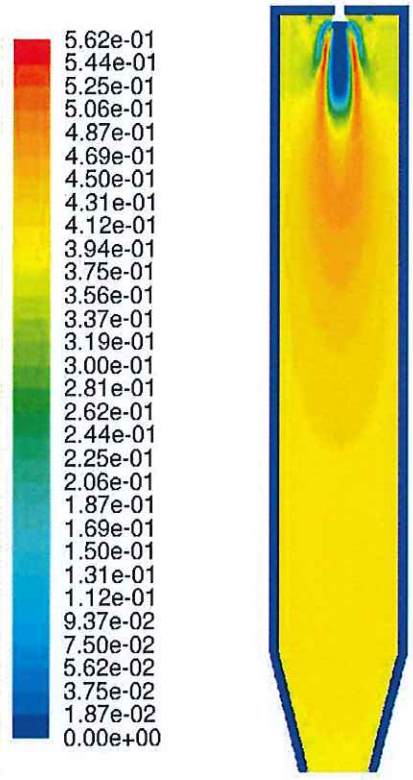

Figure 30. Mole fraction of H_2.

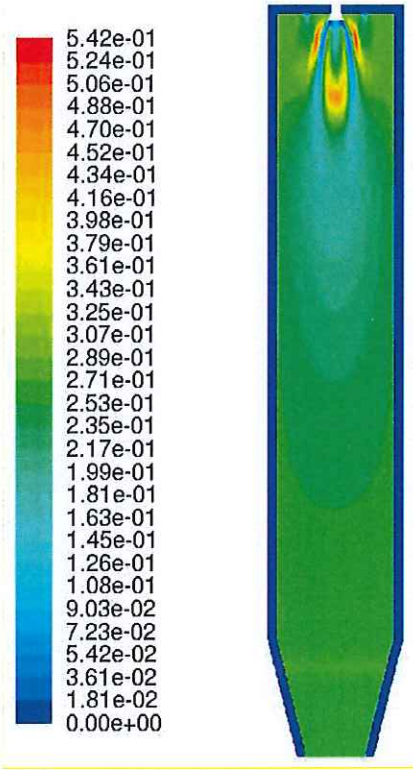

Figure 31. H_2O mole fraction.

Run #2

The temperature distribution is shown in Figure 32. The final product temperature is 1245 °C. The distributions of H_2 and H_2O mole fractions in the reactor are shown in Figures 33 and 34, respectively. The mole fractions of H_2 and H_2O at the exit of the reactor are 0.39 and 0.26, respectively.

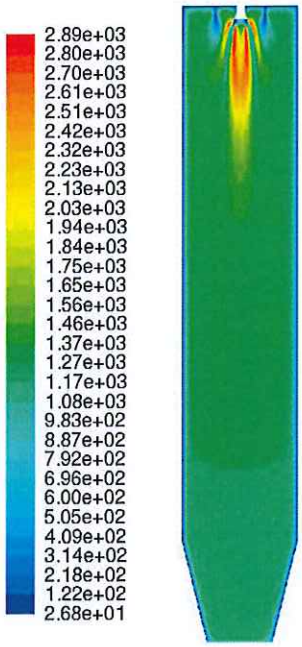

Figure 32. Temperature distribution (temperature in °C)

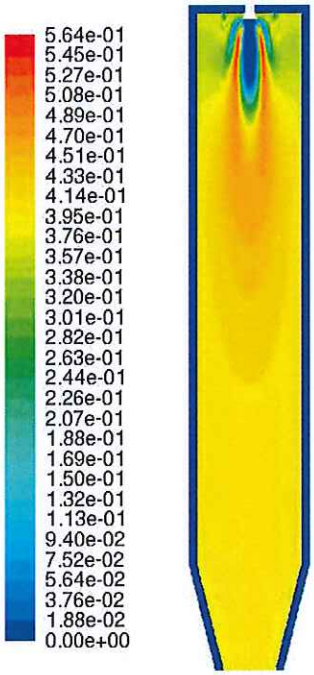

Figure 33. Mole fraction of H_2.

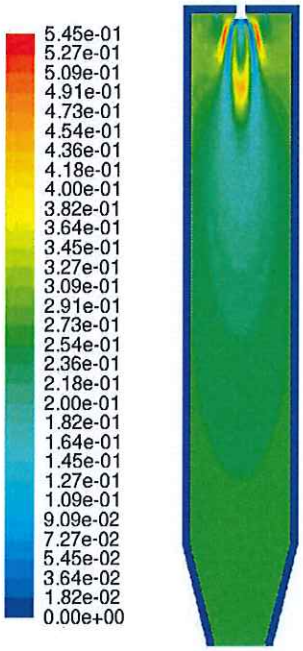

Figure 34. H_2O mole fraction.

The average particle residence time is 5.2 seconds, and reduction degree at the exit is 90%. The reduction degree in this simulation run is close to but still does not meet the 95% metallization criterion as the operating temperature is still not high enough for complete reduction of the concentrate particle at this residence time.

Run #3

The temperature distribution is shown in Figure 35. The final product temperature is 1320 °C.

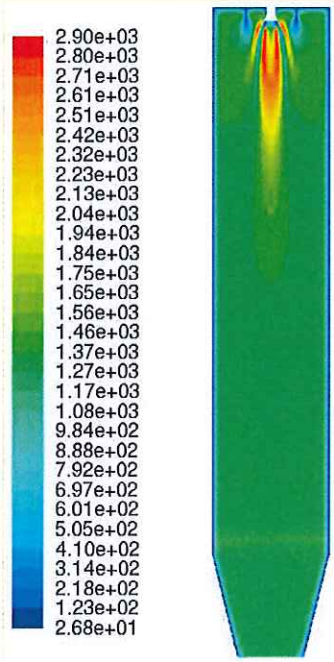

Figure 35. Temperature distribution (temperature in °C)

The distributions of H_2 and H_2O mole fractions in the reactor are shown in Figures 36 and 37, respectively. The mole fractions of H_2 and H_2O at the exit are 0.40 and 0.24, respectively.

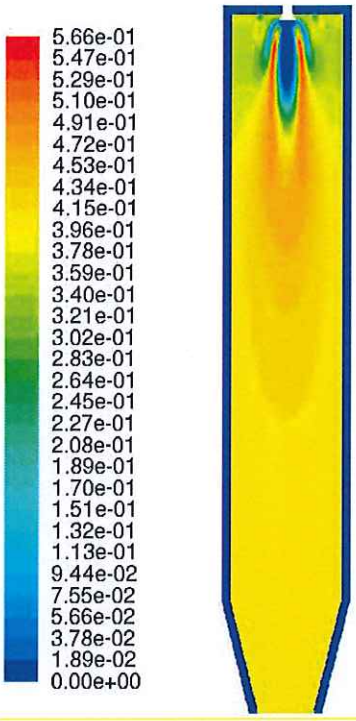

Figure 36. Mole fraction of H_2.

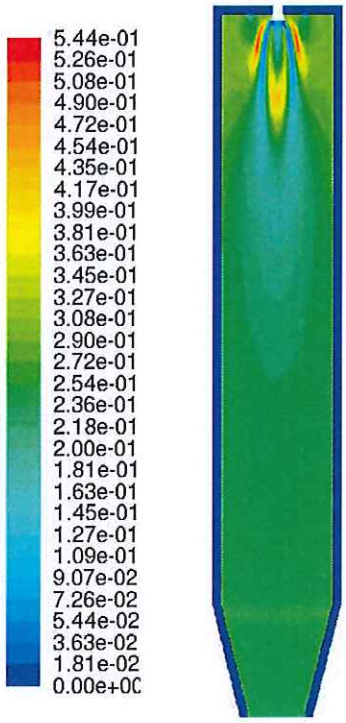

Figure 37. H_2O mole fraction.

The average particle residence time and reduction degree at the exit are 4.3 seconds and 96%, respectively. The reduction degree in this simulation run meets the 95% metallization criterion.

Run #4

The temperature distribution is shown in Figure 38. The final product temperature is 1315 °C.

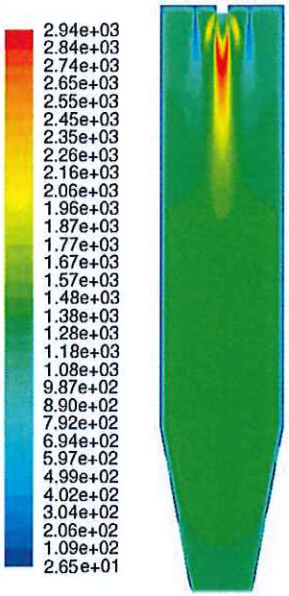

Figure 38. Temperature distribution (temperature in °C, reactor length 21 m).

The distributions of H_2 and H_2O mole fractions in the reactor are shown in Figures 39 and 40, respectively. The mole fractions of H_2 and H_2O at the exit of the reactor are 0.38 and 0.28, respectively.

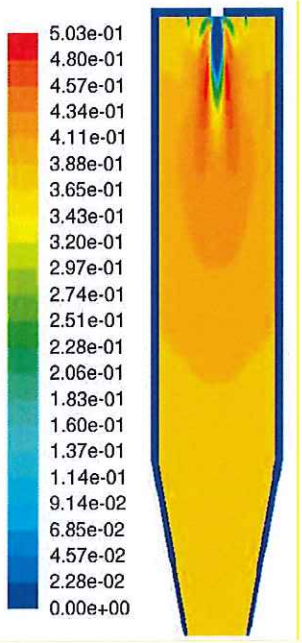

Figure 39. H_2 mole fraction.

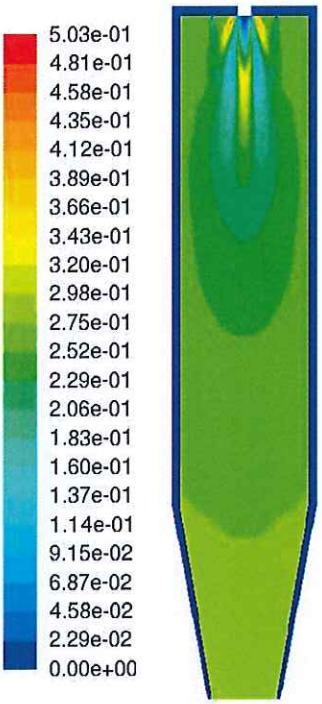

Figure 40. H_2O mole fraction.

The average particle residence time and reduction degree at the exit are 4.4 seconds and 96%, respectively. The reduction degree in this simulation run meets the 95% metallization criterion.

Run #5

The temperature distribution is shown in Figure 41. The final product temperature is 1310 °C.

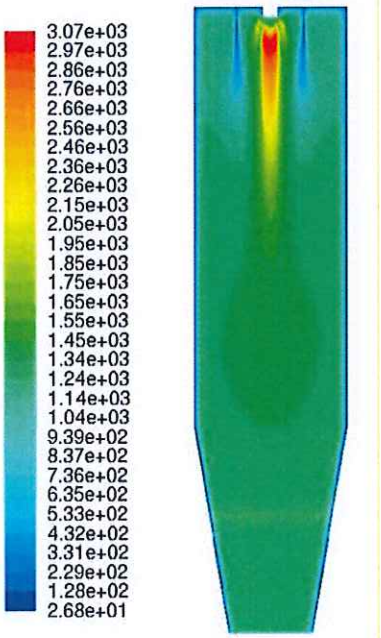

Figure 41. Temperature distribution (temperature in °C, reactor length 18 m)

The distributions of H_2 and H_2O mole fractions in the reactor are shown in Figures 42 and 43, respectively. The mole fractions of H_2 and H_2O at the exit of the reactor are 0.37 and 0.27, respectively.

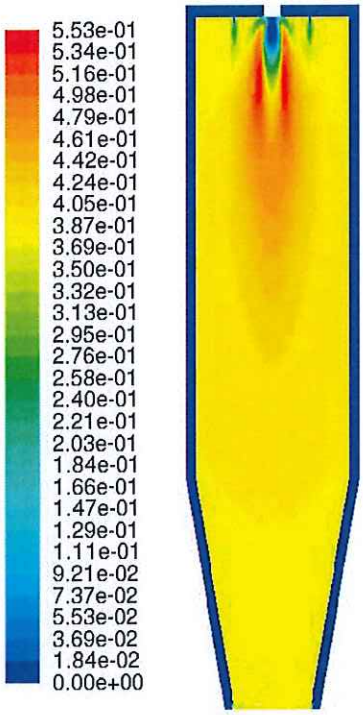

Figure 42. H_2 mole fraction distribution

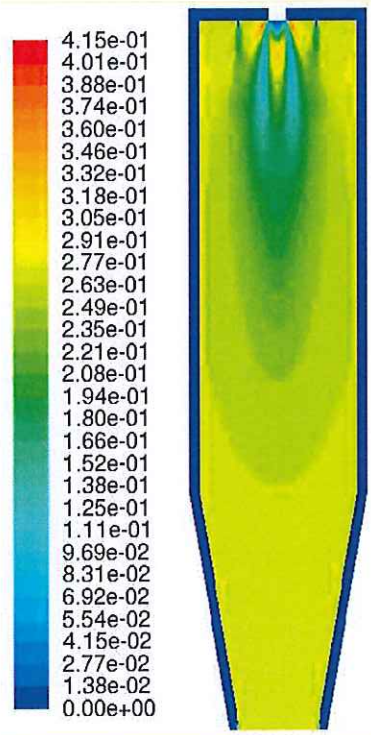

Figure 43. H_2O mole fraction distribution

The average particle residence time and reduction degree at the exit are 4.6 seconds and 97%, respectively. The reduction degree in this simulation run meets the 95% metallization criterion.

5.2.4 Elevated Pressure Reactor

In the previous section, the dimensions for a flash ironmaking reactor, with a capacity for 100,000 tons of iron per year, operating under normal atmosphere (1 atm) was simulated. In this section, a flash ironmaking reactor operating at an elevated pressure (10 atm) was simulated. The geometry of this reactor is shown in Figure 44. The wall of this pilot reactor was kept the same as in the previous simulation, which consisted of three layers, namely, the refractory layer, insulation layer and steel shell from the inner to outer surface. The thickness of each layer was also kept the same as in the previous simulations.

The four-powder feeder injection ports configuration was also maintained. The distance between the powder injection port and the centerline of the reactor was kept at 0.25 m.

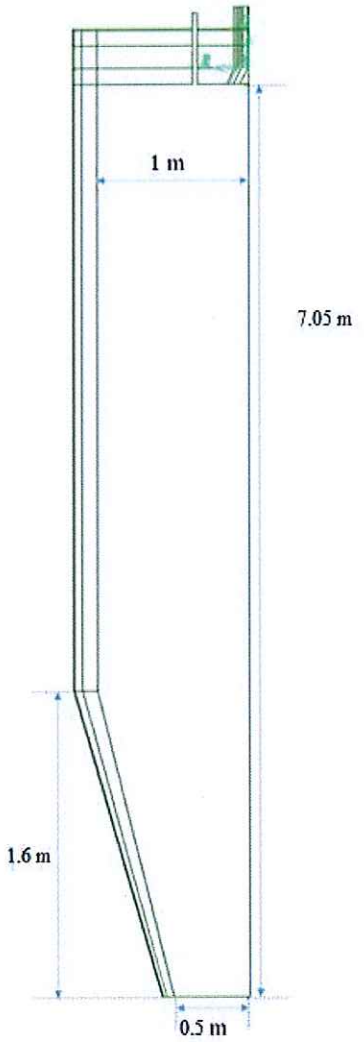

Figure 44. Geometry

(a) Burner Configuration

The non-premixed burner with two oxygen slots and one natural gas slot was also the same as that used in the previous report, which is shown in Figure 45.

The set of operating parameters tested is shown in the following Table 17. The operating pressure was kept at 10 atm for this design.

Table 17. Operating Parameters

Parameter	Value
Total Production rate, tpy	100,000
Total CH_4 (kg/s)	9,229
Total O_2 (kg/s)	13,620
Concentrate (tons/h)	16.1

The same mass flow rate was used for the two oxygen slots (50% of the total flow rate each). The O_2/CH_4 ratio of this run was kept at 0.74.

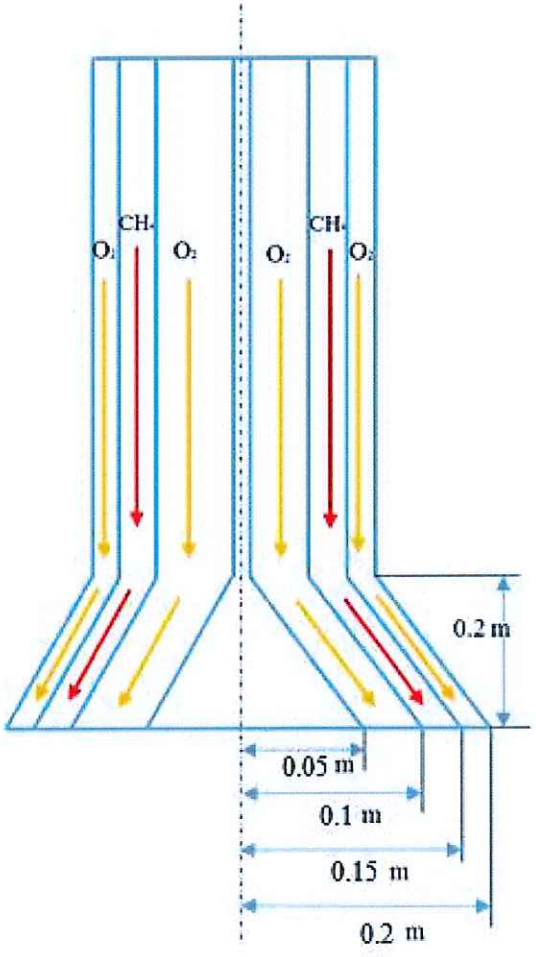

Figure 45. Burner configuration.

(b) Results

The temperature distribution is shown in Figure 46. The final product temperature is 1250 °C. The distributions of H_2 and H_2O mole fractions in the reactor are shown in Figures 47 and 48, respectively. The mole fractions of H_2 and H_2O at the exit of the reactor are 0.37 and 0.28, respectively. The distributions of CO and CO_2 mole fractions in the reactor are shown in Figure 49. The mole fractions of CO and CO_2 at the exit of the reactor are 0.255 and 0.065, respectively.

The average particle residence time and reduction degree at the exit are 3.1 seconds and 96%, respectively. The reduction degree in this simulation run meets the 95% metallization criterion although the operating temperature is relatively low and the reactor much smaller in both the diameter and length.

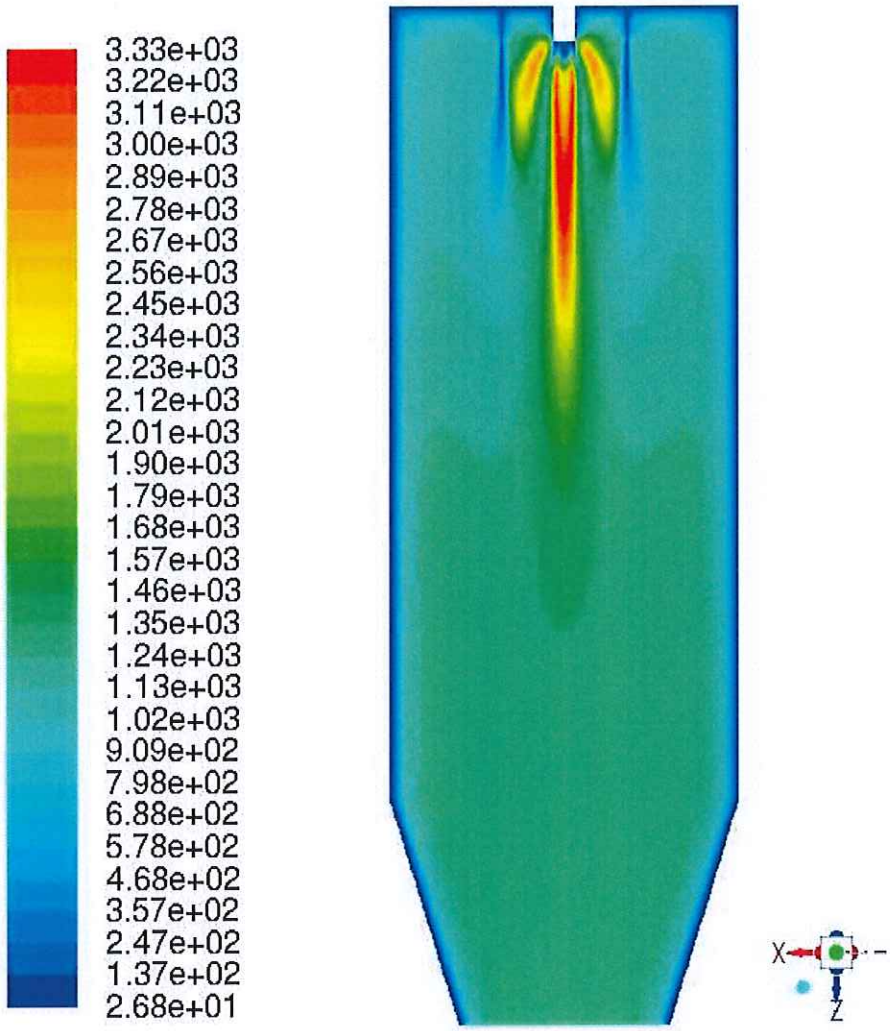

Figure 46. Temperature distribution (temperature in °C)

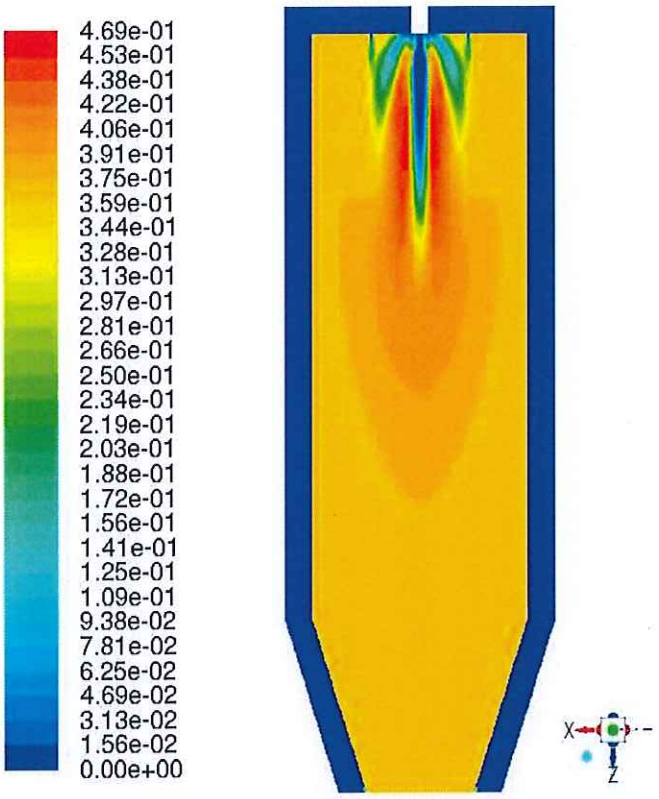

Figure 47. Mole fraction of H_2.

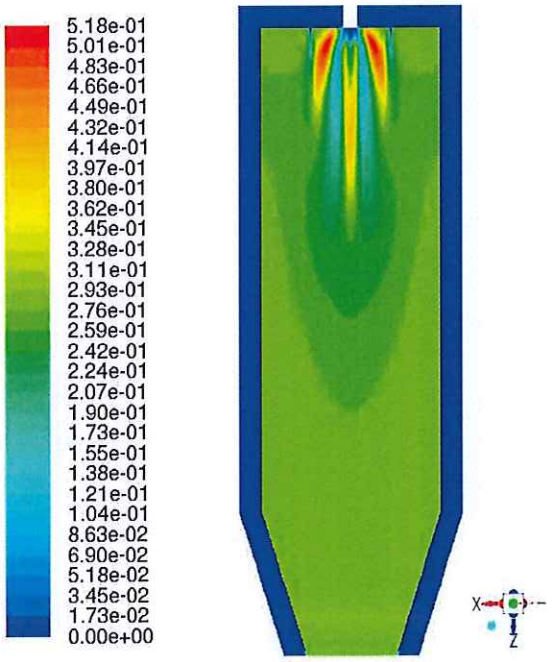

Figure 48. H_2O mole fraction.

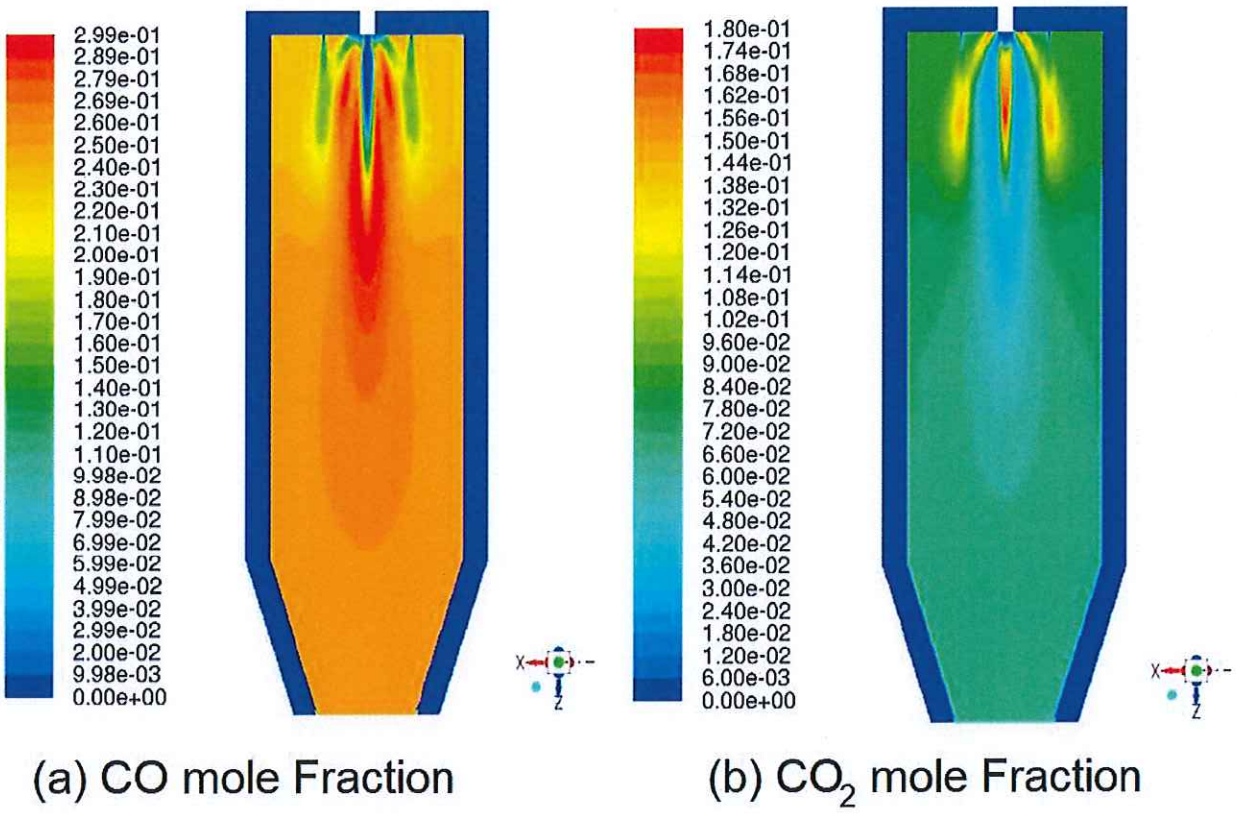

Figure 49. (a) CO mole fraction. (b) CO_2 mole fraction.

5.3 Reduction Kinetics Analysis through CFD Modeling in Drop Tube Reactor

(a) Geometry and Mesh

The flow domain simulated in the drop tube reactor (DTR) is schematically represented in Figure 50(a). The reactor was composed of a vertical split tube furnace and a cylindrical alumina tube with an inner diameter of 5.6 cm and 193 cm in length. Hexahedral mesh was used throughout the geometry, as shown in Figure 50(b).

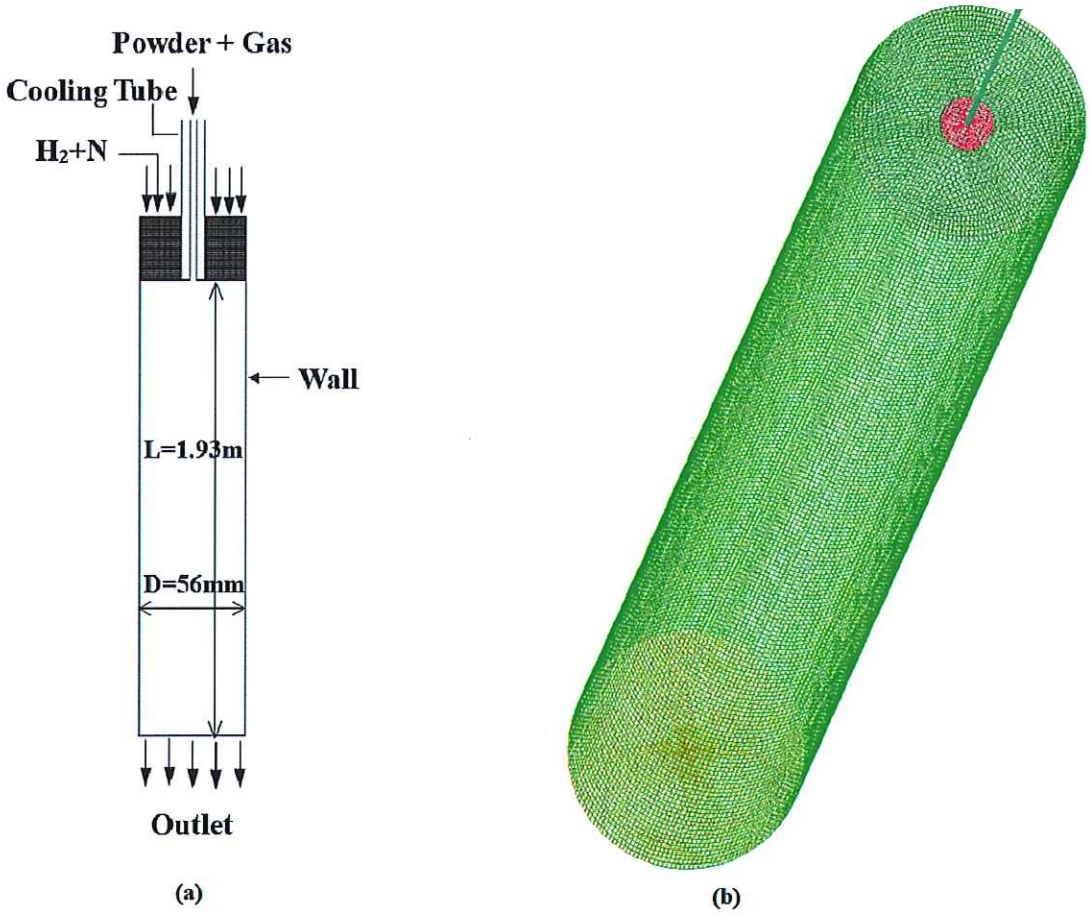

Figure 50. Geometry representation of the drop tube reactor (DTR) and the computational mesh. (a) Geometry representation and (b) Mesh.

(b) Algorithm

The kinetics parameters for magnetite reduction by hydrogen, namely, the pre-exponential factor (k_o) and activation energy (E) are both inputs for the model as well as unknowns to be determined. Sufficiently broad ranges of values for k_o and E that contain the actual values for the hydrogen reduction of magnetite were first pre-determined and discretized into pairs of k_o and E with a specified activation energy increment. Then those discretized pairs of k_o and E are then used to predict the reduction degree of magnetite particles under each set of experimental conditions and calculate the mean of the squared errors.

The wall temperature in the CFD model was first optimized until the calculated gas temperature profile agreed with the measured profile along the reactor axis as shown in Figure 51. And these optimized wall temperatures then were used as boundary conditions.

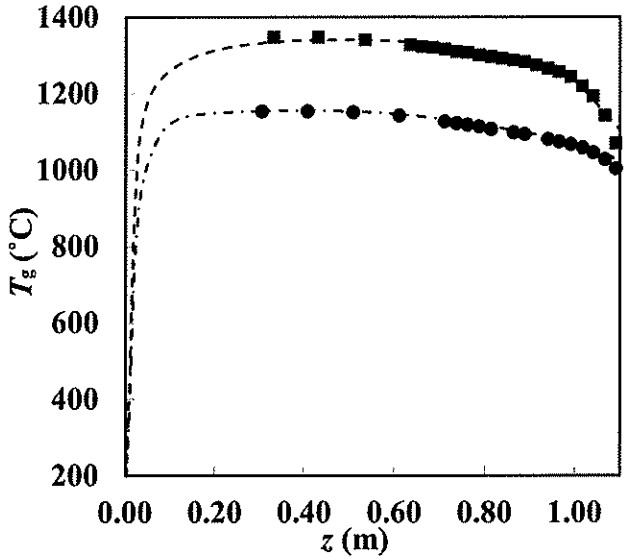

Figure 51. Comparison of the measured and calculated temperature profiles along the drop tube reactor axis. ▪, – – –, experimental and calculated temperature profiles for target temperature of 1350 °C; ●, – · – : experimental temperature and calculated profiles for target temperature of 1150 °C.

(c) Mathematical model

The gas phase was treated as a continuum in the Eulerian frame of reference, and the particles are tracked using a Lagrangian approach in which the trajectory and velocity are determined by integrating the equation of particle motion. In addition, a heat balance on the particle that relates the particle temperature to convection and radiation was also applied. The realizable k-ε model was chosen for simulating the spread of the carrier gas jet. Radiation was taken into account using the discrete ordinate (DO) model. As the volume fraction of the solid phase in the reactor is in the order of 10^{-6}, the flow is categorized as a very dilute flow. Thus, the inter-particle collisions were neglected. The energy needed to heat up the particle phase is much smaller than the amount of heat carried by the gas phase in this dilute system (usually ≤ 5 wt%), and thus the addition of particles into the reactor does not significantly affect the gas phase temperature. Similarly, the particle addition at this low level does not significantly affect the gas phase velocity profile. Therefore, the gas phase temperature and velocity profiles calculated in the absence of particles were used even in the presence of particles. This simplified approach was used to minimize the computational time since a full CFD simulation of the entire experimental data set that considers coupling between the discrete and continuous phase would have taken a prohibitive amount of computational time.

(d) Results and discussions

The following global nucleation and growth rate expression for the overall reduction of magnetite was used:

$$\left[-\ln\left(1-X\right)\right]^{1/n} = k_0 \exp\left(\frac{-E}{RT}\right)\cdot\left[\left(p_{r,g}\right)^m - \left(\frac{p_{p,g}}{K}\right)^m\right]\cdot\left(d_p\right)^{-s}\cdot t \qquad (23)$$

where $p_{r,g}$ and $p_{p,g}$ are the partial pressure of gaseous reducing agent (H_2) and product (H_2O),

respectively; n is the Avrami parameter; and s represents the dependence of rate on the particle size. K is the equilibrium constant for the reduction of $Fe_{0.947}O$ [$Fe_{0.947}O + H_2 = 0.947Fe + H_2O$]; m is the reaction order with respect to the partial pressure of gaseous reactant and product. The reaction order of the reactant and product must be equal with each other since a zero net reaction rate must be satisfied at equilibrium when $K = p_{r,g} / p_{p,g}$.

The objective function used in this study was the mean of the squared errors of all experiments as:

$$f_{\min} = \sum_i \left(X_{cal,i} - X_{\exp,i} \right)^2 / N \tag{24}$$

A wide range of values that contain the expected values were discretized and scanned for searching an optimized value. The search ranges of activation energy and pre-exponential factor are listed in Table 18.

Table 18. Searching range and optimized values of the kinetics parameter

	$n = 2, m = 0.5$	$n = 1, m = 1$
E range (kJ mol^{-1})	59 ~ 176	96 ~ 221
k_0 range(atm$^{-1/m}$ s^{-1} μm^s)	5700 ~ 2.38×10^8	131.2 ~ 4.46×10^6
Optimized values	$E = 129$, $k_0 = 3.93\times10^4$	$E = 196$, $k_0 = 1.23\times10^7$

The typical calculated particle temperature profile within the DTR is shown in Figure 52. The position where the particle temperature rises to the temperature of the isothermal zone, marked by the first dashed line on the left in Figure 52, is 0.205 m, which accounts for nearly one-third of the whole reaction zone length in this case. This length can be larger or smaller depending on specific experimental conditions. The typical calculated particle reduction degree through the reactor is shown in Figure 53 together with the corresponding experimental final value. The comparisons between the reduction degrees calculated using the optimized kinetics parameters of first-order partial pressure dependency and the values obtained experimentally are shown in Figure 54.

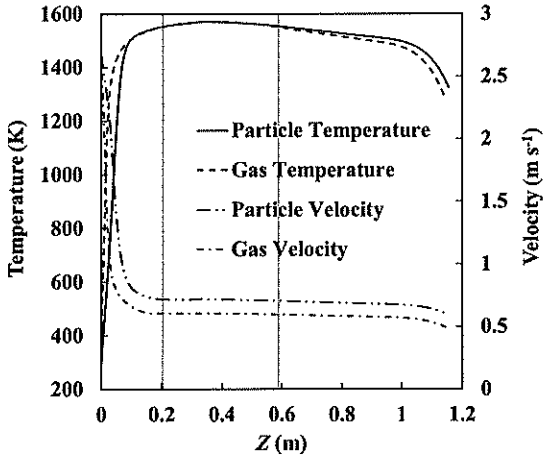

Figure 52. Particle temperature and velocity along the centerline of the reactor for T_{iso}=1573 K, pH_2 = 0.2 atm, d_p = 49 μm, total gas flow rate = 8.5 L min^{-1}. The two vertical dashed lines represent the beginning and the end of the isothermal zone (target temperature 1573 ± 20 K).

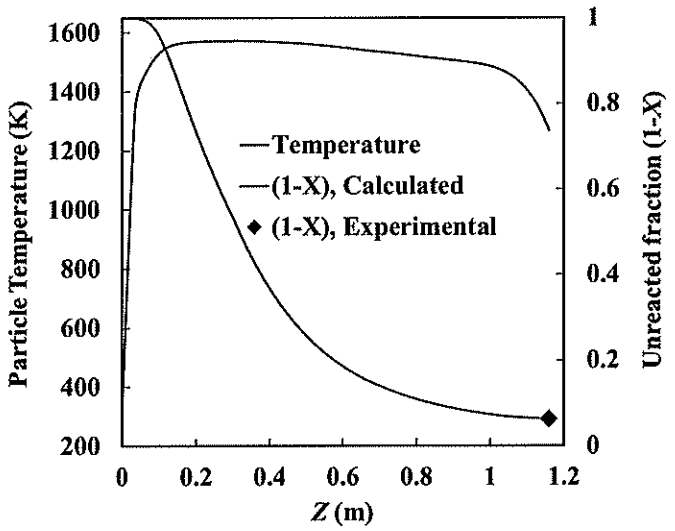

Figure 53. Particle temperature profile and unreacted fraction through the reactor for T_{iso} =1573 K, pH_2=0.2 atm, d_p=22.5 μm, gas flow rate=2.15 L min^{-1}.

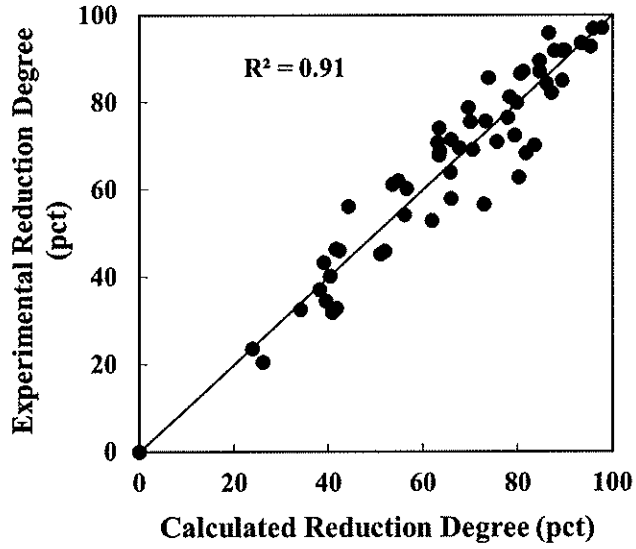

Figure 54. Comparisons between the calculated reduction degrees vs. experimental results of all runs (n=1, m=1).

(e) Complete rate expression

Combining all the rate parameters obtained through the steps described above, the complete rate equation for the hydrogen reduction of magnetite concentrate particle in the temperature range of 1150 to 1350 °C is given by:

$$\left[-\ln(1-X)\right] = 1.23\times10^{7}\times e^{-\frac{196{,}000}{RT}}\cdot\left[\left(p_{r,g}\right)-\left(\frac{p_{p,g}}{K}\right)\right]\cdot t \qquad (25)$$

where R is 8.314 J mol^{-1} K^{-1}, p is in atm, and t is in seconds.

5.4 Computational fluid dynamics simulation of Utah Flash Reactor (UFR)

(a) Geometry and Mesh

The Utah Flash Reactor (UFR) is schematically represented in Figure 55(a). The reactor had 0.19 m ID and 2.13 m length but for clarity only the top part of the reactor is shown. The configuration of the burner is shown in Figure 55(b). Hydrogen or Methane and oxygen were injected through a non-premixed burner. Two particle injection ports with an angle of 22.5° from the vertical axis of the reactor tube were installed on two sides of the burner. Hexahedral dominating hybrid mesh was generated and shown in Figure 55(d). Tetrahedral mesh was used in the top part of the reactor for capturing the complex geometric configuration of the burner and powder feeding ports as shown in Figure 55(c).

(b) Mathematical Model

The Euler-Lagrange approach is used in the CFD model in which the gas phase is treated as a continuum in the Eulerian frame by solving a set of momentum, energy and turbulent closure equations, while the trajectories and velocities of a large number of particles are tracked and integrated in the Lagrangian frame. The turbulence model chosen for simulating the spread of gas jet was the realizable k-ε model. Radiation was taken into account using the discrete ordinate (DO) model. The chemical reactions and the corresponding rate constant parameters incorporated for the gas phase combustion are listed in Tables 19 and 9. The H_2 partial combustion mechanism adopted consisted of 7 chemical reactions involving 6 species. The CH_4 partial combustion mechanism adopted here was a 4-step simplified global chemical reaction involving 5 species. The rate constant of forward reaction for all the chemical reactions was expressed in the Arrhenius form as

$$k_f = AT^{\beta} \exp\left(-\frac{E_a}{RT}\right) \tag{26}$$

The activation energy, temperature exponent and pre-exponential factor for each of the elementary reaction of H_2 partial combustion and CH_4 partial combustion are listed in Tables 19 and 9, respectively. The rate expression used for the solid phase is the optimized rate expression Eq. (25).

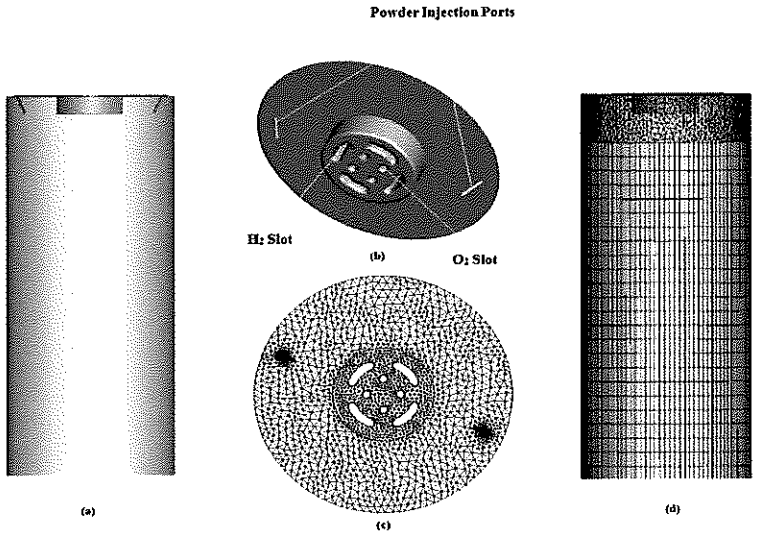

Figure 55. Geometry of the Utah Flash Reactor (UFR) and burner configuration. (a) Reactor interior and (b) Burner (c) Burner Mesh (d) Hybrid Mesh.

Table 19. Gas-Phase Reaction Mechanism for H_2-O_2 Partial Combustion

	Reaction	A (cm^3 mol^{-1} s^{-1})	β	E_a (cal mol^{-1})
1	$H_2+O_2=OH+OH$	0.170×10^{14}	0.0	48,151
2	$H+O_2=OH+O$	0.142×10^{15}	0.0	16,401
3	$OH+H_2=H_2O+H$	0.316×10^{8}	1.8	3,030
4	$O+H_2=OH+H$	0.207×10^{15}	0.0	13,750
5	$OH+OH=H_2O+O$	0.550×10^{14}	0.0	7,000
6	$H+OH=H_2O+M$	0.221×10^{23}	-2.0	0
7	$H+H=H_2+M$	0.653×10^{18}	-1.0	0

(c) Simulation Results: H_2 Runs

The CFD model was used to simulate a variety of operating conditions for the Utah Flash Reactor (UFR). The range of operating conditions simulated are listed in Table 20.

Table 20. Operating Conditions for the Utah Flash Reactor Using H_2

Parameters	Range
Concentrate feeding rate, kg h^{-1}	0.10 ~ 0.13
Mass-average particle size, μm	32
H_2 flow rate*, L h^{-1}	918 ~ 3600
H_2 input temperature, K	298
O_2 flow rate, L h^{-1}	117 ~ 579
O_2 input temperature, K	298

**Flow rates are calculated at 298 K and 0.85 atm, the barometric pressure at Salt Lake City (1 atm = 101.32 kPa).*

The temperature distributions under two typical operating conditons, H_2: 3600 L h^{-1}, O_2: 579 L h^{-1} and H_2: 1200 L h^{-1}, O_2: 177 L h^{-1}, are shown in Figure 56. It is noted that there is a recirculation region near the burner region formed by high velocity gas streams, which is depicted in Figure 57.

The calculated and measured gas phase temperature along the centerline of the reactor for the higher and lower H_2 flow rate are depicted in Figure 58. The gas temperature first spikes to the flame temperature and then drops to the isothermal temperature and stays until the gas travels out of the isothermal zone. It is noted that good agreement between the calculated and measured gas temperatures is obtained, as shown in Figure 58, except there are some slight deviations at the end of the reactor.

Table 21 lists all the experimental conditions simulated for UFR. A comparison of the calculated reduction degree of the particles and the values obtained experimentally is shown in Figure 59.

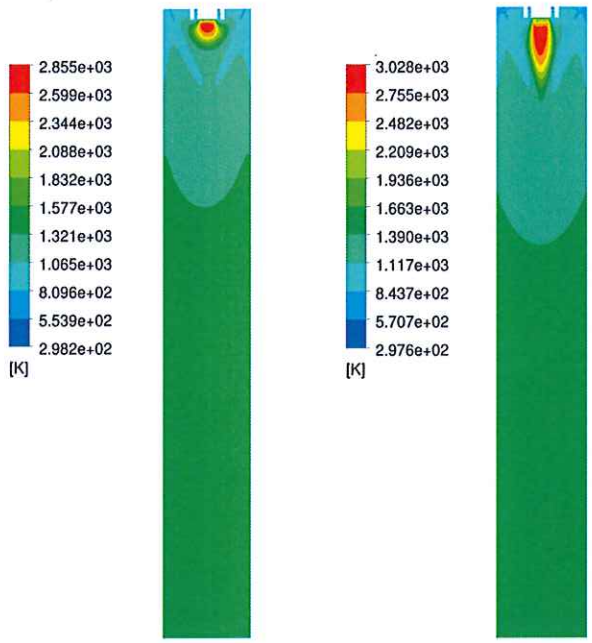

Figure 56. Temperature distribution in the Utah Flash Reactor. H_2 flow rate: (a) 1200 and (b) 3600 L h^{-1}

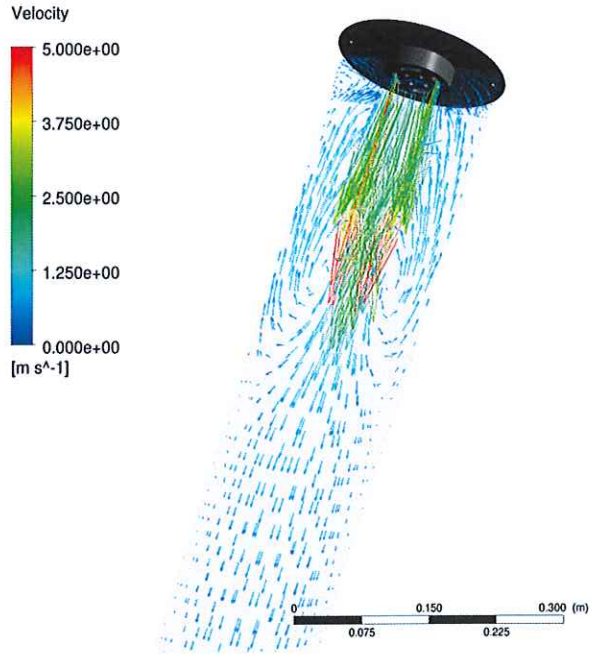

Figure 57. Velocity vector near the burner region. H_2 flow rate 3600 L h^{-1}

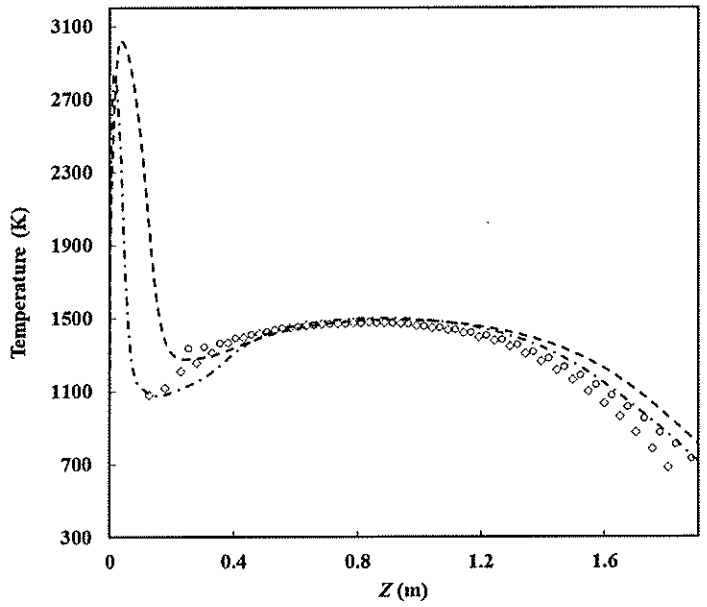

Figure 58. Gas phase temperature along the centerline of the reactor. – · –, □: experimental and calculated temperature profiles for H_2: 1200 L h^{-1}, O_2: 177 L h^{-1}; ○,– – –: experimental and calculated temperature profiles for H_2: 3600 L h^{-1}, O_2: 579 L h^{-1}.

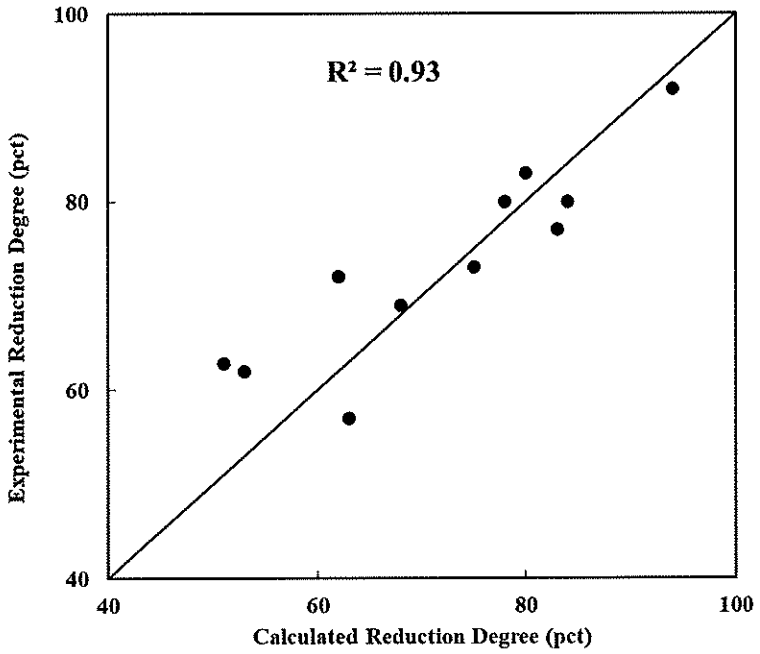

Figure 59. Comparisons between the calculated reduction degrees vs. experimental results.

Table 21. Experimental Conditions and Reduction Degrees

Exp. ID	H_2 (L min^{-1})	O_2 (L min^{-1})	Particle Flow Rate (kg h^{-1})	X_{cal} (%)	X_{exp} (%)
1	15.3	2.16	0.13	84	80
2	15.3	2.72	0.10	63	57
3	20	2.96	0.14	80	83
4	20	3.22	0.12	78	80
5	20	3.7	0.13	51	63
6	40	4.32	0.13	94	92
7	40	6.4	0.12	83	77
8	60	9.65	0.11	75	73
9	60	10.1	0.12	68	69
10	60	10.65	0.11	62	72
11	60	11.2	0.13	53	62

(d) Simulation Results: CH_4

Experimental conditions of a typical run using methane partial combustion to produce reducing gas-H_2 and CO, in the UFR is listed in Table 22.

Table 22. Experimental conditions of a typical run CH_4 in the UFR

Parameters	Values
H_2 flow rate*, L h^{-1}	120
H_2 input temperature, K	298
CH_4 flow rate*, L h^{-1}	300
O_2 flow rate*, L h^{-1}	270
O_2 input temperature, K	298

**Flow rates are calculated at 298 K and 0.85 atm, the barometric pressure at Salt Lake City (1 atm = 101.32 kPa).*

The reaction mechanism and parameters listed in Table 13 were used to simulate CH_4 partial combustion in the UFR using the above conditions. The temperature contours on the plane of powder injection ports are shown in Figure 60. It was found that flame temperature of CH_4 partial combustion is lower than that of H_2 partial combustion under the same % excess hydrogen. The species mole fractions on the same plane are shown in Figure 61.

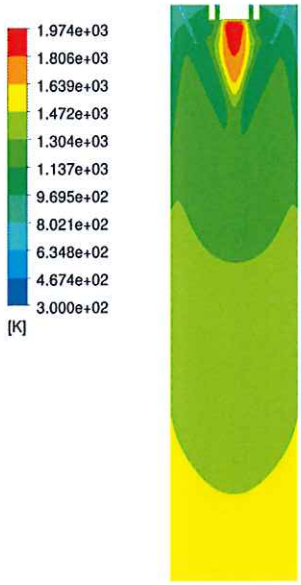

Figure 60. Temperature profile in the Utah Flash Reactor.

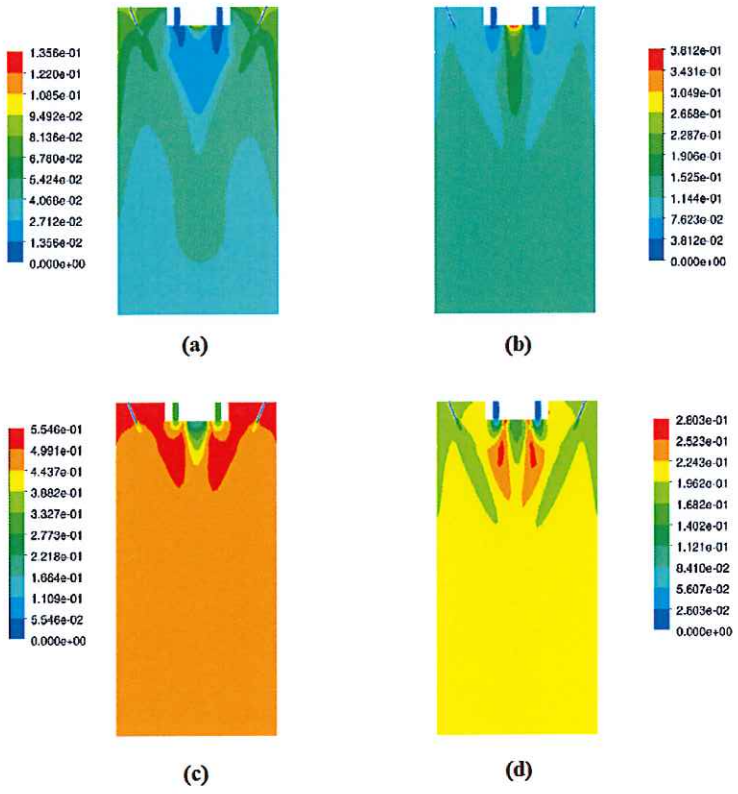

Figure 61. Species concentration distribution in the Utah Flash Reactor. (a) CO_2 mole fraction, (b) H_2O mole fraction, (c) H_2 mole fraction and (d) CO mole fraction.

6. CONCLUDING REMARKS

A novel ironmaking technology for producing iron directly from fine concentrates by gas-solid flash reduction that bypasses cokemaking and pelletization/sintering was investigated.

The major task in this project was the test of the Flash Ironmaking Technology (FIT) in a Large Scale Bench Reactor (LSBR). Additional tasks were a more detailed determination of the concentrate reduction kinetics by H_2+CO mixtures and experiments in a smaller laboratory flash reactor termed Utah Flash Reactor (UFR). All of the project objectives, milestones, and tasks were successfully accomplished.

The UTAH Team worked with Berry Metal Co. (BMC) and University Construction Services to install the Large-Scale Bench Reactor (LSBR), and the UTAH team carried out hot commissioning, with the assistance of BMC, to test the different components. After testing the LSBR facility to check whether all the components worked properly and making necessary corrections and repairs, main experiments were performed. These LSBR runs yielded many useful results, as described in the main part of this report. The results of the LSBR runs, together with the CFD simulation approach developed in this project, will be useful in designing the industrial reactor, including the identification of scale-up challenges and how to improve the various aspects of operation.

The LSBR was the first of its kind and the design and operation of such a large reactor posed a number of challenges. It took much effort to resolve many of these difficulties. Others parts of the system design were identified that must be optimized while designing the industrial reactor. The project results provided valuable findings from this large-scale testing program.

7. REFERENCES

Abdelghany, A. R., 2018, "Design of Flash Ironmaking Reactors with Computational Fluid Dynamics Modeling," Ph.D. Dissertation, University of Utah.

Choi, M. E. and H. Y. Sohn, 2010, Development of Green Suspension Ironmaking Technology Based on Hydrogen Reduction of Iron Oxide Concentrate: Rate Measurements, *Ironmaking Steelmaking*, 37, 81-88.

Fan, D., Mohassab, Y. and Sohn, H. Y., 2016a, CFD Simulations of a Laboratory Flash Reactor Relevant to a Novel Flash Ironmaking Process. *AISTech 2016 Proceedings*, AIST, 551-558.

Fan, D., Mohassab, Y., Elzohiery, M., and Sohn, H.Y., 2016b, Analysis of the Hydrogen Reduction Rate of Magnetite Concentrate Particles in a Drop Tube Reactor through CFD Modeling. *Metallurgical and Materials Transactions B*, 47, 1669-1680.

D.-Q. Fan, H.Y. Sohn, Y. Mohassab, and M. Elzohiery, "Computational Fluid Dynamics Simulation of the Hydrogen Reduction of Magnetite Concentrate in a Laboratory Flash Reactor," *Metall. Mater. Trans. B*, 47B, 3489-3500 (2016c). DOI:10.1007/s11663-016-0797-4; http://link.springer.com/article/10.1007/s11663-016-0797-4

Gran, I.R. and Magnussen, B.F., 1996, A Numerical Study of a Bluff-Body Stabilized Diffusion Flame. Part 2. Influence of Combustion Modeling and Finite-Rate Chemistry. *Combustion Science and Technology* 119(1-6), 191-217.

Hahn, Y.B. and Sohn, H.Y., 1990, Mathematical Modeling of Sulfide Flash Smelting Process: Part II. Quantitative Analysis of Radiative Heat Transfer. *Metallurgical and Materials Transactions B*, 21(6), 959-66.

Jones, W.P. and Lindstedt, R.P., 1988, Global Reaction Schemes for Hydrocarbon Combustion. *Combustion and Flame* 73, 233-249.

Kemori, N., Ojima, Y. and Kondo, Y. 1988, Variation of the Composition and Size of Copper Concentrate Particles in the Reaction Shaft. In: *Flash Reaction Processes, Proceedings of Center for Pyrometallurgy Conference*, University of Utah, Published by Center for Pyrometallurgy, Rolla, MO, 47–68.

Kimura, T., Ojima, Y., Mori, Y. and Ishii, Y., 1986, Reaction Mechanism in a Flash Smelting Reaction Shaft. In: *The Reinhardt Schuhmann International Symposium on Innovative Technology and Reactor Design in Extraction Metallurgy*, TMS/AIME, Colorado Springs, CO, 9 November, 403–18.

Mohassab, Y. , M. Elzohiery, F. Chen, and H. Y. Sohn, 2016, Determination of Total Iron Content in Iron Ore and DRI: Titrimetric Method versus ICP-OES Analysis, *EPD Congress 2016*, ed. by A. Allanore et al., TMS (The Minerals, Metals & Materials Society), pp. 125-133.

Ranz, W.E. and Marshall, W.R., 1952, Evaporation from drops: Part 2. *Chemical Engineering Progress* 48(4), 173–80.

Sohn, H. Y., *Suspension Hydrogen Reduction of Iron Oxide Concentrate*, Final Report to American Iron and Steel Institute for work under DOE Project DE-FC36-97ID13554, March 2008.

Themelis, N.J., Wu, L. and Jiao, Q., 1988, Some Aspects of Mathematical Modeling of Flash Smelting Phenomena. In: *Flash Reaction Processes, Proceedings of Center for Pyrometallurgy Conference*, University of Utah, Published by Center for Pyrometallurgy, Rolla, MO, 263–85.

Theodore, A.S.L., Bergman, L., Incropera, F. P., and DeWitt, D. P., 2011 *Fundamentals of Heat and Mass Transfer*, 7th Edition, Wiley, NJ, USA.

8. PUBLICATIONS BASED ON WORK PERFORMED IN THIS PROJECT

Dissertations and Theses:

1. M. Y. Mohassab-Ahmed, "Phase Equilibria between Iron and Slag in $CO/CO_2/H_2/H_2O$ Atmospheres Relevant to a Novel Flash Ironmaking Technology," Ph.D. Dissertation, University of Utah, 2013.
2. M. Olivas-Martinez, "Computational Fluid Dynamic Modeling of Chemically Reacting Gas-Particle Flows," Ph.D. Dissertation, University of Utah, 2013.
3. Z. Yuan, "Re-Oxidation Kinetics of Flash Reduced Iron Particles Relevant to a Novel Flash Ironmaking Process," M.S. Thesis, University of Utah, 2013.
4. M. H. Elzohiery, "Flash Reduction of Magnetite Concentrate Related to a Novel Flash Ironmaking Process," Ph.D. Dissertation, University of Utah, 2018.
5. A. R. Abdelghany, "Design of Flash Ironmaking Reactors with Computational Fluid Dynamics Modeling," Ph.D. Dissertation, University of Utah, 2018.

6. D.-Q. Fan, "Computational Fluid Dynamic Analysis of Experimental Flash Ironmaking Reactors," Ph.D. Dissertation, University of Utah, soon to be completed.

Book Chapters:

7. H. Y. Sohn, Mohamed Elzohiery and De-Qiu Fan, "Development of Flash Ironmaking Technology," in Ironmaking and Steelmaking: Processes, Applications and Technology, Nova Science Publishers, Hauppauge, NY, 2018.
8. H. Y. Sohn and Y, Mohassab, "Greenhouse Gas Emissions and Energy Consumption of Ironmaking Processes," in Ironmaking and Steelmaking Processes. Greenhouse Emissions, Control, and Reduction, Chapter 25, ed.by P. Cavaliere, Springer, New York, pp. 427-455, 2016.
9. H. Y. Sohn, "From Nonferrous Flash Smelting to Flash Ironmaking: Development of an ironmaking technology with greatly reduced CO_2 emissions and energy consumption," Treatise on Process Metallurgy, Volume 3 Industrial Processes Part B, Section 4.5.2.2, pp. 1596-1691, Elsevier, Oxford, UK and Waltham, MA, USA, 2014.
10. H. Y. Sohn, "A Novel Flash Ironmaking Technology Based on Naturally Occurring Magnetite Mineral," Chapter 1, Magnetite: Synthesis, Uses and Biological Occurrences, pp. 1-31, ed. by J. Ward, ISBN: 978-1-63321-602-0, Nova Science Publishers, Inc., Hauppauge, NY, 2014. Hardcover: https://www.novapublishers.com/catalog/product_info.php?products_id=50804 E-book: https://www.novapublishers.com/catalog/product_info.php?products_id=50817

Refereed Journal Articles:

11. Z. Yuan, H. Y. Sohn, and M. Olivas-Martinez, "Re-oxidation Kinetics of Flash Reduced Iron Particles in H_2-H_2O(g) Atmosphere Relevant to a Novel Flash Ironmaking Process," Metallurgical and Material Transactions B, 44B, 1520-1530 (2013). DOI 10.1007/s11663-013-9910-0.
12. M. Y. Mohassab-Ahmed and H. Y. Sohn, "Application of Spectroscopic Analysis Techniques to the Determination of Slag Structures and Properties: Effect of Water Vapor on Slag Chemistry Relevant to a Novel Flash Ironmaking Technology," JOM, 65 (11), 1559-1565 (2013). DOI: 10.1007/s11837-013-0742-9.
13. M. Y. Mohassab-Ahmed and H. Y. Sohn, "Effect of Water Vapor Content in H_2-H_2O-CO-CO_2 Mixtures on Manganese Distribution in Slag under the Conditions of a Novel Flash Ironmaking Technology," Steel Res. International, 85(5), 875-884 (2014).
14. M. Y. Mohassab-Ahmed and H. Y. Sohn, "Effect of Water Vapor on the Activity of Iron Oxide in Slags Relevant to a Flash Ironmaking Technology," Ironmaking Steelmaking, 41 (9), 665-675 (2014).
15. M. Y. Mohassab-Ahmed, H. Y. Sohn, L. Zhu, "Effect of Water Vapor Content in H_2-H_2O-CO-CO_2 Mixtures on MgO Solubility in Slag under the Conditions of a Novel Flash Ironmaking Technology," Ironmaking Steelmaking, 41(8), 575-582 (2014).

16. Z. Yuan and H. Y. Sohn "Re-oxidation Kinetics of Flash Reduced Iron Particles in O_2-N_2 Gas Mixtures Relevant to a Novel Flash Ironmaking Process," ISIJ International, 54, 1235–1243 (2014).
17. H. Y. Sohn, and M. Olivas-Martinez, "Methods for Calculating Energy Requirements for Processes in Which a Reactant is also a Fuel – Need for Standardization," JOM, 66 (9), 1557-1564 (2014).
18. Y. Mohassab and H. Y. Sohn, "Effect of Water Vapor on Sulfur Distribution between Liquid Fe and MgO-Saturated Slag Relevant to a Flash Ironmaking Technology," Steel Research Int., (2014). DOI: 10.1002/srin.201400197
19. Y. Mohassab, H. Y. Sohn and B. Van Devener, "An X-Ray Photoelectron Spectroscopy (XPS) Study of the Effect of Water Vapor on Slag Chemistry and Structure Related to a Novel Flash Ironmaking Process. Part 1: Experimental Work," AIST Trans., 12 (8), 179–186 (2015).
20. Y. Mohassab and H. Y. Sohn "An X-Ray Photoelectron Spectroscopy (XPS) Study of the Effect of Water Vapor on Slag Chemistry and Structure Related to a Novel Flash Ironmaking Process. Part 2: Calculation of the Degree of Polymerization," AIST Trans., 12 (9), 185–190 (2015).
21. M. Y. Mohassab-Ahmed and H. Y. Sohn, "Analysis of Slag Chemistry by FTIR-RAS and Raman Spectroscopy: Effect of Water Vapor Content in H_2-H_2O-CO-CO_2 Mixtures Relevant to a Novel Green Ironmaking Technology," Steel Research Int., 86 (7) 740–752 (2015). DOI: 10.1002/srin.201400186; *featured in MaterialsViews.com*.
22. H. Wang and H. Y. Sohn, "Reduction Kinetics of Magnetite Concentrate Particles by H_2+CO at 1673 K," ISIJ Intl, 55,706-708 (2015).
23. Y. Mohassab and H. Y. Sohn, "Effect of Water Vapor on the Equilibrium Distribution of Phosphorus between Liquid Iron and MgO-Saturated Slag Relevant to a Flash Ironmaking Technology," Ironmaking Steelmaking, 42(5), 346-350, (2015). http://dx.doi.org/10.1179/1743281214Y.0000000235
24. Y. Mohassab and H. Y. Sohn, "The Effect of Water Vapor on O^{2-} Content in Ironmaking Slag," J. Iron Steel Res. Int., 22(10), 672-680 (2015).
25. Y. Mohassab, H. Y. Sohn, and B. Van Devener, "An X-Ray Photoelectron Spectroscopy (XPS) Study of the Effect of Water Vapor on Slag Chemistry and Structure Related to a Novel Flash Ironmaking Process. Part 1: Experimental Work," AIST Trans., 12 (8), 179–186 (2015).
26. Y. Mohassab and H. Y. Sohn, "An X-Ray Photoelectron Spectroscopy (XPS) Study of the Effect of Water Vapor on Slag Chemistry and Structure Related to a Novel Flash Ironmaking Process. Part 2: Calculation of the Degree of Polymerization," AIST Trans., 12 (9), 185–190 (2015).
27. H. Y. Sohn and S. Perez-Fontes, "Computational Fluid Dynamics Modeling of Hydrogen-Oxygen Flame," Int. J. Hydrogen Energy, 41, 3284-3290 (2016).
28. D. Fan, Y. Mohassab, M. Elzohiery, and H. Y. Sohn, "Analysis of the Hydrogen Reduction Rate of Magnetite Concentrate Particles in a Drop Tube Reactor through CFD Modeling," Metall. Mater. Trans. B, 47(3), 1669-1680 (2016).

29. H. Y. Sohn and Y. Mohassab, "Development of a Novel Flash Ironmaking Technology with Greatly Reduced Energy Consumption and CO_2 Emissions," J. Sustainable Metallurgy, 2(3), 216–227 (2016).
30. D.-Q. Fan, H.Y. Sohn, Y. Mohassab, and M. Elzohiery, "Computational Fluid Dynamics Simulation of the Hydrogen Reduction of Magnetite Concentrate in a Laboratory Flash Reactor," Metall. Mater. Trans. B, 47B (6), 3489-3500 (2016). DOI:10.1007/s11663-016-0797-4; http://link.springer.com/article/10.1007/s11663-016-0797-4
31. M. Elzohiery, H. Y. Sohn, and Y. Mohassab, "Kinetics of Hydrogen Reduction of Magnetite Concentrate Particles in Solid State Relevant to Flash Ironmaking," Steel Research International, 88 (2), (14 pp.) 1600133 (2017). http://dx.doi.org/10.1002/srin.201600133
32. D.-Q. Fan, H. Y. Sohn, and Mohamed Elzohiery, "Analysis of the Reduction Rate of Hematite Concentrate Particles by H2 or CO in a Drop-Tube Reactor through CFD Modeling," Metall. Mater. Trans. B, 48B, 2677-2684, (2017). http://rdcu.be/ybnM ; https://link.springer.com/content/pdf/10.1007%2Fs11663-017-1053-2.pdf
33. R. Morales-Estrella, J. Ruiz, N. Ortiz-Lara, Y. Mohassab, and H. Y. Sohn, "Effect of Mechanical Activation on the Hydrogen Reduction Kinetics of Magnetite Concentrate," J. Thermal Analysis and Calorimetry, 130 (2), 713–720 (2017).
34. R. Sarkar and H. Y. Sohn, "Interactions of Alumina and Magnesia Based Refractories with Iron Melts and Slags - A Review," Metall. Mater. Trans. B, accepted. https://link.springer.com/article/10.1007/s11663-018-1300-1

Conference Proceedings:

35. H. Y. Sohn, "From Sulfide Flash Smelting to a Novel Flash Ironmaking Technology," keynote paper in Celebrating the Megascale: EPD Symposium on Pyrometallurgy in Honor of David G. C. Robertson, 2014, 143rd TMS Annual Meeting, San Diego, California, ed. by P. J. Mackey et al., TMS/Wiley, pp. 69-76, 2014.
36. H. Y. Sohn and M. Olivas-Martinez, "Determination of Energy Requirements for Ironmaking Processes: It's Not That Straightforward," Keynote paper in Energy Technology 2014 Carbon Dioxide Management and Other Technologies, 143rd Annual TMS Meeting, San Diego, California, 2014, ed.by C. Wang et al., TMS/Wiley, pp. 49-56, 2014.
37. M. Y. Mohassab-Ahmed and H. Y. Sohn, "Slag Structures and Properties by Spectroscopic Analysis: Effect of Water Vapor Relevant to a Novel Flash Ironmaking Technology," in 5th International Symposium on High-Temperature Metallurgical Processing, 143rd Annual TMS Meeting, San Diego, California, 2014, ed.by T. Jiang et al., TMS/Wiley, pp. 11-18, 2014.
38. M. Y. Mohassab-Ahmed and H. Y. Sohn, "Effect of Water Vapor on the Activities of FeO and MgO in Slags Relevant to a Novel Flash Ironmaking Technology," in 5th International Symposium on High-Temperature Metallurgical Processing, 143rd Annual TMS Meeting, San Diego, California, 2014, ed.by T. Jiang et al., TMS/Wiley, pp. 83-90, 2014.

39. S. E. Perez-Fontes, H. Y. Sohn, and M. Olivas-Martinez, "A Computational Fluid Dynamic Model for a Novel Flash Ironmaking Process," in Celebrating the Megascale: EPD Symposium on Pyrometallurgy in Honor of David G. C. Robertson, 2014, 143rd TMS Annual Meeting, San Diego, California, ed. by P. J. Mackey et al., TMS/Wiley, pp. 385-392, 2014.
40. M. Y. Mohassab-Ahmed and H. Y. Sohn, "Effect of Water on S and P Distribution between Liquid Fe and MgO-Saturated Slag Relevant to a Flash Ironmaking Technology," in EPD Congress 2014, 143rd TMS Annual Meeting, San Diego, California, ed. by J. Yurko et al., TMS/Wiley, pp. 203-210, 2014.
41. Z. Yuan, H. Y. Sohn and M. Olivas-Martinez, "Oxidation of Flash Reduced Iron Particles in Various Gas Mixtures under the Conditions of a Novel Flash Ironmaking Process," in Celebrating the Megascale: EPD Symposium on Pyrometallurgy in Honor of David G. C. Robertson, 2014, 143rd TMS Annual Meeting, San Diego, California, ed. by P. J. Mackey et al., TMS/Wiley, pp. 509-517, 2014.
42. H. Y. Sohn and Y. Mohassab, "Novel Flash Ironmaking Technology," in Metallurgical Fundamentals and Techniques, Proceedings of the World Congress on Mechanical, Chemical, and Material Engineering (MCM 2015), Barcelona, Spain, July 20 - 21, 2015, Paper No. 336..
43. D. Fan, Y. Mohassab, H. Y. Sohn, "Computational Fluid Dynamics Simulation of a Laboratory Flash Reactor Relevant to a Novel Ironmaking Process," CFD Modeling and Simulation in Materials Processing 2016, ed. by: L. Nastac et al., TMS (The Minerals, Metals & Materials Society), pp. 11-18, 2016.
44. M. Elzohiery, Y. Mohassab, A. Abdelghany, S. Zhang, F. Chen, and H. Y. Sohn, "Reduction Kinetics of Magnetite Concentrate Particles with Hydrogen at 1150 - 1600 °C Relevant to a Novel Ironmaking Process," EPD Congress 2016, ed. by A. Allanore et al., TMS (The Minerals, Metals & Materials Society), pp. 41-49, 2016.
45. M. Elzohiery, Y. Mohassab, J. Pal,, S. Zhang, and H. Y. Sohn, "Reduction Kinetics of Magnetite Concentrate Particles with H2 + CO at 1200 TO 1600 °C Relevant to a Novel Ironmaking Process," 7th International Symposium on High-Temperature Metallurgical Processing, ed. by: J.-Y. Hwang et al., TMS (The Minerals, Metals & Materials Society), pp. 35-41, 2016.
46. R. Morales-Estrella, J. Ruiz-Ornelas, Y. Mohassab, N. Ortiz-Lara, and H. Y. Sohn, "Hydrogen Reduction Kinetics of Mechanically Activated Magnetite Concentrate," EPD Congress 2016, ed. by A. Allanore et al., TMS (The Minerals, Metals & Materials Society), pp. 51-60, 2016.
47. Y. Mohassab, M. Elzohiery, F. Chen, and H. Y. Sohn, "Determination of Total Iron Content in Iron Ore and DRI: Titrimetric Method versus ICP-OES Analysis," EPD Congress 2016, ed. by A. Allanore et al., TMS (The Minerals, Metals & Materials Society), pp. 125-133, 2016.
48. Y. Mohassab, M. Elzohiery, and H. Y. Sohn, "Flash Reduction of Magnetite and Hematite Concentrates with Hydrogen in a Lab-Scale Reactor for a Novel Ironmaking Process," 7th International Symposium on High-Temperature

Metallurgical Processing, ed. by: J.-Y. Hwang et al., TMS (The Minerals, Metals & Materials Society), pp. 3-10, 2016.
49. D. Fan, Y. Mohassab, and H. Y. Sohn, "CFD Simulations of a Laboratory Flash Reactor Relevant to a Novel Flash Ironmaking Process," AISTech 2016 Proceedings, AIST, pp. 551-558, 2016.
50. Y. Mohassab, M. Elzohiery, and H. Y. Sohn, "Flash Reduction of Magnetite Concentrate Based on Partial Oxidation of Natural Gas Relevant to a Novel Ironmaking Process," AISTech 2016 Proceedings, AIST, pp. 713-722, 2016.
51. M. Elzohiery, D. Q. Fan, Y. Mohassab, and H. Y. Sohn, "Flash Ironmaking from Magnetite Concentrate in a Laboratory Reactor: Experimental and CFD Work," 8th International Symposium on High-Temperature Metallurgical Processing, pp. 3-10, 2017. DOI 10.1007/978-3-319-51340-9_1
52. D. Q. Fan, M. Elzohiery, Y. Mohassab, and H. Y. Sohn, "A CFD Based Algorithm for Kinetics Analysis of the Reduction of Hematite Concentrate by H2 + CO Mixtures in a Drop Tube Reactor," 8th International Symposium on High-Temperature Metallurgical Processing, pp. 61-70, 2017.
53. H. Y. Sohn, Y. Mohassab, M. Elzohiery, D.-Q Fan, and A. Abdelghany, "Status of the Development of Flash Ironmaking Technology," Applications of Process Engineering Principles in Materials Processing, Energy and Environmental Technologies: An EPD Symposium in Honor of Professor Ramana G. Reddy, pp. 15-23, 2017.
54. H. Y. Sohn, M. Elzohiery, D.-Q. Fan, and A. Abdelghany, "Development of a Flash Ironmaking Technology Based on Hydrogen or Natural Gas - Implications on Energy and Greenhouse Gas Emissions," in Proceedings of the 3rd World Congress on Mechanical, Chemical, and Material Engineering (MCM'17), Rome, Italy, June 9 – 10, 2017.
55. A. Abdelghany, D.-Q. Fan, M. Elzohiery, and H. Y. Sohn, "Flash Ironmaking from Magnetite Concentrate using a Large Scale Bench Reactor: Experimental and CFD Work," AISTech 2018 Proceedings, AIST, pp. 683-690, 2018.
56. A. Abdelghany, D.-Q. Fan, and H. Y. Sohn, "CFD Simulations of a Large Scale Bench Reactor Relevant to a Novel Flash Ironmaking Process," AISTech 2018 Proceedings, AIST, pp. 765-772, 2018.

Novel Flash Ironmaking Pilot Plant

Preliminary Design

Final Report

Project No. EE0005751

Prepared For:

AISI American Iron and Steel Institute

25 Massachusetts Avenue, Suite 800, Washington, DC 20001

Date: November 15, 2018

Novel Flash Ironmaking Pilot Plant Preliminary Design

Primary Contacts:

George Boy
Vice President – Engineering
Berry Metal Company
2408 Evans City Road
Harmony PA 16037 USA
Office: 724-453-1658
Cell: 412-445-4518
E-mail: gboy@berrymetal.com
Web Site: http://www.berrymetal.com

Ed Green
Principal Engineer
Berry Metal Company
2408 Evans City Road
Harmony PA 16037 USA
Office: 724-453-1617
Cell: 724-900-3374
E-mail: egreen@berrymetal.com
Web Site: http://www.berrymetal.com

Danyang Li
Design Engineer
Berry Metal Company
2408 Evans City Road
Harmony PA 16037 USA
Office: 724-452-8040 X678
E-mail: dli@berrymetal.com
Web Site: http://www.berrymetal.com

Submitted to:

Michael Sortwell
Senior Director Technology

REVISION HISTORY

Rev	By	Date	Description	Approved By	Approval. Date
0	**EJG**	**11/15/18**	**Final Issuance**	**GAB**	**11/15/18**

TABLE OF CONTENTS

INTRODUCTION

The project goal is to develop an entirely new transformational process for alternate ironmaking based on the direct gaseous reduction of iron oxide concentrates in a flash reduction process, with the ultimate objective of significantly increasing energy productivity and reducing environmental emissions, especially CO_2 emissions, versus the conventional blast furnace ironmaking route. The Novel Flash Ironmaking Process uses gaseous reducing agents, such as natural gas, hydrogen, other syngas, or a combination thereof.

The proposed technology is to be applied to the production of iron as a feedstock to the steelmaking process. The technology is particularly suited to EAF steelmakers by providing low-cost access to metallic iron. Metallic iron acts as a scrap supplement to dilute tramp elements (such as Cu, Ni, Sn) that cannot otherwise be processed out, enabling economical production of higher grades of steel and/or expansion of products. The highly metallized, low-acidic gangue iron produced can be traditionally charged or injected into the EAF furnace reducing raw material cost and increasing yield.

The Novel Flash Ironmaking Process eliminates the iron ore pelletizing and indurating steps removing the need for coke and coke ovens. It also overcomes issues with traditional direct reduction technologies by offering a lower-CAPEX (up to 10x less per ton), site-specific, and scalable alternative-iron solution to meet individual mill demands. This technology is especially appealing to stand alone specialty plants with geographic limitations on access to DRI or Pig Iron as the technology is suited to be located on-site thus eliminating additional barge/rail costs for merchant metallic substitutes. The technology also has the ability to use oxide fines (by-product of other ironmaking processes) as sole or blended feedstock and use byproducts and waste heat to minimize production cost.

The Novel Flash Ironmaking Process has the potential to offset and eventually replacing the blast furnace and other alternate ironmaking processes. The process can also be a part of a continuous direct steelmaking process.

BACKGROUND

One of the core technical problems facing the U.S. steel industry today is to develop a new technology to produce steel from iron ore. An ideal process would replace the blast furnace and coke oven; would use domestic iron ores especially concentrates which the US has in abundance; and would greatly reduce energy requirements. It should also be a high intensity process requiring much less capital investment than the blast furnace/coke oven combination, and must be capable of producing 5,000 – 10,000 tons of metal per day so that it can support existing steel mills.

The fundamental question regarding the feasibility of adapting the flash furnace to ironmaking concerns the speed of reaction, i.e. can iron oxide concentrates be completely reduced in the few seconds of residence time typically available in a flash furnace. Research performed under the AISI/DOE Technology Roadmap Program (DE-FC36-97ID13554) at the University of Utah using iron ore concentrates (~30 µm size) show that 90 – 99% reduction can be achieved within 2 – 7 seconds of residence time at temperatures of 1300°C or higher. This was verified by additional laboratory-scale testing. Thus, the question on whether the reduction rate of concentrate particles is fast enough for a flash reduction process was resolved conclusively in the affirmative.

The studies also established that because of the high temperature and lack of contact between the iron ore particles in flash furnaces, sticking and fusion of the particles is eliminated. Sticking is a crucial

problem that has beset other alternative ironmaking processes and eliminated them as a replacement for the blast furnace.

Additional large-scale laboratory tests supported by AISI under the CO_2 Breakthrough Program (2008-2011) included successful operation of an oxy-fuel burner as a supply source of both heat and reducing agent in an industrial operation. Detailed material and energy balances showed that Flash Ironmaking Technology can use any of the three possible reductants/fuels or combination thereof. A natural gas fired flash smelter will generate only 39% of the carbon dioxide of a blast furnace. CO_2 emissions using coal and hydrogen are 69% and 4%, respectively. The Flash Ironmaking Process also eliminates the iron ore pelletizing and indurating steps and, of course, eliminates the need for coke and coke ovens.

Once fully developed, the technology is to be applied to the production of iron as a feed to the steelmaking process, eventually replacing the blast furnace and other alternative ironmaking processes. The process can also be a part of a continuous direct steelmaking process.

General Engineering

Approach

Purpose of Pilot Plant

The pilot plant is the 1st look at a continuous process. It has significantly higher capital and operating costs than the lab scale reactors. It is used to test technologies that will be used on a larger scale. It is used to develop automation and controls for the larger scale. It is used to optimize operation and to gather data for economically scaling up to minimize capital and operating cost for commercial scale.

The purposes of the pilot plant are defined as:

a. Scaling factors
b. Reaction Kinetics
c. Chemical Equilibrium
d. Equipment material properties
e. Computational Fluid Dynamics
f. Thermodynamics
g. Equipment selection
h. Material handling
i. Yield
j. Reliability of equipment for larger scale

Goals of Pilot Plant

The goals of the pilot plant are defined as:

a. Final product properties in bulk and variation by lot
b. Product yield
c. Efficiency of system
d. Residence time
e. Particle size vs residence time and variability in final product vs residence time
f. Gas and utility usage
g. Additional chemical species formed in product and off-gas
h. Determine instrumentation critical to the process and for scaling
i. Process optimization (Sensitivity of various parameters to product yield and quality)
j. Gas and particle flow patterns, Identify dead spots and by-passes
k. Temperature profile of Reactor
l. Equipment material properties – Evaluate how they hold up to the heat

m. Equipment material properties – Evaluate susceptibility to corrosion
n. Powder injection efficiencies or deficiencies
o. Material handling issues
p. Effects of recirculation of hydrogen
q. Use of energy reduction and recovery strategies
r. Test finished product to determine the need for gas cover
s. Finished product degradation as powder in pile, as bricks, as powder sealed in bags
t. Refine control system requirements
u. Determine CO_2 emissions savings

Scaling Process

Bench Scale

The Bench Scale was a small drop tube furnace used by the University of Utah to perform early testing. It was a proof of concept batch type of process that used just a few hundred grams per batch. The main reactor uses the drop tube for a design basis.

Laboratory scale and Large-Scale Bench Reactor (LSBR)

The Laboratory Scale was a short fat batch type reactor capable of 5 kg/hour. Testing was performed by the University of Utah and lessons learned from this testing were incorporated into the main reactor.

Sizing

The size of the pilot plant needs to be large enough to gather sufficient information to meet the goals and purpose, but small enough to be able to cost effectively modify components as needed and change the operating profiles to find operating efficiencies. In order to determine the appropriate size of the pilot plant, research was conducted to determine the sizes of other pilot plants and the success of those programs per the table below:

Company or Program	Pilot Plant Size in tpy	Demonstration Plant size - tpy
Midrex DRI		80,000
HYL DRI	18,250*	25,000
ITmk3	3,000*	25,000
Fastmet	1,400	16,000
Circored	175**	
SIIL		30,000
Jindal	15,000	
Kawasaki SR	3,650	
HIsmelt	12,000/100,000	800,000

*Did not meet design expectations

**Lab scale

The team considered 3 pilot plant sizes

- Modify the current LSBR to 86 tpy, (current capability if it was 24/7 is 43 tpy)
- Pilot Plant 5,000 to 10,000 tpy
- Demonstration Plant 50,000 to 100,000 tpy

Going straight to the demonstration plant was ruled out after reviewing the Circored experience. Circored went from lab scale of 175 tpy straight to commercial 800,000 tpy and failed due to lack of knowledge that would have been gained from a pilot plant. Pros and cons for the other two size plants were evaluated below.

Plant size 86 tpy – redesign the existing reactor to be a continuous operation

Pros

1. Re-purpose some components
2. Off the shelf components
3. (Local) industrial test
4. Quick modification of process experiments
5. Reduced manpower Est. 11-13
6. Simplified Permit process

Cons

1. Limited Production Capacity
2. Known design issues with existing reactor
3. Cannot gather all the data required
4. May not show operating issues

Plant size 5,000 to 10,000 tpy – use lessons learned from the LSBR to optimize a continuous design operation

Pros

1. Can gather all of the data required
2. Modular design established for Reactor
3. Sufficient product to run industrial test
4. Limited total discharge permit
5. Most of equipment procurable from industrial suppliers

Cons

1. Slower to run experimental options
2. Formal Permit process
3. Est. Manpower 25-30

The team started down the path of 10,000 tpy but at the project meeting it was felt that 10,000 tpy was too much of a jump than the 5 to 10 X rule of thumb. The rule of thumb shows that failure rates increase dramatically when a new process or equipment is larger than 5 to 10 times the largest successfully operating process or equipment. If the current reactor were operated 24/7 it would produce 44 tpy. The next size by rule of thumb would be 440 tpy. BMC evaluated how much smaller the current system could be sized to still meet the goals and purposes of the pilot plant previously defined. One of the concepts that needs to be proven with this plant is the 'particle curtain' discussed in detail later. It is intended to use two parallel particle curtains in a rectangular shaft to maintain even heating of the particles. For a 10,000 tpy reactor these particle curtains would be 3.3 meters long. When shortened to reduce the scale it was felt that 1 meter long particle curtains were as short as could be operated without the operation being skewed with end effects on the curtain. Two parallel one-meter long particle curtains scale to use 3,000 tpy. Another rule of thumb exists for sizing continuous operation vs. batch feed. A .1 kg/sec should be batch operation and .1 kg/sec or above should switch to continuous operation. The .1 kg/sec feed rate scales to be 3,000 tpy. The size of the pilot plant will be 3,000 tpy.

The proposed site for the pilot plant is Natural Resource Research Institute (NRRI) Laboratory in Coleraine Minnesota. The site is located near the Minnesota iron range and positioned to receive material from several different mines. The laboratory's mission is to transition ideas and concepts from academia to industry. They have several pilot plants on site including an iron reducing pilot plant and they have staff with significant knowledge in the iron making processes. They also have skilled labor to operate a pilot plant during the testing phase.

Overview of Flash Iron

Chemistry & Phase diagrams

There are two main processes to reduce iron oxide

Reduction by hydrogen

1. $3Fe_2O_3 + H_2 = 2Fe_3O_4 + H_2O$
2. $Fe_3O_4 + H_2 = 3FeO + H_2O$
3. $Fe_{.947}O + H_2 = .947Fe + H_2O$

Reduction by carbon monoxide

1. $3Fe_2O_3 + CO = 2Fe_3O_4 + CO_2$
2. $Fe_3O_4 + CO = 3FeO + CO_2$
3. $Fe_{.947}O + CO = .947Fe + CO_2$

At the proposed operating temperatures (1150 to 1350°C) using CO is much slower than hydrogen and very limited by equilibrium. The graph below shows this.

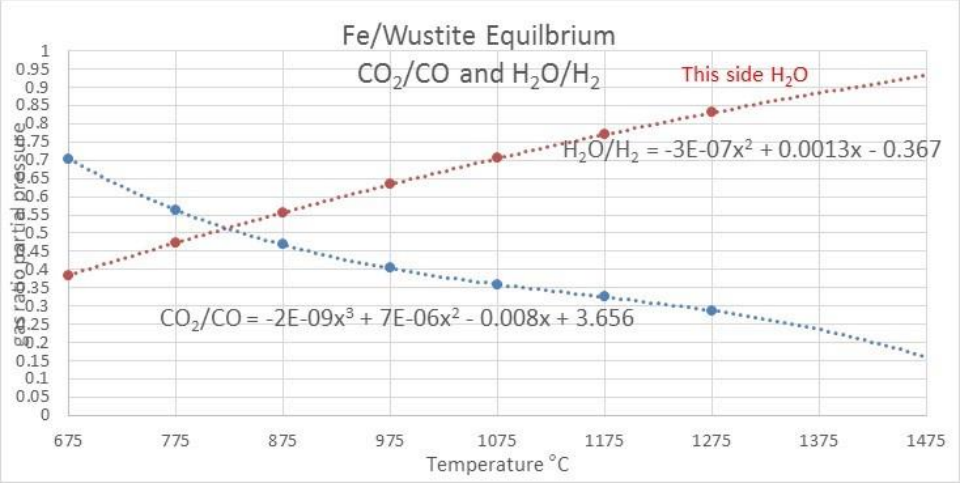

The main reactor for this pilot plant will use 100% hydrogen as CO uses more energy in heating, is not very effective at operating temperature, reacts too slowly to be useful and can cause carbon deposition in the reactor.

An iron phase diagram below shows the melting point of FeO to be 1380°C. FeO in a liquid form will react with the refractory and/or it will stick to anything in comes in contact with. Once this material is anchored, the thermal growth differential creates micro spalls creating additional imperfections and

acceleration of the mechanical wear of the refractory. It has been decided this project will stay below the melting point of the material to prevent this. 1325°C has been picked as the highest operating temperature that the reactor will operate although it will be designed to withstand 1400°C.

Iron Oxide Phase Diagram

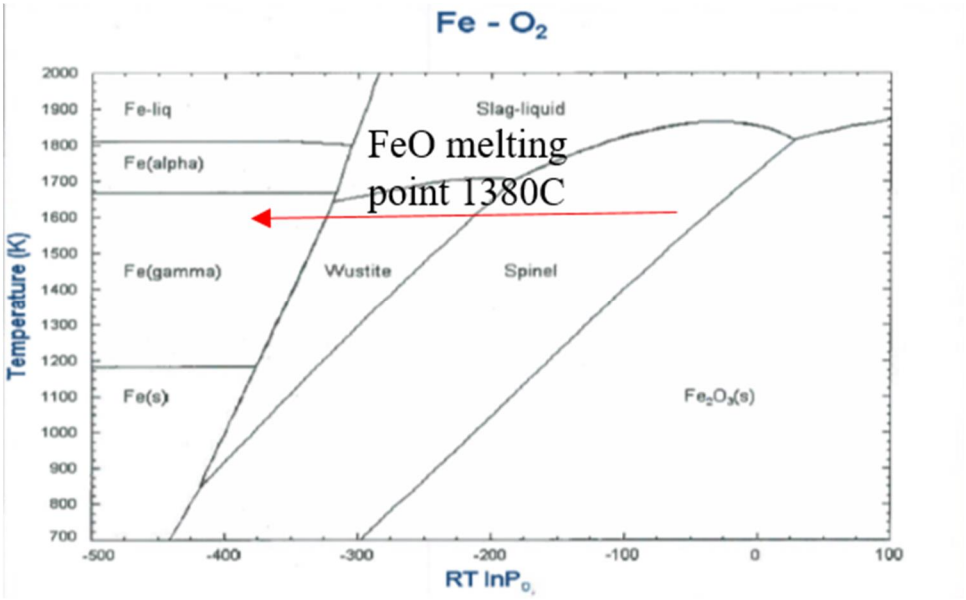

General Basis of Design

General philosophy guiding the design of the overall system is as follows:

- The magnetite concentrate is a very fine powder and when it is dry it becomes airborne easily. The concentrate is kept wet as far into the process as practical to prevent airborne yield loss before it enters the reactor.
- Minimize acid gangue content of magnetite concentrate. The concentrate that is readily available is generally not DR-Grade (low acid gangue). The main purpose of the pilot plant is to prove out greater than 95% metallization when scaled up however, proving the process material that has low acid gangue is an important marketing topic for commercialization.
- When the concentrate is dried, the maximum moisture content is to be less than 1% to prevent powder plugging.
- The target moisture into the reactor is less than 0.5% to reduce H_2O ingress into the reactor. Want to minimize H_2O as it slows and limits the reduction reaction. High moisture content requires more hydrogen to overcome the equilibrium point and therefore more energy is used to heat the process.
- Iron particles can fuse together above 600°C. Particles should be airborne in a dilute flow whenever they are above 600°C.
- Particle preheat temperature should be limited to less than 600°C to prevent particle agglomeration. Hydrogen is present in the preheater which can cause iron oxide to reduce to iron.
- Particles should be cooled below 600°C while airborne to prevent agglomeration.
- Target cooling particles below 400°C to prevent reoxidation. Reoxidation 400°C to 600°C will take 10's of minutes.
- Recycle unused hydrogen.
- Finished iron product should be protected from exposure to water vapor or oxygen in atmosphere to prevent reoxidation or fire.
- When the powder is falling in the reactor, want to control the particle path to prevent particle contact with the walls as the particles might stick.
- This project is targeting to drop the particles in a curtain to prevent contact with walls. Particle curtain is dilute flow to prevent collisions and to prevent gas entrainment that can cause vortexes eddy distorting the flow.
- Gas is laminar flow in the reactor to prevent vortexes that will distort the particle curtain. Minimize flow distortion in the reactor.
- Maintain particles Stokes number $Stk<<1$ so the particles follow the streamlines.
- Minimize or avoid Karman Street Vortex in the reactor.
- Optimization - minimize hydrogen to reduce energy consumption.
- Optimization – maximize particle density in curtain to increase throughput. May need to increase hydrogen flow and / or hydrogen pressure for reactions to occur.
- Optimization – minimize operating temperature while still reacting within residence time to reduce energy consumption.
- Optimization – minimize heat required to maintain reaction. The reaction is endothermic and the temperature can drop several hundred degrees during the reaction which may slow or stop the reaction.
- The baseline mass flow into the reactor is .0925 kg/s of dry concentrate with .007 kg/sec of hydrogen.

- The inject particles should form a particle curtain for even heating and processing.
- Maximum particle temperature should not exceed 1350°C because gangue materials will start to melt. This melted outer layer slows the reaction and reduces metallization.
- Minimize carbon introduced into reactor. CO is very inefficient at the high temperatures, at 1325°C need 10 times excess CO due to low equilibrium. As the excess CO cools, some reacts as $2CO = C + CO_2$ which can create carbon deposits downstream. Also unable to recycle and reuse the CO if it has been converted.
- Minimize yield loss when separating the finished iron particles from the exhaust gas. LSBR experiments had very high yield loss in the exhaust.
- Convert natural gas to hydrogen via steam methane reformer with water shift reactor. At the operating temperature in situ reforming uses more energy than external reforming.

STANDARDS AND SPECIFICATIONS – MASTER LIST

All product specifications, assemblies and installations are to comply with current recognized published standards and best practices as a minimum standard. The following is a list of typical standards. The IBC/Minnesota State Building Code and Standards supersede where products and installation are covered under the code. ASTM, ANSI, NFPA, UL, and FM compliance are to be specified when they exceed other standards.

AAMA – Association of Architectural Metals Manufacturers

AAMA – American Architectural Manufacturers Association

AABC – Associated Air Balance Council

ACA – American Correctional Association

ACI – American Concrete Institute

ACI 350, Code Requirements for Environmental Engineering Structures, Latest Edition.

ACI 318, Building Code Requirements for Structural Concrete, Latest Edition.

ACI 530, Building Code Requirements for Masonry Structures, Latest Edition.

AISC – American Institute of Steel Construction

AISI – American Iron and Steel Institute

ALSC – American Lumber Society

AMCA – Air Movement Control Association

ANSI – American National Standards Institute

ANSI/TIA/EIA – Electronic Industries Association/Telecommunications Industry Association (EIA/TIA)

Commercial Building Standard for Telecommunication Pathways and Spaces (No. 568)

ANSI/ISA 18.2 Management of Alarm Systems for the Process Industries

APA – American Plywood Association

API – American Petroleum Institute

ARI – Air Conditioning and Refrigeration Institute

ASHRAE – American Society of Heating, Refrigeration and Air Conditioning Engineering

ASCE – American Society of Civil Engineers 7-10, Minimum Design Loads for Buildings and Other Structures.

ASME – American Society of Mechanical Engineers (Standards)

ASME B16.5 Pipe Flanges and Flanged Fittings

ASME B31.3 Process Piping

ASME B31.12 Hydrogen Piping and Pipelines

ASME Boiler and Pressure Vessel Code Section IX

ASME B31.8 Gas Transmission and Distribution Piping Systems – Natural Gas Service

ASSE – American Society of Safety Engineers

ASTM – American Society of Testing Materials

AWI – American Woodworkers Institute

AWS – American Welding Society

AWWA – American Water Works Association

CISPI – Cast Iron Soil Pipe Institute

EIA – Electronics Industries Association

ETL – Electrical Testing Laboratory

ETL – Electro Technical Laboratory

FCC – Federal Communications Commission (EMI -Electromagnetic Interference emission Standards)

FCI – Fluid Controls Institute

FM – Factory Mutual 7

FS – Federal Specification / Military Specification / DOD- Department of Defense Specification

GA – Gypsum Association

GANA – Glass Association of North America

HI – Hydraulic Institute

IBC – International Building Code

ICEA – Insulated Cable Engineers Association

IEC 61131-3 Standard PLC Function Block Programming

IEEE – Institute of Electrical and Electronic Engineers

IES – Illuminating Engineering Society

IES – Institute for Environment and Sustainability

IFC – International Fire Code

IPCEA – Insulated Power Cable Engineers Association

ISA – Instrument Society of America

ISO – International Standards Organization

MNDOT – Minnesota Department of Transportation (Standard Specifications for Construction)

ML&PB – Minnesota Lathing & Plaster Bureau

MSS – Manufacturers Standardization Society

NAAMM – National Association of Architectural Metal Manufacturers: NAAMM Standard SW-1

NAIMA – North American Insulation Manufacturers Association

NCMA – National Concrete Masonry Association: NCMA-TEK

NCPWB – National Certified Pipe Welding Bureau

NEBB – National Environmental Balancing Bureau

NEC – Nation Electric Code (NEC, NFPA-70)

NECA – National Electrical Contractors Association

NEMA – National Electrical Manufacturers Association

NICET – National Institute for Certification in Engineering Technologies

NFPA – National Fire Protection Association

NFPA 101 Life Safety Code

NFPA 70E Standard for Electrical Safety in the Workplace

NFPA 497 Recommended Practice for the Classification of Flammable Liquids, Gases or Vapors and of Hazardous (Classified) Locations for Electrical Installations in Chemical Process Areas

NFPA 499 Recommended Practice for the Classification of Combustible Dusts and of Hazardous (Classified) Locations for Electrical Installations in Chemical Process Areas

NPCA – National Paint and Coatings Association

NRCA – National Roofing Contractors Association: Roofing and Waterproofing Manual

NRTL – Nationally Recognized Testing Laboratory Listing and Labeling

OSHA – Occupational Safety and Health Administration

PCI – Precast/Prestressed Concrete Institute

PDI – Plumbing and Drainage Institute

SDI – Steel Deck Institute

SDI – Steel Door Institute

SJI – Steel Joist Institute

SMACNA – Sheet Metal and Air Conditioning Contractors' National Association: SMACNA Architectural Sheet Metal Manual

SSPC – Steel Structures Painting Council (The Society for Protective Coatings)

SSPMA – Sump and Sewage Pipe Manufacturers Association

TEMA – Tubular Exchanger Manufacturers Association

TCA – Tile Contractors Association UL- Underwriters Laboratory

UL – Underwriters Laboratory

USASI – United States of America Standards Institute Warnock-Hersey

Minnesota State Fire Code 2007, Chapter 7511

Minnesota State Mechanical and Fuel Gas Code 2015, Chapter 1346

Minnesota State Accessibility Code 2015, Chapter 1341

Minnesota Building Code, 2016, Chapter 1305

Minnesota State Building Conservation Code, 2015, Chapter 1311

Minnesota State Plumbing Code 2015, Chapter 4715

PROCESS ENGINEERING

PROCESS DESIGN CRITERIA

General

Equipment and machinery shall be provided so that the plant can operate for at least two years without major overhaul or inspection.

Nominal Indoor Environmental Conditions	
Atmospheric Pressure	14.696 psia
Temperature	50°F
Relative Humidity	70%
Seismic	Zone 0

Nominal Outdoor Environmental Conditions	
Atmospheric Pressure	14.696 psia
Temperature	85°F/-20°F
Relative Humidity	70%
Wind Load Nominal	93 mph
Wind Load Ultimate	120 mph
Seismic	Zone 0
Ground Snow	60 psf
Roof Snow	42 psf
Roof Live Load	20 psf

Design Temperature

The design temperature is typically 25°F above the operating temperature and shall not be lower than the maximum operating temperature. Design temperature for the Particle Preheater, Main Reactor, Ruffle Fin Panel Cooler and Cyclone Separator shall be at least 50°F above the nominal operating temperature. Design minimum temperature shall be specified if the minimum operating temperature is

below 35°F. The minimum design temperature shall be at least 9°F less than minimum operating temperature. The HAZOP analysis performed in Detail Design will set final the Design Temperature.

Design Pressure

Malfunction and equipment failure shall be protected by safety relief devices or be designed for explosion proof. Maximum deflagration pressure for hydrogen is 10 bar. The design pressure is typically 30 psi or 10% (whichever is greater) above maximum operating pressure. The HAZOP analysis performed in Detail Design will set the final Design Pressure.

Flanges and Gaskets

All hydrogen flanges shall be a minimum of Class 300 size and gaskets for hydrogen service shall be Flexitallic.

Equipment on the Discharge of a Pump

Equipment which may have to bear the shut-off pressure of a pump shall have a design pressure equal to or higher than the shut-off pressure.

Thin-walled Tanks and Vessels

Atmospheric thin-walled tanks and vessels shall have a design pressure equal to the highest pressure imposed upon discharge of the pressure relief device.

Corrosion Allowance

Materials of construction and corrosion allowance for all equipment and machinery shall be for a design life of 20 years.

However, minimum corrosion allowance shall be for carbon steel (including .5 Mo alloy steels):

- Pressure vessels and other applicable equipment 0.125”
- Storage tanks 0.062”
- Piping 0.062”
- Removable parts or internals in contact with operating fluid 0.030”
- For stainless steel/titanium/aluminum 0.000”
- Carbon steel with epoxy resin coating 0.125”

Heat Exchangers

In general heat exchangers shall be designed to 110% of their operating duty.

Columns & overhead coolers shall be designed to 120% of their operating duty.

Large heat exchangers shall be split into two or more shells for easy operation and maintenance.

Pumps

Normally pumps shall be designed to 110% of their maximum required flow rate in worst case of operation.

The shut-off pressure shall be estimated according to the following criteria whichever is higher:

- Differential head at rated flow x 120% + LH (level high) suction static head + max operating pressure suction side.
- Differential head of pump at rated flow + LHH (level high high) suction static head + design pressure suction side x 120%

No overdesign shall be applied to the rated pressure.

Compressors

In general, compressors shall be designed to a minimum of 110% of their maximum required flow.

Pressure Relief Valves

Pressure relief valves shall be supplied with locked open isolating valves.

The set pressure of pressure relief valve shall be equal to or less than the design pressure.

Vent and Drain

All vessels will have a vent and drain.

The piping system will have a vent at all highest locations.

The piping system will have a drain at all lowest locations.

Hand hole or Inspection Hole

Preferable size 8".

Minimum size 6".

Storage and Bulk Handling Equipment

General Requirements & Safety Measures - The system shall be designed for personnel and environmental safety, minimization of spillage, prevention of material degradation in handling and storage, simplicity in operation and maintenance, safety during operation and failure.

Bulk Storage

- Easy to store and empty
- Material is protected from environmental effects
- Capacity is enough for smooth operation of plant for a justifiable agreed time
- Storage method will reduce the potential for explosion and ideally nullify the chance
- The storage medium is accessible and maintenance can be carried out inside when necessary
- Material entry and exit will not cause clogging in normal operating conditions. Valves such as ball and plug type should be avoided, the preference is gate type or butterfly valves.

Metallic bins and silos when used shall be made of graded steel to avoid erosion as well as internal and external corrosion.

Stored material level shall be continuously monitored through a well-established level measurement method to avoid overflow or running out of stock.

When vessels are used for storing, the construction shall be designed stiff enough to avoid vibration during filling and emptying.

Static charge accumulation shall be prevented on the storage mediums.

Storage bins and hoppers shall be designed to operate in mass flow mode to avoid ratholing/piping, slow flow, arching/bridging, incomplete emptying, segregation and caking.

The bulk material filling and emptying to and from the storage medium shall preferably be carried out through a transfer system such as an apron, belt, air slide, enclosed screw, drag chain, etc. conveyor systems.

The material flow shall be such that no spillage occurs during transfer.

Limit switches of preferably proximity type shall be employed on the transfer link.

The rotating components shall be well guarded, for protection of the mechanism and staff.

Material and construction of the transfer system components shall have previous successful service history.

A local starter panel with all central gear should be provided with a view to the transport system for local operation.

Automatic weighing and packing – Where end product weighing and packing occur the weighing type shall be electronic.

Provisions shall be made for local viewing as well as remote transfer of the weigh scale readouts as a compatible signal to the plant.

The weighing and packing system shall be interconnected with the transfer chain so that failure of either one will automatically stop the other.

The weighing and packing loop shall be a clog free design so that material will flow easily. Any abnormalities in material flow should be detected and alarmed. In severe cases this should be able to stop the transfer chain and the weighing and packing loop.

BLOCK FLOW DIAGRAM

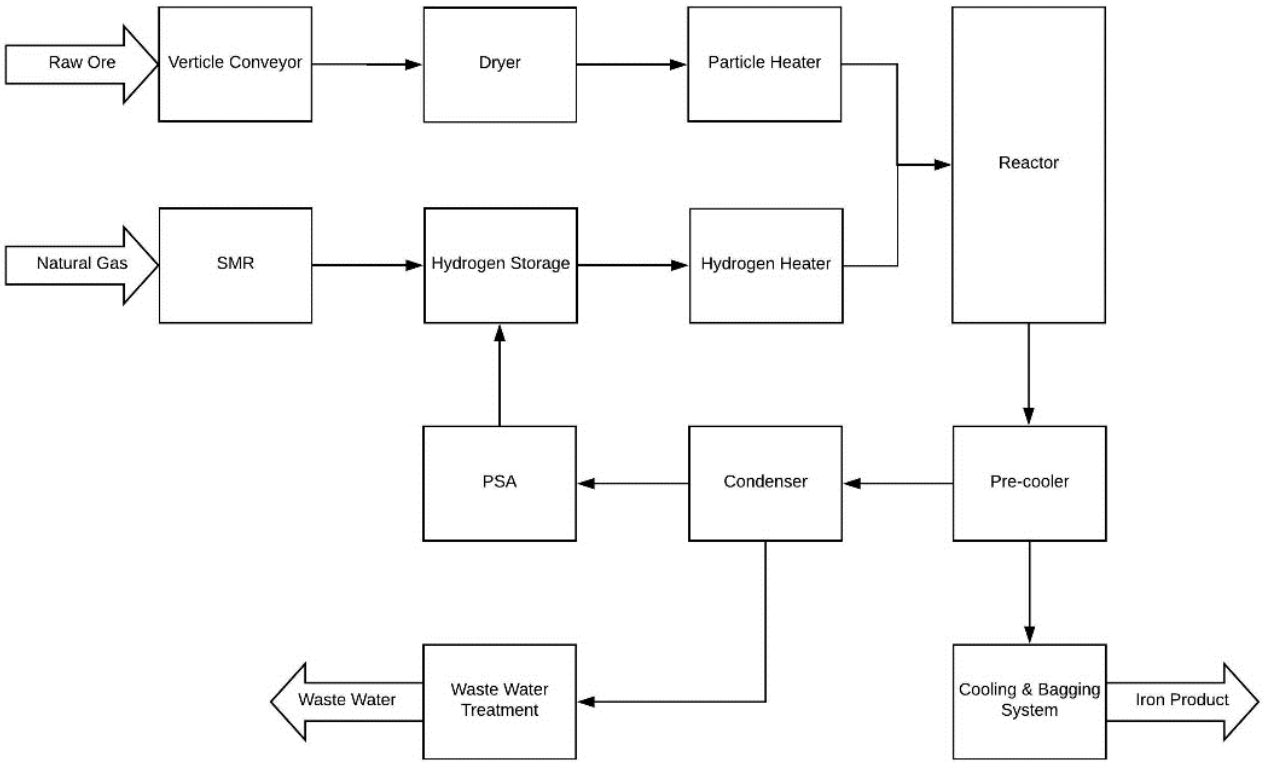

Process Flow Diagram

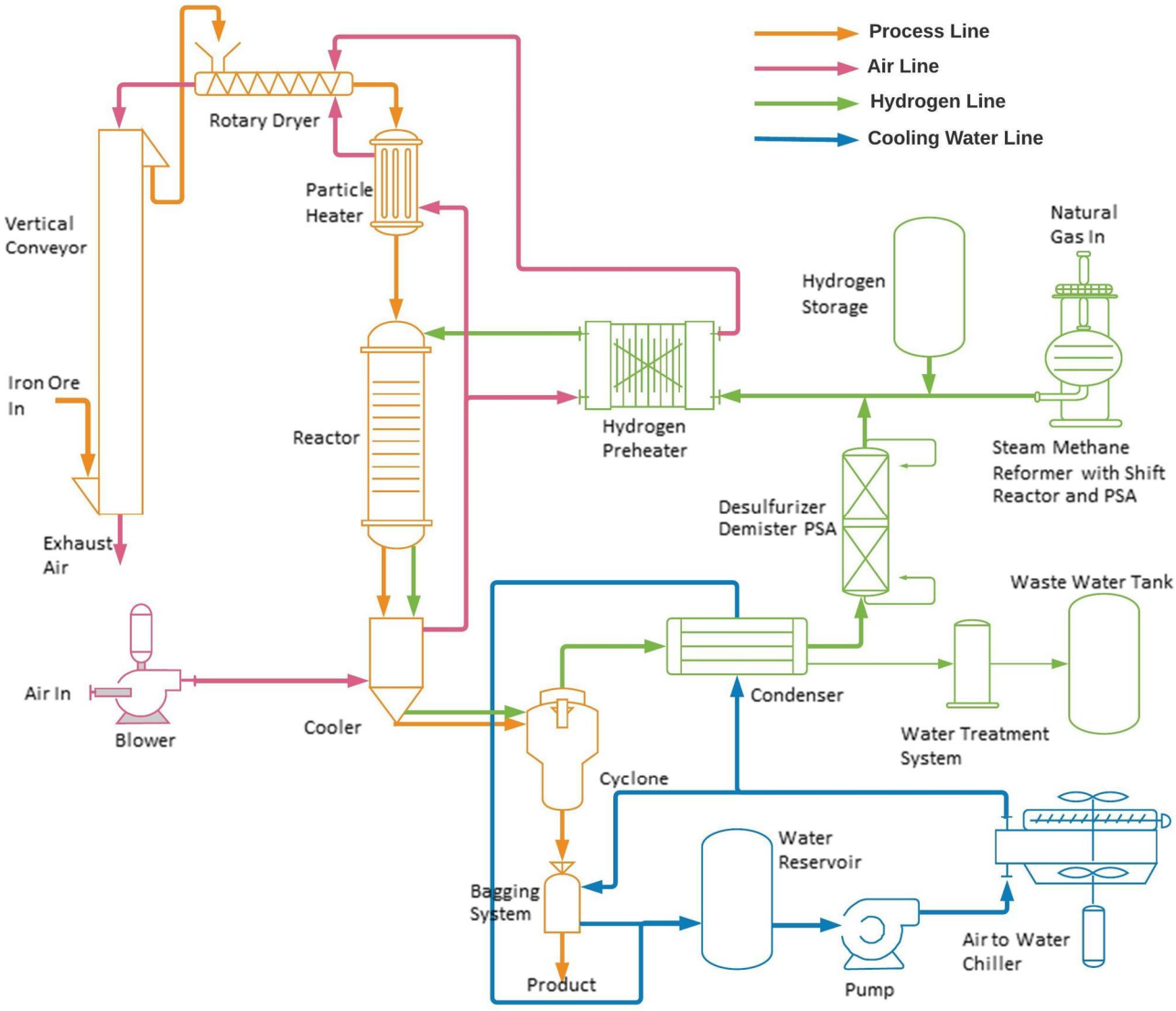

PLANT PROCESS AREAS

Pilot Plant Process Area Codes (PPA)	
010	Conveyor Feed Hopper
020	Elevator
030	Dryer Hopper
040	Rotary Dryer
050	Dryer Outlet Hopper
060	Reactor Feed Lock Hopper
070	Powder Heating & Reactor Feed Hopper
080	Reactor Induction/Resistance Heating
090	Reactor Cooler
100	Cyclone Separator
110	Bagger/Palletizer
120	Condenser
130	Hydrogen Recovery Skid
140	Waste Water Treatment
150	Air Compressor Handling Skid
160	Chiller
170	Nitrogen Purge Station
180	Cyclone Separator Lock Hopper
190	Steam Methane Reformer
200	Hydrogen Storage
210	Boiler Feed Water Treatment Skid
220	Utility Air
230	Safety Control System/Fire Suppression
240	Cooling Water Pump Skid
250	Motor Control Center
260	Feed Gas Compressor Skid
270	Hydrogen Preheater
280	Gas Sampling System

MATERIAL AND ENERGY BALANCE

MATERIAL

The Flash Iron Process is a Direct Reduced Iron (DRI) process. It is utilized to dilute the residual elements contained in scrap and as a scrap replacement. For the pilot plant it is intended to process DR Grade wet magnetite concentrate in the 5 to 50 micron size range into DRI. The finished product may be bagged, used as a powder injected directly into a furnace, or it may be processed into HBI (Hot Bricked Iron) or CBI (Cold Bricked Iron) for ease of shipping and handling. The goal is to convert the iron ore to > 95% metallization.

DR Grade Pellet or Concentrate Quality

The direct reduction process is the removal of oxygen from the iron ore without reaching the melting point. Most of the impurities that are in the ore remain in the final product except the concentration is increased due to the removal of oxygen. One exception to this is 60% to 70% of Sulphur is removed in a hydrogen reduction atmosphere, the S becomes H_2S and is removed from the product. The impurities that are in the DRI affect the economics of the EAF or BOF melting process.

Required Chemical Properties

The Fe total iron content is to be >67% with minimal gangue, moisture, and other residual elements

SiO_2, Al_2O_3 and TiO_2 are considered to be acid gangue. The industry prefers to have <2% acid content but will accept <3%.

CaO and MgO are basic oxides. Basic oxides <3% displace purchased flux in steel making

Typical Merchant DR Pellet Chemical Properties								
Chemistry %	AMMC BBS	Samarco	LKAB KPRS	VALE Tubarao	VALE Oman	IOC Standard Acid	IOC Low Silica	CAP Chile
Fe	67.70	67.90	67.90	67.75	67.75	68.00	67.00	67.33
SiO2	1.60	1.23	0.75	1.40	1.04	1.20		1.40
Al2O3	0.40	0.49	0.16	0.55	0.55	0.45	.3	0.23
TiO2	0.15	0.04	0.16	-	-	0.04		0.10
Mn	0.03	0.04	0.06	0.10	-	0.12		-
P	0.010	0.053	0.025	0.035	0.030	0.007	.007	0.033
S	0.002	0.002	0.002	0.007	0.003	0.003		0.005
V	0.005	0.003	0.110	-	-	<0.01		-
Cu	0.0002	0.003	0.001	-	-	<0.001		-
Pb	0.001	0.05	-	-	-	<0.002		-
Zn	0.0015	0.002	0.004	-	-	<0.002		-
Cr	0.018	0.05	0.002	-	-	0.012		-

For the Flash Iron Pilot Plant project the economics demand acquiring ore within trucking distance of the plant. The North American mines that currently produce DR Grade Pellets are below. It is expected that truckloads of wet DR Grade concentrate will be able to be acquired from these sources although wet concentrate is not currently marketed.

- Cliffs Northshore – 2.6 mtpy. Future will be captive.
- ArcelorMittal Mines Canada – capacity 10.2 mtpy
- Rio Tinto Iron Ore (IOC) – capacity 12.5 mtpy
- Ambershaw Metallics Canada – start up
- Chippewa Capital Prtns. formerly Essar Minnesota – 2.4 mtpy. Not expected back online until 2020

To increase potential suppliers it may be possible to acquire wet BF Grade concentrate ore from the following suppliers and final process it at the Flash Iron Plant by grinding / performing a Reverse Flotation.

- U. S. Steel MinTac
- U. S. Steel KeeTac
- ArcelorMittal Minorca
- Hibbing Taconite
- United Taconite

The world DRI pellet market is still limited and it is reported sintering ore fines are currently in oversupply. Other available material is DRI byproduct fines that are created when shipping and handling DRI. There is significant yield loss in the industry when handling DRI and the ore fines that are generated are currently a waste byproduct. The flash ironmaking process should be able to process these fines as an economical solution to recover yield loss. The major costs involved for reprocessing these fines is shipping and grinding to size before processing.

Typical Chemistry of DRI					
%	**Midrex DRI**	**Hyl HBI**	**Iron Carbide**	**Pig Iron**	**Flash Iron**
Total Fe	90-94	91-93	87	91.0-95.7	95.8
Metallic Fe	83-89	83-88	2.5	91.0-95.7	92.0
Fe_3C			69.8		
FeO/Fe_3O_4	6-14	6-13	20.2		3.8
% Metallization	88-96	92-95		100	96
Silica (SiO_2)	1.5-2.5	1.5-2.5			2.5
Silicon (Si)			1.5	0.3-3.0	
Alumina (Al_2O_3)	0.4-1.5	0.4-1.5	1.0		0.18
Mn				0.4-1.0	
P	0.02-0.09	0.02-0.05	0.033	0.08-0.5	0.014
S	0.005-0.03	0.002-0.02	<0.01	Max 0.04	0.009
CaO	1.5	0.3-1.8			0.37

MgO	0.45	0.5-1.8			0.18
Carbon	1-2.5	1.2-2.2		3.5-4.5	0.33

The table above compares commercial DRI final chemistry to Flash Iron. The Flash Iron chemistry is taken from a single sample and is dependent on the gangue content from the mine it is acquired from. From the single sample it appears the Flash Iron Process produces material with chemistry equivalent or better than the other DRI processes. From the table it can be seen percent metallization for Flash Iron is expected to be greater than 95% and metallic Fe 92% which is equal to or better than Midrex DRI or Hyl HBI. The FeO content of the Flash Iron material is also lower than Midrex, HYL or Iron Carbide. The SiO_2 is at the high end of Midrex and Hyl but the Al_2O_3 is well below them. CaO, MgO and C are all less than Midrex and HYL, slightly higher percentages are preferred.

ECONOMICS OF DRI

Flash Iron Powder and to a much lesser extent HBI are subject to oxidation. Shipping the raw ore fines is fairly easy and inexpensive. Shipping iron fines and HBI can be done but requires special regulations and controls. The Flash Iron Powder must be stored indoors to prevent moisture ingress that can cause oxidation or fire and it must be protected from air to prevent oxidation.

The chemical composition of the DRI determines important factors as yield, slag weight, energy consumption, carbon and raw material feeding rates, and oxygen usage.

The metallization percentage is important to know so the steelmaker can determine the quantity of FeO. Carbon is added or injected to final reduce the remaining FeO to Fe through the chemical reaction

$$FeO + C = Fe + CO$$

Approximately 1% C is required to balance out 6% FeO.

Gangue content in DRI is an often cited reason by steelmakers reluctance to use it in the EAF or BOF. Gangue consists of both acidic and basic components. The biggest concern with gangue materials is that they require additional lime and dolomitic lime additions in order to maintain a specific target basicity in the slag. The additional flux adds cost of material, consumes energy within the process, and increase yield loss. Failure to add sufficient basic oxides results in poor foaming and excessive refractory erosion.

It is a goal to reduce the SiO_2 percentage in the Flash Iron process. This can easily be done by using ore imported from one of the companies in the previous table with SiO_2 content averaging 1%. It may also be possible to reduce the SiO_2 by Reverse Flotation at the Flash Iron Plant before processing. The economic balance between cost of the ore, penalty of higher SiO_2 and sale price of higher grade steel can be done to determine the most optimized process.

PILOT PLANT MATERIAL & ENERGY BALANCE DIAGRAM

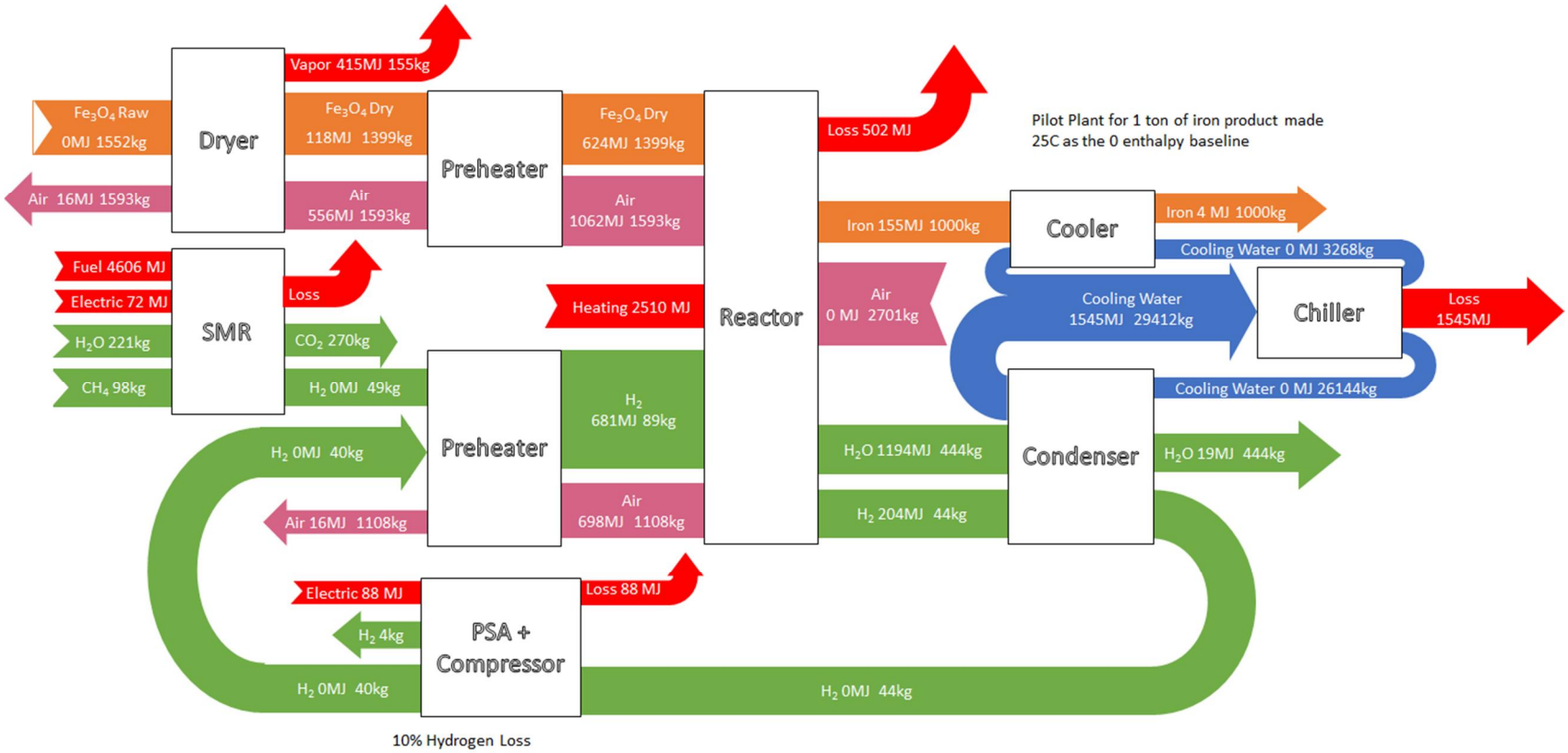

The loss from SMR is to be determined.

COMMERCIAL SCALE PLANT MATERIAL & ENERGY BALANCE DIAGRAM

The difference between pilot plant and commercial scale plant is the SMR system. In the commercial scale system, SMR efficiency of 80% is assumed, energy input is included in the CH_4 mass.

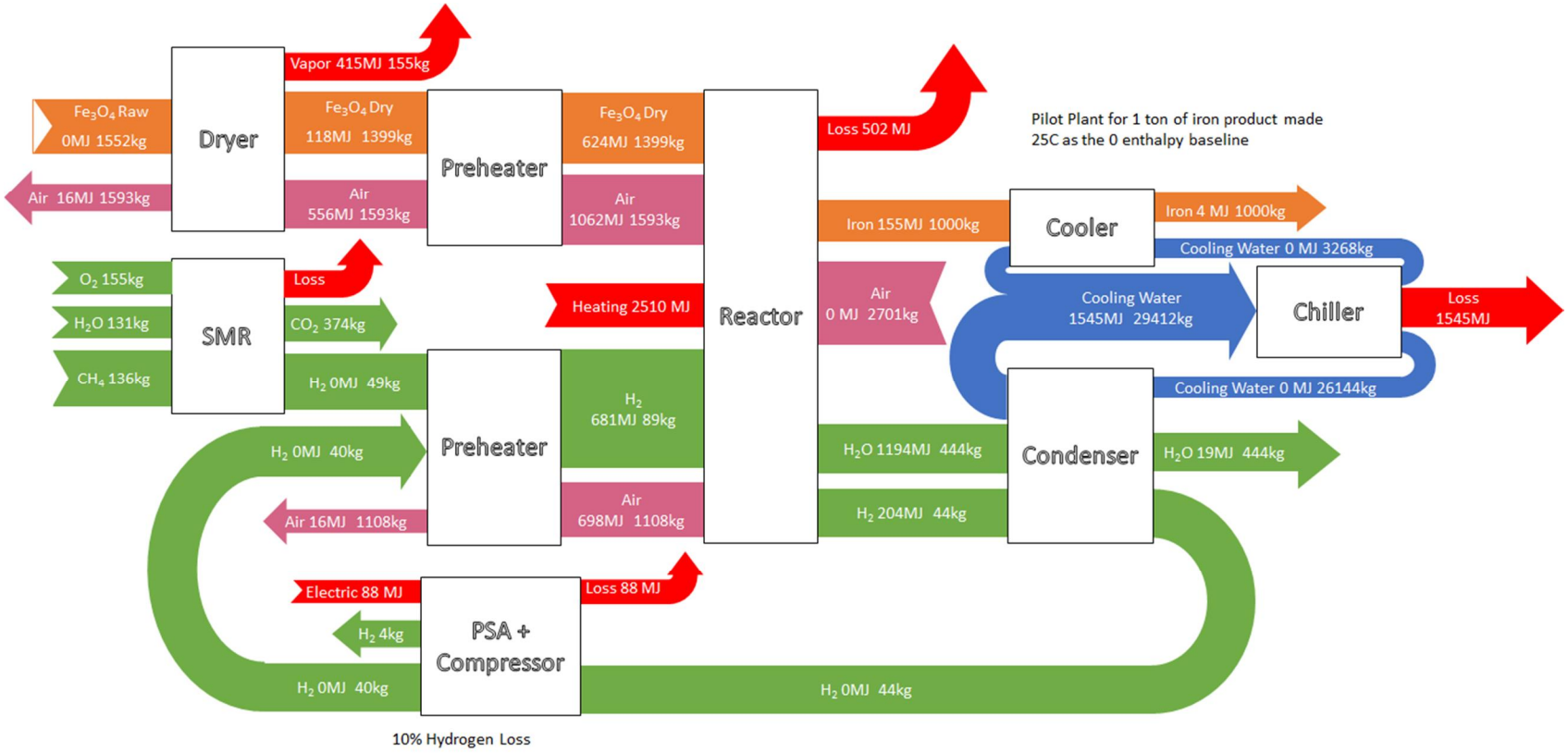

PROCESS STUDY - CFD ANALYSIS

LAB SCALE MODEL

PURPOSE OF EXPERIMENT

The lab scale model mimics the drop tube experiment conducted by University of Utah. The goal of this experiment is to validate the capability of simulating a flash iron making process in Ansys Fluent, and to tune parameters such as pre-exponential number, so that the model predicts similar residence time and reduction rate as experiment. Industrial scale model relies on these parameters for better predicting results.

PHYSICAL MODEL AND MESH INFORMATION

The lab scale model was constructed based on dimensions of the experimental test stand in University of Utah.

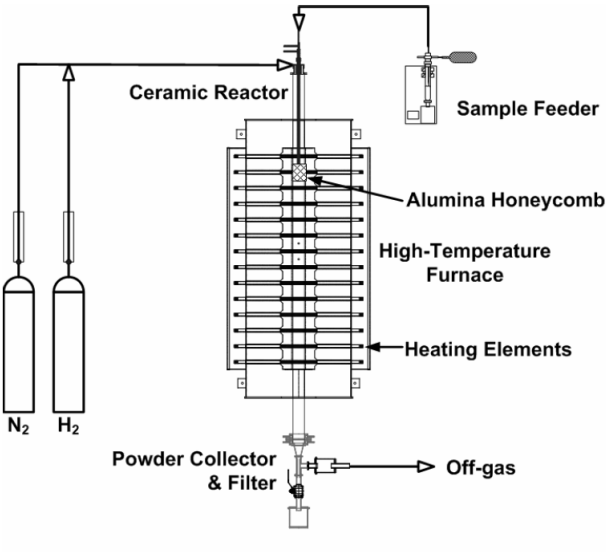

The model simulates the section after the alumina honeycomb where hydrogen and iron ore particles are heated to temperature. The reaction tube is 193cm long, with a 5.6cm I.D., ~80cm heating zone and 1 meter measured reaction zone. The particle inlet diameter is 1.2mm. Particles are purged by high pressure nitrogen in the reaction tube. A high temperature mixture of hydrogen and nitrogen gases enter the reaction tube around the particle inlet tube.

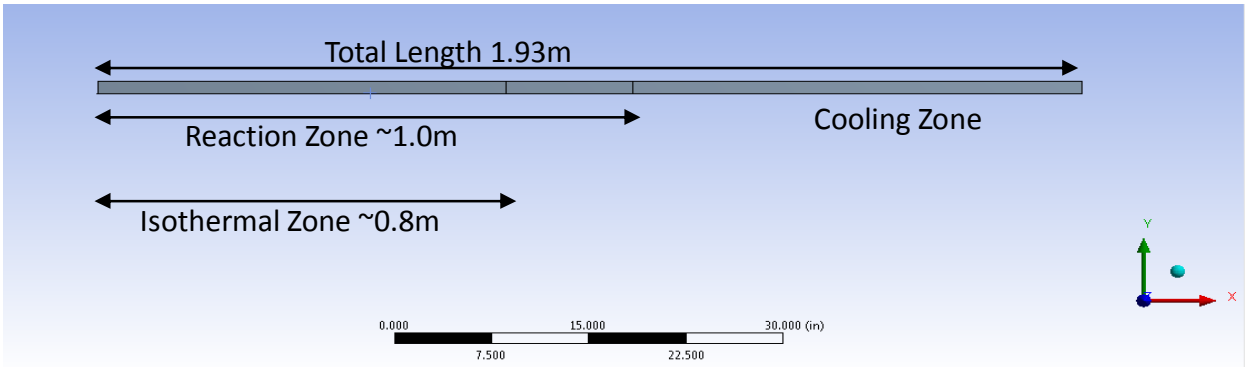

In Ansys, the reaction tube model is constructed as half of the panel cross section, and in the physical model, it would be set as axial symmetric to simulate the whole model to save time and computer resource.

The reaction tube wall is set to have an inflation layer to allow better boundary heat transfer simulation. To ensure good meshing, the growth rate should be no higher than 1.2. The maximum inflation layer is set to 10 for better transitioning.

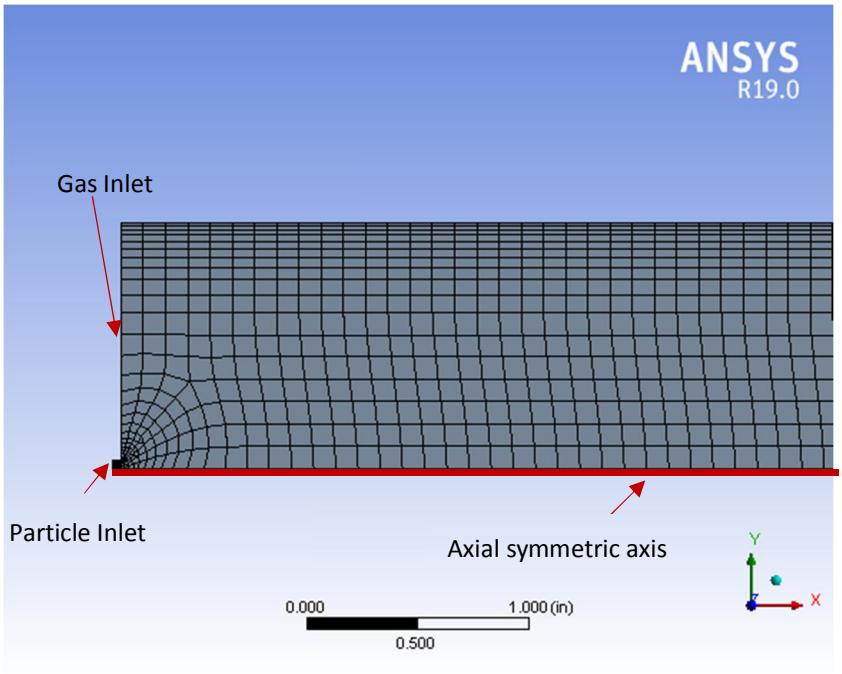

There are 7820 nodes and 7355 elements in the model. In addition to elements and nodes, there are 3 other important factors in Ansys to control good meshing quality: Skewness, Aspect Ratio and Orthogonal Quality. The best practice is to limit these parameters as well as the parameters of our model. These are listed below for comparison:

Aspect Ratio: < 50

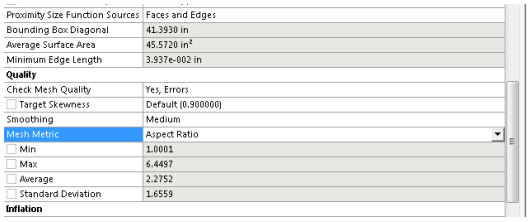

Proximity Size Function Sources	Faces and Edges
Bounding Box Diagonal	41.3930 in
Average Surface Area	45.5720 in²
Minimum Edge Length	3.937e-002 in
Quality	
Check Mesh Quality	Yes, Errors
Target Skewness	Default (0.900000)
Smoothing	Medium
Mesh Metric	Aspect Ratio
Min	1.0001
Max	6.4497
Average	2.2752
Standard Deviation	1.6559
Inflation	

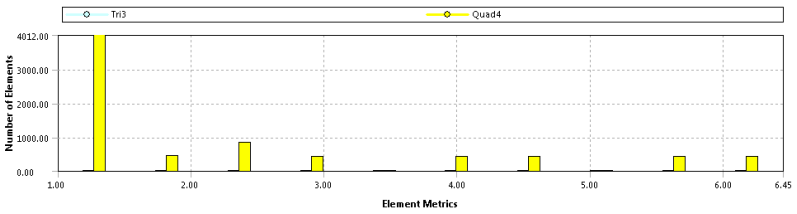

Skewness: 0-0.25 (excellent), 0.25-0.50 (very good), 0.50-0.80 (good), 0.80-0.94 (acceptable), 0.95-0.97 (bad), 0.98-1.00 (unacceptable).

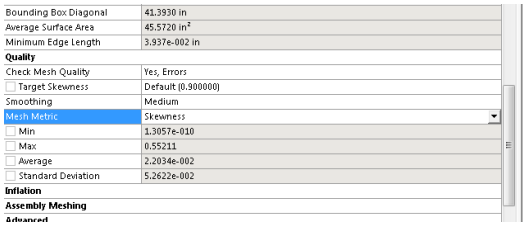

Bounding Box Diagonal	41.3930 in
Average Surface Area	45.5720 in²
Minimum Edge Length	3.937e-002 in
Quality	
Check Mesh Quality	Yes, Errors
Target Skewness	Default (0.900000)
Smoothing	Medium
Mesh Metric	Skewness
Min	1.3057e-010
Max	0.55211
Average	2.2034e-002
Standard Deviation	5.2622e-002
Inflation	
Assembly Meshing	
Advanced	

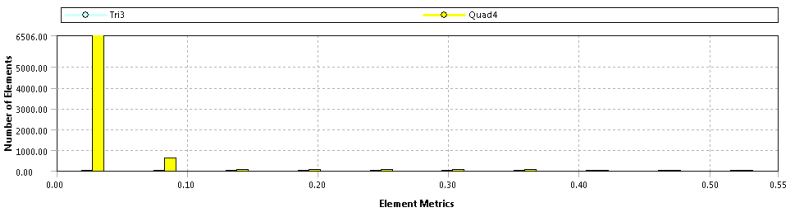

Orthogonal quality: 0-0.001 (unacceptable), 0.001-0.14 (bad), 0.15-0.20 (acceptable), 0.20-0.69 (good), 0.70-0.95 (very good), 0.95-1.00 (excellent)

Bounding Box Diagonal	41.3930 in
Average Surface Area	45.5720 in²
Minimum Edge Length	3.937e-002 in
Quality	
Check Mesh Quality	Yes, Errors
Target Skewness	Default (0.900000)
Smoothing	Medium
Mesh Metric	Orthogonal Quality
Min	0.73235
Max	1.
Average	0.99716
Standard Deviation	1.4112e-002
Inflation	
Assembly Meshing	

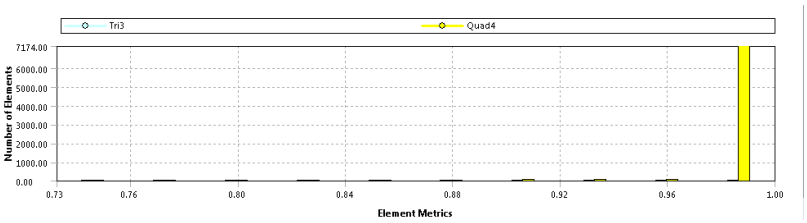

All meshing parameters are falling in the excellent range, indicating good meshing quality of model.

DATA OF COMPONENTS PROPERTY

All thermal dynamic properties of Hydrogen and Nitrogen are obtained from the database of Calhoun. In Fluent, thermal conductivity is set to use piece-wise polynomial function and viscosity is set to use polynomial function. Solid particle heat capacity is obtained from NIST database.

Hydrogen and Nitrogen heat capacity, viscosity and thermal conductivity are temperature dependent and in a form of:

$$y = A_0 + A_1 \times T + A_2 \times T^2 + A_3 \times T^3 + A_4 \times T^4 + A_5 \times T^5$$

Values of the constant A are presented in the following table:

Component	Properties	Temperature Range [K]	A1	A2	A3	A4	A5	A6
H_2	Cp	490°-1365°	14920.082	-1.997	2.541e-3	-4.759e-07		
	K	500°-1500°	0.108	2.212e-4	2.264e-7	-1.743e-10	4.649e-14	
		1500°-2000°	-0.281	1.097e-3	-5.273e-7	1.240e-10		
	viscosity	500°-2000°	2.729e-6	2.322e-8	-7.629e-12	2.926e-15	-5.289e-19	
N_2	Cp	590°-1365°	1405.508	-2.190	4.785e-3	-4.540e-6	2.085e-9	-3.790e-13
	K	100°-1500°	-1.523e-3	1.189e-4	-1.209e-7	1.156e-10	-6.365e-14	1.472e-17
		1500°-3500°	0.728	-1.5432e-3	1.354e-6	-5.516e-10	1.0845e-13	-8.268e-18
	viscosity	80°-2200°	0.026e-6	7.534e-8	-6.516e-11	4.350e-14	-1.562e-17	2.250e-21
Fe	Cp	973°-1042°	-11532	12.505				
		1042°-1100°	13495	-11.513				
		1100°-1800°	8392.7	-15	0.0096	-2e-6		
Fe_3O_4	Cp	900°-3000°	867					

Properties of water vapor are obtained from Refprop.

Viscosity and thermal conductivity of water vapor in Fluent is set to use linear function. For viscosity, take 2 point: 473°K -> 16.2E-6, 1573°K -> 58.3-6. For thermal conductivity: 473°K -> 0.0334, 1573°K -> 0.1772. Cp values are Fluent defaults due to only slight changes in temperature range.

The Enthalpy and Entropy of iron and magnetite at 25°C are obtained from NIST:

	Molecular Weight[kg/kmol]	Enthalpy [J/kmol]	Entropy [J/kmol-K]
Fe3O4	231.5	-1.12E+09	145200
Fe	55.845	0	27310

FLUENT SIMULATION MODEL SETUP

General Setup:

- Gravity is activated
- Pressure-based steady model
- Axial symmetric Model

Model Setting:

The following model modes are set for this simulation:

- Energy -> On

  This allows the energy calculation to compute, including convection, conduction and reaction heat

- Viscous -> Realizable k-e, Standard Wall Fn

  Turbulence model according to University of Utah

- Radiation -> Discrete Ordinates

  Discrete Ordinates radiation model is most appropriate for particle radiation, which is our main purpose.

- Species -> Species Transport Reaction

  Setup for the reaction. In Reaction, check Volumetric and Particle Surface. In Turbulence-Chemistry Iteration, check Finite-Rate/No TCI.

  The Mixture Properties are also defined here. Detail provided in the Mixture Setting Section.

- Discrete Phase -> On

  Particle parameters are set in this mode. First, Check 'Interaction with Continuous Phase' option (2-way coupling). Set Iteration interval between 50 -100 (recommended by ANSYS technicians)

  In Physical Models, check the Particle Radiation Iteration option to allow radiation from graphite wall to particles.

  In Numerics -> Coupled Heat-Mass Solution, check Combusting. If UDF is used for particle surface reaction, this option should be un-checked.

Parameter Setting:

The purpose of this simulation is to verify the residence time and reaction of the model to confirm with the experimental data. The testing parameters input into the model are from the published data by experiments conducted by University of Utah.

Reaction Temperature	H2 Flow Rate	N2 Flow Rate	N2 Feeder Flow Rate	Particle Flow	Particle Size	Residence Time	Reduction Rate
C	L/min	L/min	L/min	g/min	micron	s	%
1187°	1.000	0.80	0.3	0.150	22.5	4.96	82.2
	2.000	2.00	0.3	0.250	22.5	2.71	69.5
	0.600	0.80	0.3	0.090	22.5	5.97	79.8
	1.000	1.50	0.3	0.130	22.5	3.89	69.1
	2.500	4.30	0.3	0.320	22.5	1.69	32.8
	0.400	0.40	0.3	0.050	35	5.90	84.3
	0.800	1.20	0.3	0.130	35	3.86	75.5
	2.300	3.90	0.3	0.250	35	1.68	46.4
	0.300	0.20	0.3	0.030	49	4.67	68.3
	0.500	0.60	0.3	0.060	49	3.76	56.7
	2.200	3.70	0.3	0.280	49	1.55	34.6
	0.500	1.30	0.3	0.050	22.5	4.98	63.9
	2.000	6.20	0.3	0.280	22.5	1.42	20.5
1236°	1.100	1.70	0.3	0.110	22.5	3.95	91.9
	3.000	5.20	0.3	0.240	22.5	1.56	60.2
	0.300	0.70	0.3	0.030	22.5	8.33	92.8
	0.500	1.30	0.3	0.070	22.5	5.52	87.0
	1.000	3.00	0.3	0.150	22.5	2.99	68.8
	2.300	7.20	0.3	0.300	22.5	1.37	37.1
	0.300	0.70	0.3	0.040	35	6.25	91.7
	0.500	1.30	0.3	0.050	35	4.52	63.5
	2.000	6.20	0.3	0.280	35	1.47	32.0
	0.300	0.70	0.3	0.030	49	4.48	70.2

Reaction Temperature	H2 Flow Rate	N2 Flow Rate	N2 Feeder Flow Rate	Particle Flow	Particle Size	Residence Time	Reduction Rate
C	L/min	L/min	L/min	g/min	micron	s	%
	0.700	2.00	0.3	0.080	49	2.89	57.9
	0.300	2.00	0.3	0.050	22.5	4.72	54.1
	0.500	3.50	0.3	0.090	22.5	2.99	40.1
	1.000	7.20	0.3	0.190	22.5	1.56	23.5
1284°	1.000	1.50	0.3	0.140	22.5	3.87	96.8
	2.700	4.70	0.3	0.220	22.5	1.55	85.6
	0.500	1.30	0.3	0.080	22.5	4.98	93.6
	1.000	3.00	0.3	0.140	22.5	2.69	76.6
	2.000	6.20	0.3	0.260	22.5	1.40	61.9
	0.900	2.60	0.3	0.120	35	2.63	72.4
	2.200	6.90	0.3	0.230	35	1.21	45.2
	0.800	2.30	0.3	0.120	49	2.42	70.9
	2.000	6.20	0.3	0.270	49	1.21	45.9
	0.300	1.70	0.3	0.050	22.5	4.66	75.7
	0.500	3.50	0.3	0.060	22.5	2.69	61.1
	1.000	7.20	0.3	0.100	22.5	1.40	32.5
1324°	1.100	3.30	0.3	0.160	22.5	2.63	89.5
	2.200	6.90	0.3	0.240	22.5	1.36	67.8
	0.900	2.60	0.3	0.140	35	2.82	95.9
	2.000	6.20	0.3	0.300	35	1.41	74.0
	0.300	0.70	0.3	0.040	49	4.51	97.0
	0.700	2.00	0.3	0.090	49	2.85	85.0
	2.000	6.20	0.3	0.320	49	1.30	52.9
	0.300	2.00	0.3	0.040	22.5	4.55	87.0
	0.500	3.10	0.3	0.090	22.5	3.16	71.4

Pre-exponential factor provided by University of Utah is 1.23E+07 [1/atm-s] (121.4 [1/Pa-s]). Fluent requires a unit of factor [kg/m^2-Pa^N-K^{beta}-s]. According to University of Utah, the temperature factor beta is 0 and pressure factor N is 1, therefore the unit reduces to [kg/m^2-Pa-s]. The extra [kg/m^2] indicates the surface area of 1 kg particle. Density of Fe_3O_4 is 5170 kg/m^3, 1kg Fe_3O_4 has approximately 8.62E+09 particle, and total area is about 33.2 [m^2/kg], so by multiplying it by Utah's data, the pre-exponential factor for Fluent is 3.66. This is our baseline to start the simulation and this parameter would be the main parameter to be tuned in this simulation.

The activation energy provided by University of Utah is 1.96E+08 J/kmol.

Particle Setting:

Particle setting is in the Discrete Phase -> Injections.

Particle type is set to Combusting to allow chemical reaction. In Materials, there will be a new group named Combusting Particle. Vaporization Temperature should be set to a low value to allow reaction activation. Combustible Fraction is set to 100% assuming pure magnetite particles. The Combustion Model should set to multiple-surface-reactions. Set Injection Type to be surface so the particles are released from the wall surface of Particle Inlet.

In Physical Models, the Drag Law is set to be Stokes-Cunningham, to ensure the model follows Stokes Law of particle falling.

In Multiple Reactions, set the ratio of Magnetite to 1 and Iron to 0 initializing the falling particle property.

Mixtures Setting:

- Species:

  Water, hydrogen and nitrogen as selected species. Magnetite and iron as selected Solid Species. Nitrogen is necessary in the mixture group even though it's not in part of the reaction, because Ansys reaction model requires more than 2 species (excluding solid species) to enable the particle combustion model.
- Reaction:

  The Reaction Type should set to be Particle Surface since the reaction happens on the surface of the particles.
- Mechanism:

  Reaction Type of all reactions set to be Particle Surface
- Density:

  Incompressible-ideal-gas
- Cp:

  Mixing-law
- Thermal Conductivity

  Mass-weighted-mixing-law
- Viscosity:

  Mass-weighted-mixing-law
- Mass Diffusivity:

  Kinetic-theory
- Thermal Diffusion Coefficient:

  Kinetic-theory

Simulation Result and Analysis

Flow Pattern and Thermal Behavior

The experiment shows the particles injected in the center will stay in their central path, after hitting terminal velocity and will continue falling to the bottom of the reactor. This is important because if the particles are spraying out we would have particles sticking to the reactor wall and accumulate. The simulation results are in agreement with experiment that the particles stay near the center axis. They quickly hit the terminal velocity and keep at that velocity while falling.

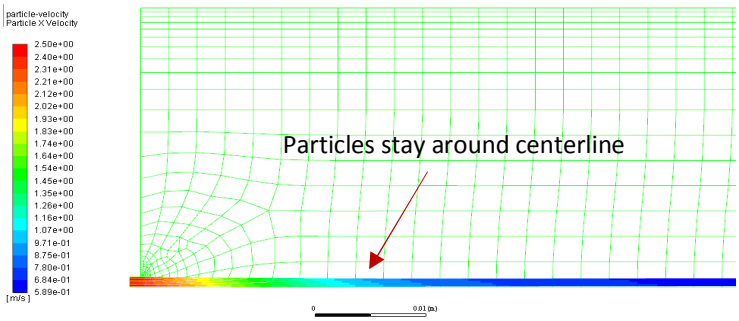

The velocity is higher at the centerline because the 2 way coupling in the simulation system is on, meaning that not only is gas dragging the particles but, the particles are also dragging the gas. This results in higher velocity at the center where particles are more present than the surroundings.

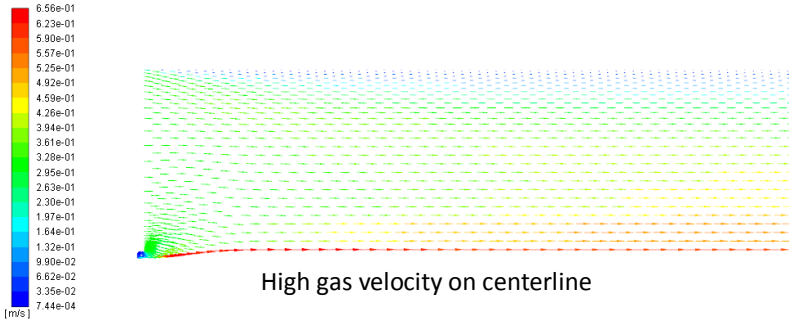

High gas velocity on centerline

Gas is heated up before entering the reaction area, while particles enter at a low temperature. This result shows that particles get heated up by hot gas immediately after entering the area. With 0.8 m of heater length, the temperature is kept for about 1 m, after that it drops due to the cooling jacket around the reaction tube (which is simulated as cool surface). The temperature profile of the gas is shown as below:

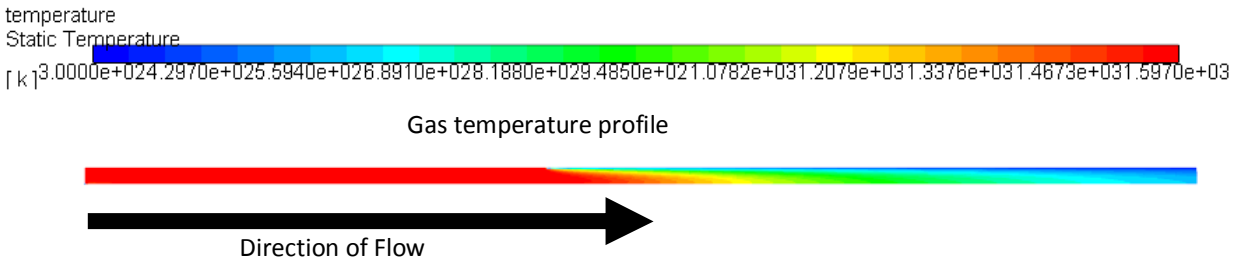

Gas temperature profile

Chemical Reaction

The below figure shows one of the cases simulated according to data provided by University of Utah. We can see that magnetite particles react and become iron particles to a certain extent, and water is generated in the same process.

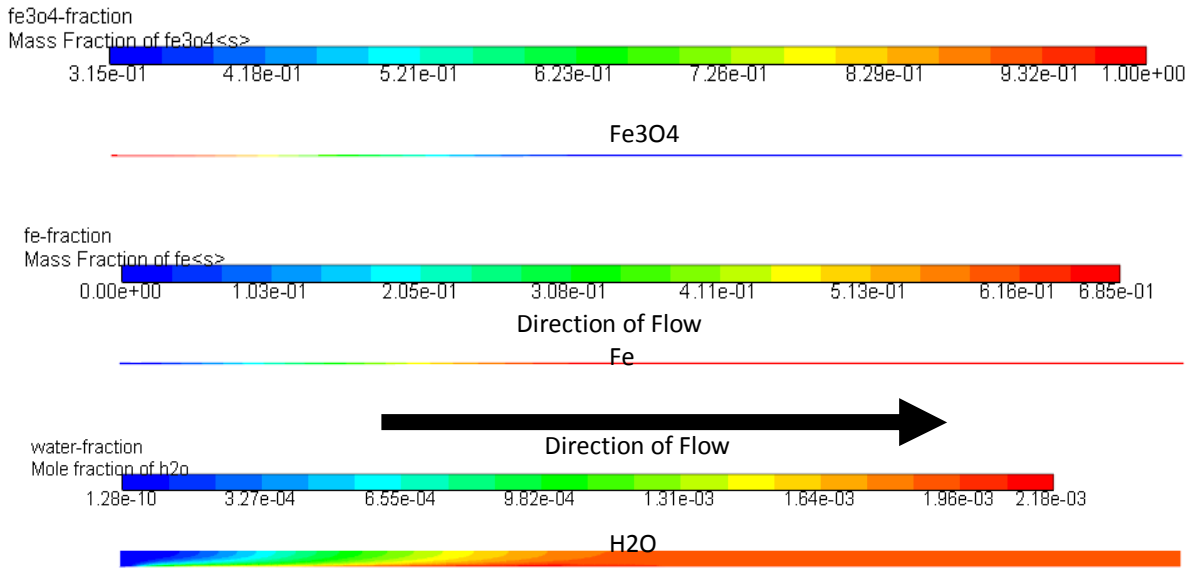

Comparison Between Simulated Results and Experiment Data

Once the parameters are fine-tuned with the above setup, BMC discovered that with a particle size less than 35µm, the best pre-exponential number is 3.0 and with particle size of 49µm, the pre-exponential number is 1.75. These numbers are different from what is obtained by University of Utah. Considering all the Assumptions University of Utah made and the uncertainty in experiment, BMC would think both numbers are of the same magnitude of the number provided by University of Utah. Therefore, they are good estimated parameters to be imported by the industrial scale model. To be more conservative, BMC choose to use 1.75 as the final input for the industrial scale model, which will result in a lower reduction rate than 3.0.

The following graph shows the relationship between simulated data and actual data acquired from the experiments. We see very good liner relationship between both residence time and reduction rate data, with R value close to 1.0. The results show that the experiment results have good agreement with the experiment results with the inputs described above. These parameters obtained from the lab scale model can be applied to the big industrial scale model to help the actual reactor design.

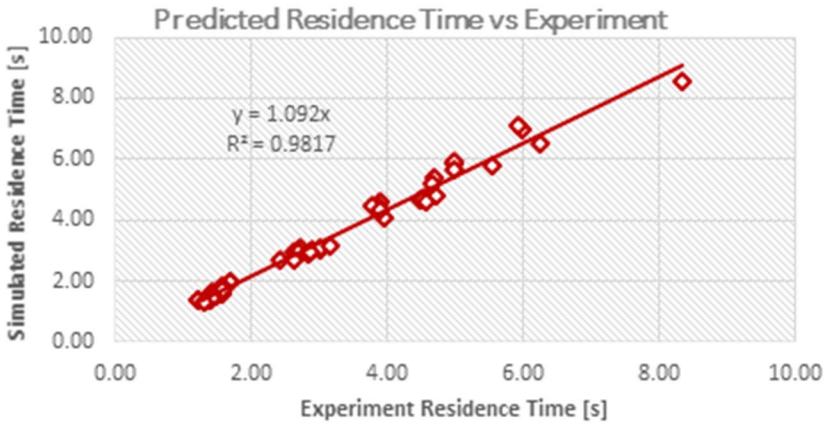
Predicted Residence Time vs Experiment
y = 1.092x
R² = 0.9817
Simulated Residence Time [s]
Experiment Residence Time [s]
0.00
2.00
4.00
6.00
8.00
10.00

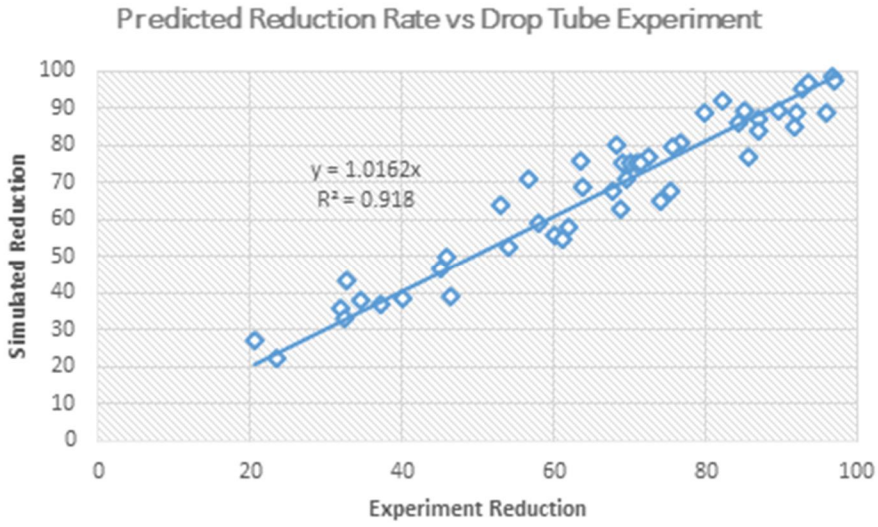
Predicted Reduction Rate vs Drop Tube Experiment
y = 1.0162x
R² = 0.918
Simulated Reduction
Experiment Reduction
0
10
20
30
40
50
60
70
80
90
100

INDUSTRIAL SCALE PILOT MODEL

PHYSICAL MODEL AND MESH INFORMATION

The heating portion of the reactor is 5ft long where induction heating coil will heat up the graphite susceptor. The susceptor heats up refractory wall by radiation. Both susceptor and refractory wall heat up the gas and particle in the 5ft long portion by convection and radiation. After being heat up to the temperature, gas and particles enter the reaction zone about 28ft in length, where good insulation is assumed so wall condition is set to be adiabatic. After the reaction zone, there is a cooling zone with length about 16ft, with cooling panel to cool

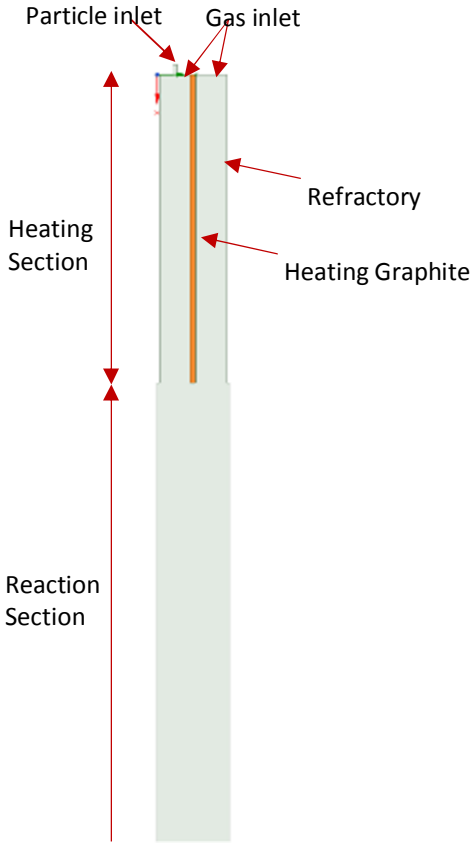

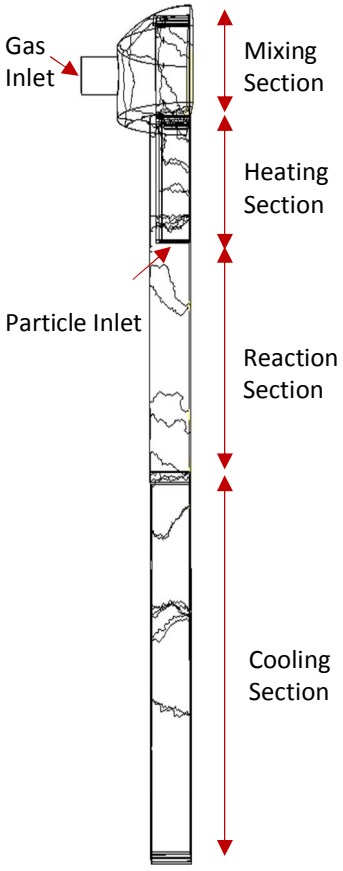

gas and particles

Two (2) models are constructed for the industrial scale pilot reactor. The 2D model includes a heating portion and reaction portion to simulate the heat transfer and chemical reactions. To ensure considerations of all flow directions, the particle falling simulation is conducted by 3D modeling, with the same setting of 2D, except the reaction is turned off to save time and space.

In 3D model, since the reaction is not simulated, the reaction section is shorted to save computational resource.

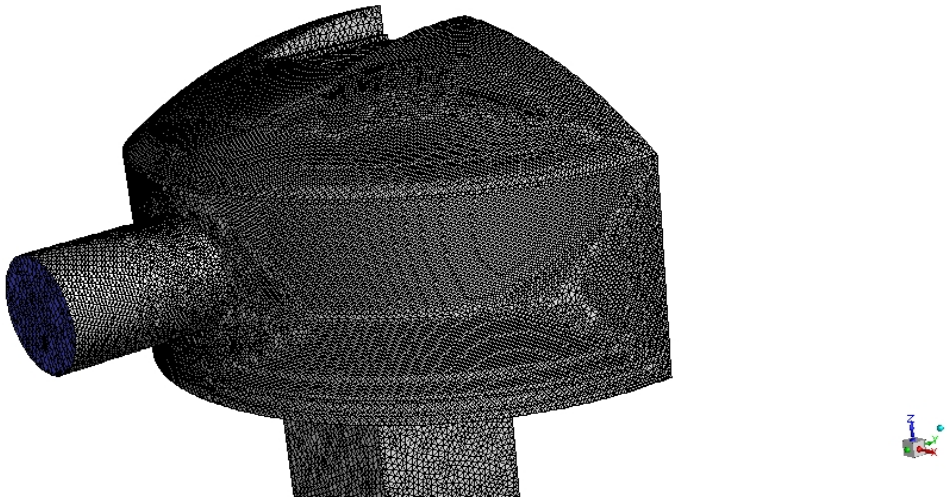

The 3D model has 7411535 nodes and 5162476 elements. Skewness, Aspect Ratio and Orthogonal Quality of the model are listed below:

Aspect Ratio: < 50

Physics Preference	Mechanical
Element Order	Program Controlled
Sizing	
Quality	
Check Mesh Quality	Yes, Errors
Error Limits	Standard Mechanical
Target Quality	Default (0.050000)
Smoothing	Medium
Mesh Metric	Aspect Ratio
Min	1.1577
Max	26.639
Average	1.8647
Standard Deviation	0.45443
Inflation	

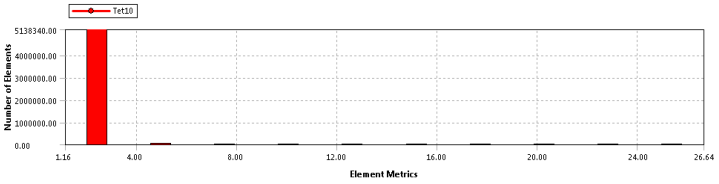

Skewness: 0-0.25 (excellent), 0.25-0.50 (very good), 0.50-0.80 (good), 0.80-0.94 (acceptable), 0.95-0.97 (bad), 0.98-1.00 (unacceptable).

Element Order	Program Controlled
Sizing	
Quality	
Check Mesh Quality	Yes, Errors
Error Limits	Standard Mechanical
Target Quality	Default (0.050000)
Smoothing	Medium
Mesh Metric	Skewness
Min	5.5594e-007
Max	0.99962
Average	0.24277
Standard Deviation	0.13217
Inflation	

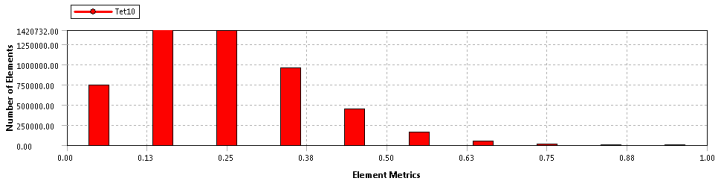

Orthogonal quality: 0-0.001 (unacceptable), 0.001-0.14 (bad), 0.15-0.20 (acceptable), 0.20-0.69 (good), 0.70-0.95 (very good), 0.95-1.00 (excellent)

Physics Preference	Mechanical
Element Order	Program Controlled
Sizing	
Quality	
Check Mesh Quality	Yes, Errors
Error Limits	Standard Mechanical
Target Quality	Default (0.050000)
Smoothing	Medium
Mesh Metric	Orthogonal Quality
Min	3.7915e-004
Max	0.99787
Average	0.75568
Standard Deviation	0.13018
Inflation	

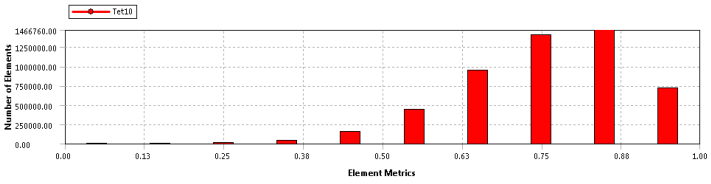

Aspect ratio is less than 27, which is good. Most cell are fallen into under 0.8 range for skewness, and most cell are fallen into more than 0.2 range for orthogonal quality, which indicate good mesh quality of 3D model.

In the 2D model, the end effect is not considered, where additional graphite will add in more heat. Ignoring the end effect is a more conservative method. Reactor walls are set to have an inflation layer to allow better heat transfer simulation. To ensure good meshing, the best practice of growth rate should be no higher than 1.2. The inflation maximum layer is set to 10 to have good transition.

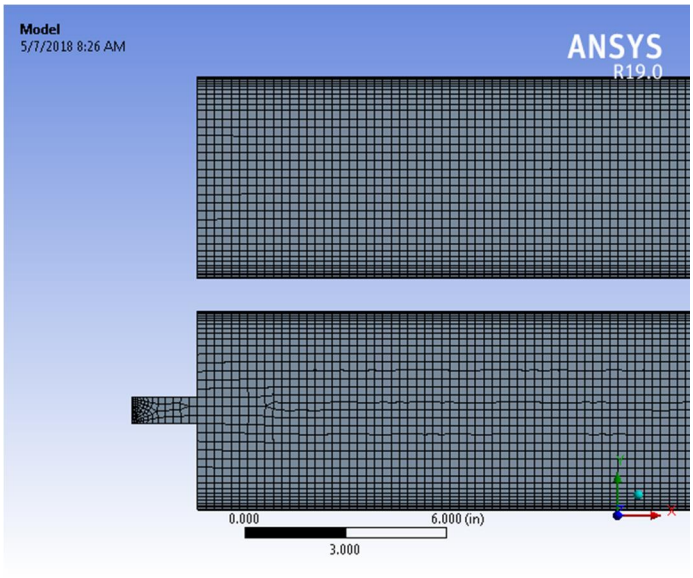

The 2D model has 100776 nodes and 98880 elements. Skewness, Aspect Ratio and Orthogonal Quality of the model are listed below:

Aspect Ratio: < 50

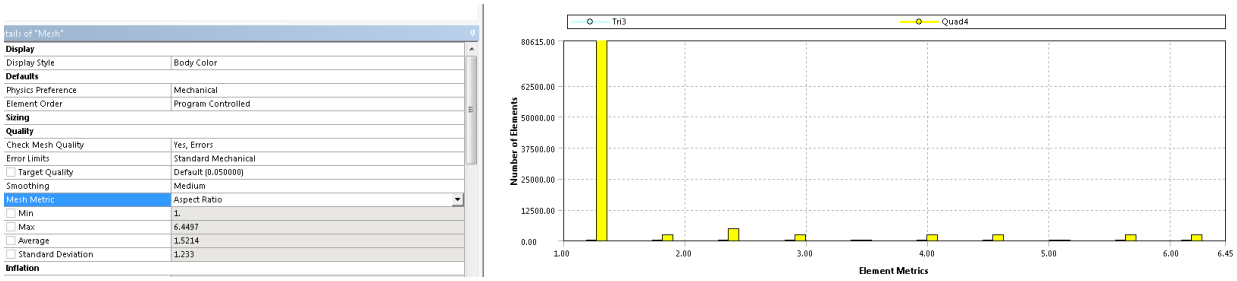

Skewness: 0-0.25 (excellent), 0.25-0.50 (very good), 0.50-0.80 (good), 0.80-0.94 (acceptable), 0.95-0.97 (bad), 0.98-1.00 (unacceptable).

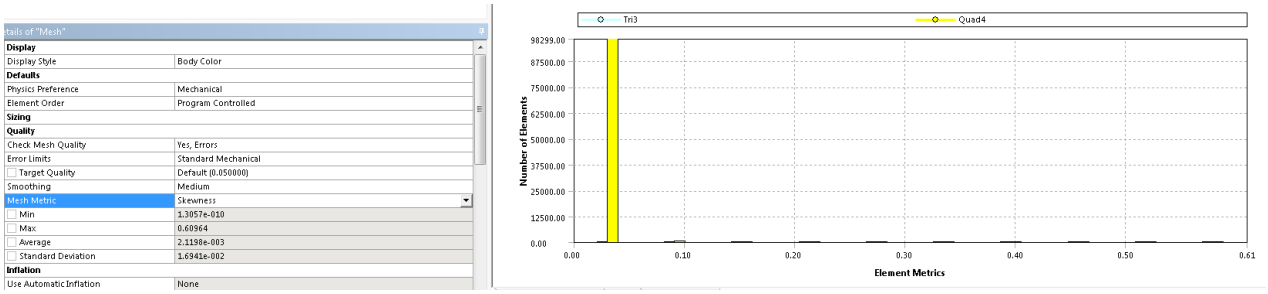

Orthogonal quality: 0-0.001 (unacceptable), 0.001-0.14 (bad), 0.15-0.20 (acceptable), 0.20-0.69 (good), 0.70-0.95 (very good), 0.95-1.00 (excellent)

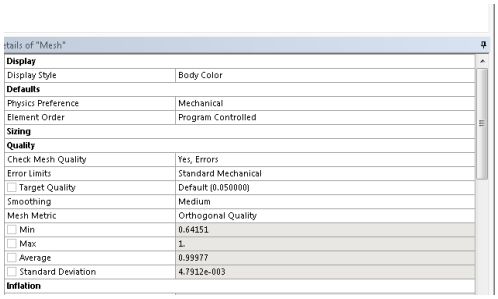

Details of "Mesh"	
Display	
Display Style	Body Color
Defaults	
Physics Preference	Mechanical
Element Order	Program Controlled
Sizing	
Quality	
Check Mesh Quality	Yes, Errors
Error Limits	Standard Mechanical
Target Quality	Default (0.050000)
Smoothing	Medium
Mesh Metric	Orthogonal Quality
Min	0.64151
Max	1.
Average	0.99977
Standard Deviation	4.7912e-003
Inflation	

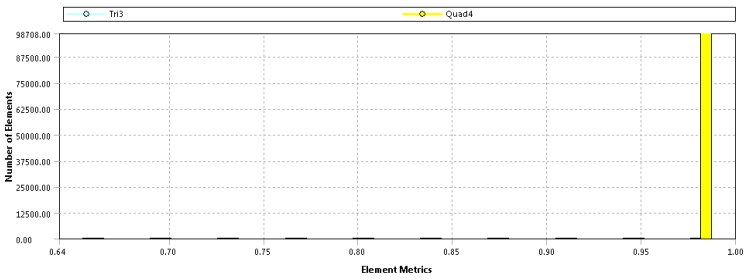

Overall, the meshing quality of the model is excellent.

Simulation Setup

Base Case Parameter Setting:

The 2-D model in Fluent is assuming 1-meter thickness, and our simulation is only simulating half of the symmetric reactor, with model set to be symmetric to include the other half. The 3-D model

The base case condition parameters are as follow:

Particle Mass: 0.047 kg/s (half of actual mass flow rate for half model)

Gas Mass: 0.0035 kg/s (assuming 100% Hydrogen) (half of actual mass flow rate for half model)

Heating Wall Temperature: 1424° [C] (Temperature set to heat particle to 1325°C)

Particle Diameter: 35 um

Activation Energy: 1.96E+08

Pre-exponential Factor: 1.75

Particle setting:

Same setting as Lab Scale Model.

Mixtures setting:

Same setting as Lab Scale Model.

RESULTS FOR 3D MODEL

1. Particle Path

For particle path study, we verified that particles follow the path of the gas without being in large turbulence that will blow the particles to walls, susceptor and cooler panels.

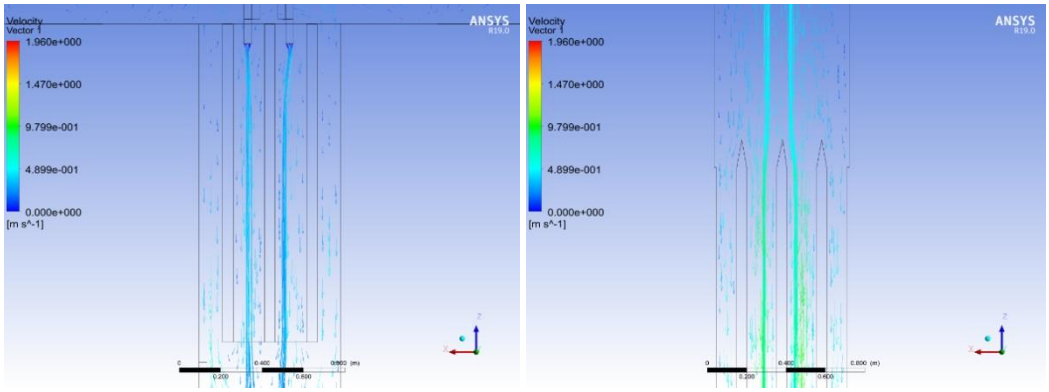

Simulation indicates that particles stay in their path and will not touch the panels.

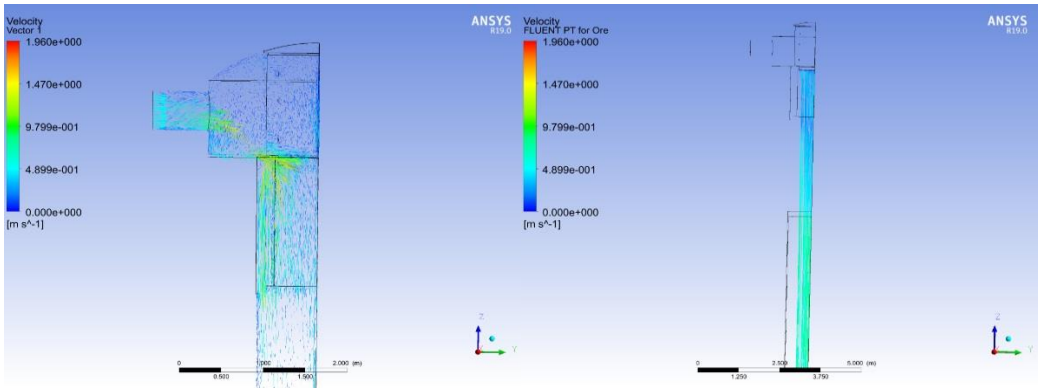

The above results indicate that particle curtain is pushing inwards when entering the reactor by the faster fluid. The influence is small compare to the length of curtain, and will be even more trivial when curtain is long.

2. Flow Distribution

Gas flow was not distributed evenly across the section plate before, based on the simulation result, we adjust the space between graphite and wall. After adjusting the space between refractory box and graphite, the flow is almost evenly distributed in the space.

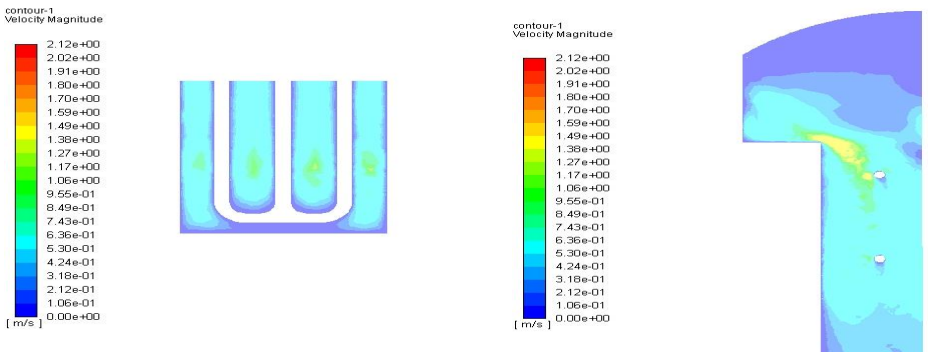

3. Temperature Profile

Fluid gets heated up to temperature while flowing through the heated graphite part. From the model we observed high temperature gas raising up to the mixing room, but most fluid flows down to the heating section.

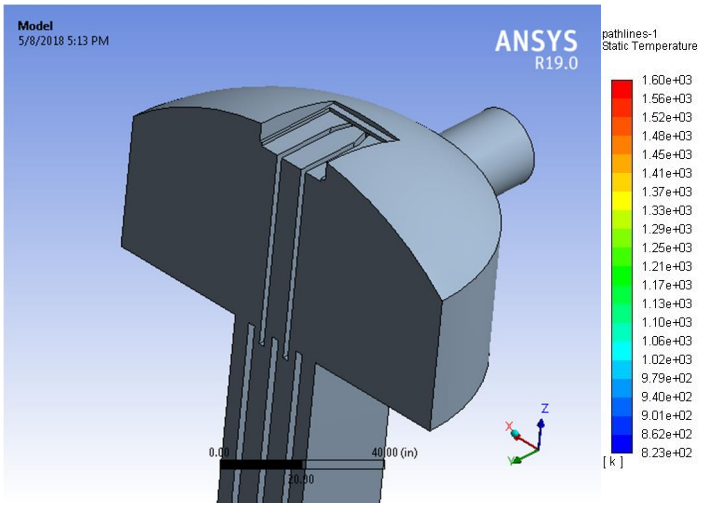

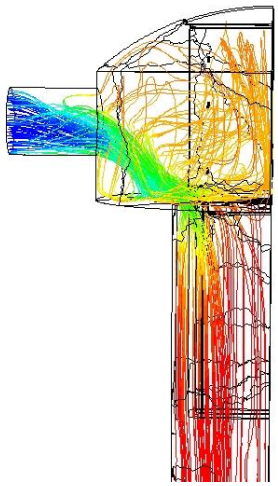

RESULT FOR 2D MODEL

The 2D model focuses on the chemical reactions to ensure enough heat and time is provided to achieve the 95% metallization goal. Apart from the base case, several other cases are investigated to discover the potential of increasing capacity or production rate of the system. The conditions and results are listed below:

Particle Starting Temperature [C]	**Wall Temperature [C]**	**Reaction Time 95% reduction[s]**	**Total Time in Reactor [s]**	**Total Energy [GJ/ton]**
1225	1325°	6	9.0	10.47
1275	1375°	4.5	9.4	10.73
1325	1600° (double)	5.8	5.8	10.81
1325	1425° (baseline)	3	10.0	10.81

There is variety in the total time in reactor, that's because in some cases there are back flow from the outlet that occupies some space in reactor, pushing the downward flow to the center, so the speed of downward stream increases.

The simulation shows that under our baseline condition, the reaction would be instant, so we can increase flowrate to achieve higher production rate or decrease the heating temperature to save energy usage per ton iron making. A comparison of baseline and double flow and particle flowrate cases are shown below. In the baseline case, the reaction reaches 95% before midpoint, while in the double flow case, the reaction reaches

95% at bottom of the reactor. As temperature decreases, it takes more time and longer distance to reach 95% metallization.

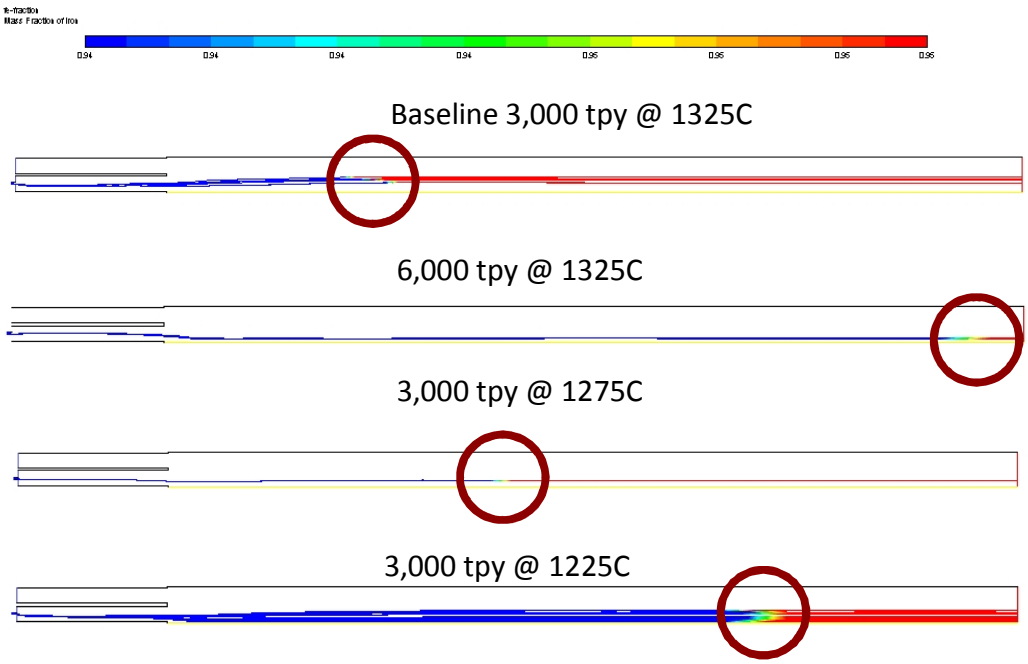

The simulation results show that the current design can achieve the baseline goal with extra capacity. We may be able to operate at lower temperature or higher flow rate with current design.

Risk Assessment of Calculation Uncertainties

- Data from Phase II has some inconsistency and the CFD was calibrated to this data.
- Formulas from Phase II were developed with large excess hydrogen - 800% to 2,000%. The pilot plant will operate with 100% excess hydrogen which is pushing the limit of the range for which it was tested.
- Most of Phase II runs consisted of a hydrogen/nitrogen mixture. The pilot plant will be 100% hydrogen which is pushing the limit of the tested range.
- Ansys Fluent Bug 1 - The endothermic reaction pulls heat from the system. We calculate by hand the temperature from reaction should drop by 200°C, Fluent results only show a temperature drop of 10°C. The heat removal is not being applied to the cells correctly. Ansys has acknowledged and recorded the bug and will work to fix it for next release. These incorrect cell temperatures affect:
    - Density of gas – colder gas increases density slowing the particle velocity increasing residence time
    - Viscosity of gas – colder gas decreases viscosity increasing the particle velocity decreasing residence time
    - Reaction rate – colder gas will slow the reaction

- The report for the heating block heat flux is reporting unrealistically high heat transfer to the particles and gas. This appears to be related to the reported temperature bug with Ansys.
- Ansys Fluent Bug 2 - crashed when simulating particles with different sizes. In actual situation, particles have size ranges from 5um to 50um, it's possible that small particles melting while the larger one not getting to desirable temperature.
- Ansys Fluent Bug/Limitation 3 – Fluent provides unrealistic particle velocity results with 2-way coupling between particle and gas for the model under certain boundary conditions.
    - In one-way coupling, the gas affects particle temperature and flow patterns but particle does not affect the gas. This is normally used for dilute flow, less than 10% volume particles to gas, to reduce computational time.
    - In two-way coupling, the gas affects the particle and the particle affects the gas. This is used for heavy particle flow where the particles entrain and drag the gas.
    - As the endothermic chemical reaction is very large the two-way coupling is required to drop the temperature and change the flow of the gas. When the two-way coupling was turned on with a fixed wall temperature boundary condition the particle velocities increased by a factor of 3. This large velocity also created an unrealistic vortex in the gas flow.
    - Ansys acknowledged the results were unrealistic and first recorded the anomaly as a bug. It went to the Developers to fix but they declared this as an oddball case (they limit dilute flow by mass ratio particles to gas) and rather than make a significant change to the software declared it as a Software Limitation.
    - We were able to get good results by using adiabatic walls instead of fixed temperature.

Risk Reduction of Calculation Uncertainties

- Possible results of missed calculations
    - Do not get the 95% metallization
    - Do not get to 3,000 tpy
    - Need more energy
- We have set the baseline to react to 95% metallization in 3 seconds with total time in the reactor of 10 seconds – significant margin
- If 95% metallization is not achieved the additional main reactor section heaters will be turned on. These heaters have 4 control sections.
- If still do not achieve the 95% metallization in 10 seconds we will reduce the particle mass flow rate. This increases the percent of excess hydrogen which increases reaction rate. With the slower particle mass flow rate we will not meet the 3,000 tpy rate.
- If 95% metallization is achieved with baseline - will increase particle and gas flow rate to reduce margin. The increase in hydrogen increases the velocity reducing residence time in the reactor.
- If 95% metallization is achieved – will reduce hydrogen flow to determine how much excess hydrogen is required.

- If 95% metallization is achieved – will increase particle flow rate and hydrogen to determine limit of particle loading density.

Piping Legend Detail							
Service	Legend	Size	Installation	Material	Joint Type	Pressure [psig]	Remarks
Natural Gas	NG	2.5	BUR EXP	CST	F	260	
Nitrogen	N2	<= 1	EXP	SST	F	100	
Cooling Water	CW	<=3	EXP	SST CST	F	50	
Hydrogen	H2	<= 24	EXP	SST	F	260	
Air	AIR	<= 8	EXP	SST	F	15	
Steam	STM	1	EXP	SST CST	F	15	
Condensate	CND	<=1	EXP	PVC	F	205	
Boiler Feed Water	BFW	0.75	EXP	SST CST	F	260	
Flue Gas	FLG	8	EXP	CS	F	TBD	
Vent	VENT	0.75	EXP	CST	F	0	
Waste Water	WW	1	EXP	PVC	F	5	
Process Water	PW	1	EXP	PVC	F	35	
Deaerator Overflow	DR	1	EXP	CS	F	TBD	
Iron Ore	IRO	TBD	EXP	SST	F	TBD	pressure high enough to prevent blow back of ore by hydrogen
Iron with Exhaust Gas	IRX	4	EXP	SST	F	15	
Exhaust Gas	EXG	<=4	EXP	SST	F	15	
Waste Gas	WG	<=3	EXP	CS	F	5	
Sodium Hydroxide	SOH	TBD	EXP	SST	F	TBD	

PROCESS FLUIDS LIST

Process Fluids List	
NG	Natural Gas
N2	Nitrogen
CW	Cooling Water
H2	Hydrogen
AIR	Cooling/Heating Air
STM	Steam
CND	Condensate
BFW	Boiler Feed Water
FLG	Flue Gas
VENT	Pressure Relief Safety Vent
WW	Waste Water
PW	Process Water
DR	Deaerator Overflow
IRO	Iron Ore
IRX	Iron with Exhaust Gas
IRN	Iron with Nitrogen Blanket Gas
EXG	Exhaust Gas
WG	Waster Gas
SOH	Sodium Hydroxide

Utility Consumption List

The pilot plant utility consumption is listed in the table below.

Utility	**Usage**
Natural Gas	1940 scfh
Electric	350 kW
Water - makeup	6 gpm
Nitrogen purge	6000 scfd
Nitrogen	350 scfh
CO2	.1 scfh
50% NaOH	.05 gph

Emissions and Effluent Summary

The pilot plant emissions are listed in the table below.

Pollutant	**Generated**
SO_2	.88 lb./hr.
CO_2	336 lb./hr.
CO	.07 lb./hr.
NO_x	.11 lb./hr.
VOC	.03 lb./hr.
Particulates	.02 lb./hr.
H_2S	.08 lb./hr.
H_3PO_4	.01 lb./hr.
Acid water neutralized with 50% NaOH	224 lb./hr.

HEALTH, SAFETY, & ENVIRONMENT (HSE)

CODES AND STANDARDS

- Minnesota State Fire Code 2007, Chapter 7511
- International Fire Code
- NFPA 497 Recommended Practice for the Classification of Flammable Liquids, Gases or Vapors and of Hazardous (Classified) Locations for Electrical Installations in Chemical Process Areas
- NFPA 499 Recommended Practice for the Classification of Combustible Dusts and of Hazardous (Classified) Locations for Electrical Installations in Chemical Process Areas

SAFETY DESIGN

The three buildings will be protected per the Minnesota Fire Code. The Process Building will have equipment that contains combustible material - hydrogen, natural gas and iron powder. NFPA classifies hazardous locations as:

Class I – the material present is a flammable gas or vapor

Class II – the material present is a combustible dust

The Classes are further subdivided into Divisions

Division 1 – the combustible material is present normally or frequently

Division 2 – the combustible material is present as a result of infrequent failure of equipment or containers

The combustible material is further broken down into groups

Hydrogen – Group B with an auto ignition temperature of 520°C

Natural Gas – Group D with an auto ignition temperature of 630°C

Iron Powder – Group E with an auto ignition temperature of 290°C

Process Building

Is an "H-2" Occupancy with a Type II-B Construction 60' x 114' x 28' high (6,900 sq. Ft). The building will be covered with an automatic wet pipe sprinkler system hydraulically calculated to provide a density of .3 gpm over the entire area utilizing 286°F, K=8.0 sprinklers spaced a maximum of 10.0 square feet. It will have an automatic sprinkler riser with a double check valve, shut-off valves, supervisory switches, water flow switch, 2" main drain with two pressure gauges and 2 ½" x 2 ½" x 4" fire department connection complete with 4" swing check valve. The building will have a minimum of two 20# surface mounted multi-purpose dry chemical fire extinguisher with UL rating of 20A:80B:C.

Equipment containing hydrogen with flanges, valves and seals is spread throughout the building. Natural gas lines are limited to the steam methane reformer area. Iron powder that can be airborne is limited to the bagging station. The most explosive rating of the two gases is hydrogen so the entire building will be rated to a Class I Division 2 Group B classification. The Iron Powder has the lowest ignition temperature but the hazard is limited to a 20 ft. radius around the bagging machine. This will require a local hazard zone of Class II Division 1 Group E within the building. The building air will be turned over a minimum of 6 times per hour to achieve adequate ventilation per the NFPA. The control room, restrooms and MCC/power electronics room will be ventilated per NFPA requirements.

Any openings in the roof will be classified Class I Division 2 Group B for a 15 ft. radius. No openings are currently planned in the roof.

Finished Product Building

Is an "H-3" occupancy with a Type II-B construction 40' x 60' x 20' high (2,400 sq. Ft.). The building will be covered with an automatic dry pipe sprinkler system hydraulically calculated at a density of .6 gpm over the entire area utilizing 286°F, K=16.8 brass upright sprinklers spaced at 100 square feet. It will have an automatic dry pipe sprinkler riser complete with a double check valve assembly, 6" dry pipe valve with 2" main drain, two pressure gauges, water flow pressure switch, high/low air switch, air compressor and fire department connection. As the building is unheated there will be a 4' x 5' heated room for dry pipe sprinkler riser complete with a 3'-0 man door, light and 5 kW heater. The building will have a minimum of two 20# surface mounted multi-purpose dry chemical fire extinguishers with UL rating of 20A:80B:C.The finish product will be contained in paper/plastic sealed bags. Per the NFPA guidelines, iron powder stored in bags does not need to be classified. Therefore, the Finished Product building will be unclassified.

Raw Ore Building

Is an "S-2" occupancy, type II-B 60' x 60' x 28' high (3600 sq. ft.). Automatic sprinklers are not required for this building. The building will have a minimum of two 20# surface mounted multi-purpose dry chemical fire extinguisher with UL rating of 20A:80B:C.

Iron ore is not combustible therefore the Raw Ore Storage building will not be classified as a hazardous location.

Outside of Buildings

The hydrogen storage tank and main reactor will be located outside the buildings. The storage tank, main reactor and a 15 ft radius around them will be designated a Class I Division 2 Group B location.

OCCUPANCY LIFE SAFETY SUMMARY

A preliminary review of building codes revealed the following:

1. The large quantity of finished iron storage (> 25 ton) requires a "detached building".
2. The Process Area requires significant ventilation. If the raw ore is in the same building, this area must be ventilated also. Will drive utility costs up especially in the winter.
3. Above 7000 SF an H-2 building must be Type II-A or Type I-B. Type II-A may be pre-manufactured metal with complete fire proofing all exposed surfaces. Type I-B may be CMU or concrete walls and roofing members.

After reviewing the building code, it was decided there would be three separate buildings:

1. Process Building
2. Raw Ore Storage Building
3. Finished Material Storage Building

Occupancy category and construction requirements of the building are limited by the materials being stored and used or produced in the process. It is understood that the building must contain the materials at the approximate quantities as noted in the table below:

Material	Process	Quantity	Hazard Class	Required Occupancy
Hydrogen Gas	Input		Flammable Gas	H-2
Natural Gas	Input	Delivered @ 20psi	Flammable Gas	H-2
Raw Ore	Input		Non-Hazardous	S-2
Liquid Nitrogen	Input		Cryogenic Inert	*
Liquid CO2	Input		Cryogenic Inert	*
Iron Powder	Product	~ 200 ton Storage	Class II Unstable (Reactive)	H-3
Hydrogen Sulfide (H2S) Gas	Byproduct	0.058 kg/hr	Toxic Gas	*
Hydrogen Phosphate (H3PO4) Gas/Liquid	Byproduct	0.105 kg/hr	Toxic Gas	*
* Quantities do not exceed Allowable Quantity per Control Area (Table 307.1(2)) and do not require Hazardous H occupancy. Control area requirements apply.				

Fire Water Demand Calculation

City water supply with a minimum static pressure of 65 psi, 60 psi residual with 1,200 gpm flowing at connection to the automatic sprinkler riser.

Process Building requires .3 gpm over the entire area of 6,900 square feet = 2,052 gpm.

Product warehouse requires .6 gpm over the entire area of 2,400 square feet = 1,440 gpm.

Flare Study

According to NASA guideline Safety Standard for Hydrogen and Hydrogen Systems, for hydrogen vent rates greater than 0.5 lb. /sec, flaring may be considered. Large quantities of unused hydrogen that can't be handled by the vent system should be flared at a remote location. This is not an issue for smaller commercial systems. For small system with vent rate below 0.5 lb. /sec, roof vent located 16 ft. above roof can be used. In our system, the maximum hydrogen generation rate is 0.009 lb. /sec (6000 scfh), the vent rate is much lower than the criteria, so a flaring system is not required.

HAZARDOUS AREA CLASSIFICATION DRAWINGS

Per NFPA 497 Figure 3-8.27 the process building will be classified Class I Division 2 Group B for flammable gases shown below. The outdoor hydrogen storage tank and main reactor will also be classified as Class I Division 2 group B for a 15 ft. surrounding radius around them shown below. A 20 ft. radius surrounding the bagging machine will be classified as Class II Division 1 Group E per NFPA 499 Figure 6.10(e) for combustible dust.

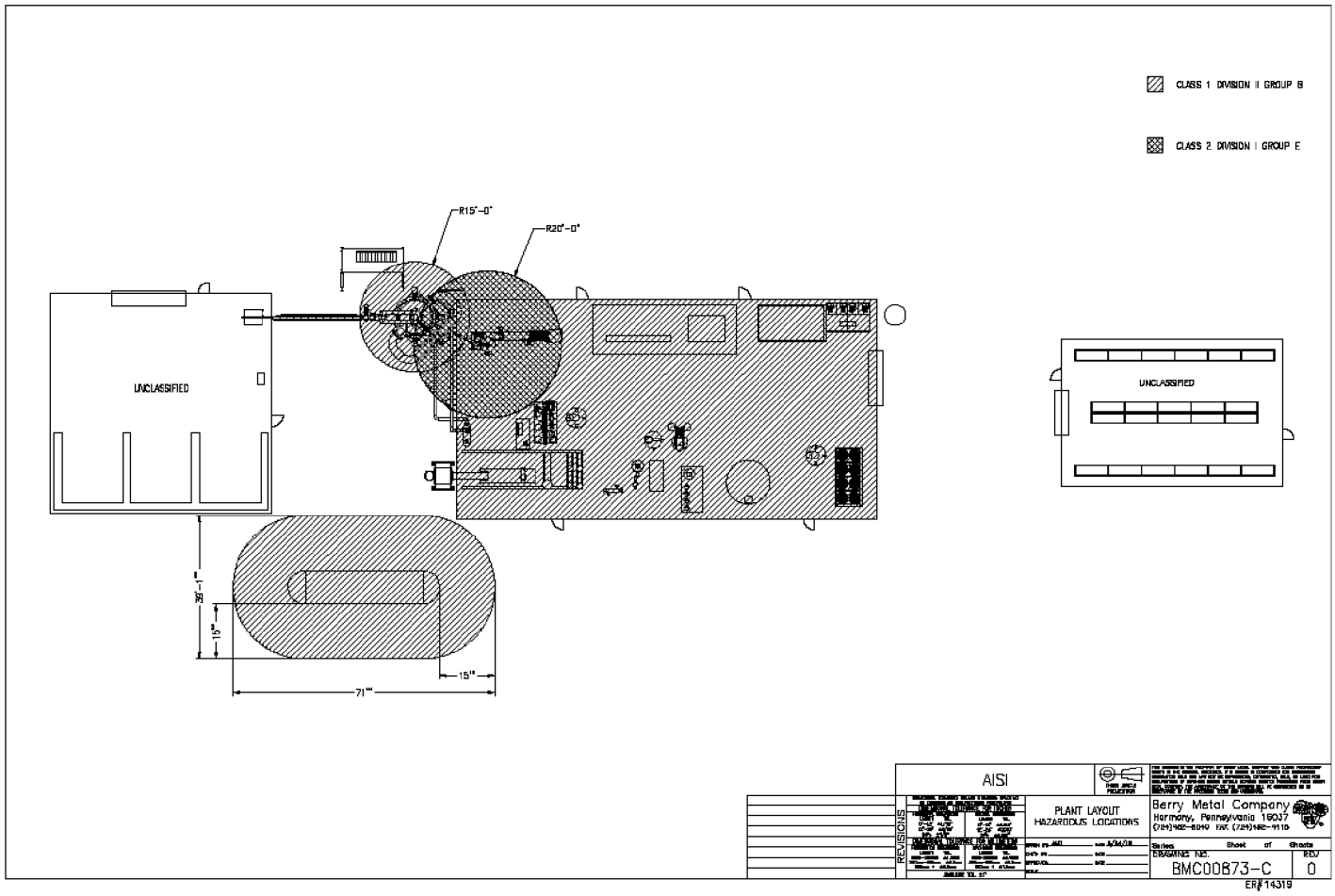

Per NFPA 497 Figure 3-8.27 the process building will be classified Class I Division 2 Group B for flammable gases

The bagging machine may have a small amount of dust escape and become airborne during use. Per NFPA 499 Figure 6.10(b) the bagging machine and a 20 ft. radius will be additionally classified as Class II Division 1 Group E.

Per NFPA 499 Figure 6.10(e) the bags of finished iron powder stored in the Finished Product Building are not required to be classified.

PYROLYTIC TENDENCIES OF FLASH IRON

All metallic iron including DRI has a natural tendency to re-oxidize on contact with air and/or moisture. This is an exothermic reaction, which in bulk scenarios can lead to a risk of self-heating and fires if the DRI is not properly stored and inerted. This is especially important in maritime transport. The International Maritime Organization's International Maritime Solid Bulk Cargoes Code classifies DRI as “Group B” (cargo with chemical hazard) and class “MHB” (material hazardous only in bulk). DRI pellets or process fines that have a large percentage of metallization are required to have an inert gas blanket, hydrogen gas detectors, temperature monitoring equipment and fire protection systems.

The flash iron process is performed at a high enough temperature that individual particles have enough energy to close down the pores created from oxygen removal. Therefore, the individual particles are far less susceptible to catching fire from rapid oxidation. The University of Utah performed research on small samples of powder and determined they are not pyrophoric. A large sample will have significant surface area and the extent oxygen or water will react with them is unknown. Testing with both water and oxygen will be performed once a significant sample size is manufactured. The finished product will be protected with a nitrogen blanket before it is removed from the bagging machine and it will be stored in bags that are plastic to prevent oxygen and moisture ingress and paper to protect the plastic.

MECHANICAL ENGINEERING

CODES AND STANDARDS

Mechanical system design will conform to the applicable U.S. codes and standards. The codes and standards of the following organizations will govern:

- American National Standards Institute (ANSI)
- American Society of Mechanical Engineers (ASME)
- American Welding Society (AWS)
- National Fire Protection Association (NFPA)
- Occupational Safety and Health Administration (OSHA)
- Minnesota State Mechanical and Fuel Gas Code 2015, Chapter 1346
- American Society of Heating, Refrigeration and air-conditioning Engineers (ASHRAE)
- Steel Joist Institute (SJI)

MECHANICAL BASIS OF DESIGN

EQUIPMENT SELECTION

Process equipment will be selected for the chosen plant process to meet the performance requirements of that process. Input from customer personnel, general contractor, site engineering firm and NRRI will be solicited throughout the design for preferred manufacturers or equipment vendors. Final process equipment selections will be made based on equipment performance requirements, reliability, cost, efficiency, experience, and the customers preferences. The process mechanical engineer(s) will be responsible for compiling the equipment specifications.

The major equipment and layout were developed to a preliminary design stage.

Reactor support and bucket elevator - The deflection of steel structural members shall not exceed that permitted by AISC 360, AISI S100, ASCE 8, SJI CJ-1.0, SJI JG-1.1, SJI K-1.1 or SJI LH/DLH-1.1, as applicable.

EQUIPMENT LAYOUT AND ACCESS

- Typically, one type of equipment will be chosen as the basis of design. This make or model is referred to as the “design standard.” Layout should be based on this selection. Where other manufacturer’s products are also suitable, the layout should be checked to ensure that the arrangement does not preclude the use of these alternatives.
- Required space for equipment removal/replacement/maintenance will be provided in the layout on the drawings.
- Mount equipment and panels on equipment pads to protect them from wash down and flooding.

- The minimum clearance on sides around rotating equipment over 10 horsepower (hp) should be 4 feet.
- Leave at least 4 feet of clearance between the outermost extremities of adjacent pieces of equipment or between a wall and a piece of equipment.
- Clearance in front of any other equipment face or panel requiring maintenance to be 4 feet.
- Pressure vessels should be at least 2 feet from the back wall and 3 feet apart. Sufficient space in front of the vessel should be provided for the face piping plus 4 feet.
- For pumps, compressors, and other rotating equipment where parallel units are provided, the orientation of the drive and the rotation should be identical.
- Provide ladders and/or hatches to access and remove equipment.
- Provide adequate lifting headroom for equipment. Also, an allowance for sling length or lifting beams between equipment lift points and crane or hoist hook needs to be included.
- Provide lifting eyes, in accordance with the design details, above equipment not otherwise provided with lifting means.
- All equipment in the Process Building is to meet Hazardous Locations Class I Division 2 Group B. Any equipment within 20 feet of the bagging machine needs to meet both Class I Division 2 Group B and Class II Division 1 Group E. Any equipment within 15 feet of the main reactor or hydrogen storage tank must meet Class I Division 2 Group B.

Equipment Removal System

- Provisions will be made to ensure all equipment is installed to allow means for its removal and replacement, as necessary.
- The primary means for removal of equipment that is mounted outdoors will be through the use of boom trucks and cranes.
- The facility designs for equipment mounted indoors shall take into consideration the method of equipment removal. Where practical, access shall be provided to allow removal by forklift, dolly, or cart. Where this type of access is not available, permanent means of equipment removal shall be provided in the design.

HVAC Design Criteria

Exterior Design Air Temperature Conditions

Design temperature data

- Winter Dry Bulb -20°F
- Winter Wet Bulb -20.6°F
- Summer Dry Bulb 84.3°F
- Summer Wet Bulb 69.6°F

Space Temperature Design Criteria

Design temperature criteria

- Raw Ore Building Winter 50°F
- Raw Ore Building Summer N/A
- Process Building Winter 70°F
- Process Building Summer N/A
- Finished Product Building Winter N/A
- Finished Product Building Summer N/A

Corrosion Protection

Protection from corrosion is a design criteria for HVAC systems. All HVAC coils will be specified with a corrosion-resistant coating. Paint will be applied to HVAC systems to protect materials exposed to chemicals used in or resulting from the process.

Duct Design

Ductwork for HVAC systems will be specified to be in compliance with SMACNA HVAC Duct Construction Standards. In general, ducts will be sized for 0.1 inch static pressure per 100 feet or less to reduce fan energy consumption.

PLANT LAYOUT

STANDARDS AND SPECIFICATIONS

- Minnesota State Accessibility Code 2015, Chapter 1341
- INTERNATIONAL BUILDING CODE 6, 2012
- MINNESOTA BUILDING CODE, 2016, Chapter 1305
- MINNESOTA STATE BUILDING CONSERVATION CODE, 2015, Chapter 1311
- MINNESOTA STATE MECHANICAL and FUEL GAS CODE, 2015, Chapter 1346
- MINNESOTA STATE PLUMBING CODE, 2015, Chapter 4715
- MINNESOTA STATE FIRE CODE, 2007, Chapter 7511

PLANT LAYOUT BASIS OF DESIGN

General

- Separate the raw ore from everything else to limit dust ingestion into equipment
- Separate finished product from everything else to minimize fire proofing
- Hydrogen and nitrogen storage are to be outside of buildings for safety
- Reactor and reactor feeding equipment are too tall to be inside buildings
- As much as practical keep water and water cooled components indoors to prevent freezing in the winter
- Raw ore to be stored in a protected building to prevent material loss due to wind and rain
- All external conveyors or ore material handling equipment is to be enclosed to prevent material loss due to wind and rain
- Use waste heat when possible to prevent material that is handled outside from freezing
- Minimize distance between exit of Process Building and entrance of Finished Product Building for ease of forklift access and minimizing snow removal to transport finished product

Raw Ore Building

- Provide minimum heat to building to prevent ore or reverse flotation skid water from freezing
- Ceiling clearance to be high enough to allow a dump truck to unload inside building.
- Ceiling must clear triaxle dump truck, if possible should clear tandem dump truck
- To have free span roof – no posts to create obstacles for dump trucks
- Bays to be sized to hold a minimum of one week worth of material
- Need multiple bays to separate product from different mines or different stages of processing.
- Floor thickness to be sized for 3 dump truck deliveries per week and 3 loaded Bobcat trips across per hour
- Inlet hopper to feed material into the system to be located in the Raw Ore Building to keep the dirty side contained

Finished Product Building

- To be sized to hold approximately one month of finished product
- Aisle way and storage shelving size for forklift access with 4'x3' pallets
- Don't heat building if practical to minimize building requirements

Process Building

- Keep size of building under 7,000 SF to minimize fire protection requirements
- Ventilate building enough to meet "adequately ventilated" requirements of NFPA 497
- Consolidate hazardous locations to this building as much as practical
- Steam methane reformer contains multiple water cooled components, keep as much of this skid as practical inside the building to prevent freezing
- Aisle way from bagger / palletizer to garage door to be sized for forklift access with 4' x 3' pallets
- Align steam methane reformer and boiler feed water treatment skid to share drains if practical

PROPOSED SITE AND PLOT PLANS

KEY PLAN

The preliminary key plan is shown below

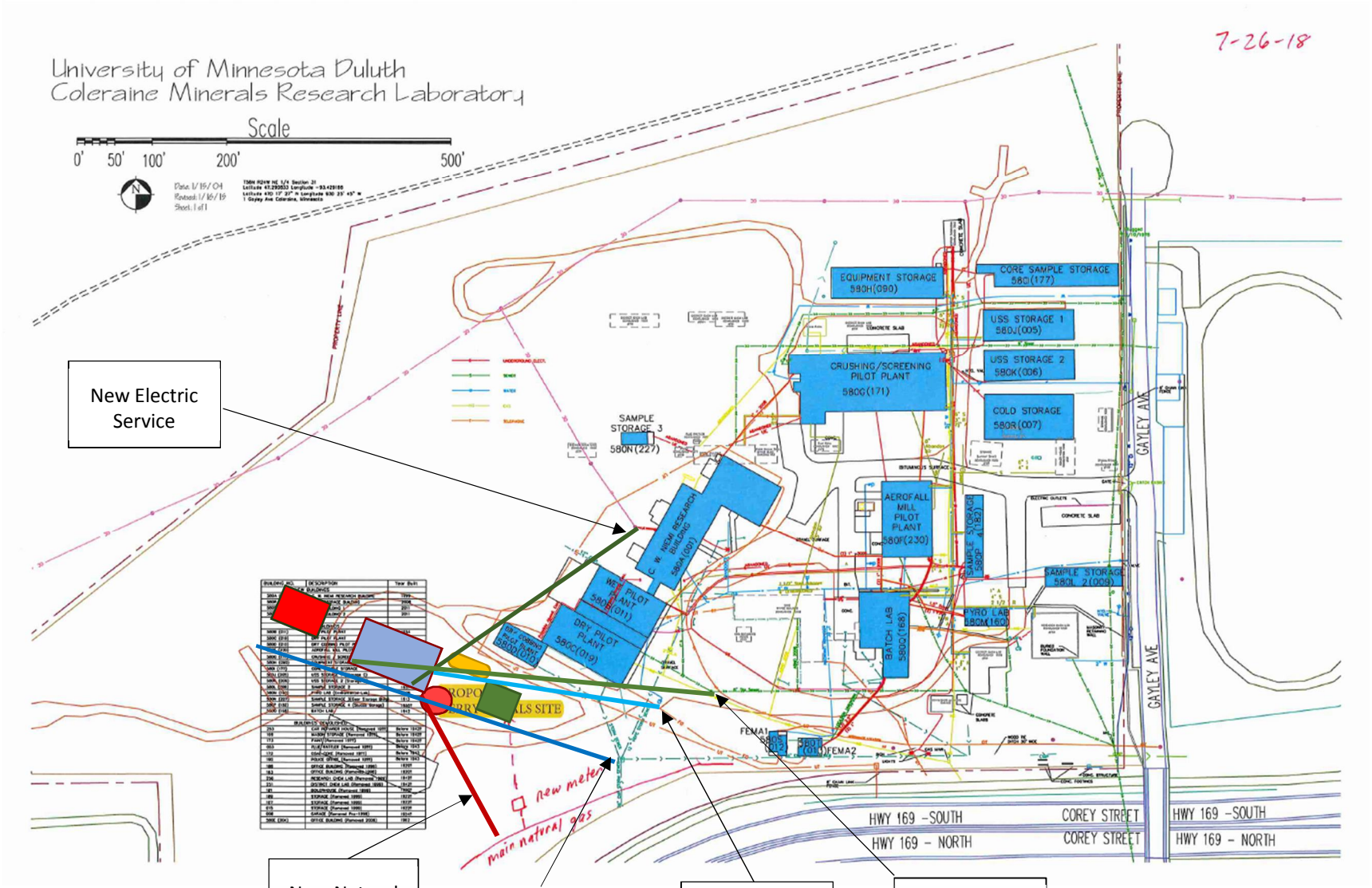

PROPOSED SITE PLAN

The preliminary site plan is shown below.

3D Model Screen Shots

All 3 buildings

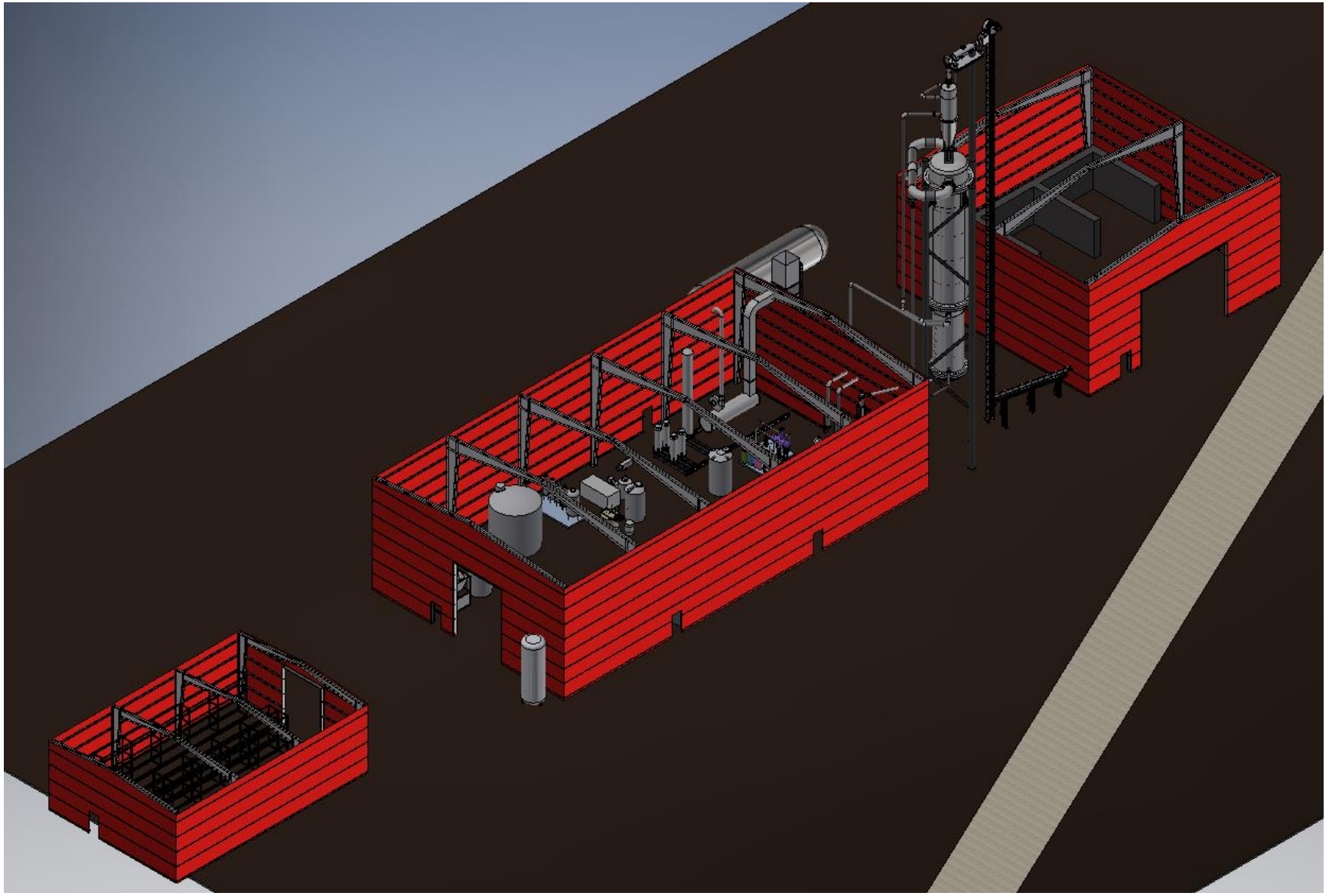

Raw Ore Building

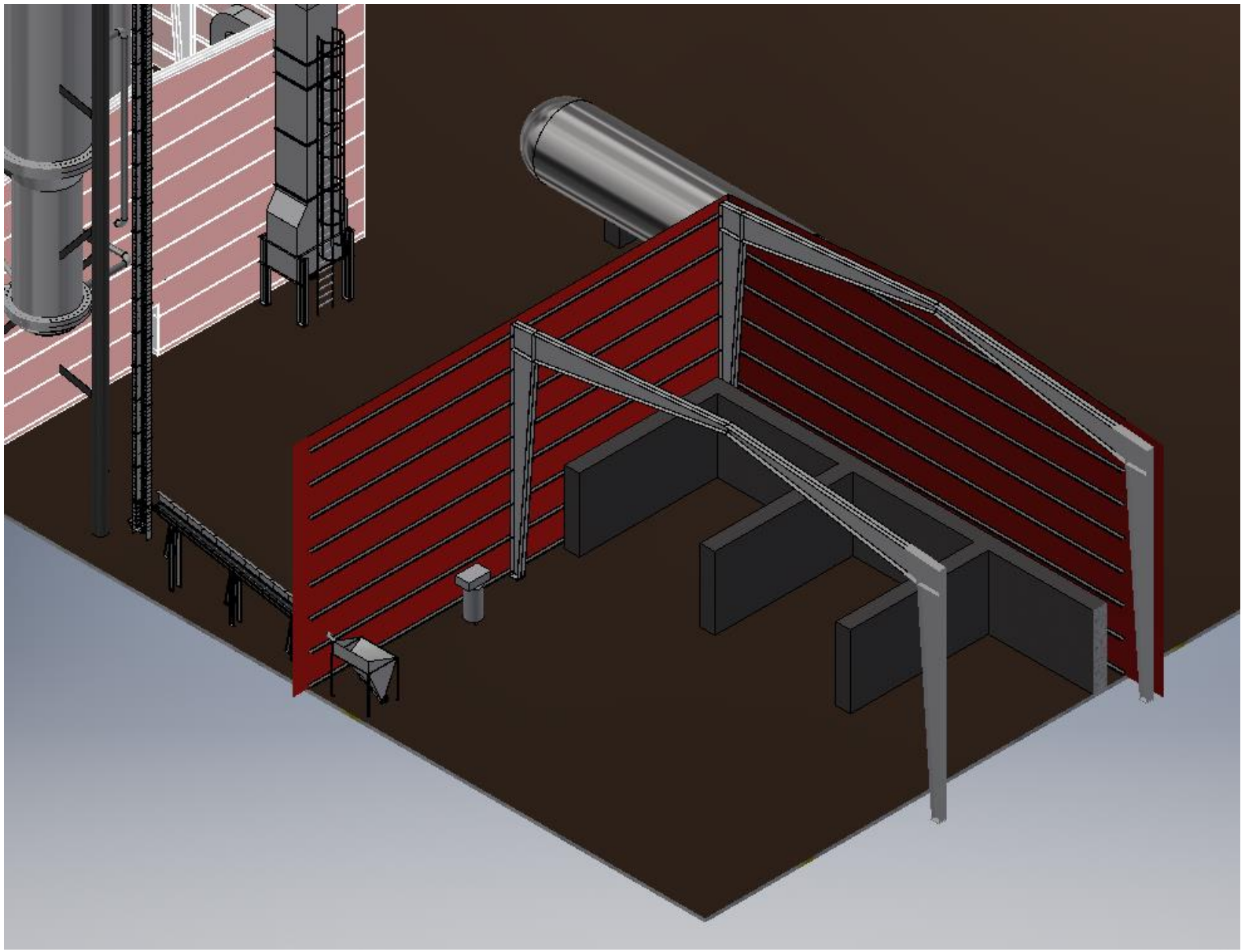

Process Building

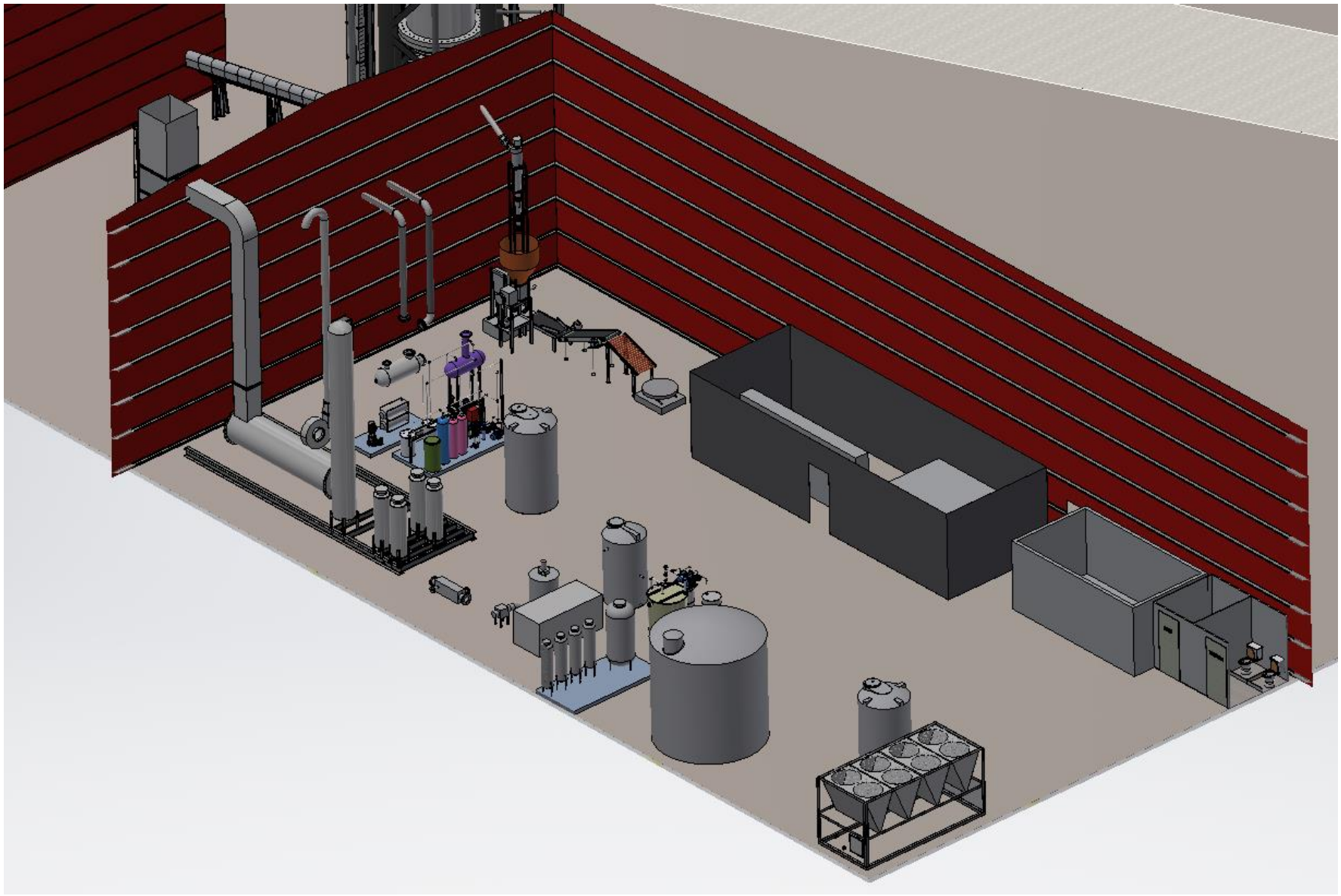

Reactor & Bucket Elevator

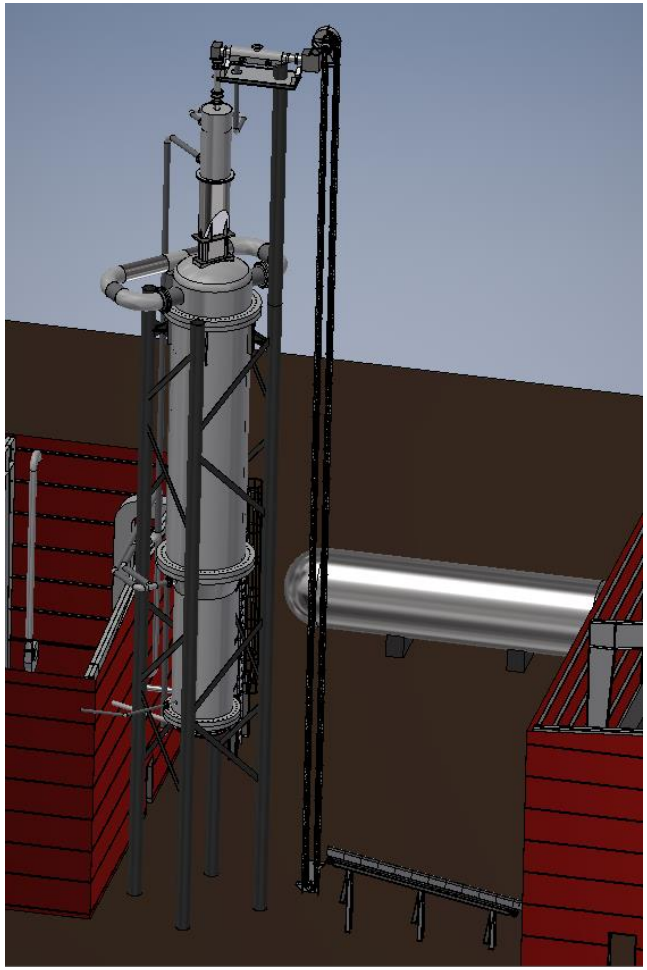

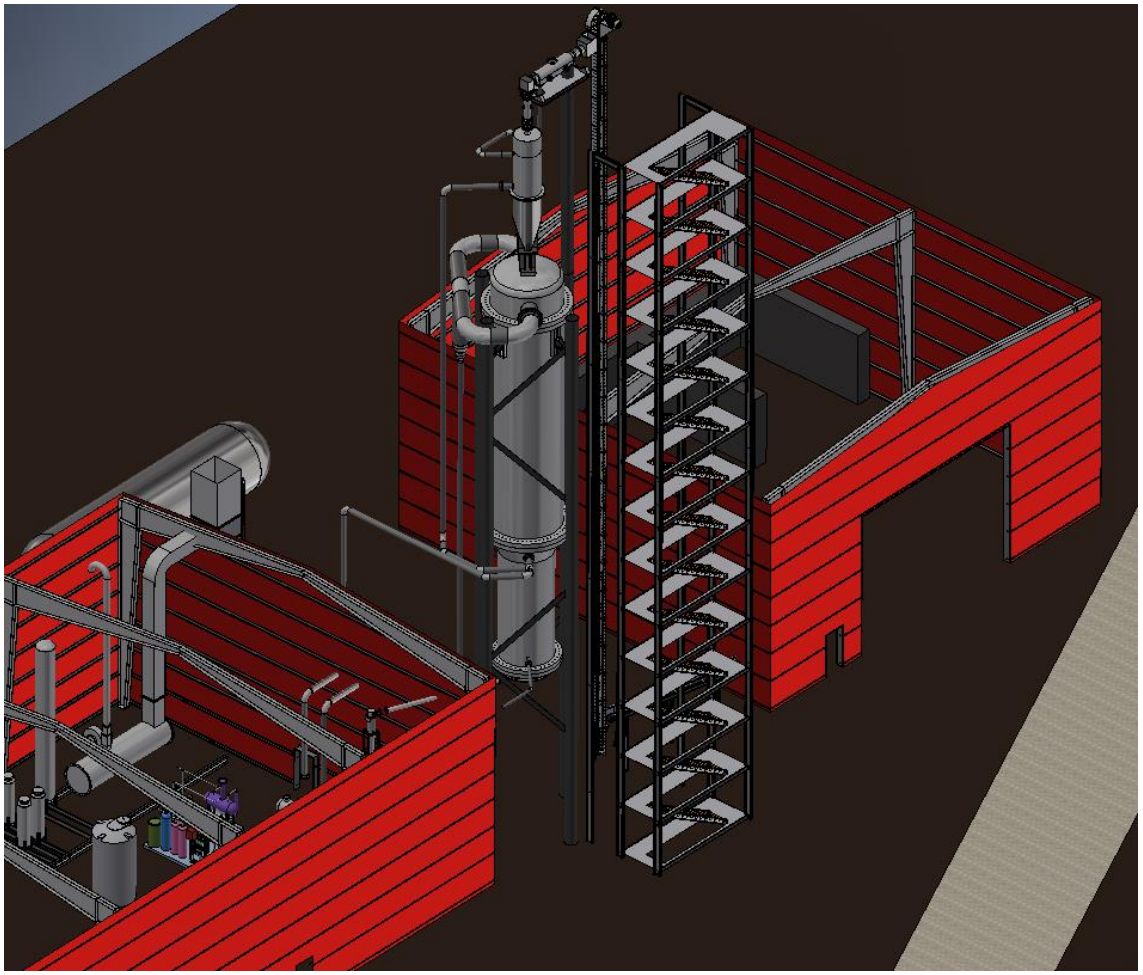

Finished Product Building

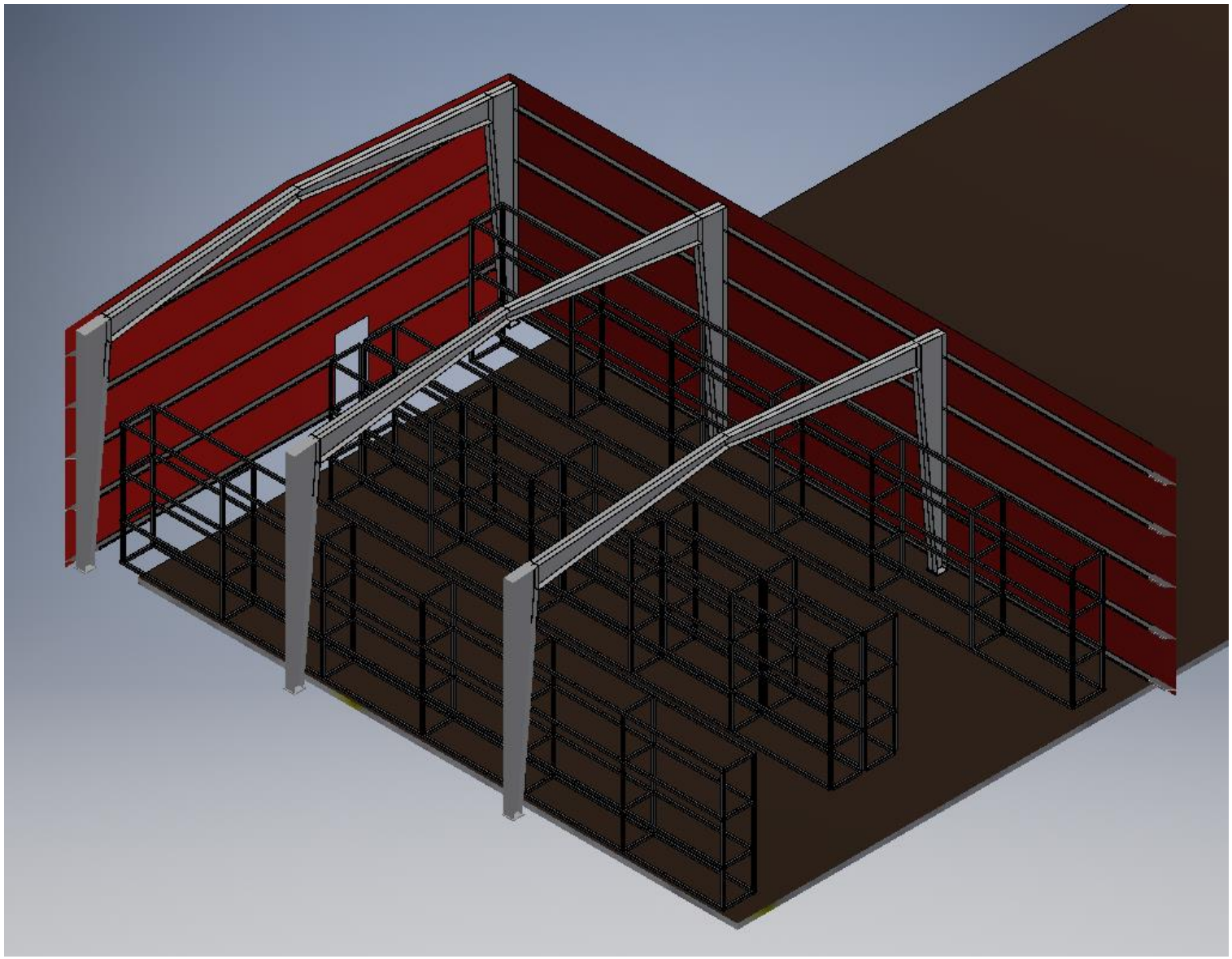

FACILITIES OVERVIEW

After reviewing the safety codes, the plant will occupy three buildings and some outdoor space.

Process Building

The Process Building is pre-engineered metal that will contain the majority of the process equipment, especially equipment that requires water cooling. The building will contain the control room, restrooms and MCC room. As this building is classified as hazardous location it will have ventilation that turns over a minimum of six times per hour. It will be heated to a minimum of 68°F to prevent water freezing and for personnel comfort.

Raw Ore Building

The raw ore building is pre-engineered metal with a clear span to allow dump trucks to back into it and dump the raw iron ore into storage bays. The ore will be moved by Bobcat or skid loader from the bays and dumped into the inlet hopper contained within the building. Because the raw ore is wet, the building will be heated to 50°F to prevent the ore from freezing.

Finished Product Building

Due to the expected large quantity of finished iron (> 25 ton), a “detached building” is required between occupancies to store finished iron powder product, otherwise the building fire proofing requirements are significant. This building is sized to store approximately 3 weeks of finished product when operating on a 24/7 basis. The building will have shelving to store pallets of the finished product until it can be shipped out. This building is not required to be heated but a heated room will be provided to prevent the sprinkler system from freezing.

Piping Installation

Piping Specifications

- Minnesota State Plumbing Code 2015, Chapter 4715
- ASME B31.12 Hydrogen Piping and Pipelines – Hydrogen Service
- ASME B31.8 Gas Transmission and Distribution Piping Systems – Natural Gas Service
- ASME B31.3 Process Piping - Water or Other Service
- ASME B16.5 Steel Pipe Flanges and Flanged Fittings

Piping Basis of Design

Piping selection

A Preliminary Pipe Schedule is included.

Steel and stainless steel pipe shall be provided with flanged joints connections to valves and other equipment. Piping materials and joint types for pressurized systems will be selected to provide thrust restraint of all joints exposed or buried.

The standard for pipe flange and pipe fitting is ASME B16.5 Pipe Flanges and Flanged Fittings.

Working pressure is location specific.

Transient pressures are to be limited to 1.33 times the working pressure.

Test pressures are to be 1.25 times the working pressure.

Valve Selection

Manually operated and power-operated valve schedules will be developed and updated as design progresses. Valve selection will generally be as follows:

- For process air system and plant water systems, valves 3 inches and larger will be butterfly valves. Valves 2-½ inches and smaller will be ball valves.
- In chemical systems, non-metallic diaphragm valves will be used.
- Check valves for wastewater will generally be swing-check valves. Check valves in chemical systems will be non-metallic ball-check valves.
- The default actuator type for power-operated valves will be electric actuators. Electric actuators will generally be 120-volt (120 V); single-phase on valves 4 inches and smaller and will generally be 480-volt; three-phase on valves larger than 4 inches.

General Piping and Valves

- All flanges for hydrogen services are to be class 300 or better.
- Spiral wound gaskets are to be used for hydrogen service.
- Cast-iron pipe and fittings shall not be used.
- Valves, gauges, regulators and other accessories for hydrogen service shall be recommended by the manufacturer.

- Hydrogen service and natural gas service - code welding per ASME BPV Section VIII Codes or ASME B31.12, B31.8 or B31.3. Procedures and qualifications in accordance with ASME BPV Section IX Welding, Brazing and Fusing Qualifications.
- Non-code welding per AISC, procedures and qualifications shall be in accordance with AWS D1.1 Structural Welding – Steel or approved equivalent.
- Locate piping so that it is not a tripping hazard, a head-banger, or a barrier to equipment access.
- To facilitate lifting, minimal piping should be located above blowers, compressors, or pumps.
- In general, lay out piping close to walls where it can be easily supported, particularly in spaces with high ceilings.
- If piping must be run close to a wall, but not supported from it, leave at least 2 feet of clearance between the outermost pipe flange and the wall.
- To permit purging of air from the pipeline while it is being filled, locate a manual vent valve on the highest point of every pipeline to be filled or is to be hydrostatically tested.
- To permit drainage, locate a manual drain valve on the lowest point of every pipeline.
- Pipe supports and seismic bracing are generally not shown on the layout drawings; however, verify that adequate space is available for installation of these supports.
- Provide flexible connections to permit easy assembly and disassembly of piping and connections to equipment.
- When laying out piping, keep the placement of anchors and expansion joints in mind. These must be located on the drawings.
- If piping reducers are required on the suction side of pumps, provide eccentric reducers that are flat on top (FOT).
- Wall penetrations should be perpendicular to the wall.
- Make an effort to keep valves within operator reach (below 8 feet). For any valve over 8 feet above the operating floor, provide a chain operator.
- Do not place swing check valves in vertical piping runs.
- Install an easy disassembly coupling or pipe joint within four pipe diameters of valves.
- Provide thrust restraint for sleeve and other couplings that are not capable of internal thrust restraint.
- Allow ample space for valve and gate actuators.
- Provide adequate clearances for rising stem valves and gates.
- Install buried valves in valve vaults, where practical.
- Provide sufficient straight runs for flow meters and other instrumentation and control (I&C) elements.

Non-Potable Water Supply

A non-potable water line will provide fire protection system water. The system will also serve for wash down stations. Hose valves, hoses, and hose rack stations will be supplied in the Process Building and the Raw Ore Storage Building.

Process Drainage, Sanitary Sewer and Roof Drainage

Process drainage includes drainage piping connected directly to process equipment or systems and area drainage in process areas. For the Process Building the steam drains are expected to be connected to the sanitary sewer. Roof and ditch drainage from the new facilities will be collected and routed to the storm drain.

Natural Gas

A new natural gas tap off will be established with a sub-meter.

Domestic Water Heating

A point of use electric water heater will serve the Process Building new restroom and service sink.

Piping Material Specifications

In general the following pipe materials apply

- Natural Gas — Steel Pipe: ASTM A53 black steel, Schedule 40
- Hydrogen — Type 316 Stainless Steel
- Process Air — Stainless steel
- Plant Air — Carbon Steel
- Nitrogen — Carbon Steel or Stainless Steel
- Cooling Water — Stainless Steel
- Steam — Carbon Steel
- Condensate — Stainless Steel or PVC
- Boiler Feed Water — Carbon Steel
- Flue Gas — Carbon Steel
- Waste Water — PVC
- Process Water — PVC
- Deaerator Drain — Carbon Steel
- Exhaust Gas — Stainless Steel
- Waste Gas — Carbon Steel
- Sodium Hydroxide — PVC

MATERIAL & CORROSION

CODES AND STANDARDS

- SSPC Steel Structures Painting Council

MATERIALS BASIS OF DESIGN

Material criteria are listed below

• Concrete	f'c = 4,000 psi at 28 days, 4,500 psi at 56 days
• Reinforcing Steel (ASTM A615, grade 60)	fy = 60 ksi
• Masonry	f'm = 1,500 psi
• Steel	
○ W-shapes	fy = 50 ksi
○ Plates, angles, shapes except W (inc channels)	fy = 36 ksi
○ Square or rectangular steel tubing	fy = 46 ksi
• Bolts	
○ High Strength Bolts	A325N
○ Machine or anchor bolts	A307
○ Stainless steel	A193 or type 316
• Aluminum	Alloy 6061-T6
• Stainless Steel	Type 316 fy = 30 ksi, Type 316L fy = 25 ksi where welded

f'c = compressive strength

fy = yield strength

ksi = kilopounds per square inch

psi = pounds per square inch

Fasteners

A fastener schedule will be provided in detail design for the appropriate type of fastener to be used for various exposure conditions.

In submerged or wet areas, type 316 stainless steel shall be used for cast-in-place anchor bolts, drilled-in wedge anchors and adhesive anchors, and aluminum beam connections.

Adhesive anchors should not be used in direct pullout, to support fire-resistive construction, or where temperatures will exceed 120°F.

Wedge or expansion anchors shall not be used to support vibrating machinery, in direct pullout unless approved for use in cracked concrete, or in masonry walls.

Painting Specification

- All carbon steel structures, pressure vessels and heat exchangers exposed to process operating temperatures less than 250°F are to be painted.
- Equipment such as pumps, motors and electrical and instrumentation housings can be supplied with the manufacturers standard finish. No field painting is required on manufacturer finished surfaces except for repair or damaged painted surfaces.
- The preparation of steel surfaces is to be in accordance with Steel Structures Painting Council (SSPC) “Surface Preparation Specifications”. The method of surface preparation is to be chosen on the exposure of the surface and painting system chosen.
- All painting operations on steel surfaces, including procedures for storage, mixing, thinning, application and drying to be in accordance with Steel Structures Paint Council PA-1 Shop, Field and Maintenance Painting and the paint suppliers printed instructions.
- Machinery non-painted surfaces for sliding or mating are to be protected during shipment with a rust preventative suitable for 6 months of storage.

Insulation Specification

Pipe Insulation

- All exterior small diameter process piping.
- Insulation will be provided on air low pressure (ALP) piping, on the discharge near the blowers, to protect personnel from potential burn hazards, and on other areas as necessary.
- Insulation to be provided on all Hydrogen piping

CIVIL, STRUCTURAL, ARCHITECTURAL ENGINEERING

CODES AND STANDARDS

- International Building Code (IBC) 2012
- Minnesota Building Code 2016 Chapter 1305
- Minnesota State Building Conservation Code 2015, Chapter 1311
- American Society of Civil Engineers (ASCE) 7-10, Minimum Design Loads for Buildings and Other Structures.
- American Concrete Institute (ACI) 350, Code Requirements for Environmental Engineering Structures, Latest Edition.
- ACI 318, Building Code Requirements for Structural Concrete, Latest Edition.
- ACI 530, Building Code Requirements for Masonry Structures, Latest Edition.
- American Institute of Steel Construction (AISC), Steel Construction Manual, Latest Edition

CIVIL BASIS OF DESIGN

DESIGN LOADS FOR BUILDINGS

Per Minnesota Building Code

RAW ORE BUILDING

Floor load

- Must withstand 3 deliveries per week of a fully loaded dump truck of iron ore
- Must withstand 3 trips across per hour of Bobcat with pneumatic wheels
- Ore bays will store iron ore at 4 ft. high and density of 195 lb. /ft^3. Bays are 19 ft. x 19 ft.

PROCESS BUILDING

Floor load

- Must withstand forklift 6 trips per hour, gross weight 15,000 lbs. Forklift Model: FL40AC-EX - EX Explosion Proof Front Loader Truck
- Local load – 10,000 gallon water storage tank - 85,000 lbs. over 141” diameter
- Local load – 1550 gallon water storage tank – 13,000 lbs. over 64” diameter
- Local load – 850 gallon water storage tank – 7,200 lbs. over 92” diameter
- Local Load Steam methane reformer 44,000 lbs. over 10’6” x 11’4”

FINISHED PRODUCT BUILDING

Floor load

- Structural Pallet Racks post spacing 108” x 36” five sections long – 3 shelves high + floor, storing 6 pallets total on shelves. 2 pallets total on floor, pallets are 3’x4’ and 3,000 lbs.
- Total load per post on continuous sections is 9,000 lb. plus 250 psf distributed floor load
- Shelving is located along the outside walls as well as the center of the building.

BUILDING DETAIL DRAWINGS

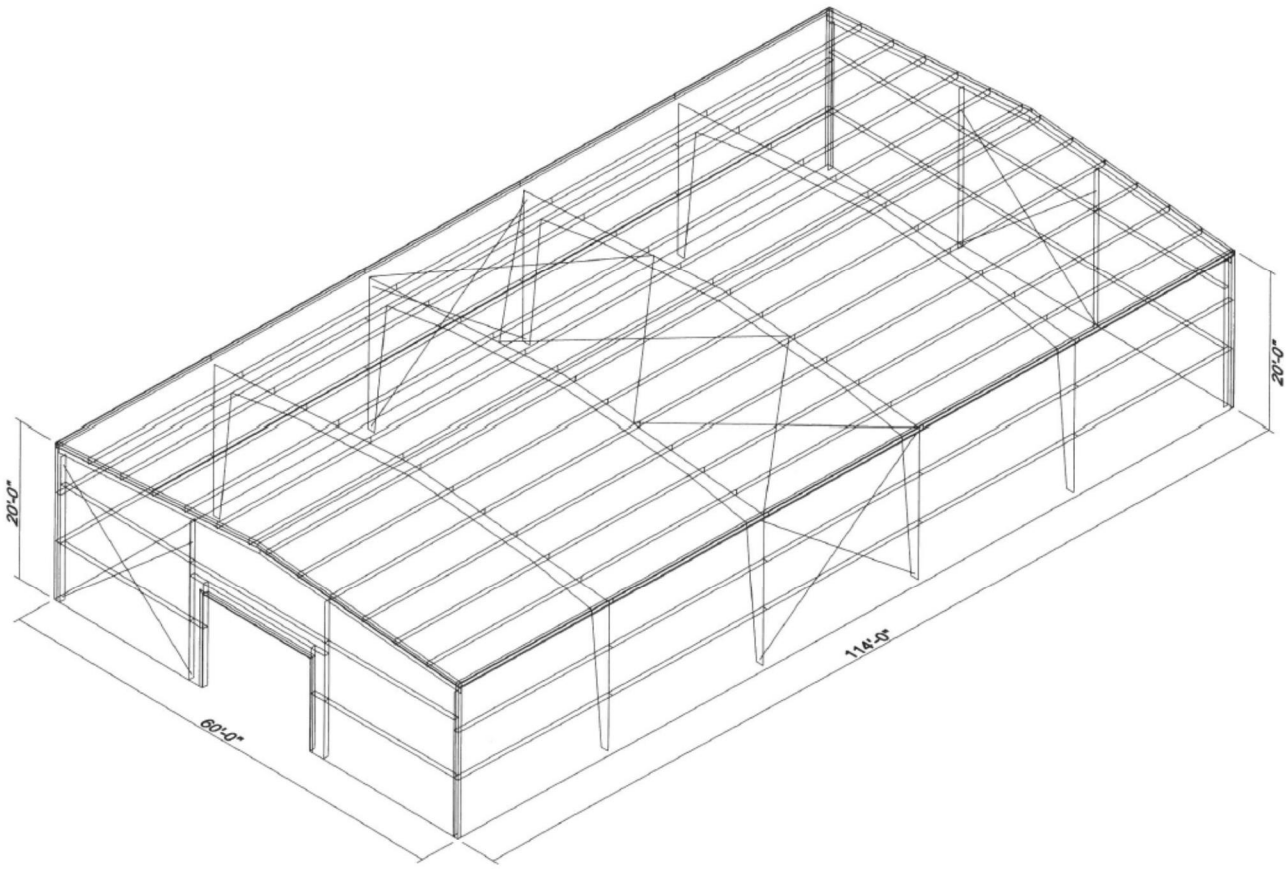

Process Building

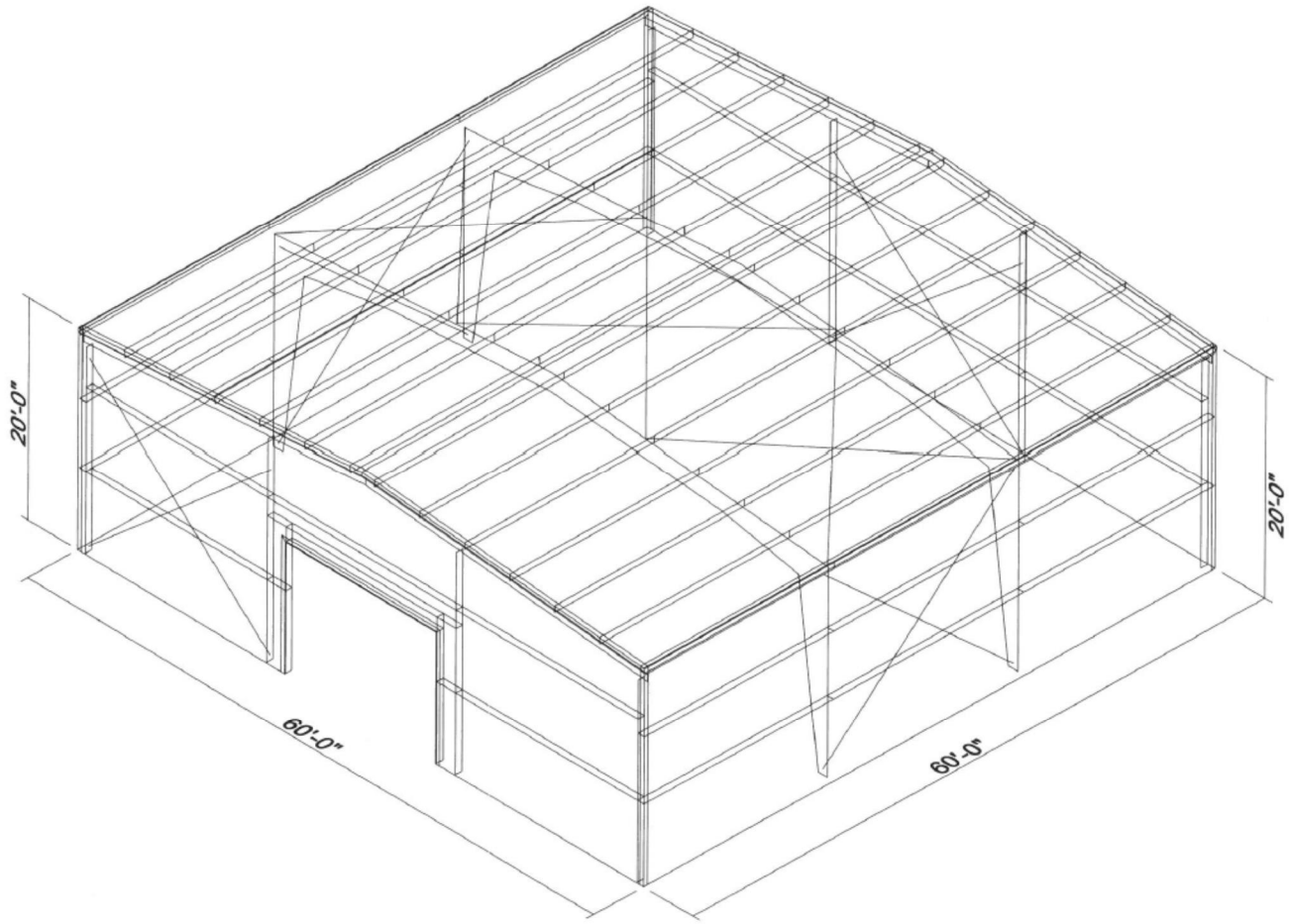

Raw Ore Building

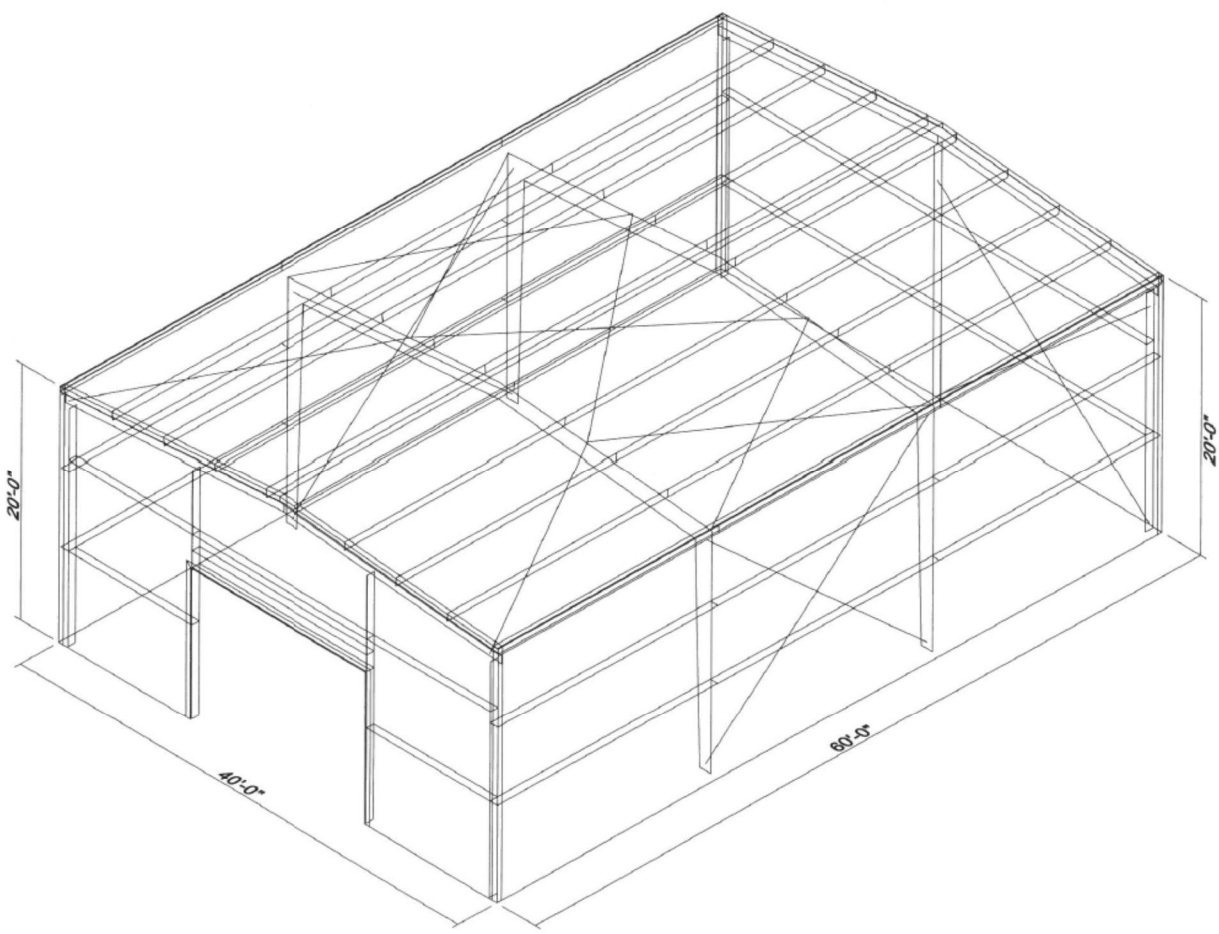

Finished Product Building

INSTRUMENTATION, CONTROLS, AUTOMATION

CODES AND STANDARDS

- NFPA 55 Compressed Gas for Industrial and Medical Facilities
- NFPA 70 National Electric Code
- NFPA 86 Standards for Ovens and Furnaces
- NFPA 325 Guide to Fire Hazard Properties of Flammable Liquids, Gases and Volatile Solids
- NFPA 496 Standard for Purged and Pressurized Enclosures for Electrical Equipment
- ISA Instrument Society of America (ISA)
- ANSI / NEMA 250 Enclosures for Electrical Equipment
- IEC 61131-3 Standard PLC Function Block Programming
- ANSI/ISA 18.2 Management of Alarm Systems for the Process Industries

INSTRUMENTATION & CONTROLS DESIGN CRITERIA

PCS – Process Control System Architecture

The PCS consists of PLC -Programmable Logic Controllers, HMI – Human Machine Interface workstations and network communication equipment. The PLC interfaces with field devices such as instruments, valves, motor starters and drives to automatically control the process. The PCS shall be designed to minimize loss of automatic control. The main control system will be an AB ControlLogix PLC with Red Lion HMI's.

Networks and Communications

The control system supervisory LAN - local area network will provide communication between the PLCs and the HMI servers and workstations. It shall use both fiber optic and category 6 copper cables.

PLC – Programmable Logic Controllers

PLCs consist of processors, communication modules, input/output (I/O) modules and I/O networks. The software the program is written in is Rockwell Software FactoryTalk View SE. The program written in this software provides the automatic control functions necessary for plant operations. In the event of failure the system is to be shutdown safely. Consideration will be given to providing redundant controllers and redundant backup power in the event of failure as the design progresses.

Package Control System PLCs

Package control system PLCs shall be small processor systems that communicate with the main PLC. Package control PLCs are anticipated for the following systems:

- Steam Methane reformer
- Induction Heating equipment
- Boiler Water Treatment System
- Bagger Palletizer
- PSA Hydrogen Recovery System
- Waste Water Treatment System

Field I/O Networks

Field I/O networks are device-level networks that connect multiple signals from devices, such as VFD - Variable Frequency Drives and electric motor operators, to a PLC via a dedicated communications link instead of hardwired I/O.

HMI Human Machine Interface System

The HMI system consists of operator workstations that are controlled by Rockwell Software FactoryTalk View SE. The software provides a graphical operator control interface to the PLCs including process status, alarms, data collection, trending and reports. The design shall be based on using Rockwell Software FactoryTalk View SE software for all PC - Personal Computer based plant HMI and data history functions.

Alarm Handling

Alarms shall be displayed and acknowledged via the HMI workstation. Alarm history shall be stored in the database at the plant.

Software Development

Delivery of the PCS application software will follow a rigorous testing, review and approval cycle. The following delivery approach will be used.

- Programming Standards Review
- Preliminary Process Graphic Review
- Factory Acceptance Test – Demonstrates all aspects of application software, simulating I/O states by forcing in software
- Functional Test 1 – Verifies field devices (instruments, starters, drives, etc.) are properly wired and providing correct input and output functions.
- Functional Test 2 – Verifies all aspects of application software function as described in the process control narratives
- System Acceptance Test – Verifies that the PCS functions as a complete operating system

DESIGN STANDARDS

Single Point of Failure

In general, single points of failure will be avoided. This does not mean that all control and equipment has to be duplicated, but there are specific components for which redundancy is required for safety or continued operation. Redundancy will be used for the following components to be determined.

PLC Input / Output Signals

PLC I/O signal types shall follow industry standards:

- Discrete inputs: dry contact field devices such as level or pressure switches and motor starter auxiliary contacts shall be powered from 120 VAC source in the PLC cabinet. PLC digital input modules shall be designed to accept isolated input signals if external power sources are necessary.
- Discrete outputs: PLC digital outputs shall be individually isolated, rated for 2 amps at 120 VAC. For current requirements greater than 2 amps, interposing relays mounted in the PLC cabinet shall be used.

- Analog inputs: PLC analog input signals shall be 4 to 20 mA at 24 VDC. PLC analog inputs shall be individually isolated, allowing for 2-wires transmitters powered from independent DC power supplies in the PLC cabinet and 4-wire transmitters powered from 120 VAC UPS supply from the PLC cabinet.
- Analog Output: PLC analog output signals shall be isolated 4 to 20 mA at 24 VDC into 750 ohms, powered from the PLC.
- Special signals: 1 to 5 VDC analog inputs may be used within control cabinets.

Failsafe Alarms

All alarm signals shall be designed as failsafe. This means a field service device shall provide a powered signal back to the PLC during normal process conditions, with power being disrupted during an alarm condition. Therefore, if power is lost or a device or wiring fails, an alarm shall be generated.

Emergency Stop Control

Selected equipment shall have a mushroom-type emergency stop (E-STOP) pushbutton. This pushbutton is hardwired to the motor starter. The E-STOP pushbutton must be surrounded by a metal guard.

Personnel Safety

Switches and relays hardwired to the equipment starter or controller shall be used for personnel safety interlocks, such as E-STOP pushbuttons and conveyor/press trip wires. The operation of these interlocks shall be independent of, but monitored by the PCS. Local RESET pushbuttons shall be used to reset lockout functions as required at the MCCs.

Equipment Protection

Switches and relays hardwired to the equipment starter or controller shall be used for protective interlocks, such as motor overload and critical process conditions. The operation of these interlocks shall be independent of, but monitored by the PCS. Local RESET pushbuttons shall be used to reset lockout functions, as required.

Valve and Gate Control

Actuated valves and gates will be provided with local OPEN/STOP/CLOSE pushbuttons and LOCAL/REMOTE selector switches integral with the actuator. OPEN/CLOSE service valves will be provided with OPEN and CLOSED limit switches that actuate at the end of travel. Modulating valves will be provided with OPEN and CLOSED limit switches that actuate at the end of travel, and with continuous 4-20 milliamp position feedback and transmitters.

Indicating Light Colors

Indicating lights shall follow the convention as listed below.

- GREEN to indicate an inactive condition such as motor OFF, valve CLOSED
- RED to indicate operation, such as motor RUNNING, valve OPEN
- YELLOW/AMBER to indicate an abnormal condition, such as high pressure or level, or motor ALARM
- WHITE to indicate remote control
- BLUE to indicate local control

UPS - Uninterruptible Power Supply

Uninterruptible power supply shall be provided for the following loads (at a minimum)

- PLC power supplies
- Power for all 4-wire analog devices monitored by a PLC
- Loop power for all analog I/O monitored or controlled by a PLC
- All computer equipment and panel-mounted HMI components (including workstations, keyboard/video/mouse modules and panel mounted operator interface components)
- All network equipment (including network switches and firewalls)

The UPS shall provide a minimum 30 minutes of backup power, allowing adequate time for the standby generator to startup and transfer. The UPS shall receive incoming power from either utility or standby generator power. The UPS will include a bypass switch to allow removal and/or repair to the UPS without disrupting power to the load.

Fire Alarms

The Fire Alarms will be provided and coordinated with the control system.

I/O List & Allocation Table

I/O Count	
Digital Inputs 120VAC	81
Digital Outputs 120 VAC	81
Analog Inputs 4-20 mA	200
Analog Outputs 4-20 mA	55
Thermocouple Inputs	106
RTD inputs	36
Ethernet cards	2
ControlLogix PLC	1
Monitors + FactoryTalk Software	4

Process Control Strategies

Three different control modes will be available – Local, Remote Automatic and Remote Manual. Each serves a different purpose and provides a different level of automation.

Local

Local refers to control interface local to the equipment being controlled. A hardwired local control option shall be provided for all equipment (excluding minor items such as solenoid valves). A local indication and a Local/Remote control switch shall be provided at or near the field device where practical (for example, open/close controls and indicators on valve actuators, start/stop controls and indicators at the MCCs starters, and integral process displays on field instruments).

The local control will provide local manual control only and does not require the PLC to be operational. All automatic functions and interlocks provided by the PLC are bypassed in this mode. This mode is intended for maintenance purposes and is not recommended for long-term operations.

Remote

Remote refers to a control interface remote from the equipment being controlled. When the Local/Remote control switch is in the Remote position, the equipment is controlled by the PLC. Once remote is selected, the operator can the select Remote Automatic or Remote Manual from the HMI.

Remote Automatic

In Remote Automatic, the equipment is automatically sequenced and adjusted by the PLC, as described in the process control narratives, based on the automatic set points entered by the operator. This is the primary operating mode that will be used.

Remote Manual

In Remote manual, the equipment can be manually operated from the HMI through the PLC. This provides a method for operators to manually operate the equipment from the control room. All automatic functions and interlocks provided by the PLC are bypassed in this mode. This mode is intended for maintenance purposes and is not recommended for long term operations.

ELECTRICAL ENGINEERING

CODES AND STANDARDS

- National Electric Code (NEC, NFPA-70)
- NFPA 497 Recommended Practice for the Classification of Flammable Liquids, Gases or Vapors and of Hazardous (Classified) Locations for Electrical Installations in Chemical Process Areas
- NFPA 499 Recommended Practice for the Classification of Combustible Dusts and of Hazardous (Classified) Locations for Electrical Installations in Chemical Process Areas
- Life Safety Code (NFPA-101)
- International Fire Code (IFC)
- Standard for Electrical Safety in the Workplace (NFPA-70E)
- American National Standards Association (ANSI)
- National Electrical Manufacturers Association (NEMA)
- Institute of Electrical and Electronic Engineers (IEEE)
- Instrument Society of America (ISA)
- Insulated Cable Engineers Association (ICEA)
- Occupational Safety and Health Administration (OSHA)
- American Society for Testing Materials (ASTM)
- Underwriters Laboratory (UL)
- Illuminating Engineering Society (IES)
- National Fire Protection Association (NFPA)

ELECTRICAL DESIGN CRITERIA

DISTRIBUTION SYSTEM

The distribution system will be designed for the capacity of the process, under the scope of this contract, with additional capacity for future process equipment. A new tap will be pulled from an existing 30 kV power line on the property. The transformer will be a 30 kV to 480 VAC at 1,000 amps. The new power line will be routed underground to the MCC cabinet located in the Process Building. Power to the Raw Ore Building and the Finished Product Building will be routed from the Process Building to sub panels located in the respective buildings.

BACKUP POWER

UPS Uninterrupted Power Supply units will be provided for the PLC Programmable Logic Controller and appropriate instrumentation. A site backup power supply system will be available from NRRI Coleraine Lab in the event that detail design shows the need for more backup power.

Listed and Labeled Equipment

Electrical equipment, materials, or services to be provided will have an attached label, symbol, or other identifying mark of an organization that is concerned with product evaluation, compliance with appropriate standards, and performance of the equipment. Typically, this is the Underwriter's Laboratories Label or Listing (UL).

Area Classifications

Area classifications (such as hazardous locations, corrosive areas, wet areas, and high temperature locations) will be called out on the drawings. All materials and methods used will be rated for use in such areas. The following areas are classified as Class 1, Division 2, Group B areas:

- Process Building ventilated at 6 air changes per hour
- Hydrogen storage tank with a 15 ft. radius around it
- Main Reactor with a 15 ft. radius around it

The following areas are classified as Class 2, Division 1, Group E areas:

- Bagger / Palletizer with a 20 ft. radius around it.

Distribution Voltage Selection

Standard distribution systems are to be used as follows:

- 480 volts, ungrounded delta, 3-phase, 3 wire
- 480 Y/277 volts solidly grounded wye, 3-phase, 4 wire
- 208Y/120 volts solidly grounded, 3-phase, 4 wire

Utilization Voltages

• Indoor Lighting	120 VAC	single phase
• Outdoor Lighting	120 or 277 VAC	single phase
• Convenience Outlets	120 VAC	single phase
• Motor Control	120 VAC	single phase
• Motors less than ¾ hp	115 VAC	single phase
• Motors ¾ hp and greater	460 VAC	three phase

Voltage Drop

Steady-state voltage drop calculations will be prepared for heavily loaded or long branch circuits and feeders. Calculations for motor circuits will be based on an 80 percent power factor and loading consistent with the maximum expected peak load (will not include standby motors). The following total voltage drop from the transformer secondary to the point of utilization, including feeder, branch circuit, and transformation, will not be exceeded:

- Lighting 3%
- Motors 4%
- Receptacles 4%

Voltage dip calculations for motor starting will be made whenever an individual motor exceeds 20% of the serving transformer capacity.

DEMAND FACTORS

The following demand factors listed below will be used for sizing power switchboards, motor control centers (MCCs), panelboards and transformers. Connected load will be used for circuit and equipment sizing per NEC requirements. Ten to twenty percent spare capacity will be provided at MCCs and panelboards.

- Lighting 1.0 x Connected load
- Emergency Lighting 1.0 x Connected load
- Air-conditioning Equipment 1.0 x Connected load
- Ventilation Equipment 1.0 x Connected load
- Convenience Receptacles 180 VA each
- Process Loads Sum of constant speed + adjustable speed + 25% of largest motor
    - Constant speed 1.0 x Connected load of non-standby loads
    - Adjustable speed 0.85 x Connected load of non-standby loads

BRANCH CIRCUITS

Connected load and NEC requirements will be used for sizing branch circuit breakers and conductors.

A minimum wire size of No. 12 American gauge (AWG) copper will be used for lighting and receptacle branch circuits. No. 10 AWG will be used when voltage drop requires a larger conductor on lighting circuits, and when receptacle circuits are longer than 75 feet. Where electronic ballasts are specified for fluorescent lighting a dedicated neutral will be provided for each lighting circuit.

In general, lighting branch circuit loads will be limited to 1,500 watts.

Lighting and receptacle branch circuits will be combined into common conduits, where appropriate.

The number of convenience receptacles, on any one branch circuit, will be limited to five duplex in process areas and six duplex in office areas.

PANELBOARDS

Branch circuits or feeders on the drawing will identify the panelboard and device protecting the individual circuit or feeder.

Each panelboard will be equipped with a minimum of 20 percent spare breakers with spaces, bus work and terminations to complete the standard size panelboard.

Panelboard schedules will be prepared indicating circuit identification, protective device trip rating, number of poles, and load in volt-amps by phase, rating of main lugs or main circuit breaker, neutral bus size, ground bus size and integrated short circuit rating of the panelboard.

A separate panelboard will be provided for instrumentation and controls devices (I&C) and field panels, if needed.

MOTOR CONTROL

Elementary (ladder type) control diagrams will be prepared for each motor showing control wiring, pilot devices, auxiliary contacts and external connections. A single diagram will be used for more than one motor having the same control.

Graphic symbols shown on the electrical legend sheet will be used. Each component will be identified with a unique letter or name. Wiring and devices inside the controller will be shown as solid lines, and wiring and devices remote from the controller with a dashed line. The location of remote devices will be indicated by symbol or description.

Remote control assemblies that have complex internal wiring will be shown as dashed rectangles. Only the interconnecting terminal or interface will be identified, and the location of the unit or responsibility of the internal wiring will be referenced.

Motor controllers provided will either be mounted inside a MCC or as a standalone piece of equipment.

DISTRIBUTION SYSTEM EQUIPMENT

Distribution equipment criteria include the following:

- 480-volt switchboard with group mounted feeder circuit breakers
- 480-volt MCCs with combination motor starters, of the motor circuit protector type, rated for the available fault current. Starters larger than NEMA size 3 (50 horsepower) will be the solid-state, soft-start type or adjustable speed drives. MCCs will be sized to accept future loads and either allow for space in the structures or floor space for future sections.
- 480-volt and 208Y/120-volt power distribution and lighting panelboards with molded case, bolt-in-place and plug-in, respectively, circuit breakers with integrated short-circuit rating suitable for the available fault current.

WIRE AND CABLE

Wire and cable criteria include the following

- Stranded copper conductors will be used for all except lighting and receptacle wiring. Solid conductors #10 AWG and smaller will be used for lighting and receptacle wiring.
- Minimum conductor size of No. 12 AWG will be used for power and lighting branch circuits. Type thermoplastic high heat resistant nylon coated (THHN)/ thermoplastic high heat and water resistant nylon coated (THWN-2) insulation will be used for No. 10 AWG and smaller conductors (conduit will be sized for Type THW conductors). Type cross-linked high heat water resistant (XHHW-2) insulation will be used for No. 8 AWG and larger conductors (conduit will be sized for THW conductors). 60°C conductor ampacity ratings will be used for sizing conductors No. 1 AWG and smaller. 75°C ratings will be used for sizing conductors larger than No. 1 AGW.
- Minimum conductor size of No. 14 AWG will be used for individual 120-volt control circuits.
- Minimum conductor size of No. 12 AWG will be used for 120-volt control circuits routed in a common conduit with the power conductors to the motor circuit controls. Combining individual motor power and control conductors in a common conduit will be done up to a maximum power conductor size of #2 AWG.
- Power and control conductors will be color-coded. Conductors No. 8 AWG and smaller will have colored insulation. Conductors No. 6 AWG and larger will be color-coded with tape at each end and at accessible intermediate points.
- Conductors and control cables will be tagged with a permanent sleeve or nylon marker plate attached with a nylon strap. Conductor tags with approved tag number will be provided by the contractor and will be located at each termination and in accessible locations.
- Under normal conditions, the maximum wire size will be limited to 600 kcmil. Parallel conductors will be used for circuits requiring greater capacity.

- 120-volt control circuits will be combined in control cables containing multiple #14 AWG stranded coper conductors with type THHN insulation and a common PVC outer jacket.
- 600-volt multi-circuit control cable will be used where grouping control circuits is practical, and the number of individual wires exceeds six conductors. When selecting control cable size, 25 percent spare (plus or minus 10 percent) conductors will be used.
- Low-voltage status/control (less than 100 volts) and analog signal circuits will be routed in 600-volt single twisted shielded pair instrumentation control cables. The cables will consist of #16 AWG stranded copper conductors with combination PVC/nylon insulation, drain wire, shield and PVC outer jacket. Signal circuits will be combined in multi-twisted shielded pair instrumentation control cables with common overall shield. The cables will consist of #18 AWG stranded copper conductors, with a combination PVC/nylon insulation, pair and common drain wires, pair and common shields, and PVC outer jacket. Low-voltage status/control and analog signal circuits will not be routed in the same control cable or conduit with 120-volt control or power circuits. Low-voltage status/control and analog signal circuits will be routed in the same conduit, but not in the same control cable.
- Adequate separation of power and I&C wiring will be provided to avoid signal interference. Long parallel runs will be avoided and analog wiring will be installed in steel conduit.
- Shielded power cables will be used between adjustable frequency drives and the driven motor when the motor is greater than 150 feet from the drive.

COLOR CODING

Conductor insulation colors will be as below

• All systems	Ground	Green
• 208Y/120 Volts	Neutral	White
	Phase A	Black
	Phase B	Red
	Phase C	Blue
• 480Y/277 Volts	Neutral	White
	Phase A	Brown
	Phase B	Orange
	Phase C	Yellow

CIRCUIT IDENTIFICATION

Circuit names will be assigned based on device or equipment at load end of circuit. Circuit identification will be at each termination and in accessible manholes and pull boxes. Plastic sleeves for conductor #3 AWG or smaller and plastic marker plates for larger conductors will be used.

For lighting circuits, the panel and circuit number for each fixture will be identified.

ENCLOSURES

NEMA 1 enclosures will be used for equipment in electrical rooms and finished areas. NEMA 12 enclosures will be used for electrical equipment in dry industrial locations. NEMA 4X enclosures will be used in exterior locations and interior corrosive locations. NEMA 7 enclosures will be used for equipment in classified locations.

Fiber Optics Cabling

Where used, fiber optic cabling will be installed either in conduit (2-inch diameter minimum) or in a cable tray. Routing of the raceway system will provide for large-radius turns to prevent breaking of the fiber optic cable.

Convenience Receptacles

General service duplex receptacles will be spaced no more than 50 feet apart in process areas. Receptacles will be surface-mounted on walls or columns.

Waterproof receptacles will be installed in damp areas or areas subject to washdown.

Outlet-mounted ground-fault circuit-interrupters will be provided, where required by the NEC. Panelboard or feed-through type devices will not be used.

General System Protection

General

Equipment will be selected with adequate momentary and interrupting capacity for the point in the system where it is used. Series rated criteria will not be used, except for self-contained equipment.

Phase and ground fault protective devices and device settings will be selected that will function selectively to disconnect that portion of the system that is malfunctioning with as little disturbance to the rest of the system as possible.

Preliminary Fault and Coordination Analysis

A preliminary analysis of the fault duty and device coordination will be made to produce a design that can be accurately bid by the contractor.

Maximum fault duty will be analyzed with sufficient accuracy to establish the required interrupting ratings of circuit protective devices specified. An infinite bus will be assumed on the source (primary) side of the utility service substation transformer.

Final coordination studies based on actual equipment purchased will be made by the contractor to establish the range of protective device settings that will result in reasonable selectivity of device operation for both three-phase and ground faults. The following protective device characteristics will be specified:

- Circuit breaker frame size, trip setting range, time delay range
- Current transformer ratios

Motor Protection and Control

General

- Each motor will be provided with a suitable controller and devices that will protect the equipment and perform the functions required.
- MCC-type construction will be used

- MCCs located in the same room with the switchboard that powers them will not have a main circuit breaker. MCCs located in areas remote from the common MCC or switchboard that powers them will have a main circuit breaker.
- MCCs will include feeder circuit breakers and motor starters. Motor starters for motors through 50 hp will be the full voltage, non-reversing, combination type with magnetic-only circuit breaker. Motor starters for motors larger than 50 hp will be the solid-state, soft-start, reduced voltage, combination type with magnetic only circuit breaker.

Overload Protection

Each constant speed motor, 50 hp and larger, and all adjustable frequency drive motors will be provided with thermal overload protection in ungrounded phases. Controller-mounted relays will be provided with external manual reset.

Motor Control

Oil-tight devices will be specified for mounting on unit starters.

Motor control circuits will be designed at 120 volts and an individual control power transformer with 120-volt control voltage will be provided in each motor starter.

Grounding

Electrodes

An integrated grounding system will be installed throughout the project facilities. A facility ground system will be installed near each of the buildings. This ground system will consist of a bare copper ground wire and driven ground rods at or near each corner of the building. Each facility ground system will be connected to an adjacent facility ground system, and routed with the site power ducts to provide an overall integrated grounding system.

Grounding electrode embedded rods and cables will be designed for a maximum resistance of 5 ohms. Where more than one rod is required, rods will be installed at least 20 feet apart. Minimum of No. 3/0 AWG stranded bare copper cable will be used for interconnecting to ground rods and footing rebar.

Separate grounding systems will be provided for communication and computer systems. Grounds will be tied together per NEC requirements.

Equipment Grounding

A separate ground conductor sized in accordance with NEC requirements will be installed in raceways for power feeders and branch circuit raceways for motor control, lighting and receptacle loads.

Shields of shielded instrumentation cables will be grounded to the ground bus at the power supply for the analog or low voltage discrete signal circuit. Shielded instrumentation cables will not be grounded at more than one point.

Lighting

General Requirements

Interior and exterior areas will be provided with lighting. Interior lighting will include switched lights, continuous-on (24 hour) lights, emergency egress lights and exit lights. Emergency egress and exit lights will each include a battery charger and battery. Exterior lighting will include photocell-controlled lights mounted on buildings near doors or on structures.

Lighting levels in maintained foot-candles will be designed to meet recommendations of the Illuminating Engineering Society of North America (IESNA), IES Lighting Handbook and the guidelines provided in this document.

Exterior lights will be sharp cut-off type to minimize light trespass outside the project site. Exterior lighting will be laid out to minimize any impacts to future site expansions, both above and below grade.

Luminaires are to meet UL requirements for intended use.

LIGHTING CALCULATIONS

Recommended foot-candle levels for each space will be calculated for maintained illumination per IESNA procedures. The following assumptions will be made unless specific information is available:

Reflectance for finished rooms:

Ceilings	80 percent reflectance
Walls	50 percent reflectance
Floors	20 percent reflectance

Reflectance for unfinished rooms

Ceilings	50 percent reflectance
Walls	30 percent reflectance
Floors	10 percent reflectance

Maintenance factor (light loss factor)

Fluorescent Lighting	.80

INTERIOR ILLUMINATION

Interior light fixtures will be fluorescent type. Fluorescent recessed luminaires will be used in control room type areas with lay-in ceilings. Fluorescent “enclosed and gasketed” luminaires of non-metallic type construction will be used for applications in locations subject to saturation with water, or locations exposed to weather and unprotected. Units will be specified to carry the UL “suitable for wet locations” label.

Fluorescent lights will typically be ceiling mounted; however, their use will be examined on an individual room basis. The final location for luminaires will be field-verified to provide easy access for maintenance. Lower mounting heights may be specified for individual task lighting.

EXTERIOR ILLUMINATION

Outdoor illumination will be provided outside exterior doors, on roads and parking lots and where deemed appropriate for visibility.

Exterior lights will be the light-emitting diode (LED) type powered at 120 or 277 volts, single phase and controlled by a photocell. Exterior lighting will be full cutoff, limiting the migration of light.

EMERGENCY AND EGRESS LIGHTING SYSTEMS

Emergency illumination will be provided in appropriate spaces as required by code to provide life safety, property and equipment protection.

Adequate lighting levels will be provided to maintain safe build egress and critical process plant functions. Emergency lighting will be located near MCCs and any equipment locations that need to be monitored on a continuous basis.

In large process areas, emergency standby lighting units with a battery pack, and two lamps and lighted exit signs with a battery pack will be provided. The battery pack will power the lights for at least 90 minutes.

Continuous on (24 hours) lights will be provided along egress paths, where required by code.

Circuiting and Switching

Each room will be circuited and switched to provide adequate lighting for the anticipated use, and reduced or no lighting when not occupied by switching alternate luminaires, or by switching alternate ballasts. Occupancy and daylight sensors will be used to automatically adjust light levels to save energy, where appropriate.

Exterior lighting will be controlled by an ON/OFF/AUTO selector switch and roof-mounted photocell. In the AUTO mode, lights turn on at dusk and off at dawn via the photocell.

Lamps

Energy efficient lamps will be installed in fluorescent light fixtures.

LED lighting is preferred for exterior lighting.

High bay fluorescent lamps are preferred for use in large areas where calculations indicate low bay fluorescent lamps will be inadequate for the tasks to be performed.

Outdoor lighting in landscaped areas and areas visible to the public will be planned in concert with architectural input.

Ballasts

Energy efficient two-lamp fluorescent ballasts will be used whenever possible. Fluorescent ballasts are sound-rated by a letter code with “A” used to designate the quietest and “D” for the loudest. Lamp ballasts with a code designation of “A” will be used whenever possible.

Lamp/ Luminaire Combinations

The following conditions will be considered in selecting lamp / luminaire combinations:

- Higher lumen per watt rapid start and high-output type fluorescent lamps will be used whenever possible.
- Fluorescent luminaires will be used in damp area applications with an enclosed and gasketed lamp compartment. Fluorescent lamps will not be exposed to the weather.
- Types of lamps will be kept to a minimum to reduce the inventory requirement for spares.

Explosion-Proof Luminaires

Any room or space listed as a hazardous atmosphere area will have explosion-proof type luminaires UL listed for installation in the hazardous area classifications, as required by Article 500 of the NEC.

Damp Atmosphere Luminaires

Rooms with a damp atmosphere will preferably have non-corrosive-type enclosed and gasketed fluorescent luminaires.

LIGHTING LEVELS

Design lighting levels in maintained foot-candles will be as shown below:

- General Lighting 20
- Control Rooms 30-50
- Laboratories 50
- Lavatories 10-20
- Stair Landings 10-20
- Corridors 10
- Storage 10-20
- Process Areas 30
- Offices 30-50
- Pump Areas 30
- Maintenance Area 30-50
- Electrical Room 30-40
- Mechanical Room 30

FIRE ALARM SYSTEM

A fully addressable fire alarm system will be installed in all facilities that connect together via a dedicated network. The network will allow the status of any one panel to be checked at any fire panel on the network. Each major facility will have a fire alarm panel that will monitor devices in that facility, as well as those in nearby facilities. The master fire panel will provide the status of the remote panels and will be connected to the plant control system to notify plant operators, as well as a central monitoring station. The central monitoring station will alert the local responding agency to the nature of the alarm and the location. The fire alarm system will monitor for presence of fire as well as combustible has detection and ventilation presence in hazardous areas where required by code.

TRAINING

Training to run the plant HMI and overall system will be provided during commissioning. A vendor representative will supply both classroom instruction and practical experience for the following subcomponents of the system:

- Methane Steam Reformer
- Boiler Water Treatment Skid
- Hydrogen Purification Skid –PSA Pressure Swing Adsorption skid
- Feed Gas Compressor skid
- Induction Power Heating system
- Bagger Palletizer
- Rotary Dryer

Testing Plan

The test plan is broken into three separate phases 4 months long each.

Commissioning

Commissioning will take place immediately after construction is complete. This is to perform functional testing to verify all equipment is hooked up properly and working and to double check accuracy. This check will include documenting and testing

- HMI – open and closed feedback, alarm status, hand off remotes, units associated with each instrument
- every valve in the system for proper function and alarm
- VFDs
- solenoid valves
- functionality all motor starters
- temperature transmitters
- pressure transmitters
- level transmitters
- weight transmitters
- other miscellaneous instrumentation

Training will take place during commissioning stages. Generally commissioning is a 5 days per week with a possible 12 hour staggered shift. Overtime is expected to occur irregularly. A small amount of iron ore will be required during this test period.

Testing Phase 1

Testing Phase 1 is generally expected to be 5 days per week with a 12 hour staggered start to allow time for system startup and shutdown. During this period material will be tested from different mines and parameters will be varied from the baseline (highlighted) to optimize the process. Multiple parameters are to be varied including temperature, flow rate hydrogen, flow rate particles and muffle heating sections on or off. Furthermore, the material from the different mines will be different size and chemical makeup. If materials are gathered from 10 mines the testing will have approximately 8 days testing for each material. Eight days of testing will consume approximately 22 tons of iron ore or approximately one truck load of iron ore. This testing will be adjusted or varied as lessons are learned.

Testing Phase 2

Testing Phase 2 is a 24/7 operation. The best combination of test parameters will be picked for testing. This extended test is expected to show erosion, corrosion or operating issues that will need to be accounted for to move forward with a demonstration unit. At the baseline operating condition the process is expected to consume just under 8 tonnes per day or 975 tonnes for the period. This consumption can go up or down depending on the operating condition selected.

Site Work and Landscaping

Description

The proposed site will be cleared of trees and graded for construction of 3 buildings for the Flash Iron Pilot Plant. These buildings will have foundations and slabs and new underground utilities will be routed to them. A road exists that will need to be slightly modified and repaired with gravel.

Permitting

Permits will be pulled in construction phase.

Grading

The existing topography in the proposed area of the buildings has a slight slope of 2 feet. After removal of the trees and excavation for the slab and subbase, the grade will be leveled in the building are and blended to the outer boundary of the excavation.

Road

An existing gravel road will be repaired and restored with gravel after construction is complete.

Drainage

The site generally slopes from the Northwest to Southeast corner. A storm sewer runs near the back side of the Raw Ore Building proposed location. All downspouts and drains the proposed buildings will be tied together and tied into the storm sewer.

Utilities

A new 30 kV to 480V electrical tap with transformer and 1200 amp circuit breaker will be installed behind building 580(A) next to the existing tap and transformer. An underground electric line will be routed west and south to the 3 new flash iron buildings.

A new gas line service will be tied into the main gas service to site with its own meter. The main natural gas line follows HWY 169 and will be a northward underground run to the Process Building and from there routed above ground to the Dryer and Raw Ore Building.

A sanitary sewer line will be run from the Process Building Eastward past building 580(C) where it will be tied into the existing sanitary sewer.

All storm drains will be routed underground South and East to the existing storm sewer.

An underground potable water line will run from the Process Building and Raw Ore Building eastward to tie into existing water lines near building 580(Q). This same line will provide for the fire sprinkler system in the Process Building and the Finished Product Building.

Process Piping

Process piping will extend outside the Process Building to the Reactor and Dryer.

Equipment Located Outside

The Main Reactor, Dryer, Bucket Elevator, Hydrogen Storage Tank and Liquid Nitrogen Storage Tank will be located outside the buildings. This equipment will have foundations.

Landscaping

The site will be landscaped by leveling and reseeding with grass after construction is complete.

COMMERCIAL SIZE

A commercial plant reactor size estimate was laid out to verify scaling. The center heating section (induction coil, refractory and susceptor) was used as the unit size. The unit size of 1 meter of susceptor length = 3,000 tpy was lengthened to increase capacity of the reactor. If hydrogen pressure is increased to increase throughput a circular reactor housing will be required to minimize the wall thickness and therefore cost. If hydrogen pressure is not increased a rectangular section can be used as the reactor housing and reactor units can fit more compactly. A 30' circular reactor housing can have an output of 130,000 tpy while a rectangular housing can have an output of 175,000 tpy. The pilot plant test data will be used for an optimization study for the design of the commercial reactor.

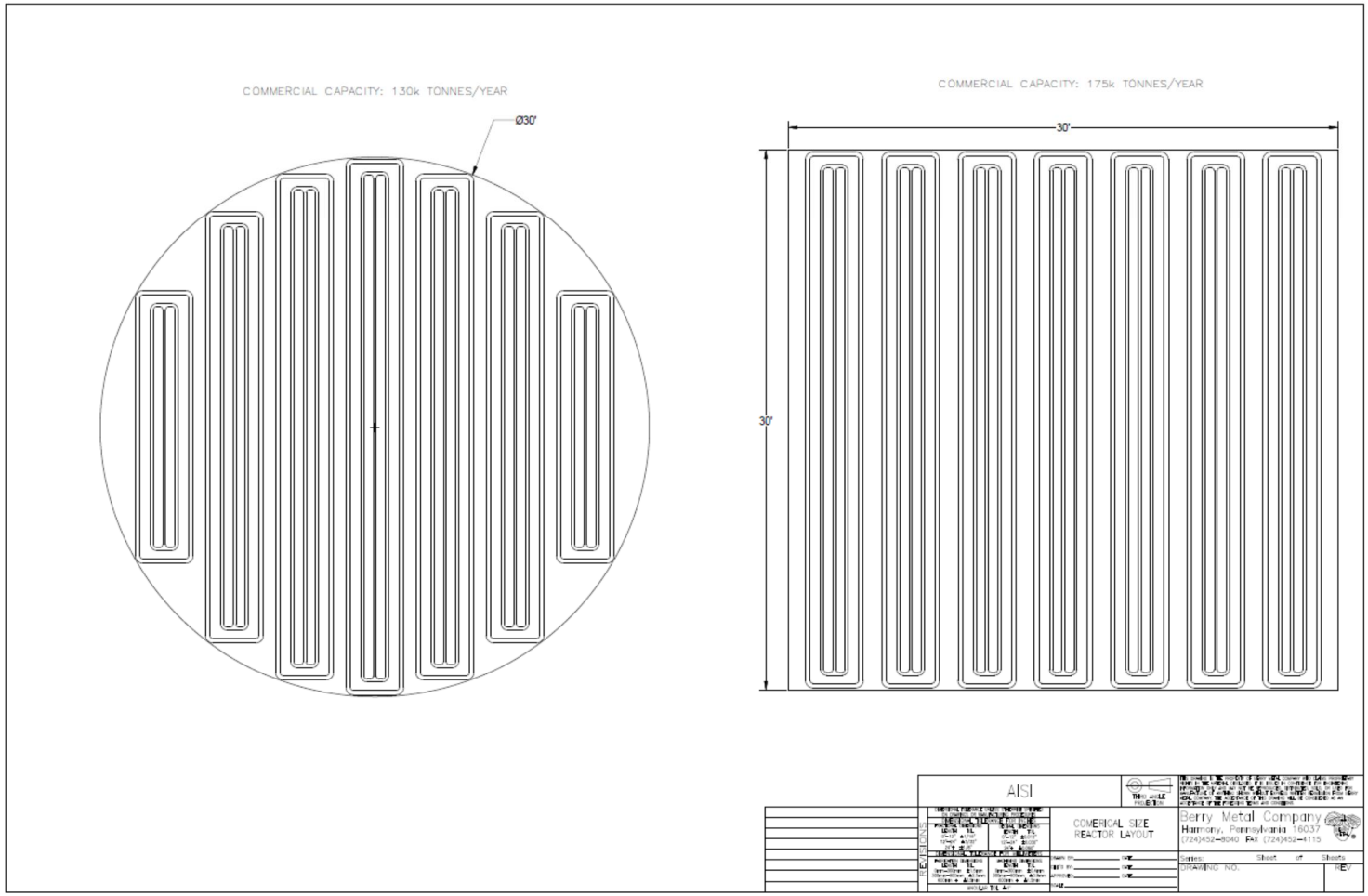

OPINION OF PROBABLE COST

ESTIMATE CLASSIFICATION AND METHODOLOGY

An opinion of cost budget to final design, manufacture equipment, erect a pilot plant and test has been developed. A Class 3 cost estimate was prepared for the Preliminary Design. This level of cost estimate, as defined by AACEI – Association for the Advancement of Cost Engineering International, is for projects at a 10 to 40 percent level of definition and uses a detailed, unit cost approach with an expected accuracy range of -15% on the low end range and +40% on the high end range. Major equipment was specified and 80% of the major equipment was vendor quoted with the remaining estimated in house. Site preparation and erection costs were supplied by an international Architectural and Engineering firm in Minnesota. This estimate was established using a combination of their in-house historical knowledge and a contractor ROM - Rough order of magnitude price including some $/SF for certain components. A testing proposal was developed and a budget of time and material was developed. A summary of these costs are in the table below.

MAJOR ASSUMPTIONS

The estimate is based on the assumption the work will be done on a competitive bid basis and the contractor will have a reasonable amount of time to complete the work. All contractors are equal, with a reasonable project schedule, no overtime, constructed as under a single contract, no liquidated damages. This estimate should be evaluated for market changes after 90 days of the issue date. It is assumed that much of the fabricated equipment and material will be acquired domestically.

This cost estimate has been prepared for guidance in project evaluation and implementation from the information available at the time of the estimate. The final costs of the project will depend on actual labor and material costs, competitive market conditions, final project costs, implementation schedule and other variable factors. As a result, the final project costs will vary from the estimate presented herein.

Summary of Flash Ironmaking Pilot Plant Cost		
	Low End $1,000s	High End $1,000s
Direct Costs	$13,289	$18,798
Indirect Costs	$2,130	$3,991
Testing	$3,216	$5,531
Total	**$18,635**	**$28,320**

The opinion of Probable Cost does not include insurance or the cost of financing. It assumes the plant and equipment will become the property of NRRI after testing is complete, no allocation has been appropriated for disposal of equipment or to restore the land to as found condition.

Risk Matrix

Risk	Impact	Risk Reduction
Iron ore powder plugs or creates bridge in piping, hoppers, or other equipment	Production stops	Remove moisture in ore to less than 1%. Create access areas
Radiant heating section may not heat particles evenly	Will not achieve 95% metallization	Create a curtain of the particles so they are all the same distance from the carbon graphite wall. Verify with CFD
Radiant heating section may heat particles too fast or too slow	May fuse the outer layer preventing the center from becoming metalized	Limit wall temperatures to slightly above desired particle temperature
Hydrogen recovery may not work as desired	Not enough EDF to get 95% metallization	Reduce particle flow rate
Heat of reaction drops the temperature too low	May not get 95% metallization	Add additional heat in second radiant heating section
High loss of material at transfer points such as conveyors, hoppers, briquette station etc.	Yield will drop	Use enclosed conveyors where possible. Use guides and enclosures at all transfer points
Lock hopper seals fail	Hydrogen can leak	Use pressurized seals that seal gas will leak into hydrogen rather than hydrogen leaking out
Induction Coil Fails	Possible reduced load	Multiple coils and two main heating zones
Feed rate too fast	Will not get 95% metallization	Create mockup to verify feed rate
Residence time calculations have uncertainty	Reactor may not be long enough to get 95% metallization	Have large margin in reactor length Cut back particle flow rate